β-delayed charged particle decays of neutron-deficient nuclei ^{20}Mg and ^{22,23}Si

M. Babo

Normandie Université

THESE

Pour obtenir le diplôme de doctorat

Spécialité Physique

Préparée au sein de l'Université Caen - Normandie

β-delayed charged particle decays of neutron-deficient nuclei ^{20}Mg, ^{23}Si and ^{22}Si

Présentée et soutenue par

Mathieu BABO

Thèse soutenue publiquement le 16 Septembre 2016 devant le jury composé de		
Dr Olivier SORLIN	Directeur de Recherche, GANIL, Caen	Directeur de thèse
Dr Bertram BLANK	Directeur de Recherche, CENBG, Gradignan	Rapporteur
Dr Daniel BAZIN	Professeur, NSCL, East Lansing	Rapporteur
Dr Riccardo RAABE	Professeur, KU Leuven, Leuven	Examinateur
Dr Etienne LIENARD	Professeur, Université de Caen / LPC, Caen	Examinateur

Thèse dirigée par Olivier SORLIN, GANIL

UNICAEN UNIVERSITÉ CAEN NORMANDIE

Ecole Doctorale SIMEM

ENSICAEN

Université de Caen-Normandie

GANIL laboratoire commun CEA/DRF – spiral2 – CNRS/IN2P3

GANIL T 2016 02

Université de Caen Normandie
U.F.R. de Sciences
ÉCOLE DOCTORALE SIMEM

Thèse de doctorat

présentée et soutenue le : 16 Septembre 2016

par

M. Mathieu Babo

pour obtenir le

DOCTORAT de l'UNIVERSITÉ de CAEN

Spécialité : Constituants élémentaires et physique théorique

β-delayed charged particle decays of the neutron-deficient nuclei ^{20}Mg, ^{23}Si and ^{22}Si.

MEMBRES du JURY :

Dr. Olivier Sorlin	Directeur de recherche, GANIL, Caen	(***Directeur de thèse***)
Dr. Bertram Blank	Directeur de recherche, CENBG, Gradignan	(***Rapporteur***)
Dr. Daniel Bazin	Professeur, NSCL, East Lansing	(***Rapporteur***)
Dr. Riccardo Raabe	Professeur, KU Leuven, Leuven	
Dr. Etienne Liénard	Professeur, LPC, Caen	

Résumé

Les ions d'intérêts riches en protons de ^{20}Mg, de ^{23}Si et de ^{22}Si ont été produits par fragmentation au laboratoire NSCL, à MSU (USA), puis implantés dans un dispositif composé de 3 détecteurs Si à pistes (DSSD) entouré de 16 détecteurs HPGe. Cet ensemble a permis la détection des particules chargées émises depuis les états non liés, en coincidence avec les rayons γ émis par la désexcitation des noyaux fils. La décroissance βp du ^{20}Mg, particulièrement bien connue, a été étudiée afin de tester et d'optimiser l'analyse. En particulier, les voies de décroissance βp peuplant les 3 premiers états excités du ^{19}Ne ont pu être identifiées. Le temps de demi-vie, les rapports d'embranchement des transitions et les énergies d'excitation des états, y compris l'état isobarique analogue (IAS), ont été mesurés. L'étude de la décroissance β du ^{23}Si a permis l'identification de 14 états dans l'^{23}Al. L'émission de deux protons depuis l'IAS dans l'^{23}Al a pu être mise en évidence avec certitude. La mesure de l'énergie de l'IAS a permis une détermination plus précise de la masse de l'état fondamental du ^{23}Si, à 23.27 (7) MeV. Une possible transition $\beta 3p$ a également été observée. La plupart des prédictions théoriques de la masse du ^{22}Si sont en accord avec une radioactivité 2-protons (2p). Les décroissances $\beta 2p$ vers le premier état excité et l'état fondamental du ^{20}Na ont été identifiées. Le rapport d'embranchement vers l'IAS est de 2.05 (44) %, et son énergie d'excitation a été mesurée à 9040 (54) keV. La mesure supplémentaire du temps de demi-vie, $T_{1/2} = 30.38$ (45) ms, a permis de calculer le temps de vie partiel de cette transition. Dans cette étude, nous proposons une paramétrisation de la fonction statistique de Fermi f pour les décroissances de Fermi super-permises, permettant la première mesure indirecte de l'excès de masse de l'état fondamental du ^{22}Si, à 31.49 (14) MeV. L'énergie seuil correspondante est alors $S_{2p} = 645$ (100) keV, et ne permet pas une radioactivité 2p depuis l'état fondamental.

Abstract

The neutron-deficient nuclei ^{20}Mg, ^{23}Si and ^{22}Si were produced by fragmentation at NSCL, at MSU (USA), and implanted into an array of 3 double sided stripped Si detectors, surrounded by 16 high-purity Ge detectors. This novel arrangement allowed the detection of the charged particles emitted by the unbound excited states in coincidence with the γ rays emitted by the de-excitation of the daughter. The βp decay of ^{20}Mg is very well-known and therefore was used to test and optimize the analysis programm. The β-delayed proton transitions to the first 3 excited states in ^{19}Ne were identified and compared to previous measurements. The half-life, the branching ratio of the transitions and the excitation energies, including the IAS, were measured and are in good agreement with the adopted values. The study of the β^+ decay of ^{23}Si allowed the identification of 14 excited states in ^{23}Al. The emission of 2 protons from the IAS was unambiguously identified. The measurement of the IAS energy allowed a better determination of the mass excess of ^{23}Si, giving 23.27 (7) MeV. A possible $\beta 3p$ decay channel was also tentitavely identified. Most of the theoritical predictions are in favor of a 2-proton radioactive ^{22}Si. The $\beta 2p$ decays to the first excited state and the ground state of ^{20}Na were identified. The branching ratio of the decay to the IAS is 2.05 (44) %, and the IAS excitation energy was measured to be 9040 (54) keV. The additional measurement of the half-life gives $T_{1/2} = 30.38$ (45) ms, and allowed the determination of the partial half-life. In this study, we propose a parametrization of the statistical rate function f for the superallowed Fermi β decays. This allow the first indirect mass measurement of ^{22}Si ground state, 31.49 (14) MeV. The two-proton threshold is then $S_{2p} = 645$ (100) keV and does not allow 2p radioactivity.

Contents

A ma mamie bleue,

Remerciements

Il est intéressant de se pencher, une fois l'épreuve de la rédaction du manuscrit touchant à sa fin, sur l'enchaînement d'évènements qui me mena en cet instant précis. Nul n'est besoin de s'attarder sur ces détails, mais il convient de remettre dans son contexte la naissance de cette thèse. Et c'est ainsi que, plutôt que d'entamer les remerciements par le côté hiérarchique, je vais vous les énoncer par ordre chronologique.

Les expériences de physique nucléaire ne sont pas sans rappeler ces kits de petit physicien en herbe que l'on m'offrait les jours de fêtes. Les nombreux shifts de nuit qui les accompagnent ressemblent d'ailleurs fortement à ces nuits passées dans le jardin familial, à observer les étoiles et les planètes, le nez tremblant, et l'œil appuyé sur la lunette ou le télescope. Ce sont là mes premières expériences de physique, d'astronomie et de chimie, mises en œuvre sous les yeux attentifs et protecteurs de mes parents. C'est ainsi que me vient naturellement l'envie de les remercier. Maman, Papa, mais aussi mes frères Thomas et Marc, vous avez su me porter et me soutenir malgré les durs efforts que cela pouvait parfois représenter. Vous avez déclenché en moi cette puissante envie de découverte, de compréhension du monde qui m'entoure. Vous l'avez accompagnée, en visitant un observatoire pendant nos vacances, ou même en parcourant quelques centaines de kilomètres pour assister à une éclipse. Et au-delà du physicien, c'est ladulte que je suis devenu qui vous remercie.

Cet attrait pour les sciences me permet d'effectuer un stage, en MPSI/MP, auprès de l'accélérateur TANDEM à l'IPN d'Orsay. C'est ici que se joue l'évènement le plus déroutant de ma vie, dans le sens où il me mènera, non sans embûche et contre toute attente, à mon doctorat. Je me dois, en me rappelant cette semaine de faisceau qui m'était entièrement dédiée pour mettre en évidence ce qu'était la magicité d'un noyau, de remercier Tonton Fadi. Grâce à toi, j'ai goûté à la physique nucléaire (et au Coca Cola cherry), et je n'ai pas réussi à m'en défaire. Je te remercie de m'avoir accompagné et de m'avoir soutenu, dans les moments de doute et de faiblesse, mais aussi dans ceux où je n'avais plus assez de batterie. Tu as vu en moi cette étincelle de chercheur que je n'avais pas même souponnée. Assez naturellement et sans honte, je peux affirmer que ce doctorat, c'est à toi que je le dois. A toi et au Père Fouettard, qui m'aura poussé au bord de mon ignorance, et qui m'aura appris ce qu'était une raie à 511 keV. Une drôle de transition, introuvable dans les tables, et qui me poursuit depuis lors. Il m'est impossible d'oublier ces autres chercheurs du groupe Nester ; les incroyables Faïrouz, Nicolas, Iulian, Iolanda, Dominique et Matthieu, qui ont également apporté leur pierre à l'édifice.

La consécration de toutes ces années d'études vient alors que je m'y attends le moins, avec l'obtention d'une bourse de doctorat au GANIL. Pour cette thèse, je dois remercier Olivier, d'avoir accepté de m'encadrer officiellement. Je ne peux que me reprocher d'avoir si peu interagi, mais je te remercie pour ton honnêteté lors de la dernière ligne droite, qui m'aura permis de me recadrer. De toute l'équipe avec laquelle j'ai travaillé, je dois aussi remercier Geoffrey-Fathom, qui a su me faire confiance en me confiant ce jeu de données à analyser. La tâche ne fut pas

facile, et la communication parfois complexe, mais nous avons su mener à bien ce projet. Et dans la suite logique, je souhaite remercier Thomas, sans qui mon caractère de breton m′aurait empêch d′avancer.

Il ne serait pas convenable de terminer ces remerciements sans parler de mes acolytes de thèse : Pierre (avec qui je n'aurai pas pu dormir dans un lit en forme de cœur à Venise mais avec qui j'ai partagé une fin de thèse digne des grandes épopées grecques), Marine (sans qui mes nerfs auraient lâché depuis belle lurette), Coralie (ma copine bretonne et alcoolique), Quentin (courage p′tit chat, le prochain c'est toi), Alex et Samantha (thank you so much for your support and your help for this last year), Guillaume (tu ne liras même pas ma thèse, mais ton cynisme me manque), Dennis, Benoît, Aldric, Adrien, Simon, Patrick, Hong Liang, Yung Hee, et j′en oublie sûrement ...

Ces trois années de thèse n'auraient pas pu être un succès sans les interactions avec les autres chercheurs du GANIL (François, Anthéa, Fanny, Carme, Julien, Beyhan, Emmanuel), de l′IPN (Marion), du CIMAP (Yannick, Lucas, Arek) de l′INFN (Barbara, Marco R., Marco S., Alberto), de NSCL (Daniel) et de Cologne (Mickael). J'en oublie sûrement, mais je dois avouer que le manque de sommeil de la fin de thèse n'arrange pas ma mémoire.

Dans une autre sphère, celle du privée, j'aimerais remercier plus particulièrement Xtoulov, pour ces coups de mains gauches et ses phrases qui ne veulent rien dire. Merci aux copains Guillaume, Richard et Julien (eh non, pas de Babo bingo cette fois-ci). Merci à Jérôme et Francis, pour cette drôle de famille. Merci à Guigui, Juju, Cécile et la déesse Britney. Merci à Romain, qui m′a aidé à accoucher de ce beau bébé qu'est Pint of Science à Caen. Merci aux femmes du GANIL : Myriam, Ketel, Sabrina, Virginie, Marie-Laure, Catherine, et toutes les autres.

En dernier lieu, il est de mon devoir de vous remercier, vous qui ouvrez ces quelques pages, et qui prenez le temps de parcourir mon travail accompli ces trois dernières années. J'ai bon espoir qu'il vous soit utile, qu'il vous inspire et qu'il vous invite à le dépasser.

Chapter 1

Introduction

One of the simplest ways to describe the mass of atomic nuclei is to ignore the fact that the nucleus consists of protons, neutrons and the complex N-body forces acting between them and to instead assume that the entire system can be treated as a charged liquid drop. A semi-empirical description would require both volume and surface terms as well as a uniform Coulomb contribution that is required to describe the overall electric charge. By adding additional terms for pairing and symmetry effects, the binding energy of this liquid drop is described by the well-known Bethe-Weizsacker mass equation [Wei35]. The predictive power of this formula is shown in Figure 1.1. It is immediately apparent that this description works reasonably well for most nuclei with the exception of a select few that have a very specific number of protons and/or neutrons. These numbers were deemed magic numbers since they seemed to provide excess nuclear binding.

Today, the concept of magic numbers is well understood. They originate from the fact that nuclei exhibit shell structure in a completely analogous way to electron shell structure in atoms. The nuclear shell model was developed [May48] to explain why these magic nuclei, with proton or neutron numbers equivalent to 2, 8, 20, 28, 50, 82, or 126, are the most strongly bound and why doubly magic nuclei (nuclei with a magic number of both protons and neutrons) provide the strongest possible nuclear configuration. Although tremendously successful, it was assumed that the nuclear shell model with its fixed set of magic numbers is universal and should persist even in unstable isotopes. Following decades of research and with the recent advent of rare-isotope beam facilities, this simple picture is now known to be incorrect. The classical shell gaps and magic numbers used to describe nuclei near stability evolve towards the extremes of nuclear binding and often give rise to spectacular phenomena such as exotic structures, unique shapes, and rare modes of nuclear decay. The delicate and subtle forces that drive these dramatic structural changes challenge our understanding and demand further investigation in regions where they may be enhanced. Experimental studies of nuclear structure and decay for the most exotic nuclei are thus essential for understanding the limits of nuclear binding

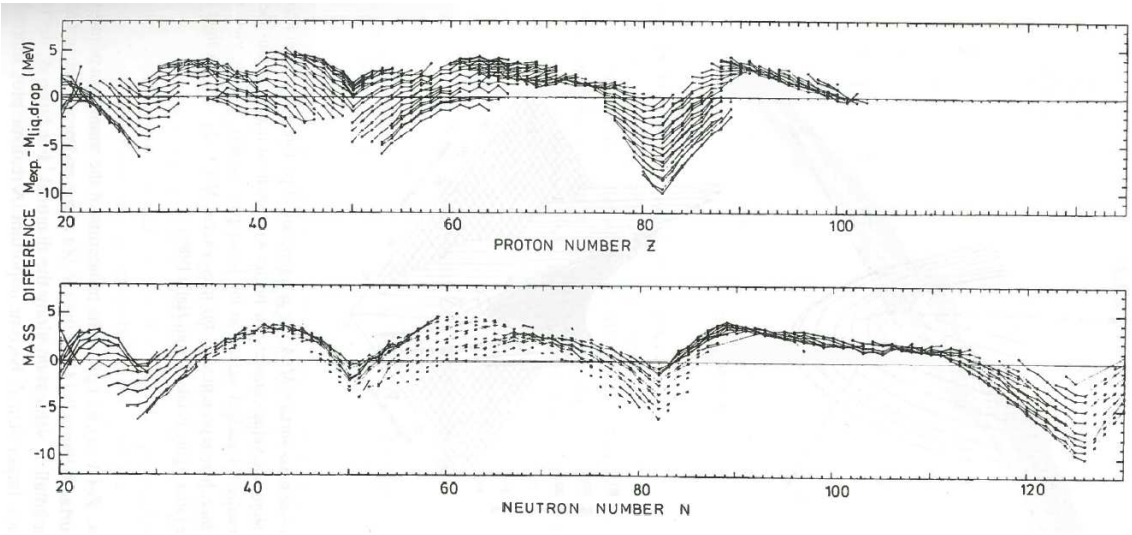

Figure 1.1 – Differences between the mass measurements and the predictions of the Bethe-Weizsäcker formula, as a function of the proton and neutron number. For discrete numbers of nucleons, the differences suddenly increase and translate more stable nuclear configurations. (Figure taken from [Hey04])

and for improving theoretical predictions in areas of the nuclear chart that cannot be accessed experimentally. The primary focus of this thesis is the study of the β decays of the neutron-deficient nuclei ^{22,23}Si and ^{20}Mg that are located at the limits of nuclear stability. For these nuclei, the energy available for β decay is significant and this energy (or Q value) opens new decay channels. The parent can decay to excited states above the particle separation threshold and these β-delayed particle decays are a powerful spectroscopic tool to study the structure of unbound excited states in weakly-bound nuclei. On the proton rich side of the nuclear chart, where the Coulomb force is less repulsive in the β^+ daughters, it is possible that the parent decays to its own isobaric analogue state (IAS). Under the assumption of that the nuclear force is isospin-independent, the IAS in the daughter (situated at high excitation energy) can be described by the exact same nuclear wave functions as the ground state of the parent nucleus. The only difference between these states is the exchanged nucleon. The difference in binding energy between these states is thus only due to the Coulomb force. The Coulomb shifts between all isobaric analogue states are well described by a quadratic function of the total isospin T and the isospin projection T_z, which is known as the Isobaric Mass Multiplet Equation (IMME). Experimental measurements of isobaric analogue states, combined with the IMME, provides a powerful tool to deduce nuclear masses when direct mass measurements are not feasible.

In this chapter, an introduction to the theoretical framework of nuclear β decay and the origins of Fermi theory will be presented. A particular focus will be on Superallowed Fermi β decays between isobaric analogue states. The IMME, which will be used in Chapter 4 to

derive the mass excess of the ($A = 23$, $T = -5/2$) nucleus ^{23}Si will also be described in detail. The different decay modes that can appear on the neutron deficient side of the nuclear chart will be provided in the context of delayed charged particle decays from the IAS in β-decay daughters.

1.1 Nuclear β-decay

Nuclear β-decay is the process by which an unstable nucleus with atomic number Z and neutron number N gains binding energy by transforming into a more stable nucleus with $Z \pm 1$ and $N \mp 1$ while conserving the total mass number $A = Z+N$. The decay is accompanied by the emission of a β particle $e^{\pm}$ and a neutrino ν_e or $\bar{\nu_e}$. The two possible β-decay processes can be expressed as:

$$ {}^{\mathrm{A}}_{\mathrm{Z}}\mathrm{X}_{\mathrm{N}} \xrightarrow{\beta^+} {}^{\mathrm{A}}_{\mathrm{Z-1}}\mathrm{W}_{\mathrm{N+1}} + \mathrm{e}^+ + \nu_{\mathrm{e}}, \tag{1.1} $$

$$ {}^{\mathrm{A}}_{\mathrm{Z}}\mathrm{X}_{\mathrm{N}} \xrightarrow{\beta^-} {}^{\mathrm{A}}_{\mathrm{Z+1}}\mathrm{Y}_{\mathrm{N-1}} + \mathrm{e}^- + \bar{\nu}_{\mathrm{e}} \tag{1.2} $$

In competition with β^+ decay, a third weak-interaction process called *electron capture* (EC) can also occur. In this process, an electron from the internal atomic orbitals is captured by the nucleus and an electron neutrino ν_e is emitted in the transformation of a proton into a neutron. This decay can be written as:

$$ {}^{\mathrm{A}}_{\mathrm{Z}}\mathrm{X}_{\mathrm{N}} + \mathrm{e}^- \xrightarrow{\text{EC decay}} {}^{\mathrm{A}}_{\mathrm{Z-1}}\mathrm{W}_{\mathrm{N+1}} + \nu_{\mathrm{e}} \tag{1.3} $$

All of the above decays release the excess rest mass energy in the unstable parent nucleus by transforming it into the more stable daughter nucleus. The energy difference between the parent and the daughter nuclei is defined as the Q-value of the decay. The Q-value, if positive, implies that the parent is less stable than the daughter and the nucleus can spontaneously decay. On the contrary, a negative Q value means that the parent is more stable than the daughter and spontaneous decay cannot occur. The Q-values of the different β decay processes described above are given by:

$$ Q_{\beta^-} = M({}^{\mathrm{A}}_{\mathrm{Z}}\mathrm{X}_{\mathrm{N}})c^2 - M({}^{\mathrm{A}}_{Z+1}Y_{N-1})c^2\,, \tag{1.4} $$

$$ Q_{\beta^+} = M({}^{\mathrm{A}}_{\mathrm{Z}}\mathrm{X}_{\mathrm{N}})c^2 - M({}^{\mathrm{A}}_{Z-1}W_{N+1})c^2 - 2m_ec^2\,, \tag{1.5} $$

where $M(X)$ is the atomic mass of the nucleus X, and m_ec^2 is the mass of the electron.

The Q-value for electron capture is defined as:

$$Q_{EC} = M(^{\mathrm{A}}_{\mathrm{Z}}\mathrm{X_N})\mathrm{c}^2 - M(^{\mathrm{A}}_{\mathrm{Z-1}}\mathrm{W_{N+1}})\mathrm{c}^2. \tag{1.6}$$

The difference between the Q values for EC and β^+ decays, $Q_{EC} - Q_{\beta^+} \approx 2m_e c^2$, implies that for nuclei in which β^+ decay is energetically possible can also decay by EC. The reverse is not necessarily possible as there are situations in which the Q_{EC} value is positive while the Q_{β^+} value is negative. In these cases, electron capture is the only possible decay mode. The ratio of EC in comparison with the β^+ process can be determined through the observation of the Auger electrons ad X-rays emitted by the electrons from the outter shells.

1.1.1 Fermi Theory of β Decay

In 1934, Enrico Fermi developed a successful theory of nuclear β decay that was based on an analogy with electromagnetic radiation theory. The transition rate of the β-decay process can be derived using Fermi's Golden Rule:

$$\lambda_{fi} = \frac{2\pi}{\hbar}|M_{fi}|^2 \frac{dn}{dE_f}, \tag{1.7}$$

where $|M_{fi}|$ is the matrix element of the interaction Hamiltonian $|\langle\Psi_f|H_{int}|\Psi_i\rangle|$ that connects the initial state Ψ_i (the nuclear wave function of the parent Ψ_P) and the final state Ψ_f (the daughter Ψ_D, the emitted β particle Ψ_e and the neutrino Ψ_ν). The matrix element can be expressed as an integral over all nucleons as well as the β particle and neutrino coordinates:

$$M_{fi} = \int \Psi_D^* \Psi_e^* \Psi_\nu^* \hat{H}_{int} \Psi_P \, \mathrm{d}^3\vec{r} \tag{1.8}$$

In his theory, Fermi treated the weak interaction as a point interaction that leads to the following expression for the Hamiltonian:

$$\hat{H}_{int} = g\delta(\vec{r}_n - \vec{r}_p)\delta(\vec{r}_n - \vec{r}_e)\delta(\vec{r}_n - \vec{r}_\nu)\hat{O}(n \leftrightarrow p), \tag{1.9}$$

where $\hat{O}(n \leftrightarrow p)$ is the operator that converts a neutron into a proton (or vice versa) and g is the interaction strength. In contrast to electromagnetic decay where a photon is exchanged between charged particles and is infinite range ($m_\gamma = 0$), nuclear β decay appears to be short range. To explain the short-range nature of nuclear β decay, it was hypothesized that a massive particle (the intermediate $W^\pm$ boson) must be exchanged. In 1983, this particle was discovered at CERN with a mass of 83 ± 5 GeV, which confirmed the short-range nature of nuclear β decay ($\approx 10^{-16}$ m or 0.1 fm).

In order to derive the matrix element $|M_{fi}|$, it is assumed that the neutrino wave function can be approximated by a plane wave normalized in a volume V:

$$\Psi_\nu = \frac{1}{\sqrt{V}} e^{-i\vec{p}_\nu.\vec{r}/\hbar} \tag{1.10}$$

For the electron, one has to take into account the Coulomb distortion caused by the interaction between the emitted charged β particle and the positively charged nucleus. This Coulomb distortion is described by the Fermi function [Fer34], and can be approximated as:

$$F(Z, p_e) = \frac{2\pi\eta}{1 - e^{-2\pi\eta}} \quad \text{with } \eta = \pm\frac{Ze^2}{4\pi\varepsilon_0\hbar v_e}, \tag{1.11}$$

where the positive (negative) sign describes the β^- (β^+) processes, and v_e is the velocity of the β particle. Assuming, as above for the neutrino, that the β particles wave function can be approximated by plane waves and including the Fermi function for the Coulomb distortion yields:

$$\Psi_e = \frac{1}{\sqrt{V}} |F(Z, p_e)|^{\frac{1}{2}} e^{-i\vec{p}_\nu.\vec{r}/\hbar}. \tag{1.12}$$

Note that for small values of η, which implies small Z and large v_e (and large Q-value), this function is close to unity.

The daughter and the parent nuclear wave functions can be approximated by single-particle wave functions, in such a way that the wave functions of the $A-1$ nucleons not involved in the β decay cancel each other yielding:

$$M_{fi} = g \int \psi_D^*(\vec{r}) \Psi_e^*(\vec{r}) \Psi_\nu^*(\vec{r}) \hat{O}(n \leftrightarrow p) \psi_P(\vec{r}) \, \mathrm{d}^3\vec{r}, \tag{1.13}$$

where ψ_D and ψ_P represents the wave functions of the proton (neutron) in the parent and the neutron (proton) in the daughter that are involved in the decay process. To simplify the notation, the modified matrix element M'_{fi} will be used which removes all of the Coulomb effects and the volume normalization from the transition matrix element:

$$|M_{fi}|^2 = g^2 \frac{F(Z, p_e)}{V^2} |M'_{fi}|^2. \tag{1.14}$$

Substituting Eqns 1.9, 1.10 and 1.12 into Eqn. 1.8 yields:

$$M'_{fi} = g \int \psi_D^*(\vec{r}) e^{i(\vec{p}_\nu + \vec{p}_e).\vec{r}/\hbar} \hat{O}(n \leftrightarrow p) \psi_P(\vec{r}) \, \mathrm{d}^3\vec{r} \tag{1.15}$$

For a β particle with momentum $p \sim 1$ MeV/c, the quantity $\vec{p}/\hbar$ in the electron wave function is only ~ 0.005 fm^{-1}. With the approximation that the electron wave and neutrino wave length

is small compared to the typical nuclear radius, $\vec{p}/\hbar \ << \ \vec{r}$, the above expression can be simplified further using a Taylor expansion:

$$M'_{fi} = \Bigg[\int \psi^*_D(\vec{r}) \hat{O}(n \leftrightarrow p) \psi_P(\vec{r}) \, \mathrm{d}^3\vec{r} + \, i \frac{(\vec{p}_\nu + \vec{p}_e)}{\hbar} \int \psi^*_D(\vec{r}) \vec{r} \hat{O}(n \leftrightarrow p) \psi_P(\vec{r}) \, \mathrm{d}^3\vec{r} + \cdots \Bigg]. \quad (1.16)$$

The first term of this expansion (zeroth order, $L = 0$) is the transformation of a proton into a neutron (or vice versa), and the integral is equal to the overlap between the parent and daughter nuclear wave functions. The parity operator $\hat{P}(\vec{r} \rightarrow \vec{r})$ applied to this term gives a non-zero result only if the parity of the daughter and parent wave functions are identical. The second term (L =1) is negative under the parity operator due to the presence of the factor $\vec{r}$ in the integral. This operation creates the first *selection rule* for nuclear β decay: the eigenvalues from the even L terms are positive with respect to the parity operator, whereas the odd L terms are negative.

Returning to Eqn. 1.15, the term $e^{i(\vec{p}_\nu + \vec{p}_e).\vec{r}/\hbar}$ can be expressed as the decomposition of a plane wave into two spherical harmonics

$$e^{i(\vec{p}_\nu + \vec{p}_e).\vec{r}/\hbar} = \sum_{L,M} (4\pi) i^L j_L(kr) Y_L^M(\hat{k}) Y_L^{*M}(\hat{r}), \quad (1.17)$$

where $\vec{k} = (\vec{p}_\nu + \vec{p}_e)/\hbar$, $j_L(x)$ are the spherical Bessel functions, and $\hat{k}$ and $\hat{r}$ stand for the angular coordinates. This leads to the expression of the matrix element:

$$M'_{fi} = g \sum_{L,M} 4\pi \, i^L Y_L^M(\hat{k}) \int \psi^*{}_D(\vec{r}) j_L(kr) Y_L^{*M}(\hat{r}) \hat{O}(n \leftrightarrow p) \psi_P(\vec{r}) \, \mathrm{d}^3\vec{r}. \quad (1.18)$$

In the case of protons and neutrons treated as single particles in the parent and daughter nuclei, the wave functions can be further separated into their radial and angular components:

$$M'_{fi} = g \, 4\pi \, i^{L_\beta} \sum_{M=-L_\beta}^{+L_\beta} Y_{L_\beta}^M(\hat{k}) \int Y_{L_D}^{*M_D}(\theta, \phi) Y_{L_\beta}^{*M}(\theta, \phi) Y_{L_P}^{*M_P}(\theta, \phi) \, \mathrm{d}\Omega \quad (1.19)$$

$$\times \int R^*_D(r) j_{L_\beta}(kr) \hat{O}(n \leftrightarrow p) R_P(r) r^2 \, \mathrm{d}\vec{r}, \quad (1.20)$$

where $L_\beta = L_e + L_\nu$. Applying the Wigner-Eckart theorem to the first term results in a second selection rule as the integral over the angular term is non-zero only if the following condition is satisfied:

$$\vec{L}_P = \vec{L}_D + \vec{L}_\beta. \quad (1.21)$$

This is the angular momentum selection rule for nuclear β decay. Substituting the spherical harmonics expression of Eqn. 1.17 into Eqn. 1.16, we can explicitly write the parity selection rule as:

$$\pi_P = (-1)^{L_\beta} \pi_D. \tag{1.22}$$

The angular momentum and parity selection rules play a crucial role in classifying nuclear β decays.

1.1.2 Classification and selection rules

Because of the presence of the spherical Bessel functions, the relative importance of the L-terms in the Taylor expansion of the transition matrix element (Eqn. 1.16) decreases rapidly. In other words, only the lowest L terms will significantly contribute to the decay probability. This leads to the well-known classification of nuclear β-decay, in terms of angular momentum L:

$$\begin{aligned} L_\beta &= 0 \quad \text{“allowed” decays} \\ L_\beta &= 1 \quad \text{“first forbidden” decays} \\ L_\beta &= 2 \quad \text{“second forbidden” decays} \\ &\vdots \end{aligned} \tag{1.23}$$

It should be emphasized that the $L > 1$ “forbidden” decays are not strictly speaking forbidden. These decays occur in nature but they are highly suppressed compared to the allowed decays. There is approximately 3 orders of magnitude suppression in the decay rate for every additional L value.

The neutrino, the β particle and the nucleons involved in the decay are all fermions (spin 1/2 particles) and this intrinsic spin must also be included in the Hamiltonian. The β-particle and the neutrino spins can couple to either S_β =0 or S_β =1. This leads to the addition of a new term in the transition matrix element:

$$\int \sum {\Psi_D}^* \hat{\sigma} \Psi_P \Psi_\beta^* \hat{\sigma} \Psi_\nu \, \mathrm{d}^3\vec{r} \tag{1.24}$$

where Ψ are the wave functions of the particles, including the spin and the orbital angular momentum terms, and $\hat{\sigma}$ are the Pauli matrices. There are thus two classifications of nuclear β decays with respect to the spin angular momentum carried by the β-particle and the neutrino:

$$\begin{aligned} S_\beta = 0 \quad & \left[\hat{O}(n \leftrightarrow p)\right] \quad \text{Fermi } \beta \text{ decay} \\ S_\beta = 1 \quad & \left[\hat{\sigma}\hat{O}(n \leftrightarrow p)\right] \quad \text{Gamow} - \text{Teller } \beta \text{ decay} \end{aligned} \tag{1.25}$$

The β decay selection rules can thus be written as:

$$\vec{J}_P = \vec{J}_D + \vec{J}_\beta \quad \text{with } \vec{J}_\beta = \vec{L}_\beta + \vec{S}_\beta \tag{1.26}$$

$$\pi_P = (-1)^{L_\beta}\pi_D. \tag{1.27}$$

Allowed Fermi decays ($L_\beta = 0$, $S_\beta = 0$) occur between states with the same spin and parity, i.e $\Delta J = 0$ and $\pi_D = \pi_P$. For the case of allowed Gamow-Teller transitions ($L_\beta = 0$, $S_\beta = 1$), one can have $\Delta J = -1, 0, +1$ and the same parity $\pi_D = \pi_P$. Another special class of decays are the $0^\pm \rightarrow 0^\pm$ decays which are pure Fermi decay since a Gamow-Teller component would be strictly forbidden according to the angular momentum selection rule ($\vec{0} \neq \vec{0} + \vec{1}$).

The strength of the Fermi and the Gamow-Teller contributions in the transition matrix element differ. The transition matrix element for the general case in which both components contribute can be written as:

$$g|M'_{fi}|^2 = g_F^2|M'_{fi}(F)|^2 + g_{GT}^2|M'_{fi}(GT)|^2 \tag{1.28}$$

where g_F and g_{GT} are the vector (Fermi) and the axial-vector (Gamow-Teller) strengths, respectively. In the case of pure Fermi transitions $0^\pm \rightarrow 0^\pm$, the Gamow-Teller component is zero and the total matrix element can be simplified to $g|M'_{fi}|^2 = g_F^2|M'_{fi}(F)|^2$.

1.1.3 The ft value

Computing the transition rate of Eqn. 1.7 requires the density of the final states, $\frac{\mathrm{d}n}{\mathrm{d}E_f}$. The number of final states n for a particle of a momentum p in 3 dimensions is given by:

$$n = \frac{1}{(2\pi\hbar)^3}\int \mathrm{d}^3x \int \mathrm{d}^3p \tag{1.29}$$

$$= \frac{V}{(2\pi\hbar)^3}\int \mathrm{d}^3p, \tag{1.30}$$

where V is the arbitrary volume in which the particles wave function has been normalized, while the second integral is performed over a sphere in momentum space with a volume $\frac{4\pi}{3}p^3$. The differential form of the density of final states can then be expressed as:

$$\frac{\mathrm{d}n}{\mathrm{d}E_f} = \frac{V}{(2\pi\hbar)^3}4\pi p^2\frac{\mathrm{d}p}{\mathrm{d}E}. \tag{1.31}$$

Using relativistic energy conservation, $E^2 = p^2c^2 + m^2c^4$, the density of final states can be simplified further:

$$\frac{\mathrm{d}n}{\mathrm{d}E_f} = \frac{V}{2\pi^2\hbar^3c^2}pE \tag{1.32}$$

$$= \frac{1}{2\pi^2}\frac{V}{(\hbar c)^3}E\sqrt{E^2 - m^2c^4}. \tag{1.33}$$

In the decay process, the β particle, the neutrino and the recoil of the daughter nucleus contains the full kinematics. Energy and momentum conservation for this three-body process implies that:

$$\vec{p}_e + \vec{p}_{\nu_e} + \vec{p}_{\mathrm{recoil}} = 0 \tag{1.34}$$

$$E_e + E_{\nu_e} + E_{\mathrm{recoil}} = E. \tag{1.35}$$

With these conservation rules, the recoil ions energy and momentum can then be expressed in terms of the electron and neutrinos energy and momenta. The resulting density of states integrated over the angles $\mathrm{d}\Omega_e$ and $\mathrm{d}\Omega_\nu$ is thus:

$$\frac{\mathrm{d}n}{\mathrm{d}E_f} = \frac{V^2}{(2\pi\hbar)^6}\frac{\mathrm{d}}{\mathrm{d}E}\int p_e^2\mathrm{d}p_e\mathrm{d}\Omega_e p_\nu^2\mathrm{d}p_\nu\mathrm{d}\Omega_\nu. \tag{1.36}$$

Evaluating the density of states for a β particle with an energy between E_e and $E_e + \mathrm{d}E_e$ and ignoring the nuclear recoil energy yields:

$$\left.\frac{\mathrm{d}n}{\mathrm{d}E_f}\right|_{(E_e,p_e)} = \frac{V^2}{(2\pi\hbar)^6}\mathrm{d}p_e\, p_\nu^2\frac{\mathrm{d}p_\nu}{\mathrm{d}E}\int \mathrm{d}\Omega_e\mathrm{d}\Omega_\nu \tag{1.37}$$

$$= \frac{V^2}{4\pi\hbar^6c^3}p_e^2\,(E - E_e)^2\left[1 - \frac{m_\nu^2c^4}{(E - E_e)^2}\right]^{1/2}\mathrm{d}p_e. \tag{1.38}$$

From this equation, a continuous β energy spectrum is obtained between $E_e = 0$ and the maximum energy that is available for the decay (the Q-value). Assuming the neutrino mass is negligible, $m_\nu \approx 0$, substitution of Eqns. 1.28 and 1.38 into Eqn. 1.7 yields the decay rate:

$$\lambda_{fi} = \frac{g^2}{2\pi^3\hbar^7c^3}|M'_{fi}|^2\int_0^{p_emax} F(Z,p_e)p_e^2(E - E_e)^2\mathrm{d}p_e. \tag{1.39}$$

It is customary to convert the energy and momentum into dimensionless unites using $\rho = \frac{p_e}{m_ec}$ and $W = \frac{E_e}{m_ec^2} = \frac{T_e}{m_ec^2} + 1$. The relativistic energy-momentum relation thus becomes $W^2 = \rho^2 + 1$. The decay constant can then be expressed as,

$$\lambda_{fi} = \frac{m_e^5c^4g^2}{2\pi^3\hbar^7}|M'_{fi}|^2\int_1^{W_0} F(Z,W)W\sqrt{W^2 - 1}(W_0 - W)^2\mathrm{d}W, \tag{1.40}$$

where $W_0 = \frac{E_e^{max}}{m_e c^2} \approx \frac{Q_\beta}{m_e c^2} + 1$. The integral in Eqn. 1.40 is referred to as the statistical rate function f:

$$f = \int_1^{W_0} F(Z,W) W \sqrt{W^2 - 1} (W_0 - W)^2 \mathrm{d}W. \tag{1.41}$$

The decay constant is then:

$$\lambda_{fi} = g^2 \frac{m_e^5 c^4}{2\pi^3 \hbar^7} |M'_{fi}|^2 \, f \tag{1.42}$$

The decay constant can also be expressed as a function of the partial half-life for the decay to the final state of interest that is defined as $t = \frac{\ln 2}{\lambda_{fi}} = \frac{T_{1/2}}{BR}(1 + P_{EC})$, where BR is the branching ratio to the final state, and P_{EC} represents the fraction of electron capture decays compared to positron decays (for β^- decay, $P_{EC} = 0$). Combining these expressions, one can express the ft value for nuclear β decay as:

$$ft = \frac{1}{g^2 |M'_{fi}|^2} \frac{2\pi^3 \hbar^7 \ln 2}{m_e^5 c^4} \tag{1.43}$$

The ft value for a nuclear β decay is a quantity that can be measured experimentally. The partial half-life t is obtained by measuring the decay half-life and the branching ratio to the particular daughter state interest. The phase space integral f is a function of the charge of the daughter nucleus and the Q-value of the β decay. Thus, if one can measure the Q-value of the β decay between the parent and daughter states, the f value can be calculated using Eqn. 1.41.

1.1.4 Superallowed Fermi β Decays

In 1932, Heinsenberg proposed to treat the neutron and the proton as the same particle (the "nucleon") with a new quantum number t, called *isospin* [Hei32], and with projection numbers $t_z = -\frac{1}{2}$ for the proton, and $t_z = +\frac{1}{2}$ for the neutron. This is analogous to the intrinsic spin s of the nucleons. This concept can be extended to the entire nucleus, giving the total nuclear isospin $T_Z = \frac{(N-Z)}{2}$ where N is the number of neutrons and Z the number of protons.

Isospin is a relatively good quantum number since it is conserved by the strong interaction. In analogy with the algebra for the spin angular momentum, the total isospin of the nucleus can be any integer between $|T_Z|$ and $(N + Z)/2$. For most nuclei, the ground state has the lowest possible isospin $T = \frac{(N-Z)}{2}$. Continuing with the analogy to spin, for every isospin T there exists a multiplet of states with a total of $2T+1$ members. For $T = 1$ states, for example, there exists a triplet of states with $T_Z = (-1, 0, +1)$.

Nuclear β decay, which describes the transformation of a proton into a neutron (or a neutron into a proton), can thus be considered as a simple isospin raising or lowering "ladder operator".

The ladder operation connecting nuclei in the same isospin multiplet with the same T, but with different projections T_Z, can be written as:

$$\hat{T}^{\pm}|T, T_Z\rangle = \sqrt{(T \mp T_Z)(T \pm T_Z + 1)}|T, T_Z \pm 1\rangle. \tag{1.44}$$

Thus, the Fermi β decay operator is simply the isospin operator $T^{\pm}$ whereas the Gamow-Teller operator is $\sigma T^{\pm}$. This implies that the selection rules for isospin in nuclear β decay are linked to those for spin and angular momentum. Fermi decays are forbidden unless the isospin of the daughter is the same as that of the parent (ΔT = 0), while Gamow-Teller decays can occur for ΔT = 0,$\pm$1.

The term "superallowed" Fermi β decays refers to a specific class of decays that are allowed ($L_\beta = 0$), pure Fermi ($S_\beta = 0$) and are transitions between isobaric analogue states (ΔT = 0) of the same isospin multiplet. In this very special case, and assuming that isospin is an exact symmetry of the nuclear Hamiltonian, the wave functions of the parent and daughter states are identical. Using this assumption, the transition matrix element for nuclear β decay $|M'_{fi}|$ can be calculated exactly using the isospin ladder operator:

$$|M'_{fi}|^2 = (T \mp T_Z)(T \pm T_Z + 1). \tag{1.45}$$

The coupling strength for superallowed Fermi decays, as defined in Eqn. 1.28, is uniquely made of the Fermi (vector) component ($g = g_F$). In the late 1950s, it was assumed (in analogy to electromagnetism) that the vector part of the weak interaction was a fundamental constant that is conserved in the nuclear field. This Conserved-Current-Vector (CVC) hypothesis is one of the pillars of the Standard Model and has been tested through very precise measurements of the ft values for several superallowed Fermi β decays. These tests require several small theoretical terms to be applied to the experimental ft values to correct for radiative effects (the interaction of the β particle in the presence of the Coulomb field of the daughter nucleus) and isospin symmetry breaking (isospin symmetry is broken by Coulomb and nuclear-structure dependent effects). The corrected ft values, written as the $\mathcal{F}t$ values, have been determined very precisely for fourteen $T = 1$ decays between ^{10}C and ^{74}Rb. As shown in Fig. 1.2, the $\mathcal{F}t$ values are clearly nucleus independent and this constancy confirms the CVC hypothesis at the level of 10^{-4}[Har15]. With CVC verified, the average $\mathcal{F}t$ value obtained from these 14 cases is $\overline{\mathcal{F}t} = 3072.7 \pm 0.72$ s [Har15].

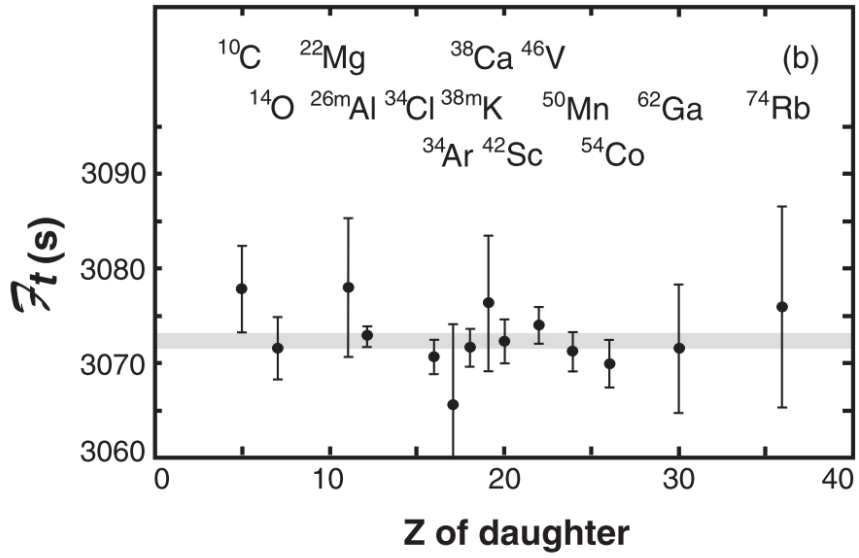

Figure 1.2 – Fourteen most precisely determined superallowed Fermi β decay $\mathcal{F}t$ values. Their constancy confirms the CVC hypothesis and yields an average value of $\overline{\mathcal{F}t} = 3072.7 \pm 0.72$ s. (Figure taken from [Har15])

1.2 β-delayed charged particle decays

At the beginning of the 1960s, Goldansky proposed several possible decay modes that can only occur very close the proton drip line including β-delayed proton and multi-proton emission as well as two-proton radioactivity [Gol60]. The first observation of these decays was at Dubna in 1962 [Kar63] but this was only after the identification of the first β-delayed proton precursor ^{25}Si [Bar1963] one year later. The interest in studying these β-delayed charged particle decays increased and today there are now more than 150 β-delayed α and β-delayed proton emitters, called precursors, that have been discovered across the nuclear chart [Har76, Lor12].

The appearance of these decays at the proton drip line can be understood through the isobaric mass differences and the increase of the decay Q-value as one moves further from the valley of stability. In addition, the binding energy of the last nucleon, which is referred to as the "separation energy", decreases towards the drip line and allows the β decay to feed particle-unbound resonances in the daughter nucleus. This opens the different decay channels, as shown schematically in Figure 1.3. The Q-value of these β-delayed charged particle decays are defined in a similar way as in Equation 1.5:

$$Q_{\beta p} = M(^{\mathrm{A}}_{\mathrm{Z}}\mathrm{X}_{\mathrm{N}})c^2 - M(^{\mathrm{A-1}}_{\mathrm{Z-2}}\mathrm{Q}_{\mathrm{N+1}})c^2 - m_p - 2m_e c^2\,, \tag{1.46}$$

$$Q_{\beta\alpha} = M(^{\mathrm{A}}_{\mathrm{Z}}\mathrm{X}_{\mathrm{N}})c^2 - M(^{\mathrm{A-4}}_{\mathrm{Z-3}}\mathrm{R}_{\mathrm{N-1}})c^2 - m_\alpha - 2m_e c^2, \tag{1.47}$$

where m_p and m_α are the masses of the proton and the α particle, respectively.

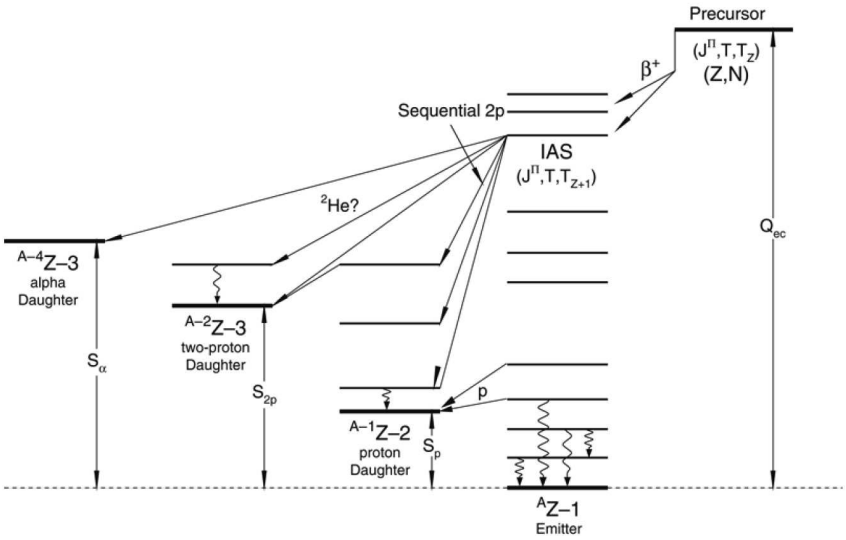

Figure 1.3 – Schematic decay scheme of the different decay channels (β, βp, β2p, and $\beta\alpha$) that can occur near the proton drip line. (Figure taken from [Bla08]).

In the case of β-delayed proton emission, referred to simply as βp decay, the precursor ${}^{A}Z$ decays from its ground state to excited levels in the emitter ${}^{A}Z-1$ which are above the proton separation threshold S_p. The state can decay by proton emission and the decay $Q_{\beta p}$-value is related to β-decay Q value according to:

$$Q_{\beta p} = Q_{\beta} - S_p(A, Z). \tag{1.48}$$

The proton separation energy can be calculated from the binding energies of the parent and daughter nuclei:

$$S_p(A, Z) = B(A-1, Z-1) - B(A, Z) \tag{1.49}$$

$$= M(A-1, Z-1) + m_p - M(A, Z). \tag{1.50}$$

As shown in Figure 1.3, the decay of the parent can also populate states in the daughter that are below the proton-separation energy. When this occurs, these states will decay by γ-ray emission. The β-delayed decay channels thus depend on the relative position of the particle separation threshold with respect to the Q_{β}-value.

In even more exotic nuclei, states in the β-decay daughter may be populated that are above the two-proton separation energy (S_{2p}). These states could then decay by the emission of two protons to states in the ${}^{A-2}Z-3$ daughter. This decay could proceed either by the direct emission of two simultaneous protons or via a sequential decay that passes through an intermediate unbound state in the ${}^{A-1}Z-2$ daughter.

Because the proton is a charged particle, proton emission can only occur when there is sufficient energy to penetrate the centrifugal barrier. The probability of emission depends primarily on this energy and on the angular momentum it carries. The intensities of the βp and β2p transitions are defined as the product of the branching ratios of the proton transition and of the β-decay transition from the ground state of the precursor to the particle-unbound levels. Because of the Coulomb shift between the precursor and the emitter, the most energetic level to be populated in the emitter is usually the isobaric analogue state (IAS) of the precursor.

1.2.1 The Isobaric Mass Multiplet Equation

The IAS energy is linked to the mass excess of the ground state of the precursor through the Isobaric Mass Multiplet Equation. This relation was first investigated and proposed by E.P. Wigner in 1957 [Wig57] to describe the mass excess for a set of the IAS in the same isobaric multiplet (A,T_Z). This relation is a function of T_Z (or Z) and the splitting of the mass excess between each member of the multiplet is due only to the Coulomb interaction, which lowers the energy of the IAS of the lower-Z isobars in the multiplet.

The eigenstates $|\alpha, T, T_Z\rangle$ of the charge-independent Hamiltonian H_{ind} that conserves isospin T, will be completely degenerate for the IAS characterized by the same value of T_Z. The addition of a charge-violating Coulomb interaction lifts this degeneracy and the result can be described as a perturbation to the nuclear force. The total binding energy is given by:

$$B(\alpha, T, T_Z) = \langle \alpha, T, T_Z | (H_{ind} + H_{Coulomb}) | \alpha, T, T_Z \rangle. \tag{1.51}$$

Considering only two-body forces, the eigenvalues of the Coulomb perturbation are defined by:

$$\Delta B(\alpha, T, T_Z) = \langle \alpha, T, T_Z | \sum_{i=0}^{2} H^{(k)}_{Coulomb} | \alpha, T, T_Z \rangle. \tag{1.52}$$

Applying the Wigner-Eckart theorem, the T_Z dependence of the energy splitting for the multiplet can be extracted:

$$\Delta B(\alpha, T, T_Z) = \sum_{i=0}^{2} (-)^{T-T_Z} \begin{pmatrix} T & k & T \\ -T_Z & 0 & T_Z \end{pmatrix} \langle \alpha, T || H^{(k)}_{Coulomb} || \alpha, T \rangle. \tag{1.53}$$

The 3-j coefficients have a simple analytical form for the three values of k, and the binding energy can be expressed as:

$$\Delta B(\alpha, T, T_Z) = \frac{1}{\sqrt{2T+1}} \left[M^{(0)} + \frac{T_Z}{\sqrt{T(T+1)}} M^{(1)} + \frac{3T_Z^2 - T(T+1)}{\sqrt{T(T+1)(2T+3)(2T-1)}} M^{(2)} \right], \tag{1.54}$$

where $M^{(k)}$ are the three sets of reduced matrix elements $\langle \alpha, T||H^{(k)}_{Coulomb}||\alpha, T\rangle$, which depend on T and α. This result can be rewritten to highlight the familiar quadratic form of the IMME:

$$\Delta B(\alpha, T, T_Z) = a + bT_Z + cT_Z^2 \tag{1.55}$$

This splitting can be observed in the case of two mirror nuclei that have the same isospin T but with opposite isospin projections T_Z. It is also useful to compare three nuclei from the same multiplet to highlight the quadratic form of the IMME.

The isospin triplet ^{14}O ($T_Z = -1$), ^{14}N ($T_Z = 0$), and ^{14}C ($T_Z = 1$) is presented in Figure 1.4. The set of states with the same T and the same configuration J^π in this triplet (for example, the triplet of 0^+ states at 0.156 MeV, 2.31 MeV, and 5.15 MeV in Fig. 1.4) is a good example of the evolution of the IAS excitation energy with isospin. The binding energy is lowest in ^{14}C (the member with the lowest Z) due to the influence of the Coulomb interaction. Because ^{14}N is $T = 0$, while ^{14}C and ^{14}O have $T = 1$, ^{14}N has several additional states that are part of the singlet ($A = 14$, $T = 0$).

Systematic studies across several masses and isospin multiplets have been performed by MacCormick *et al.* [Mac14] to deduce the values of the quadratic coefficients a, b and c for the IMME. The b coefficient is due to the first order of the Coulomb energy and based on the assumption that the nucleus is a homogeneously charged sphere, one expects b to be proportional to $(A-1)/A^{1/3}$. The function, fitted on the average of the current measurements of the IMME for multiplet from $T = 1/2$ to $T = 3$ gives:

$$b = \Delta_{nH} - S_b \times (A-1)/A^{1/3} + C_b \ \text{ in MeV}, \tag{1.56}$$

where Δ_{nH} is the neutron-proton mass difference, and S_b and C_b are coefficients obtained by the fit and are a function of the multiplet. In a similar way, the c coefficient can defined by:

$$c \simeq 3 \times (260 \times S_c/A^{1/3} + C_c) \ \text{ in MeV} \tag{1.57}$$

where S_c and C_c are the fitting coefficients. With these considerations, an approximate estimation of the ratio $|b/c|$ can be made:

$$|b/c| = 0.96 \times (A-1) - 2.8 \tag{1.58}$$

The improvement in the precision of experimentally determined IAS energies in several multiplets have indicated that there are some small contributions that require the inclusion of a cubic term into the IMME. Up to now, five non-zero d coefficients have been deduced but additional experimental investigations are needed to assess the importance and significance of the cubic term in the IMME mass prediction formula.

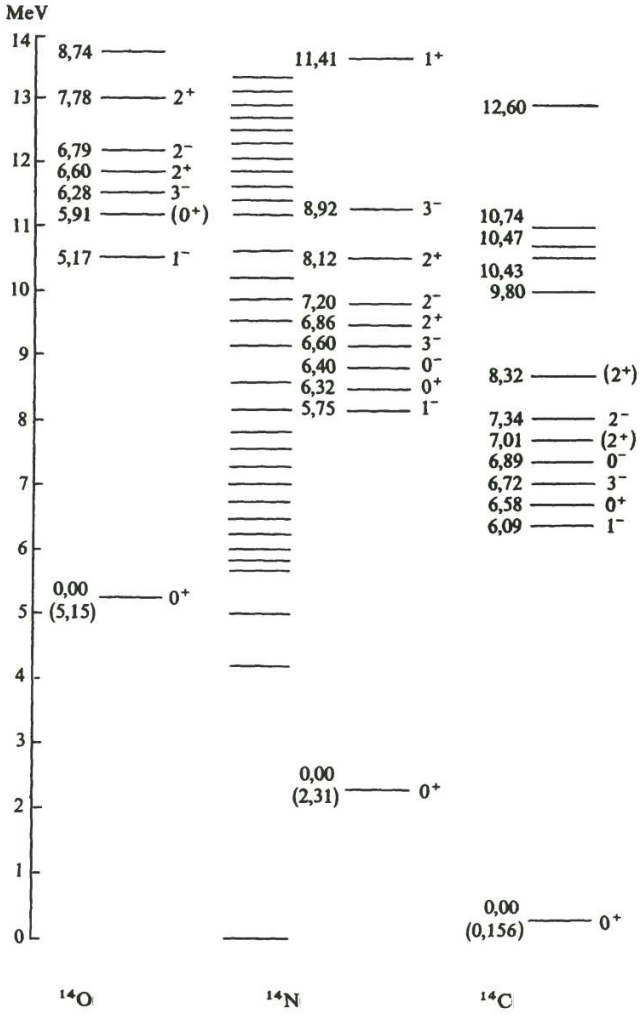

Figure 1.4 – Level schemes of ^{14}O ($T_Z = -1$), ^{14}N ($T_Z = 0$), and ^{14}C ($T_Z = 1$). Based on the charge-independence of the nuclear force, the three level schemes would be identical with the exception of the Coulomb interaction. The energies are normalized to the ground state mass of ^{14}N. Several additional states present only in ^{14}N are those belonging to the ($A = 14$, $T = 0$) singlet and are not labelled in this figure. (Figure taken from [Val09]).

1.2.2 β-delayed multiple charged particle decays

β-delayed emission of two protons (β2p decay) was first discovered in the $T_Z = -2$ nucleus ^{22}Al by Cable *et al.* in 1984 [Cab84]. The βp decay of this proton-rich Al isotope was already established as were several proton-unbound levels in the β-decay daughter ^{22}Mg. The results by Cable *et al.* included a measurement of the energies of the individual proton groups. These energies were identified as one-proton transitions to and from unbound levels in the daughter

^{21}Na, while the sum corresponded to the energy expected for a two-proton decay from the IAS to both the ground state and the first excited state in ^{20}Ne. Figure 1.5 shows the energy-sum and the individual proton spectra. The order of the individual proton transitions was deduced from the Doppler-shift induced by the kinetic energy of the recoil ion after the first proton emission. This was the first identification of a β-delayed sequential two-proton emission from an IAS. As explained above, one of the main interest in the β2p is to be able to determine if the decay proceeds by a sequential emission of single protons or a direct and simultaneous emission of two protons. New experimental techniques have since been developed to identify the decay sequence that will be described in detail below.

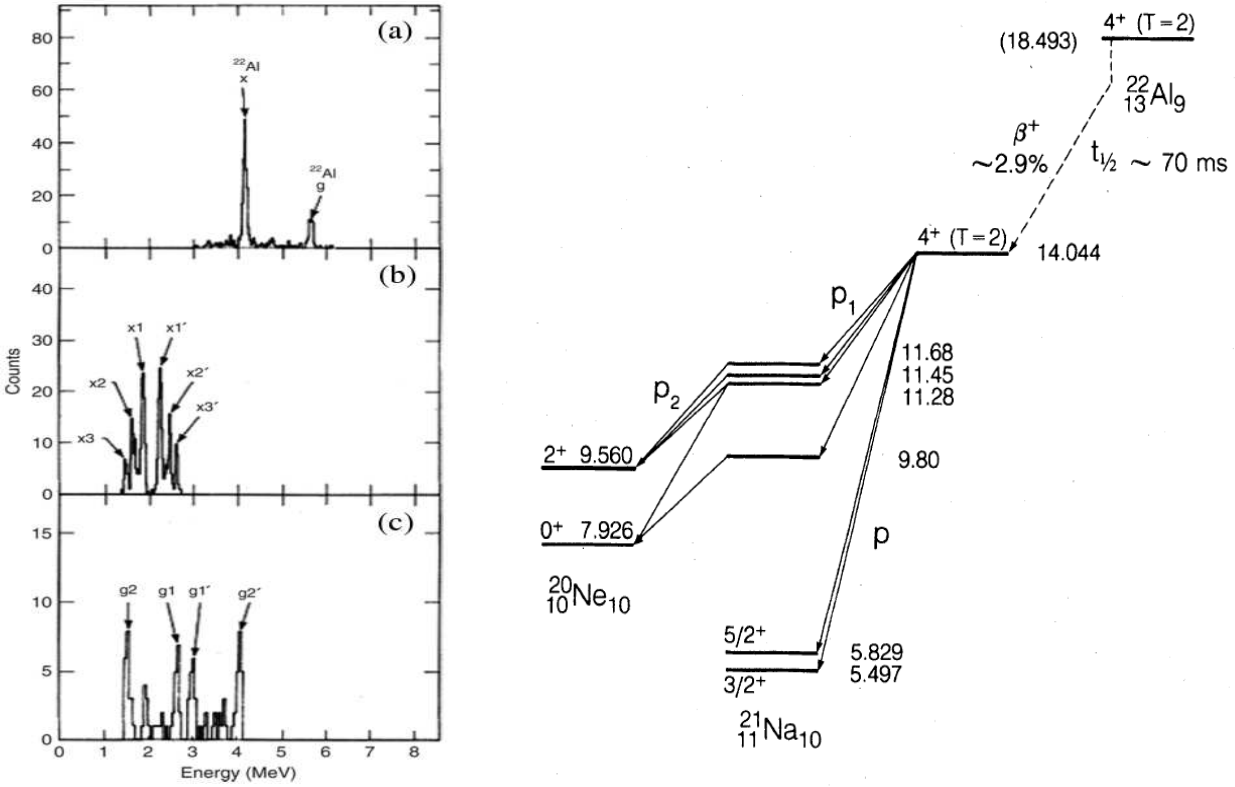

Figure 1.5 – (a) The total charged-particle energy detected in ΔE-E telescopes were measured and matches the expected values for a decay from the IAS in ^{22}Mg to the ground state and the first excited state in ^{20}Ne. The individual proton energies (x_i, $g\prime_i$) and (g_i, $g\prime_i$)were mesured and allowed to determine the order of the one-proton decay paths to the excited state (b) and the ground state (c).

In Figure 1.6, predictions for many different β-delayed decay modes which have been, or could be, observed are presented. Most of β-delayed one-proton emitters with $A < 60$ have been observed (filled symbols in Fig. 1.6) and their decay Q-values and partial half-lives have

been measured. Based on the estimated Q-value of these decays, the lightest β2p and β3p candidates are ^{22}Si and ^{23}Si, respectively.

As shown in Fig. 1.6, the β-delayed three-proton emitters are extremely rare and are even more difficult to observe because of the competition with other decay channels that involve less protons. Even if this process is less interesting from a nuclear-structure point of view, this decay channel could help to identify and measure the excitation energy of the isobaric analogue state. For now, β3p has been observed in only three nuclei : ^{31}Ar [Kol14], ^{45}Fe [Mie07] and ^{43}Cr [Pom11a, Aud12] with decay branching ratios ranging from 0.1 to a few %. Figure 1.7 presents the particle trajectories observed in a time projection chamber for these three decay paths (βp, β2p and β3p) following the decays of ^{45}Fe.

From the systematics in Figure 1.6, the Q_{3p}-value for ^{23}Si suggests a possibly observable β3p decay branch. However, when several β-delayed decays are in competition, the more exotic branch is also the less probable. In Chapter 4, an experimental search for the β3p decay from ^{23}Si will be presented in detail.

1.3 One-Proton and Two-Proton radioactivity

In addition to β-delayed proton and multi-proton decays, direct single-proton emission from the ground state of nuclei were predicted in the early 1960's [Zel60]. These decays occur when the S_p value is negative, and are referred to as proton radioactivity provided that the half-life is sufficiently long enough. First cases of proton radioactivity were observed from an isomeric state in ^{53}Co, and from the ground states of ^{147}Tm [Sch82], ^{109}I and ^{113}Cs [Fae84]. Today, there are now more than 25 proton emitters that have been discovered. Based on the similarities with the Barrier-Penetration model already used to describe α-particle emission from ground states, it was found that the partial half-life for proton radioactivity depends primarily on the decay Q-value (Q_p) and the angular momentum carried by the emitted proton. This momentum is directly related to the single-particle orbit of the emitted proton. In addition, a nuclear-structure component that describes the wave-function overlap between the parent and the daughter must be applied. Because of the Coulomb barrier, which is determined by the charge of the nucleus, it becomes evident that single-proton radioactivity is more common in medium mass and heavier nuclei.

1.3.1 Two-proton radioactivity

Very quickly after his prediction of β delayed charged particle decays, Goldanksy [Gol61] proposed the existence of an even more exotic type of decay called two-proton radioactivity. This decay mode was predicted to occur from the ground states of even-Z nuclei close to the drip

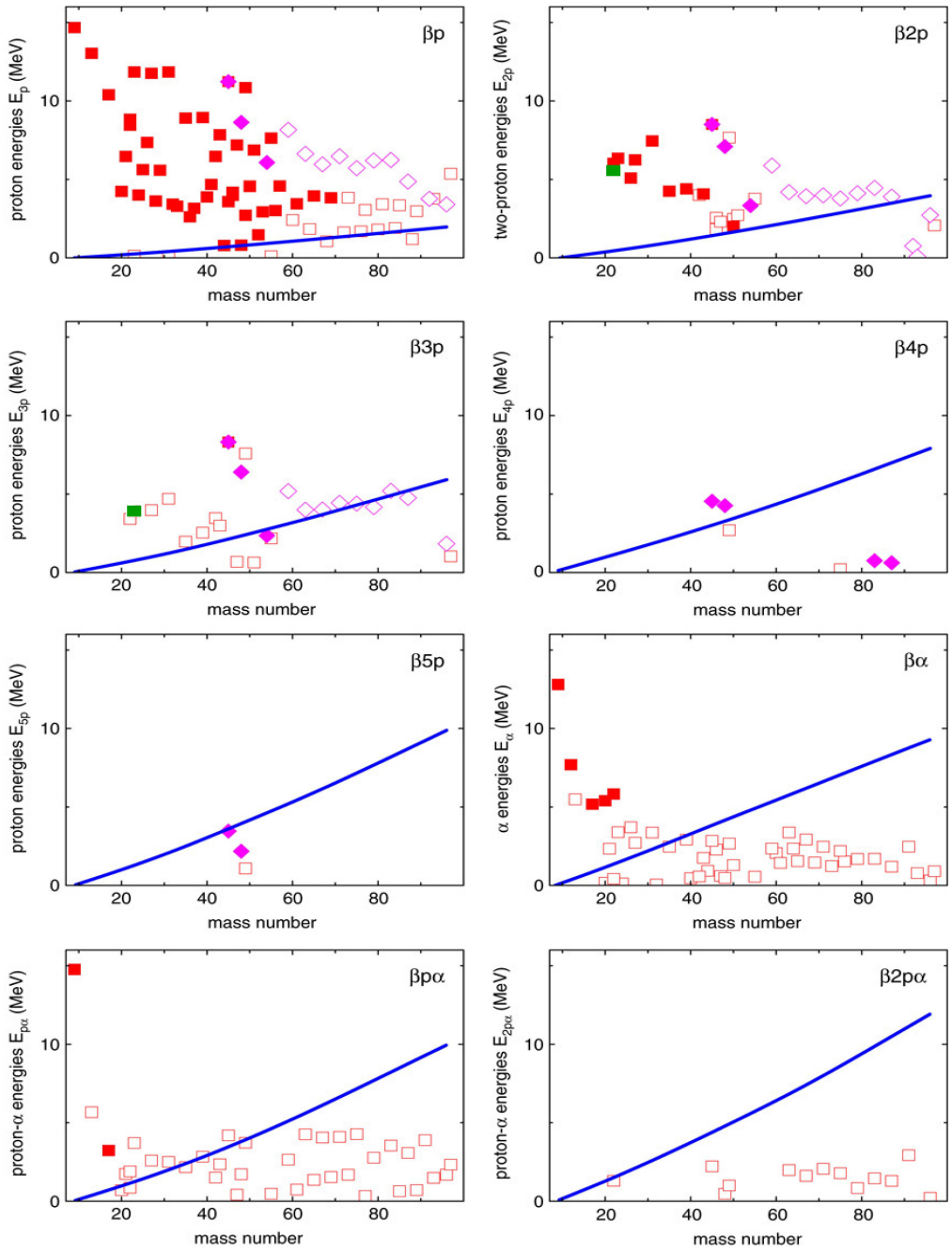

Figure 1.6 – Survey of β-delayed particle decays from proton-rich nuclei through their IAS. the y-axis is the proton energy assuming an equal sharing of the available energy. Known emitters are indicated with filled squares while the open squares are those nuclei that have a favourable decay Q-value, but which have not (yet) been observed. In green, the lightest precursors and subject of the present thesis work ^{23}Si and ^{22}Si are highlighted. The solid blue lines indicate the limit where the competition between γ-decay and particle emission is expected to be significant. (Figure taken from Ref. [Bla08]).

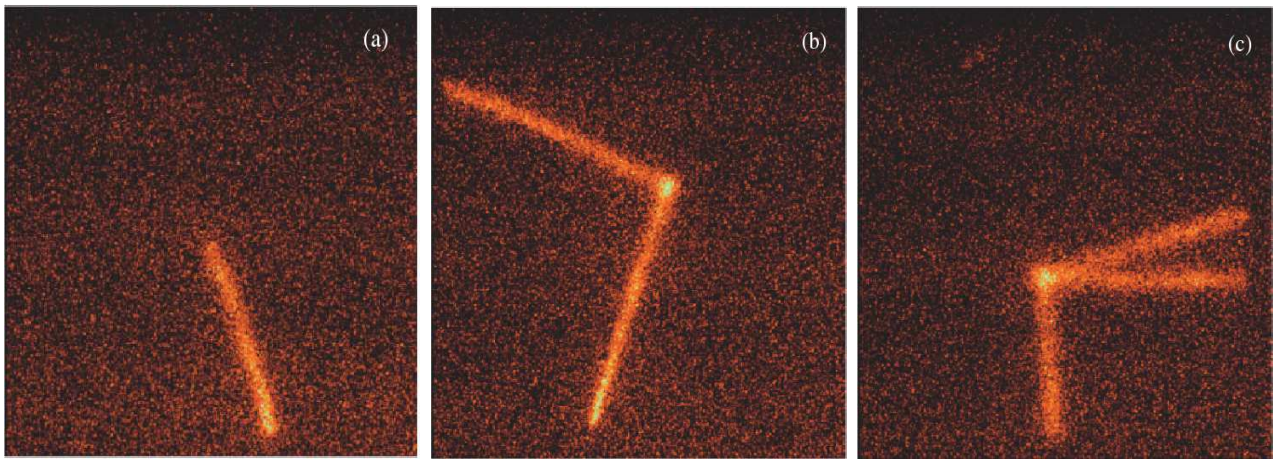

Figure 1.7 – First observation of β-delayed three proton emission (c) from the ground state of ^{45}Fe. This rare decay mode is in competition with β^+, βp (a) and β2p (b) decay channels. The branching ratio for β3p decay was measured to be 3.30% from 125 total decays. (Figure taken from [Pfü12]).

line, for which the pairing energy creates a unique situation where the S_p separation energy is positive while the S_{2p} value is negative. Decay by the emission of two protons is therefore possible while the emission of a single proton is energetically forbidden. This is shown schematically in Fig. 1.8. In this case, two-proton radioactivity cannot be a sequential decay through the one-proton daughter unless (as in light nuclei) the ground state of (A-1, Z-1) daughter is a very broad resonance. Sequential decay of two protons in this case could then occur through its low-energy tail.

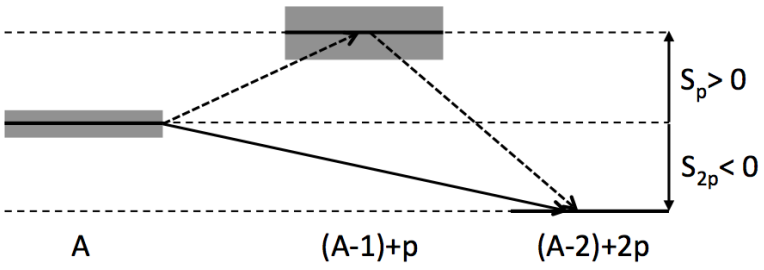

Figure 1.8 – Schematic view of the two-proton radioactivity: the single-proton channel is forbidden because of the negative Q_p-value, while the direct two-proton decay channel is open with respect to the binding energies.

For direct two-proton emission, the partial half-life is determined by the height of the Coulomb and centrifugal barriers, and is therefore expected to be more probable in medium-

mass nuclei. The two-proton decay rate can be calculated using the same tunnelling model as used for α decay. The product of the two barrier-permeability exponentials, which translates into the probability that the charged particle will tunnel through the barrier can be written as:

$$\omega = \exp\left\{\frac{-2\pi(Z-2)e^2\sqrt{m_p}}{\hbar\sqrt{E_{pp}}}\left[\frac{1}{\sqrt{(\varepsilon)}}+\frac{1}{\sqrt{(1-\varepsilon)}}\right]\right\}, \tag{1.59}$$

where E_{pp} is the total decay energy, and ε and $1-\varepsilon$ correspond to the fractions of this total energy that is available to each of the protons. The charge of the parent nucleus Z and the mass of the proton m_p are also required. This distribution reaches a maximum when there is an equal sharing of the proton energy ($\varepsilon = 0.5$). From this observation, two scenario were proposed to describe the nature of two-proton emission:

- the two emitted protons are correlated because of the pairing and nuclear interaction and form a $l = 0$ proton resonance. This system is not bound because of the Coulomb force and decays by emitting the two individual protons simultaneously.
- the process is a three-body decay where only energy and angular momentum conservation have to be respected. In this case, the angular distribution between the two protons is isotropic and the energy sharing distribution uniform.

One has to keep in mind that in addition to this simple kinematic aspect, the theoretical models must also take into account the structure of the parent and daughter nuclei, which tends to suppress the decay and increase the half-life. To be competitive with β^+ decay, the proton emission half-life has to be faster. Known 2p emitters have half-lives that range from tens to hundreds milliseconds.

1.3.2 Discovery of Two-Proton Radioactivity

Ground-state two-proton radioactivity was discovered in 2002 in experiments performed simultaneously at GANIL [Gio07] and at GSI [Pf03] following decays of ^{45}Fe. The secondary beams of ^{45}Fe were implanted into a position-sensitive Si-strip detector that were surrounded by scintillators for the detection of β-particles. The experimental measurements used spatial and time correlations between implantation events and decay events in the Si detector to study and discriminate between the different decay modes. In these experiments, the 2 low-energy protons emitted following the 2p decay are stopped in the vicinity of the implantation and the energy recorded by the Si detector is always equal to their sum. One therefore expects to observe a peak in the charged-particle spectrum with a characteristic energy. Contrary to all β-delayed charged particle decays, a β-particle is not emitted following a true 2p decay. The width of a 2p peak is expected to be narrower than a βp peak since the latter is degraded by the summing of

the proton with some fraction of the energy deposited in the Si by the outgoing β particle. The experiments clearly showed that the 2p candidate peak was narrower than the widths observed for the βp peaks. By taking an anti-coincidence with the β-particle detectors that surrounded the Si, they also showed that this peak is not accompanied by a β particle. The β-particle anti-coincident proton energy spectrum obtained in the GANIL experiment [Gio07] is shown in Figure 1.9. The energy and the partial half-life of this transition were in good agreement with the various theoretical predictions as shown in the same Figure 1.9. All of these evidences were convincing enough to claim the discovery of this rare decay mode in ^{45}Fe nearly 50 years after it was predicted to exist. Today, there are now 4 known 2p emitters: ^{45}Fe (discovered in 2002) [Gio07], ^{48}Ni (2005, confirmed in 2011) [Dos05, Pom11b], ^{54}Zn (2004) [Bla05] and ^{67}Kr (2016) [Goi16].

Following these discovery experiments that were not able to measure the individual proton energies and search for possible p-p angular correlations, experimental research in this field turned towards the development of a time projection chamber (TPC). After implanting the 2p precursor into a gas volume, the emitted protons will ionize the atoms or molecules of the gas all along their trajectories. The ionization electrons can be collected in an applied electric field onto a position-sensitive pad plane in order to provide a two-dimensional charge projection. The third dimension can be deduced using the time it takes the electrons to reach the pad plane. This method provides the means to create a full 3-dimensional image, on an event-by-event basis, which allows the decay channel to be clearly identified. In addition, the full kinematic reconstruction of each event can be used to deduce the individual energies of the emitted protons and measure the angle of emission between them.

The first direct observation of two-proton radioactivity from ^{45}Fe in a TPC took place at GANIL in 2007 where a total of 10 implant-decay correlated events were identified [Gio07]. In a subsequent experiment at GANIL on ^{54}Zn using the same device, 7 fully reconstructed, correlated implant-and-decay events were identified that allowed a measurement of the half-life and branching ratio that were in good agreement with a previous experiment using a Si detector [Asc11]. Figure 1.10 presents a single event that was reconstructed in 3 dimensions. The TPC provided additional information on the energy and angular correlations between the emitted protons that was used to study the nature of the decay mode (sequential or simultaneous). Figure 1.11 (left) shows that the energy is equally shared between the two protons, which is in good agreement with the three-body model of Ref. [Gri00]. Figure 1.11 (right) compares the angular distribution between the two protons to the three-body model in order to estimate the nuclear shell orbital where the protons originated. The shell model was then added to include nuclear structure effects into the dynamics of the decay. By comparing the partial half-lives, they were able to conclude that nearly all of the 2p decay strength in ^{54}Zn goes through the $(0p)^2$ configuration.

The emission of two protons from a nucleus is not limited to ground-state 2p radioactivity

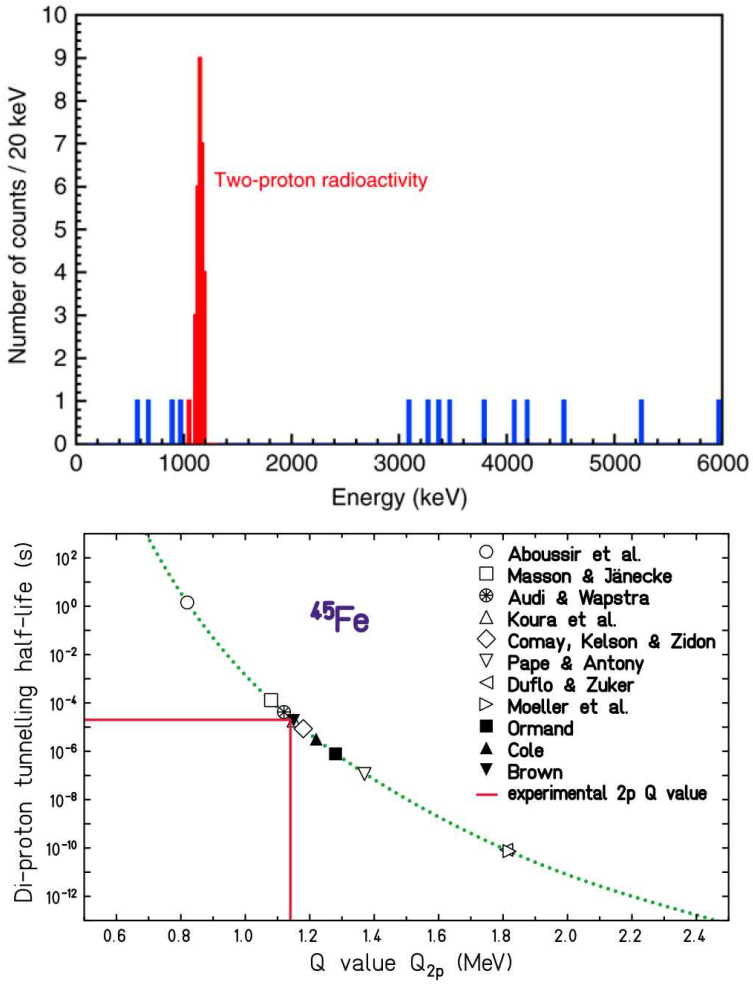

Figure 1.9 – The top figure presents the energy spectrum of the decay events recorded in a Si detector that were identified as two-proton decay from ^{45}Fe (taken from [Bla08]). The bottom figure compares the partial half-life deduced for the two-proton decay branch with different theoretical models (taken from Ref. [Gio07]).

but this decay mode can also occur from unbound excited states. These states can be populated from the β decay of a precursor (this is β2p decay that was described above) or from a nuclear reaction. Once the state is populated, and the 2p emission identified, the experimental goals are identical to the studies described above for ground-state 2p radioactivity. Measurements of the individual energies of the protons and the search for possible angular correlations between them provides unique insight as to the nature of this rare decay mode. The benefit to using a reaction to populate a 2p emitting state, as opposed to studying ground-state 2p decay, is the overall statistical yield. There are very few ground-state emitters known and their production cross sections are extremely small. One is often limited to overall yields of only $\sim$ 10 to 100 events

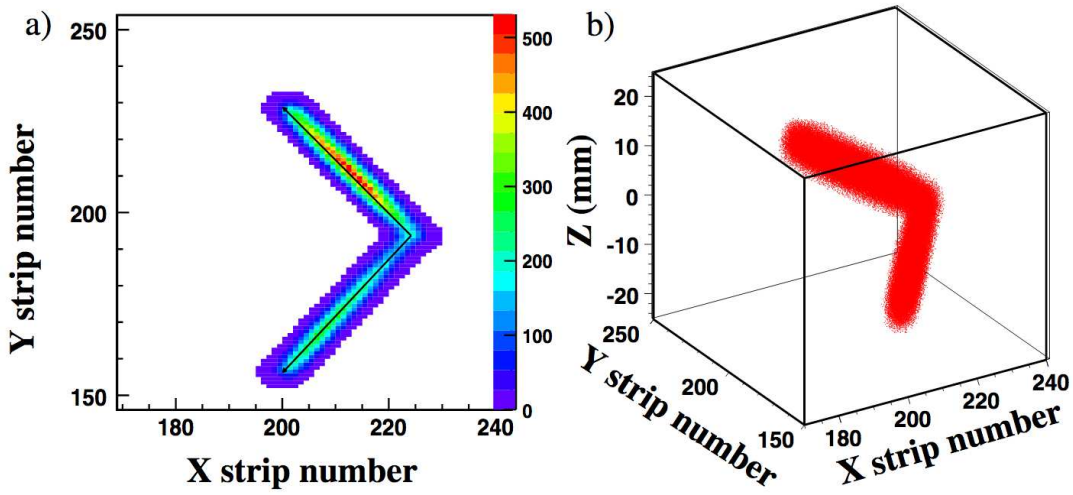

Figure 1.10 – The two-dimensionnal projection of the two proton trajectories (a) observed in the TPC after implantation of ^{54}Zn. The colors are here to indicate the energy loss detected in the strips. (b) The third dimension is obtained using the drift time of the electrons, allowing the measurement of the full kinematic. (Figure taken from [Asc11])

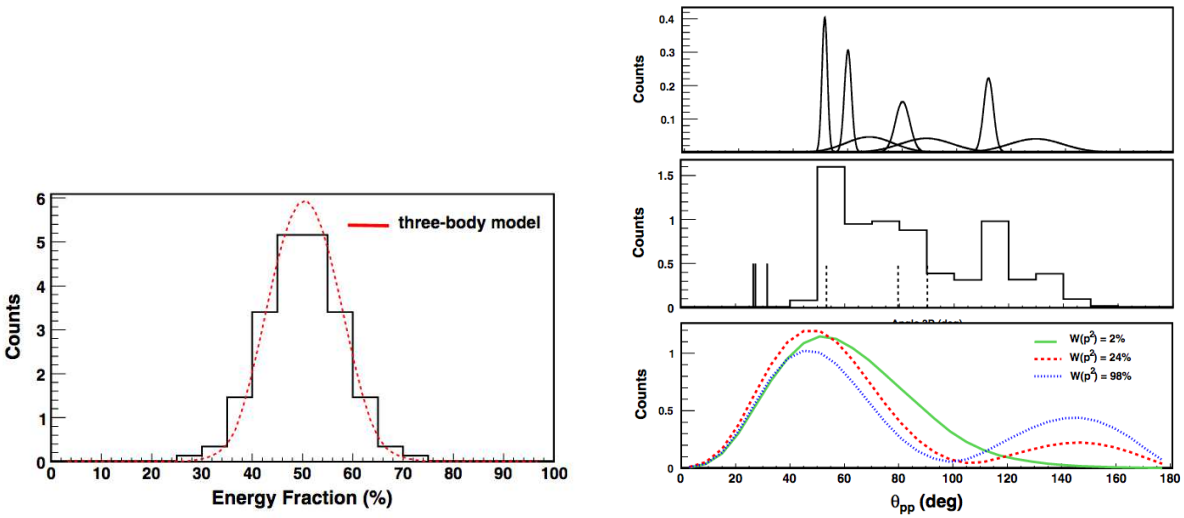

Figure 1.11 – The energy sharing bewteen the two charged particles is in good agreement with the three-body model of two-proton radioactivity. The angular distribution allows the identification of the two-proton initial orbitals. (Figures taken from [Asc11])

maximum after an experiment lasting several days. Depending on the β2p decay branching ratio or the reaction cross sections for populating these states, yields could be significantly higher. The other advantage, is that the energies of the protons emitted from excited states are much larger than the typical energies for ground-state decays ($\sim$ 500 keV per proton) and thus their detection is conceptually simpler. An example of a reaction study to populate 2p emitting states in ^{22}Mg and ^{23}Al was recently performed at RIKEN [Ma15]. Beams of ^{22}Mg and ^{23}Al were produced using the RIPS fragment separator and were sent to a ^{12}C reaction target. Following breakup reactions on the target, heavy fragments (^{20}Ne and ^{21}Na, respectively) were identified using the B$\rho - \Delta E-$TOF method, while the position and energy of the protons emitted from the excited states were measured using position-sensitive Si telescopes. Figure 1.12 shows the angular and energy correlations between the two protons that were obtained. The data were fitted using a Monte-Carlo simulation to identify whether the decays were two sequential single proton decays or the direct emission of two protons decay. The wide and isotropic energy and angular distributions that were measured for ^{23}Al is in agreement with a sequential emission of two protons. However, the narrow angular distribution centered at 30° in ^{22}Mg is in better agreement with a simultaneous correlated process.

1.3.3 Summary and Motivation

Nuclei that are situated at, or close to, the proton drip line often exhibit several rare decay channels that are not open to nuclei closer to stability. These decay modes appear naturally from the combination of the increasing decay Q-values with the decreasing particle separation thresholds. Following the β decays of these near drip-line nuclei, branching ratios to particle unbound states give rise to β-delayed particle emission. Depending on the separation energies several different β-delayed decay channels may be open and can compete with each other. Delayed decays including βp, β2p, β3p, $\beta\alpha$ and $\beta\alpha$p have all been observed experimentally. Delayed decay spectroscopy is an extremely useful experimental tool to study the structure of the unbound excited states in the daughter nuclei as they are populated with a reasonably high yield and these states can be inaccessible using other techniques such as transfer and scattering reactions or in-beam γ-ray spectroscopy. Studies of β2p decay can provide additional insight on the nature of the 2p-decay mechanism with higher statistical yield than ground-state 2p radioactivity that is produced with very limited intensities.

As described in this Chapter, the Coulomb force on the neutron-deficient side of the nuclear chart splits the degeneracy of an isospin multiplet of isobaric analogue states giving the highest energy to the lowest T_Z member of the multiplet. It is then possible that the isobaric analogue state decays to the ground state of the lowest T_Z member is accessible through nuclear β^+ decay. The use of β-delayed proton decay is also of crucial importance as the energy of this isobaric analogue state can be deduced via proton-decay spectroscopy. Once this key state is identified and its energy deduced, the isobaric mass multiplet equation (IMME) can be used to deduce

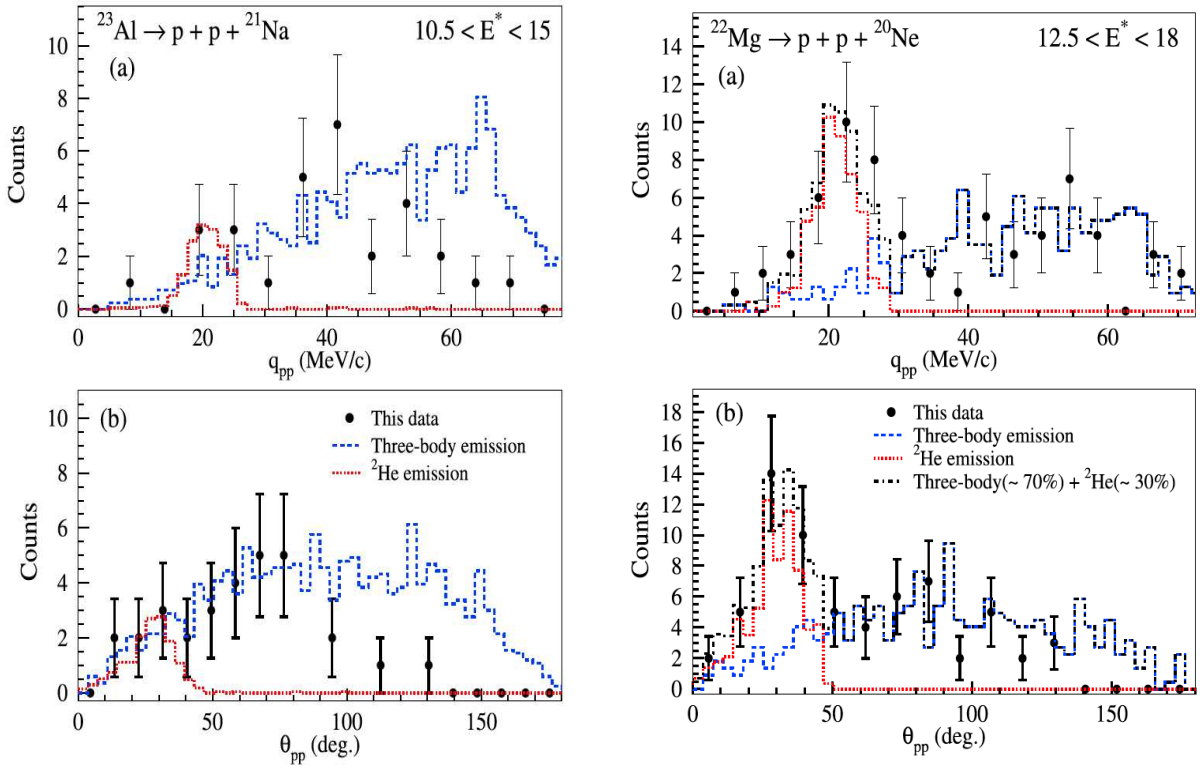

Figure 1.12 – Angular and energy correlations between the two protons emitted from the IAS in both ^{23}Al and ^{22}Mg show two different decay mechanisms. An isotropic angular and energy distribution is observed for ^{23}Al which can be explained from a sequential decay of two protons. The peak observed in the case of ^{22}Mg suggests a strongly correlated simultaneous emission of 2 protons. (Figures taken from [Ma15]).

the masses for other unknown states of the multiplet. Measuring the energy of an IAS through its proton decay can thus be used to deduce the mass of the parent nucleus. Nuclear masses are essential and fundamental quantities in nuclear physics whose trends can be used to study the evolution of nuclear shell structure in unexplored regions of the nuclear chart, deduce the limits of nuclear binding and delineate the location of the drip lines, predict the onset of rapid shape changes and deformation effects and explore new and exotic decay modes.

As the single-particle separation energy gets even closer to zero, pairing effects can create situations where the nucleus is bound with respect to single proton emission but is unbound to the emission of two protons. Ground-state 2p radioactivity has now been experimentally observed in 4 cases (^{45}Fe, ^{48}Ni, ^{54}Zn and ^{67}Kr) and 2p emission from excited states populated either through the β2p decay channel or via nuclear reactions is a rapidly accelerating field. The big question surrounds the nature of the 2p decay mechanism and whether the protons are emitted sequentially or simultaneously. Recent technical developments in nuclear physics

include time projection chambers that have been extremely successful despite the difficulty associated with the overall statistical yield since the production cross sections for these exotic nuclei are very limited. The emission of 2 protons from excited states could yield higher statistics and the development of next-generation active targets (a TPC where the gas is also used as a reaction target) will certainly be an extremely efficient choice to continue with these types of experimental investigations.

In his original reviews of two-proton radioactivity [Gol61, Gol60], Goldansky proposed ^{22}Si as the lightest possible candidate that could decay via this rare decay mode. Presently, very little is known about this nucleus. It is the lightest bound isotope with isospin projection $T_Z = -3$ and is the most neutron-deficient Si isotope that is bound. It is known to β decay with a half-life of approximately 30 ms [Bla97], which is short enough to allow the possibility of an appreciable 2p decay branch. The mass, however, has never been measured and so the S_{2p} value can only be extracted from model extrapolations. Based on the current mass evaluation AME2012 [Wan12], the two-proton separation energy is $S_{2p} = -1200$ (500) keV. In the previous evaluation of AME2003 [Aud03], a value of $S_{2p} = -16$ (202) keV was proposed. The discrepancy between these two predictions and the large uncertainties do not permit any firm conclusions to be drawn. A precision mass measurement is clearly required to assess whether or not ^{22}Si could decay by ground-state 2p radioactivity

Because Si isotopes are refractory, the production of these nuclei using the isotope separation online technique (ISOL) is not possible. Laboratories such as ISOLDE at CERN and TRIUMF-ISAC in Vancouver that have powerful precision Penning traps to measure nuclear masses simply cannot produce the Si beams required. Production of Si beams can be achieved using in-flight fragmentation reactions at facilities like LISE at GANIL and the A1900 at NSCL but the half-life of ^{22}Si is too short to allow these beams to be slowed down and injected into a trap. The only option to measure the mass of ^{22}Si directly would be using the time-of-flight technique at a fragmentation facility but purifying the secondary cocktail beam would constitute a significant experimental challenge.

In this thesis, an indirect mass measurement using the β-delayed charged particle emission from the decay of ^{22}Si will be presented. Secondary beams of the neutron-deficient nuclei ^{20}Mg, ^{23}Si and ^{22}Si were produced at NSCL (MSU, USA) by fragmentation. After purification, the nuclei of interest were implanted into the Beta Counting System to detect the β-delayed protons and α particles. Identification of the daughter nuclei and the corresponding decay paths was performed using coincident γ rays that were detected in the 16 HPGe detectors of the Segmented Germanium Array (SeGA). In the next chapter (Chapter 2), the production of the secondary beam and the implantation-and-decay station will be presented along with the calibration techniques and the analysis program that will be used throughout this thesis. Chapter 3 presents the β-delayed decay spectroscopy of ^{20}Mg that is a well-known decay and

that was delivered in the cocktail beam. Its decay was studied in the present work to test and verify the analysis protocol.

In Chapter 4, a β-decay study of the $T_Z = -5/2$ nucleus ^{23}Si was performed that is compared to a previous study of Ref. [Bla97]. In the present work, the γ-ray detection capabilities not used in the previous study have allowed several new levels to be identified. The β2p channel was unambiguously established and is in agreement with the hypothesis of the previous experiment. This nucleus is also a candidate for β3p decay, whose search will be described in detail. Chapter 4 will conclude with a presentation of the level scheme obtained in the present work and its detailed comparison to the previous experiment and a theoretical shell-model calculation. From the energy of the IAS, the mass of ^{23}Si will be derived using the IMME and compared to previous mass-model predictions.

In Chapter 5, the detailed decay spectroscopy of ^{22}Si will be presented. Results will be presented in the context of a previous experiment and compared to a shell-model calculation. The β2p decay branch has been identified and the energy of the IAS deduced. From the IAS energy, the mass of ^{22}Si was deduced in order to assess whether or not this nucleus is a candidate to decay by ground-state 2p radioactivity.

Conclusions and perspectives for future experiments and further improvements regarding the study of the β-delayed charged particle decays of these nuclei, will eventually be presented in Chapter 6.

Chapter 2

Beam Production and Experimental Setup

In this chapter, a detailed overview of the production of the secondary beams of ^{20}Mg, ^{22}Si and ^{23}Si, the experimental implant-and-decay station and the analysis techniques will be presented. These unstable nuclei were produced and selected by the A1900 Fragment Separator and were further purified by the Radio Frequency Fragment Separator at the National Superconducting Cyclotron Laboratory (NSCL) at Michigan State University. The resulting purified beams were then delivered to an experimental decay station, where the nuclei were implanted into a central Double Sided Silicon Strip Detector (DSSD) of the Beta Counting System (BCS). The calibration of the DSSD detector was performed using a ^{228}Th α source to first align each strip of the DSSD. An absolute energy calibration was then performed using previously known β-delayed protons from decays of ^{20}Mg and ^{23}Si that were implanted in DSSD2. An array of 16 HPGe detectors of the Segmented Germanium Array (SeGA) surrounded the BCS and were used to detect γ-rays in coincidence with the decays registered in the DSSD. The energy and efficiency calibrations of the DSSD and the HPGe array, the data selection and analysis protocol as well as the implant-and-decay correlation logic that was developed in the context of the present thesis work will be presented in detail.

2.1 Isotope Production

2.1.1 Secondary Beam Production

The neutron deficient isotopes of ^{20}Mg, ^{22}Si and ^{23}Si are situated at, or very near, the proton drip-line. Production of these exotic nuclei at NSCL was performed using a primary beam of ^{36}Ar that was accelerated to 150 MeV per nucleon in the K500 and K1200 coupled cyclotrons (see Figure 2.1). The ^{36}Ar beam impinged a 1030 mg/cm^2 natural Be target located at the

entrance of the A1900 fragment separator [Mor03a]. Since the products of the fragmentation reaction have nearly the same velocity, the A1900 was required to purify the beam and select the ions of interest from the rest of the fragmentation products. The A1900 filters and purifies the beam in-flight according to differences in magnetic rigidity (denoted Bρ) and the energy loss ΔE of the ions through the separator.

In a magnetic field, charged particles follow circular trajectories in the plane orthogonal to the direction of the field itself. The radius of these trajectories depends upon the momentum and the charge of the ions. Ion selection based upon their mass-to-charge ratio is a commonly used purification method and follows the relation:

$$B\rho = \frac{p}{q} = \frac{m}{q}v \tag{2.1}$$

where B is the strength of the magnetic field, p is the impulsion of the ion, m is the mass of the ion, q is the charge of the ion, v its velocity and ρ its radius of curvature.

A second selection step in the A1900 fragment separator is based on energy-loss filtering at the dispersive plane using a $\sim$300 mg/cm^2 Al degrader wedge. This degrader operates in a similar way to an optical prism; the energy loss through the Al foil is proportional to the mass of the ion, its charge and its total energy.

After the wedge, two additional purification steps using the magnetic rigidity Bρ allow an ultimate selection of the ions of interest. Figure 2.1 summarizes the production and selection steps of secondary beam production at the A1900. The magnetic field and the thickness of the energy degrader must be optimized for every experiment to select and maximize the purity and transmission of the secondary beams. The typical energies of the secondary beams of ^{22}Si^{14+} and ^{23}Si^{14+} were 82.4 MeV/u and 93.7 MeV/u respectively.

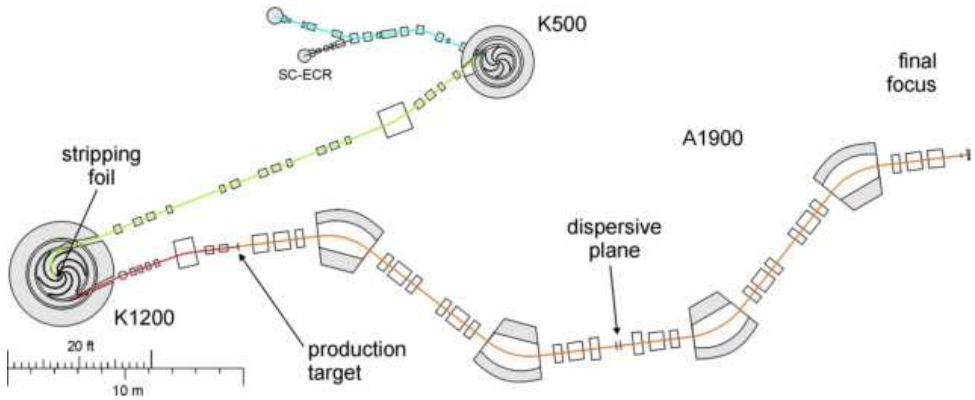

Figure 2.1 – Secondary beam production and selection at the NSCL coupled cyclotron facility. The K500 and K1200 accelerate the primary beam and the A1900 Fragment Separator is used to select and purify the secondary beam.

2.1.2 The Radio Frequency Fragment Separator

At the exit of the A1900 separator the secondary beam is never pure. It is always a "cocktail" beam consisting of several different isotopes. The momentum distribution of the fragmentation products is asymmetric and presents a low-momentum tail due to collisions in the production target. Because of the momentum selection, the tails of more stable and more abundant nuclei overlap the distributions of the more exotic isotopes of interest as shown in Figure 2.2 for the case of ^{22}Si production. Despite the precise Bρ selection at the A1900 fragment separator, the production tails of the near-stable and stable nuclei is typically several orders of magnitude higher than the production rate of the most exotic nuclei such as ^{22}Si. High rates of these unwanted contaminants are often detrimental to experiments aiming to study the most exotic nuclei and additional purification steps are essential.

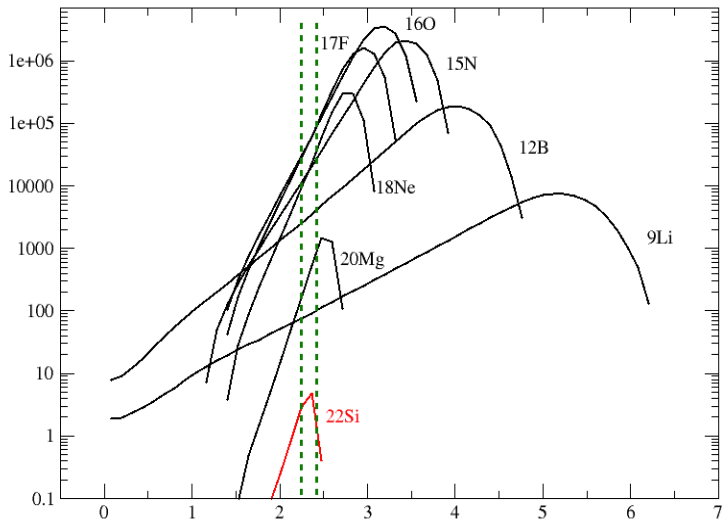

Figure 2.2 – LISE++ [Baz02] simulation of different production rates after the A1900: in red, the rate of ^{22}Si is much lower than the rates from the momentum tails from the contaminants closer to stability. The green dashed line shows the momentum acceptance of the A1900 Fragment Separator ($\Delta p/p = \pm 2.5\%$) centred on ^{22}Si production.

To further improve the purity of the secondary beam, the Radio Frequency Fragment Separator (RFFS) [Baz09] was employed. The RFFS is located in the S1 vault just after the A1900 separator. The RFFS uses a radio-frequency coupled electric field that is applied to two in-vacuum parallel plate electrodes that are 1.5 m long, 10 cm wide, and 5 cm apart (see Figure 2.3). The alternating current that supplies the electrodes in phase opposition induces a magnetic field that is orthogonal to the beam axis. As an ion passes through the device, it will experience a deflection in the vertical direction that is proportional to its velocity. The

ion trajectories follow the shape of a stationary wave with a node located at the center of the vacuum cavity. As the device is a velocity filter, the initial trajectory is deviated but the amplitude of the deviation at the end of the RFFS is less effective for the most energetic ions, as shown schematically in Figure 2.4. At the end of the RFFS cavity, a set of adjustable vertical slits is used to select the ions of interest.

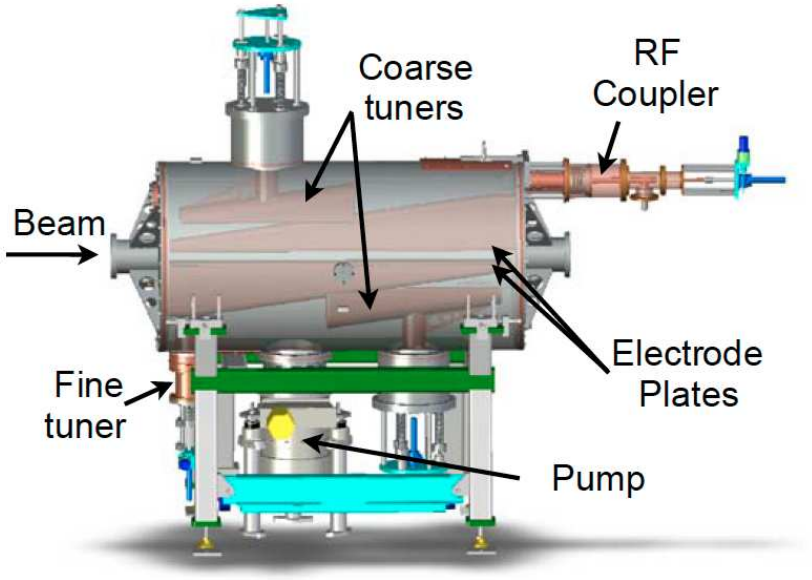

Figure 2.3 – The RFFS device is made of a radio-frequency (RF) coupling system. Two horizontal parallel electrodes cause a deviation of the particle trajectories, and two vertical slits select the nuclei of interest from the incident cocktail beam.

The RFFS was essential in this experiment to decrease the total secondary beam intensity and to thus minimize the number of implantations in the central DSSD detector. An implantation rate that is too high would significantly increase the dead time of the data acquisition and the probability of false implant-and-decay correlation events. For the ^{22}Si part of the experiment, the RFFS was also crucial as it was able to almost entirely eliminate ^{16}O and ^{20}Mg from the cocktail beam. A summary of the beam intensity and purity for the ^{22}Si production setting both with and without the RFFS is provided in Table 2.1. It should be emphasized that these rates were obtained after a reduction in the primary beam intensity by a factor of 10. The available intensity was significantly higher than the maximum rate that could be accepted by the DSSD detector. The particle identification (PID) was performed in Fig. 2.5 using the energy-loss and time-of-flight ΔE-ToF method. The time-of-flight was deduced using the time difference between a scintillator located at the exit of the A1900 and a silicon detector at the exit of the RFFS, while the ΔE energy-loss signal was from this same Si detector. Figure 2.5 shows the PID of the outgoing beam when the slits of the RFFS are either open (Fig. 2.5a) or

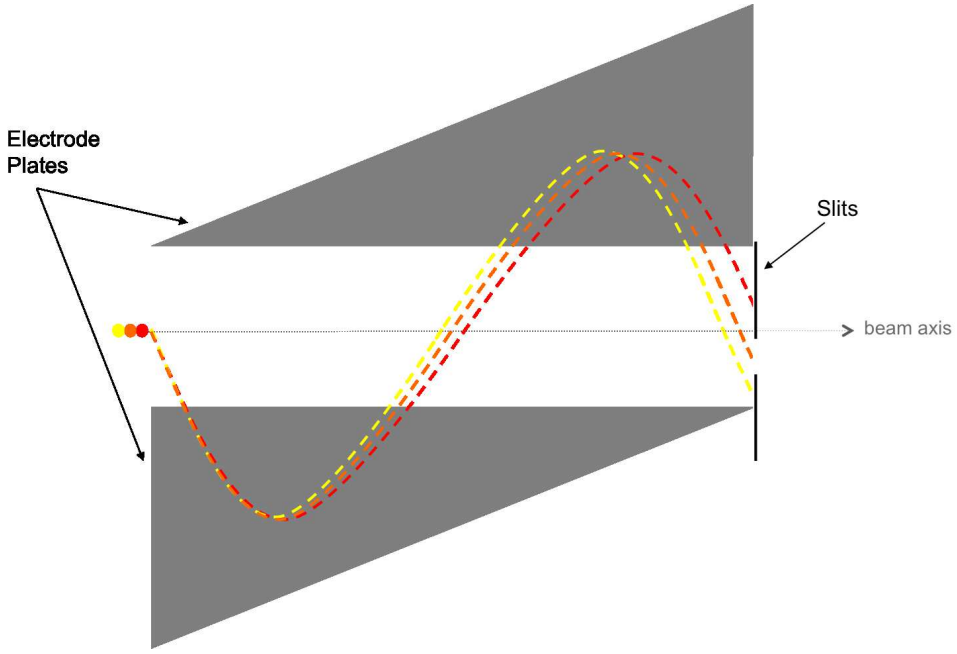

Figure 2.4 – Principle of operation of the RFFS. The fastest ions (in red) travel through the RFFS device and are less deviated by the magnetic field than the slowest ions (in yellow), which are more deviated. A set of adjustable vertical slits at the exit of the cavity are used to select the ions of interest.

Parent	RFFS Open		RFFS Closed	
Nucleus	Purity (%)	Rate (ions/s)	Purity (%)	Rate (ions/s)
^{22}Si	0.006	0.22	0.03	0.47
^{20}Mg	0.16	6	0.004	0.05
^{18}Ne	5.9	219	12.3	169
^{17}F	31.4	1160	83.7	1147
^{16}O	61.7	2280	2.1	29
$\sum$	99.2	3665.22	98.1	1345.52

Table 2.1 – Summary of the beam purity.

closed (Fig. 2.5b). Without the RFFS, the total secondary beam intensity (after the factor of 10 attenuation in beam intensity) was ∼3700 ions/s. Of this, ^{22}Si represented only 0.006% of the total intensity (approximately 0.22 ^{22}Si/s) while 0.2% (∼6 ions/s) was ^{20}Mg, a well-known β-delayed proton emitter. After the RFFS slits were closed and optimized for ^{22}Si, the ^{16}O and ^{20}Mg contaminants were almost entirely eliminated and the total intensity was reduced to ∼1300 ions/s. Even with the RFFS, the remaining cocktail beams are still not entirely pure.

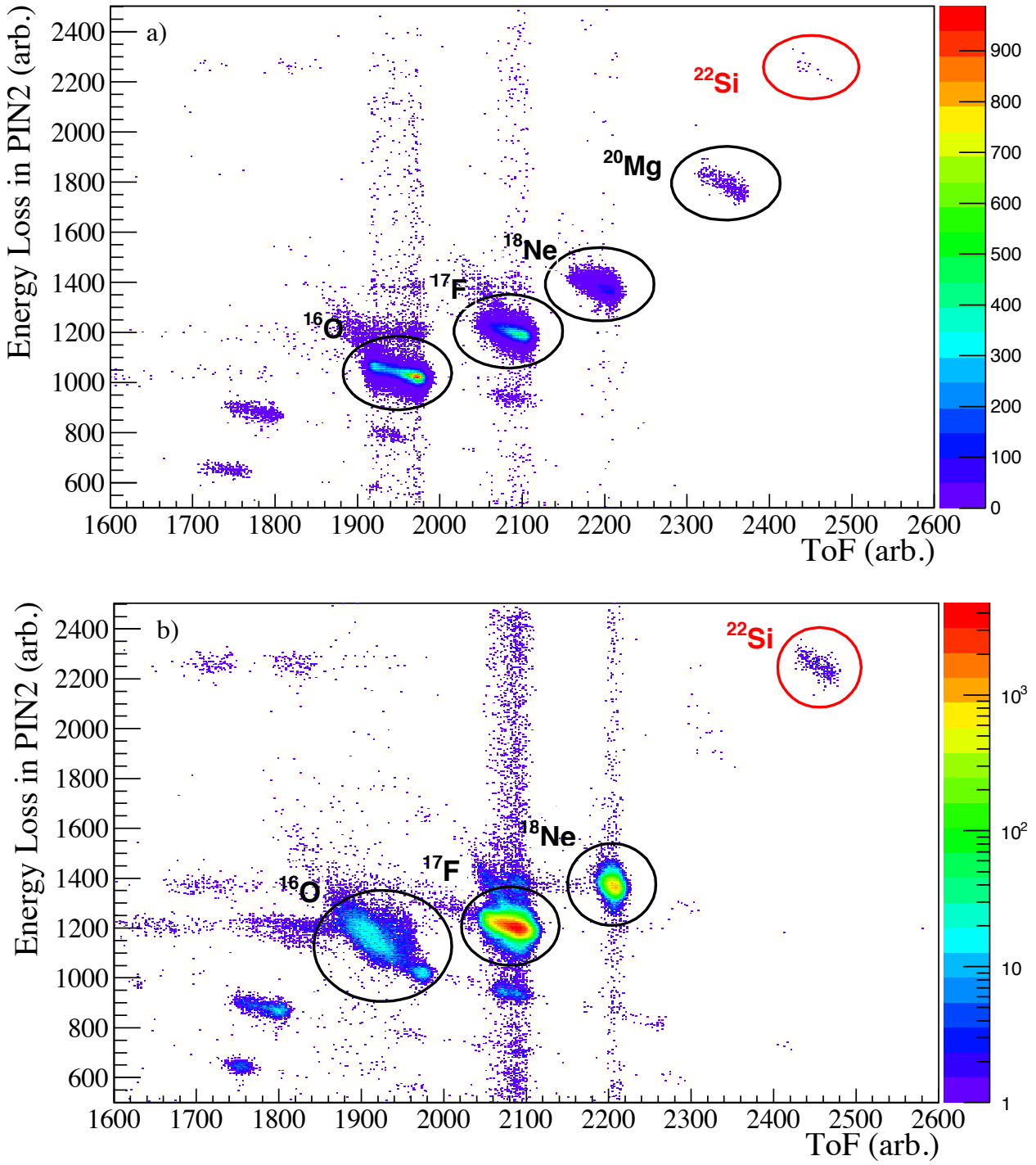

Figure 2.5 – Particle identification of fragments in the secondary beam optimized for ^{22}Si production using the ΔE-ToF method. (a) When the RFFS slits are open the purity of ^{22}Si is 0.006% while ^{20}Mg is 0.16% of the overall production rate. (b) When the RFFS slits are closed the 0.033% of the beam is ^{22}Si, and only 0.004% is the ^{20}Mg contaminant.

For the cases of ^{22}Si and ^{23}Si described in the following chapters, some contaminants that are also β-delayed charged particle emitters did remain in the beam.

2.2 Implantation and Decay Detection Station

Once the secondary beam was selected and purified, two detector arrays were used at the implantation and decay station to detect charged particles from the decay (protons, α particles and β particles) and coincident γ-rays emitted by excited states in the daughter nuclei.

2.2.1 The Beta Counting System

When the ^{22}Si and ^{23}Si ions β decay, particle unbound excited states may be populated in the daughters ^{22}Al and ^{23}Al, respectively. To ensure the detection of these emitted charged particles, the Si beams were implanted in the Beta Counting System (BCS) [Pri03, Mor03b]. This setup was traditionally dedicated to the detection of low-energy β decays but was modified in the present experiment into a novel arrangement of three 525 μm thick DSSDs that was optimized for detecting protons with high efficiency. A schematic of the experimental setup is shown in Fig. 2.6. Each of the DSSDs was segmented into 40 1-mm strips in the X and Y directions, providing 1 mm^2 pixels that were used to measure the implant and decay energies, times and positions. Ions of interest are implanted into the center of the central detector (DSSD2). Depending on the specific implantation depth for each ion, the full energy for the majority of protons with $E_p \leq 6$ MeV will be stopped in DSSD2. The exterior DSSD detectors (DSSD1 and DSSD3) could therefore be used to detect the residual energy of even higher-energy protons that escape DSSD2 and, as described below, were used as a β-particle veto as an attempt to improve the DSSD2 energy resolution. As shown in Figure 2.6, these DSSDs were located downstream with respect to three silicon PIN detectors. The thicknesses of the PINs were chosen to ensure that the Si beams were implanted in the middle of DSSD2. More than simple energy degraders, these active PIN detectors also provide energy loss and time signals that were used to identify the ions.

Electronics Diagram and Correlation Logic

The electronics diagram of the BCS detectors is shown in Fig. 2.7. The output signals of the DSSDs were split and sent into two separate pre-amplifiers with different gains. A low gain amplification was used to measure the energy deposited by the *implantation* of a heavy ion. A time signal was also generated upon implantation that was used as a time reference for the event. A high-gain amplification was used for the measurement of the energies of the charged particles emitted following the decay of an implant. These events could be β-particles, protons or α particles. A second time signal was then generated and used in the analysis process to

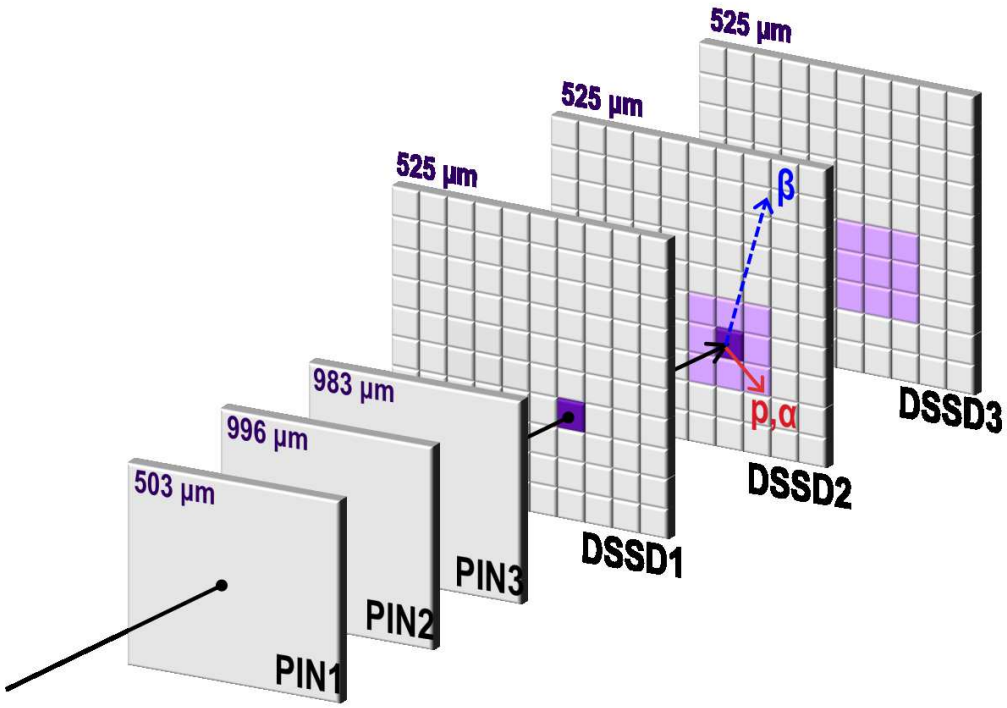

Figure 2.6 – Schematic of the Beta Counting System optimized for β-delayed charged particle decay. Three closely packed DSSDs were used with each DSSD having 40 strips in the X and Y directions to allow spatial and time correlations between implants and decays. The three PIN detectors upstream were used to degrade the beam energy and to identify the implanted ions.

deduce the time difference between the decay event relative to its implant. These signals were used to define the logic that was developed in this analysis to correlate the implant and the corresponding decay event in both space and time.

In the analysis, an implant event was defined according to the following event sequence (i) a signal was detected in PIN1, PIN2 and PIN3, (ii) low-gain signals were present in both DSSD1 and DSSD2 and (iii) a low-gain signal in DSSD3 was absent. A low-gain signal from DSSD3 implies that the ion was not implanted in DSSD2 but penetrated through and was implanted in DSSD3. This low-gain signal in DSSD3 was therefore used to veto the low-gain implant event in DSSD2. A decay event was defined by (i) a high-gain event in DSSD2 and (ii) no signals in PIN1, PIN2, and PIN3. The implant and decay identification logic is presented in Table 2.2.

	PIN1	PIN2	PIN3	DSSD1	DSSD2	DSSD3
IMPLANT	1	1	1	low-gain	low-gain	0
DECAY	0	0	0	-	high-gain	-

Table 2.2 – Logic of the analysis software to identify correlated implant-and-decay events.

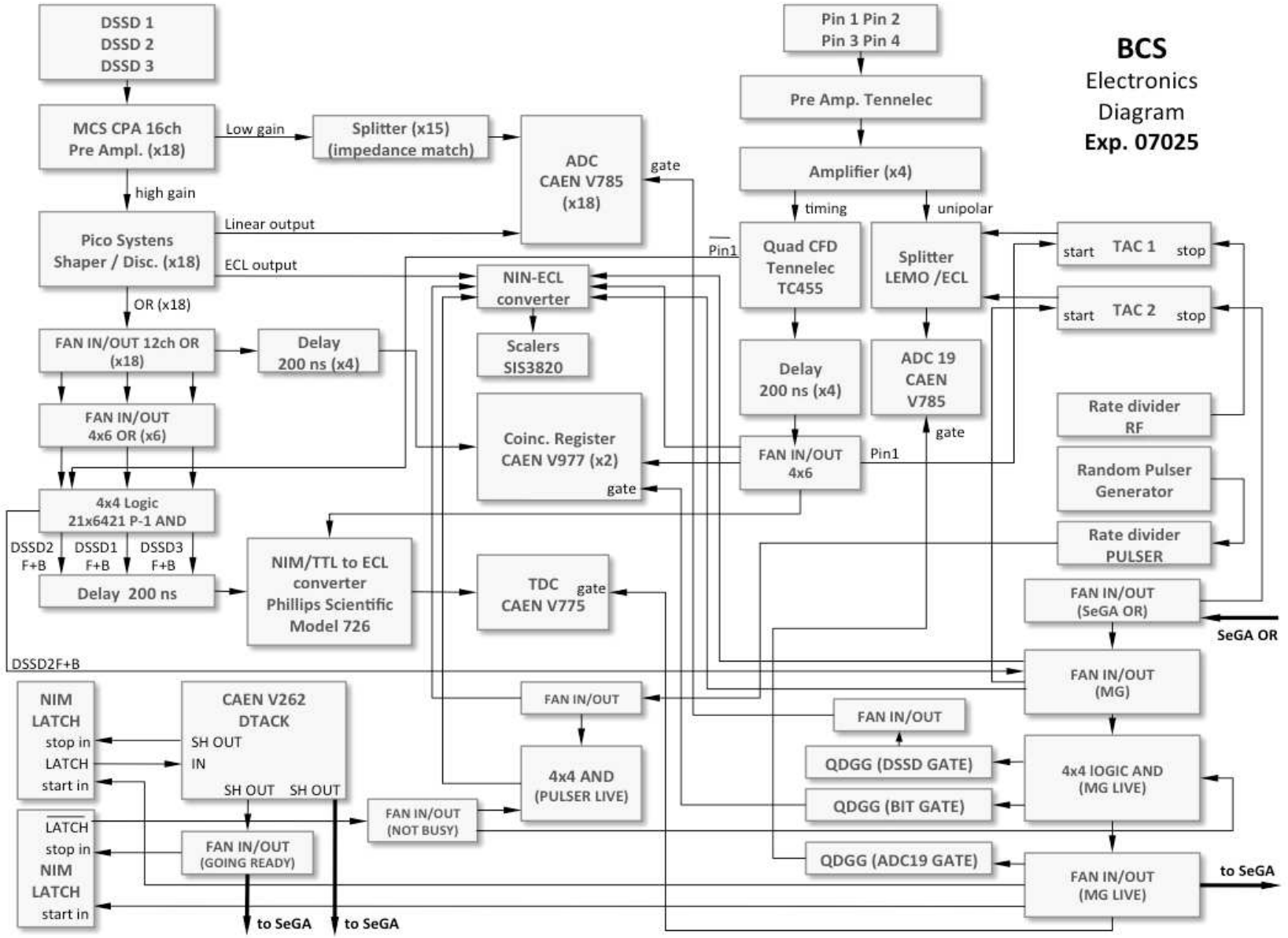

Figure 2.7 – Electronics diagram for the BCS detectors.

This time differences between implant and decay events were bound by a maximum correlation time T_{max} that was fixed for each nucleus of interest. Using the intensity of the proton branches following the implantation and decay of ^{20}Mg ($T_{1/2}$ ~90 ms), and taking into account the β-delayed α decay of its daughter ^{20}Na ($T_{1/2}$ ~450 ms), a T_{max} value was chosen to maximize the ^{20}Mg/^{20}Na ratio. A comparison of the areas for two particular transitions is shown in Figure 2.8. The intensity ratio for the proton group at 1.7 MeV (from ^{20}Mg decay) relative to the α-particle group at 2.7 MeV (from ^{20}Na decay) saturates at $T_{max} = 0.5$ s, which corresponds to approximately 5 times the half-life of ^{20}Mg. Taking a shorter correlation time would not be ideal as it would decrease the overall ^{20}Mg statistical yield. As shown in Figure 2.8, the ratio is saturated and thus extending the correlation time to $T_{max} = 1.0$ s (10 times the half-life of ^{20}Mg) would not introduce any significant bias. Based on similar analyses performed for the other nuclei in this work (^{22}Si and ^{23}Si), it was found that the most appropriate value for the maximum correlation time parameter is $T_{max} = 10 \times T_{1/2}$, where $T_{1/2}$ is the half-life of the parent nucleus of interest.

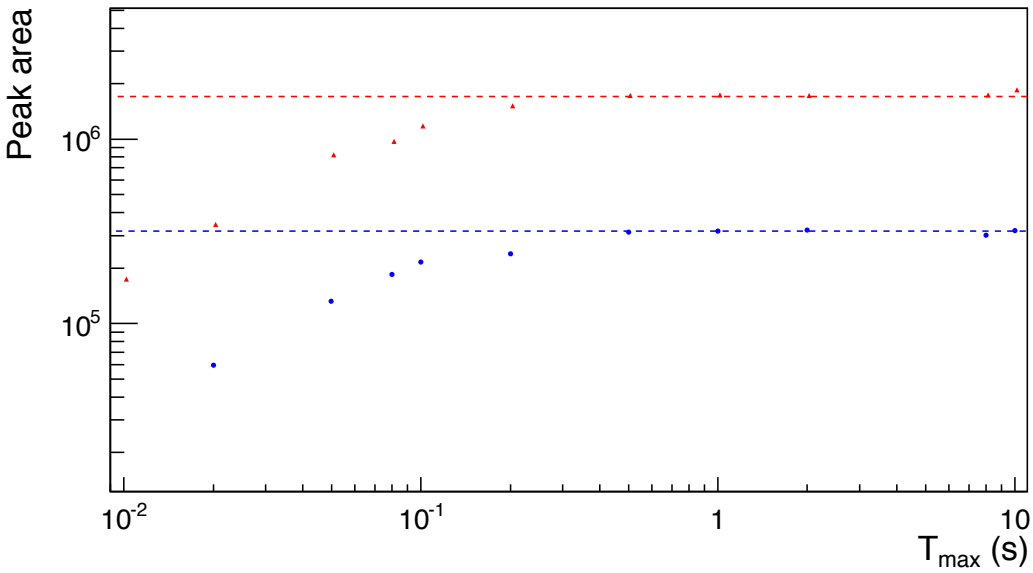

Figure 2.8 – Evolution of the area of the 1.7 MeV β-delayed proton group from ^{20}Mg and the 2.7 MeV β-delayed α-particle group from the ^{20}Na daughter after implantation and correlation of ^{20}Mg. After $T_{max} = 0.5\ s$, which roughly corresponds to $5 \times T_{1/2}$, the ratio of the area of these peaks reaches saturation.

For every event, the energy signal of the decay was taken to be the maximum of all strips surrounding the implantation pixel. This area was defined with a spatial parameter in the analysis software. According to the mean free path of the most energetic β-delayed protons, this parameter was defined as 2, meaning that only decays occurring in the implantation pixel

itself or in any of the 8 nearest-neighbour pixels that surround the implantation pixel were considered in the correlation analysis and used to determine the proton energies.

One of the challenges associated the present approach is that radioactive ion beams produced by projectile fragmentation have a relatively large energy spread. This requires the use of a thick central DSSD to ensure that all of the ions are stopped within the implantation detector. The consequence is that the additional energy deposited in the DSSD by the β particle will sum with the energy of the proton that is emitted nearly simultaneously creating an extended tail on the high energy side of the proton peak. This β-summing effect will thus decrease the resolution of the Si detectors. In an attempt to minimize this effect, correlations with decay particles (high-gain events) detected in DSSD1 and DSSD3 were investigated. If the β particle emitted following the decay of an ion implanted into DSSD2 escapes and deposits energy in either DSSD1 or DSSD3, it was assumed that the β-summing effect in DSSD2 was minimal. However, if neither DSSD1 or DSSD3 observed a β particle in coincidence with the decay in DSSD2, then it was assumed that the majority of the β energy must therefore have been recorded in DSSD2 and thus the β-summing effect was maximal. A NOT condition in DSSD1 or DSSD3 was therefore used to veto the decay event in DSSD2. A potential problem with this logic is that the thresholds of the DSSD detectors were optimized for proton detection ($\geq$ 300 keV). Any β particle that deposits less than this in either DSSD1 or DSSD3 would go undetected and the veto on the DSSD2 decay event would be applied.

To test this logic, the analysis considered a 9-pixel and 25-pixel spatial correlation window in DSSD1 and DSSD3 that was applied around the geometrical center of the 9-pixel window described above to correlate implant and decay events in DSSD2. As presented in Table 2.3 for the ^{20}Mg, ^{23}Si and ^{22}Si decays of interest, the efficiency of this correlation process increases slightly with the number of pixels. Increasing the number of neighbouring pixels further could increase the number of false correlations.

Correlation area	Efficiency for ^{20}Mg	Efficiency for ^{23}Si	Efficiency for ^{22}Si
9 pixels	4.7	3.3	2.8
25 pixels	7.4	6.1	5.9

Table 2.3 – Evolution of the correlation efficiency as a function of the number of pixels used to correlate the β particles in DSSD1 and DSSD3 for the ^{20}Mg, ^{23}Si and ^{22}Si decays.

From the results presented in Table 2.3, the efficiency of this process is very low ($\approx$ 5%). This is likely due to the relatively high energy thresholds that were applied to the DSSD detectors. The efficiency of this process is slightly better for ^{20}Mg, that was implanted near the surface of DSSD2: the β particle were detected in DSSD1 with a higher geometrical efficiency

than Si isotopes. Despite these losses, the energy resolution is certainly improved when this correlation analysis between neighbouring detectors is applied. An example is shown in Fig. 2.9 for the case of ^{20}Mg decay where the spectra with a 9-pixel and 25-pixel correlation areas in DSSD1 and DSSD3 are compared to the spectrum obtained without correlations. Several weak α and proton groups can now be resolved and the number of low-energy events has been reduced. This spectrum is comparable to the resolution obtained in similar experiments with even thinner detectors [Wal12]. Unfortunately, since this correlation process suffers from an extremely low efficiency, it will not be applied in the present work.

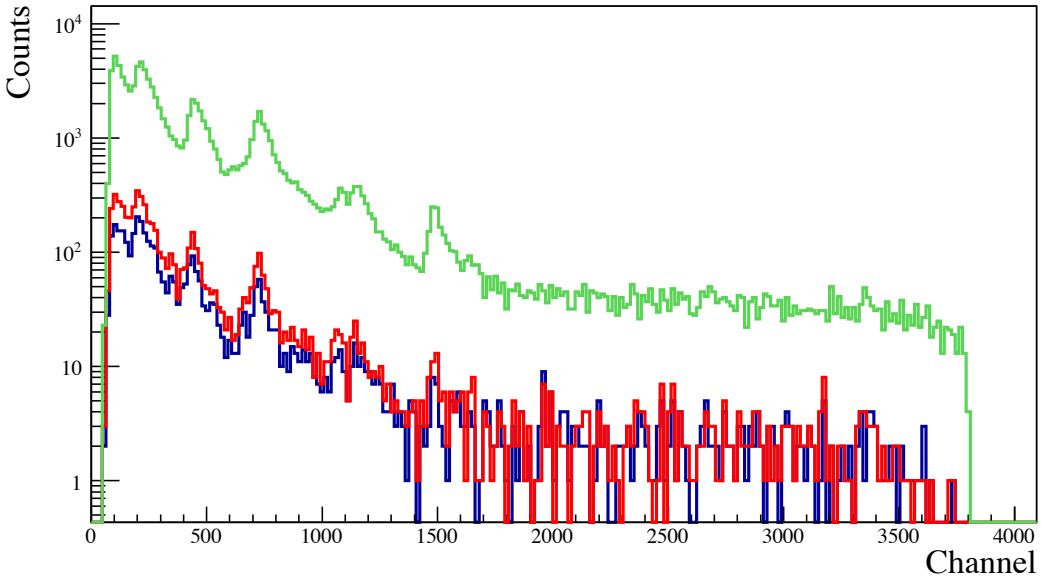

Figure 2.9 – (Green) The charged particle spectrum following β decays of ^{20}Mg where tail due to β summing is clearly visible and deteriorates the overall energy resolution. The same spectrum after correlation with β particles detected in DSSD1 and DSSD3 for a correlation area of 9 pixels (blue), or 25 pixels pixels (red). The energy resolution is improved, allowing some of the weaker transitions to be observed, but the statistics are very limited due to the efficiency of this correlation process.

DSSD energy calibration

A relative energy calibration for the strips of the DSSD detectors was performed using a ^{228}Th α-particle source. The energies and branching ratios of the α particles emitted by the source are summarized in the decay scheme presented in Figure 2.10. All strips were gain matched relative to a reference strip. Front strip #21 was selected because of its central position and increased statistics compared to the edge strips. Figure 2.11 shows the α-particle energy spec-

trum of this single reference strip.

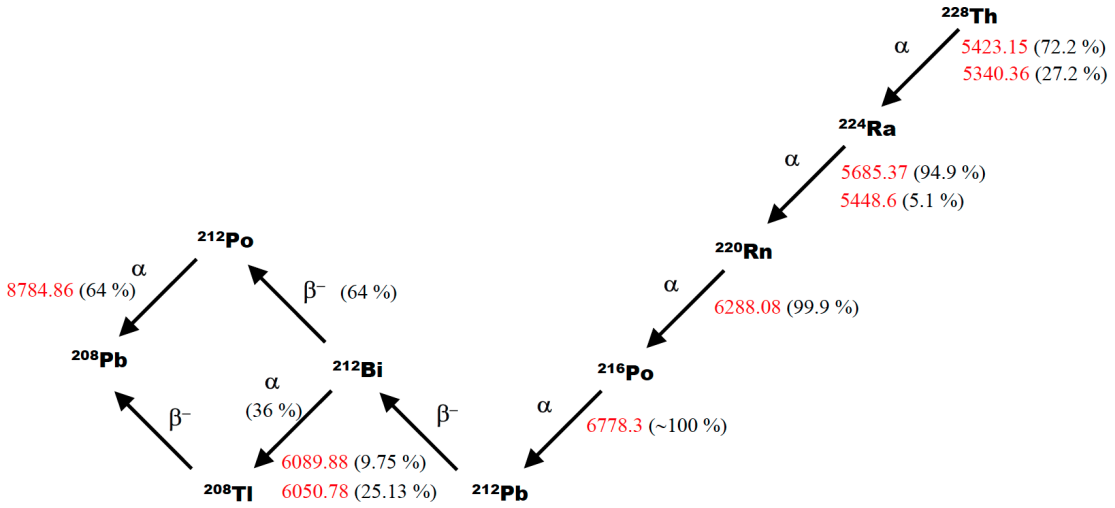

Figure 2.10 – Decay scheme of the ^{228}Th source ($T_{1/2} = 1.913$ y) with the energy of the α-particles used for the DSSD strip gain matching.

The centroids of the α-particles were obtained using a ROOT [Bru97] program. The fit function employed consisted of a Gaussian distribution convoluted with a low-energy exponential tail to reproduce the charge collection default [Sik12]. The definition of this total skewed Gaussian fit function is:

$$y = \frac{1}{2\tau} \exp\left(\frac{-(\mathrm{x}-\mu)}{\tau} + \frac{\sigma^2}{2\tau}\right) \operatorname{erfc}\left(\frac{1}{\sqrt{2}}\left(\frac{\mathrm{x}-\mu}{\sigma} + \frac{\sigma}{\tau}\right)\right) \tag{2.2}$$

where μ is the centroid of the peak, σ the standard deviation of the Gaussian, and τ the decay constant of the exponential tail on the low-energy side.

During the experiment, ions were implanted into DSSD2. Since this detector is a semiconductor, the output signal is proportional to the energy deposited by the charged particle that ionized the Si atoms. An absolute energy calibration using the α source is insufficient since the α particles would lose energy in the dead layer on the detectors surface that would not be seen by particles emitted from decays of ions implanted inside the detector. Also, these α particles from the ^{228}Th source cover a small energy range, and thus the extrapolation of the calibration at low energy would be hazardous. The amplitude of the electrical signal was

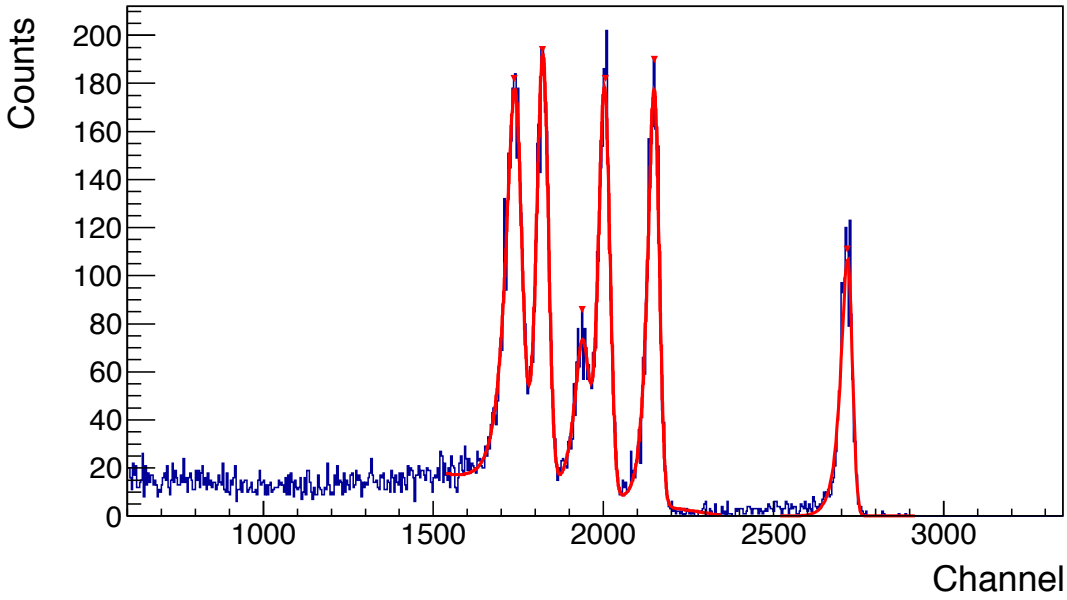

Figure 2.11 – Spectrum of the ^{228}Th α particles recorded in the reference strip (front strip 21) of DSSD2. In red, the fit function used to reproduce these data.

therefore calibrated in absolute terms using several β-delayed charged particles from nuclei that were delivered as contaminants and whose proton or α energies are well known. This method ensures that the energy calibration and the measurements were performed under the exact same experimental conditions.

One of these, ^{20}Mg, is a well known β-delayed proton emitter. Approximately 30% of ^{20}Mg decays populate excited states in the daughter ^{20}Na that are higher than the proton separation threshold (Sp = 2190 keV) and leads to proton emission. The remaining 70% populates the 1^+ excited state at 984 keV in the daughter ^{20}Na that decays by γ-ray emission to the ground state. The decay of ^{20}Na has an appreciable β-delayed α-decay branch (about 20% of the ^{20}Na decays) and these α particles can also trigger the data acquisition and be detected in DSSD2. A detailed study of the decay of one of the nuclei of interest, ^{23}Si, was previously performed by B.Blank *et al.* [Bla97]. The proton energies with the highest intensities were also included in the energy calibration of DSSD2 despite their relatively large uncertainties.

In a Si detector, heavy ions lose energy by both ionization and inelastic collisions in the

matrix of the crystal. These inelastic collisions lead to vibrational (phonon) excitations that are not detected. This phenomenon is known as the Pulse Height Defect (PHD), and can be calculated depending on the recoil ion using the phenomenological approach presented in Ref. [Rat75]. In this experiment, the mass and the charge of different recoil ions imply the need for slightly different PHD corrections, as shown in Figure 2.12. Thus, the absolute energies that were used to calibrate the DSSD are given by:

$$E_{cal} = E_p + E_{ion}(1 - \epsilon_{PHD}), \tag{2.3}$$

with

$$E_{ion} = \frac{M_p}{M_{ion}} E_p \quad \text{and} \quad E_{ion} + E_p = Q_p\text{−value}, \tag{2.4}$$

where ϵ_{PHD} is the fraction of the energy lost to phonon excitations and E_{ion} and E_p are the kinetic energies of the recoil ion and the charged particle, respectively. The Q_p-value is the energy difference between the proton-unbound state in the β-decay daughter (^{20}Na for the case of ^{20}Mg decay) and the final level in the β-delayed proton daughter (^{19}Ne for the case of ^{20}Mg decay).

In Equation 2.3, an additional term needs to be added in order to take into account the β-summing effect in the DSSD, E_β. Detailed GEANT4 simulations [Mei16] were performed to determine the experimental implantation depth and the β-summing contribution for both ^{20}Mg and ^{23}Si decay. The β-summing values were found to be 18(6) keV and 79(12) keV, respectively. In this work, the DSSD energy calibration was performed in order to analyse the β-delayed proton emission of ^{23}Si and ^{22}Si whose total Q_β-values are both larger than 15 MeV and vary by only about 10%. Since these differences are small, and given that the ion implantation profile and depths were similar for both cases, the energy calibration in the present work assumed that the β-summing correction for both ^{22}Si and ^{23}Si decays were the same. An average systematic uncertainty of 70 keV was added to the energies derived from all data sets. The energies of the protons and the α particles that were used in the calibration, and their effective energies after PHD corrections are summarized in Table 2.4.

The resulting data used in the energy calibration of DSSD2 are presented in Fig. 2.13. Two fit functions, a linear and a quadratic, were tested. The quadratic was used to ascertain if there were any evidence for non-linearities in the electronic chain and/or in the detector itself. The difference between both of these fits and the data for both calibration functions are also provided in Fig. 2.13.

In the present measurement, we are primarily interested in high-energy protons emitted from the IAS. These transitions, in the case of a decay from the IAS to the ground state can potentially be as high as ∼11 MeV. Therefore, as there are no calibration data available, one has to be extremely careful in the extrapolation of this DSSD calibration outside of the range

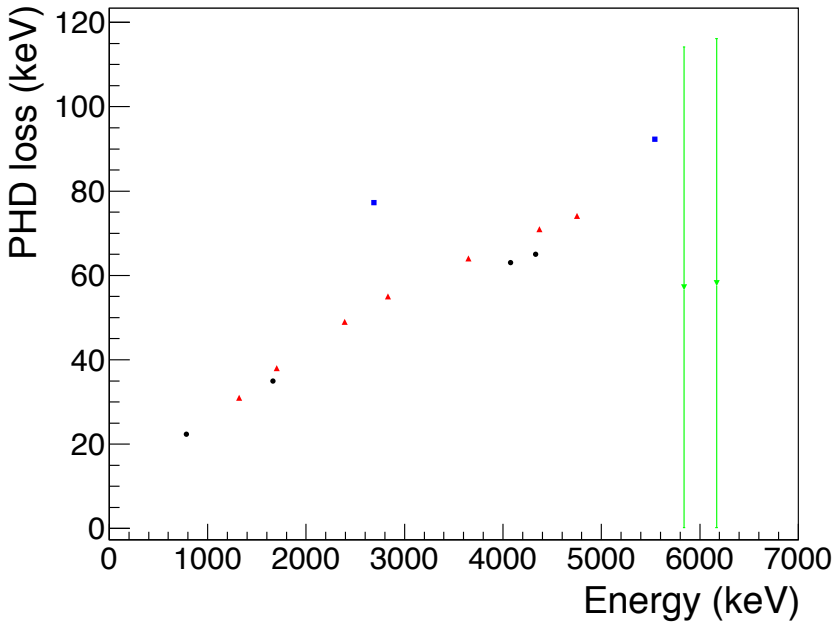

Figure 2.12 – The PHD loss to vibrational excitations of the Si crystal is a function of the mass, charge and the energy of the recoil ion. In black and blue, the PHD loss (in keV) for a ^{20}Mg implant, with the βp and $\beta\alpha$ emission from the ^{20}Na ground state, respectively. In red, the PHD loss for the β-delayed proton groups of ^{23}Si used in the calibration. The green data show the possible ranges of the PHD for the case of the β-delayed two-proton decay, as proposed in [Bla97]. The uncertainties are due to the different emission possibilities (parallel or anti-parallel) for these protons.

of energies used. The energy-difference plots for both functions (linear and quadratic) show similar agreement within the calibration range. The linear function will therefore be adopted in order to avoid potentially large uncertainties that could arise from the extrapolation of the quadratic function. The energy dependence of the systematic uncertainties due to the calibration parameters from the linear fit are provided in Figure 2.14.

At low energy, a software threshold was applied to every strip to remove the pedestal generated in the analogue-to-digital converter (ADC) from the analysis. This threshold was deduced on a strip-by-strip basis using a ^{90}Sr β-particle source and was determined when the overlap of the β background and the Gaussian pedestal was minimal. An example is shown in Figure 2.15 for the case of a single strip.

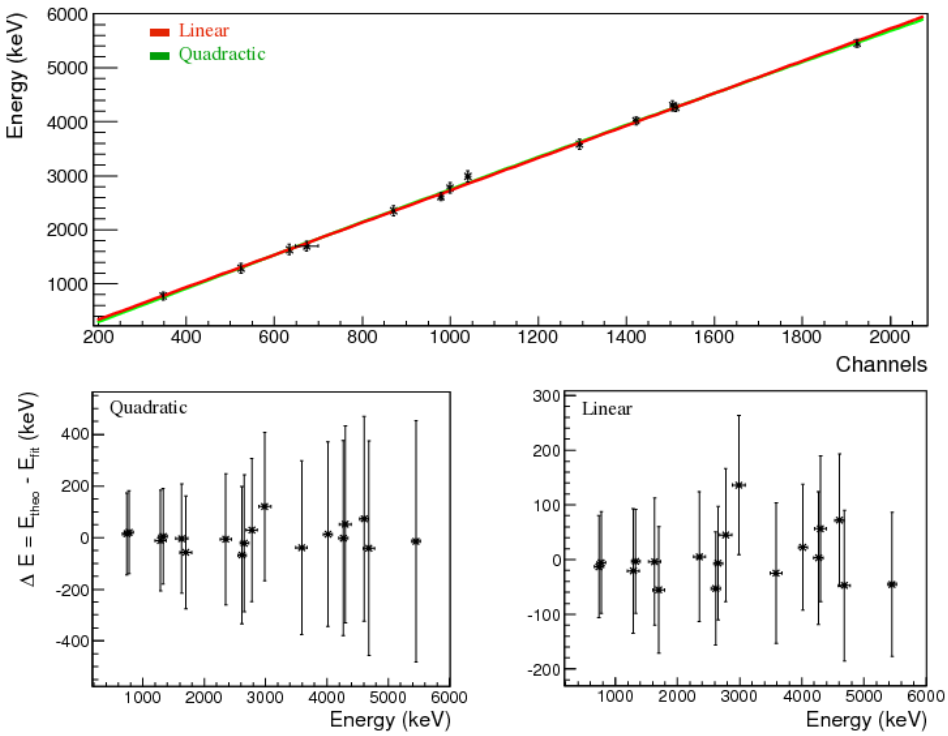

Figure 2.13 – (Top) Energy calibration for DSSD2 performed with the energy of β-delayed protons and α particles (see Table 2.4) versus the raw channel number. (Bottom) Differences between the fit function and the data, for the quadratic fit (χ^2/ν=0.97) and the linear fit (χ^2/ν=0.86).

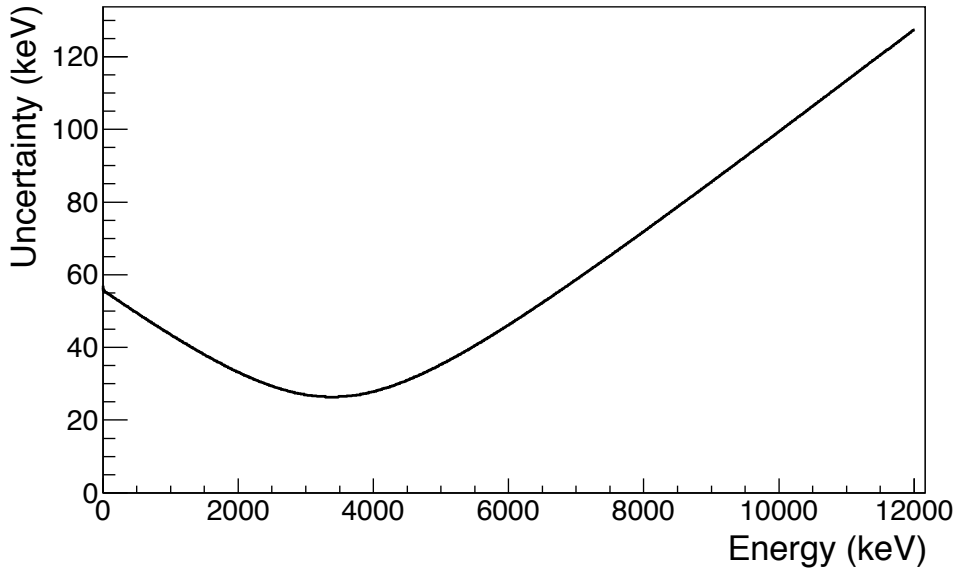

Figure 2.14 – Evolution of the calibration uncertainties, calculated within one sigma of the peak uncertainty.

Precursor	β-delayed decay	Q_p-value (keV)	E_{cal} (keV)
^{20}Mg	proton	797 (2)	775 (70)
^{23}Si	proton	1320 (40)	1289 (94)
^{20}Mg	proton	1670 (10)	1635 (71)
^{23}Si	proton	1700 (40)	1662 (94)
^{23}Si	proton	2400 (60)	2351 (94)
^{20}Mg	α	2692 (2)	2615 (70)
^{23}Si	proton	2830 (60)	2775 (94)
^{23}Si	proton	3650 (60)	3586 (94)
^{20}Mg	proton	4080 (16)	4017 (72)
^{20}Mg	proton	4332 (16)	4267 (72)
^{23}Si	proton	4370 (60)	4299 (94)
^{23}Si	proton	4760 (60)	4686 (94)
^{20}Mg	α	5543 (3)	5451 (70)

Table 2.4 – Table of energies E_{cal} used in the energy calibration of DSSD2 from decays of ^{20}Mg and ^{23}Si. The difference between the uncertainties on the Q-values and the energy E_{cal} used in the calibration is primarily due to the 70 keV systematic uncertainty that was added to account for β summing.

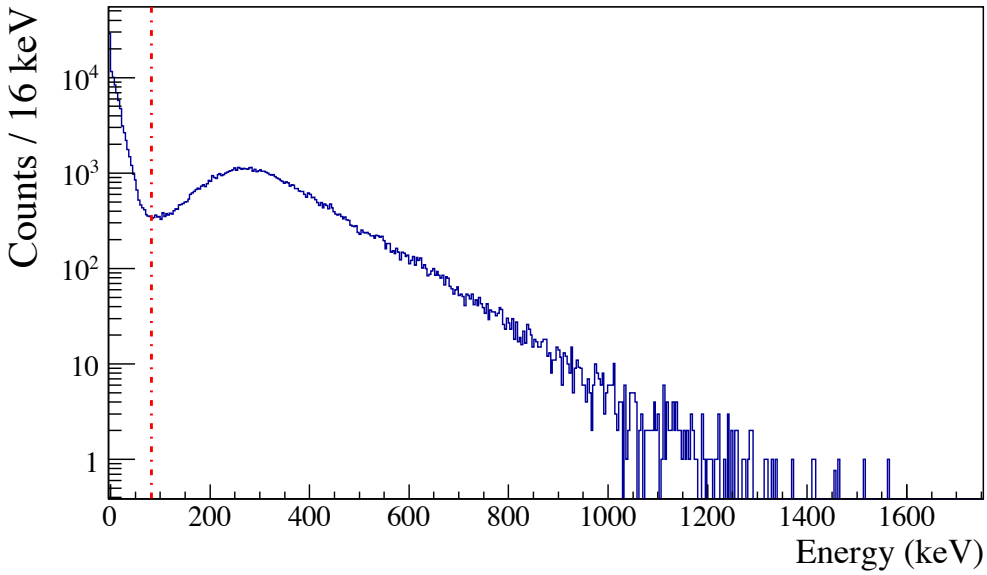

Figure 2.15 – Total β-particle spectrum from a ^{90}Sr source for a single strip in DSSD2. The dashed red line shows the software threshold that was applied to this strip and corresponds to the channel above which the number of counts is dominated by true β-particle events rather than the ADC pedestal.

DSSD efficiency calibration

In addition to the energy calibration, the DSSD2 detection efficiency as a function of the proton energy must also be derived. When a proton is emitted from the decay of an implant, its energy could be sufficient to escape from the 525 μm thick DSSD. In this case, the proton would be detected in DSSD1 or DSSD3. From the GEANT4 simulation that was performed, the ^{23}Si mean implantation depth was 250(40) μm [Mei16] so nearly perfectly centered in DSSD2. A Monte-Carlo simulation was then used to determine the detection efficiency as a function of the proton energy. In this simulation, a proton was generated with an energy between 5 MeV to 32 MeV and the corresponding mean free path in the silicon matter was obtained using LISE++[Baz02]. The simulation generated a random isotropic distribution of proton angles according to a fixed kinetic energy. The efficiency was then defined as the number of protons detected (stopped) in the 3x3 pixel area compared to the total number of decay events.

As presented in Figure 2.16 (in red), the DSSD efficiency is 100% below 5.74 MeV, i.e. no proton escapes the 262-μm half-thickness of the silicon detector. Above 5.74 MeV, the proton energies are sufficient to escape and would leave only a fraction of their energy in DSSD2. From 6 to 25 MeV, the efficiency decreases smoothly until it reaches a second drop, due to the fact that the proton has now a sufficient energy to exit the spatial correlation area. All protons from the decays studied in the present thesis work are all expected to have a kinetic energy $\leq$ 12 MeV.

Because the energy of the ^{20}Mg beam was not optimized to implant the ions in the center of DSSD2, the implantation depth and hence the efficiency for detecting the β-delayed protons was different. Based on the value of the β-summing and the shape of the tail due to the detection of the β^+ particles in the thick central DSSD, Meisel *et al.* [Mei16] were able to determine that ^{20}Mg ions were implanted with an average depth of 27(6) μm.

The same simulation as described above for ^{23}Si was used to determine the effective correction in efficiency: for a defined proton energy, the efficiency is defined as the number of protons which escape either the 27-μm layer upstream or the 528-μm Si thickness. The efficiency curve for the ^{20}Mg decay is presented in Figure 2.16 (in green). Since ^{20}Mg ions are implanted near the surface of the DSSD, the efficiency quickly drops for protons with an energy above 1 MeV and is distinctly lower than the efficiency calculated for ^{23}Si implants.

These efficiency functions were fitted with a 5^{th}-order polynomial function in order to correct the branching ratios measured in the present work.

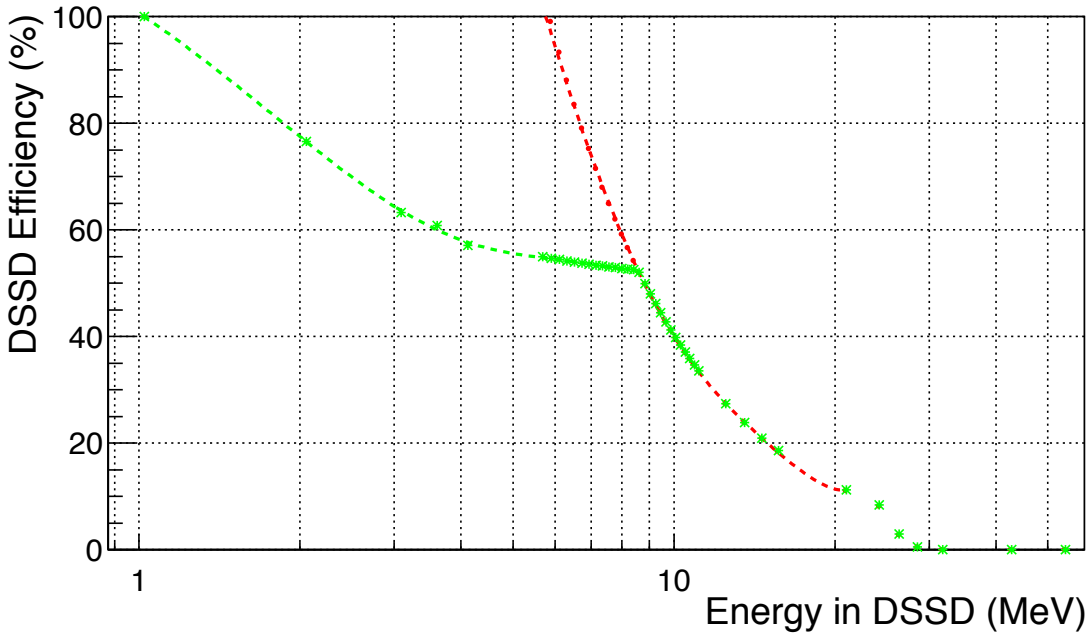

Figure 2.16 – Proton efficiency curve for the 525 μm thick DSSD detector assuming that the ^{23}Si ions (in red) are implanted in its center. Protons with a given energy were generated with an isotropic distribution and the efficiency is the number of protons stopped in the DSSD relative to the total number of protons emitted. In the case of ^{20}Mg ions (in green) with an implantation depth of 27 μm, 100% efficiency is only achieved for protons with an energy below 1 MeV. The efficiency curves were fit with a 5^{th}-order polynomial function to guide the eye.

2.2.2 The Segmented Germanium Array

The Si detectors of the Beta Counting station were surrounded by 16 detectors from the Segmented Germanium Array (SeGA) [Mue01] that were used to detect γ rays in coincidence with the protons detected in the DSSD. These high-purity germanium detectors must also be calibrated in energy and in efficiency. Calibrations were performed using two γ-ray sources, positioned at the center of the array, and data were collected for sixty minutes for each detector individually. The output signal after discrimination was used to provide the trigger signal to the acquisition data system, as presented in the electronics diagram of Figure 2.17.

The first source was a mixed source of ^{155}Eu and ^{154}Eu whose absolute activity was well known. The intensities and the energies of the γ-rays emitted by this source (on the day of the calibration) are summarized in Table 2.5. A second source of ^{56}Co was used to cover a wider range of energies from 100 keV to 3450 keV. The ^{56}Co γ-ray spectrum obtained from the sum of all sixteen detectors is presented in Figure 2.18. The characteristics of the γ rays are provided in Table 2.6.

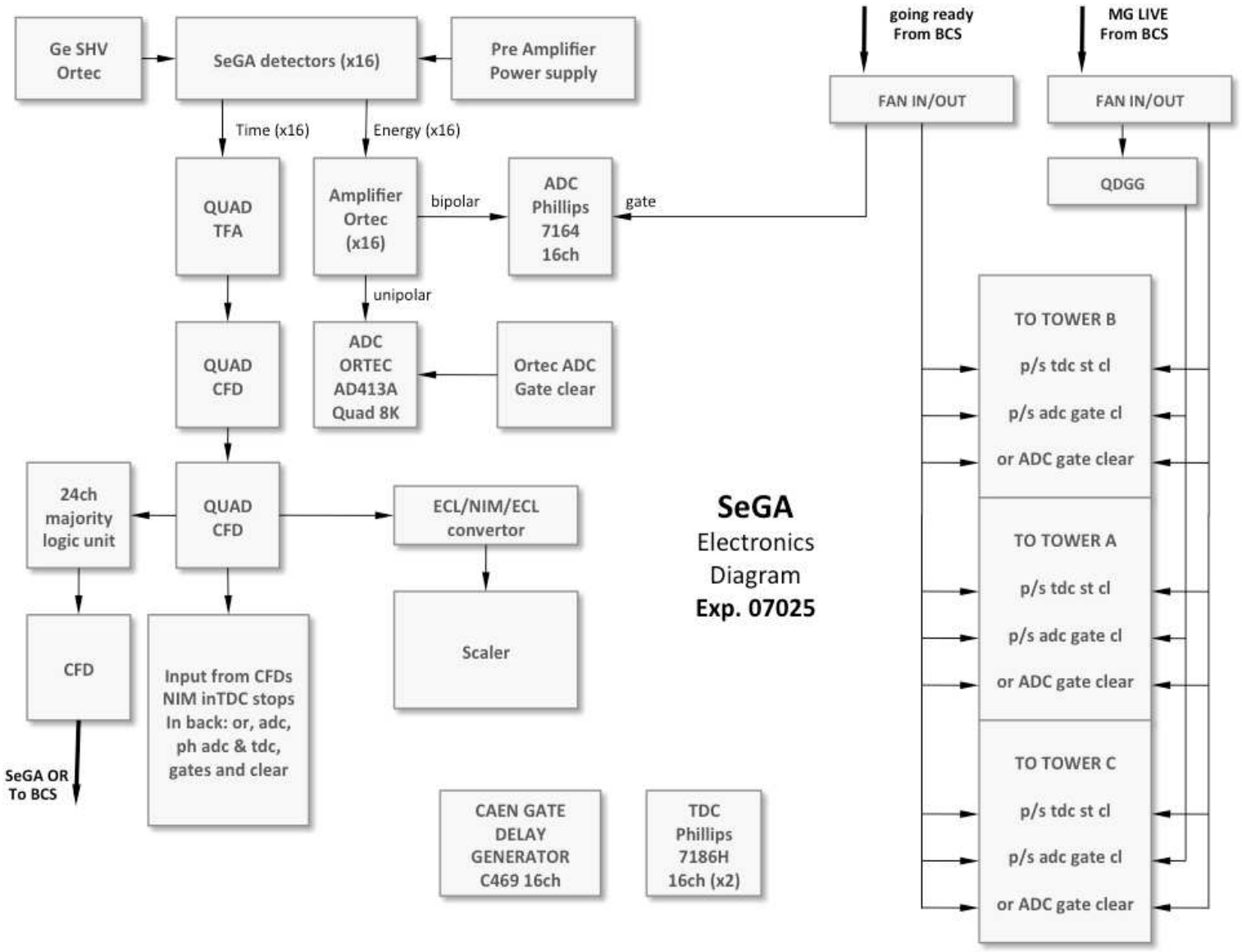

Figure 2.17 – Electronics diagram of the output signal of one SEGA detector.

Nucleus	Energy (keV)	Intensity A_γ (γ h^{-1})	Uncertainty (%)
^{155}Eu, ^{154}Eu	42.8	1.39×10^7	1.3
^{155}Eu	86.5	1.31×10^6	0.9
^{155}Eu	105.3	9.12×10^5	1.3
^{154}Eu	123.1	2.18×10^7	0.8
^{154}Eu	247.7	3.69×10^6	0.6
^{154}Eu	591.8	2.64×10^6	0.6
^{154}Eu	723.3	1.07×10^7	0.6
^{154}Eu	873.2	6.50×10^6	0.7
^{154}Eu	996.3	5.57×10^6	0.9
^{154}Eu	1004.7	9.65×10^6	0.7
^{154}Eu	1274.5	1.86×10^7	0.5
^{154}Eu	1596.4	9.45×10^5	0.7

Table 2.5 – Energy and absolute intensities of the γ rays emitted from the ^{155}Eu/^{154}Eu mixed source as of May,1st 2010.

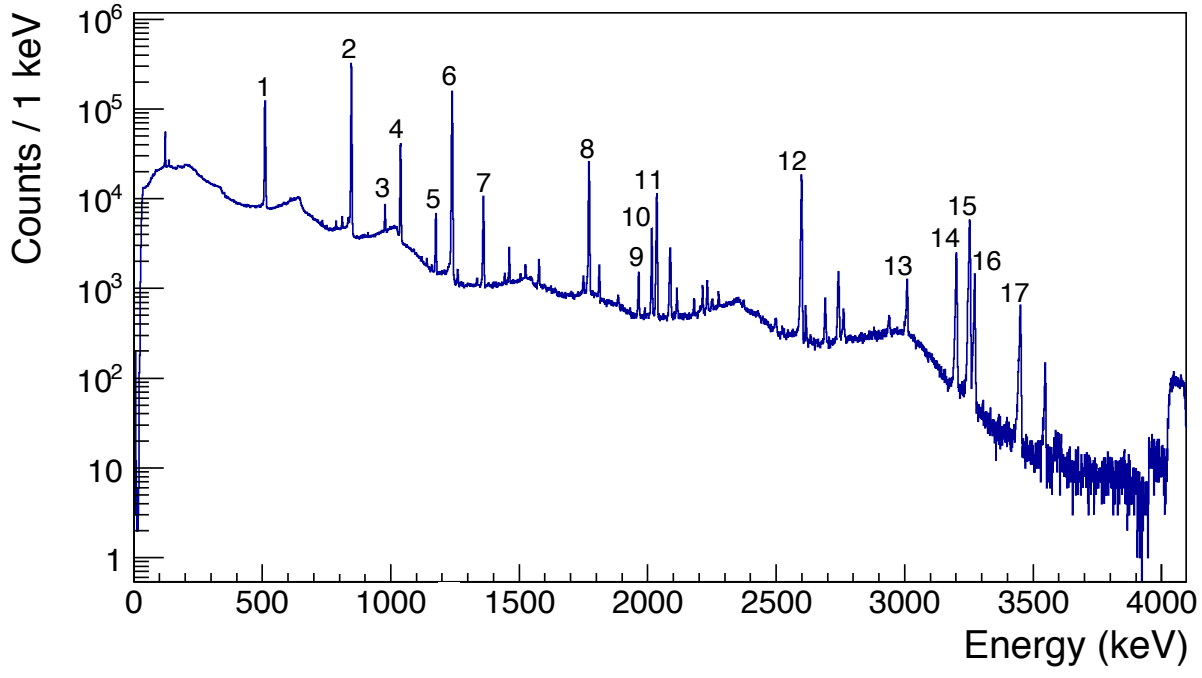

Figure 2.18 – Calibrated sum γ-ray spectrum of all 16 HPGe detectors of SeGA for the ^{56}Co source. The labels refer to the γ-ray energies summarized in Table 2.6.

#	Energy (keV)	Relative Intensity I_γ(%)
1	511.0	39 (3)
2	846.77	99.939 (9)
3	977.37	1.421 (6)
4	1037.84	14.05 (4)
5	1175.10	2.252 (6)
6	1238.29	66.46 (12)
7	1360.21	4.283 (12)
8	1771.36	15.41 (6)
9	1963.74	0.707 (4)
10	2015.22	3.016 (12)
11	2034.79	7.77 (3)
12	2598.50	16.97 (4)
13	3009.65	1.036 (13)
14	3202.03	3.209 (12)
15	3253.50	7.923 (21)
16	3273.08	1.8759 (20)
17	3451.23	0.949 (5)

Table 2.6 – Energy and relative intensities of the γ rays emitted from the ^{56}Co source.

The function used to fit the γ-ray spectra is the same as the one defined in the *GF3 RadWare* program [Rad]. It consists of a Gaussian distribution (Equation (2.5)), a skewed Gaussian (Equation (2.6)) to take into account the charge collection default at low energies, and a step function (Equation (2.7)) to account for the Compton background underneath the γ-ray photopeak. The functions are:

$$y = A\, e^{\frac{-(x-\mu)^2}{2\sigma^2}} \tag{2.5}$$

$$+ \frac{A}{\nu}\, e^{\frac{(x-\mu)}{\beta}} \operatorname{erfc}\left(\frac{(\mathrm{x}-\mu)}{\sqrt{2}\sigma} + \frac{\sigma}{\sqrt{2}\beta}\right) \tag{2.6}$$

$$+ B \operatorname{erfc}\left(\frac{(\mathrm{x}-\mu)}{\sqrt{2}\sigma}\right) \tag{2.7}$$

where μ is the centroid of the Gaussian and σ is its standard deviation. The parameter β is the decay constant on low-energy side of the peak and ν is the reduction factor of the skewed Gaussian. Both were fixed at the values given by the fit of the 996.3-keV and 1004.7-keV γ-ray transitions from ^{154}Eu.

The SeGA energy calibration was performed using a quadratic fit function, as shown in Figure 2.19. After the SeGA detectors were each calibrated individually, all 16 spectra from each detector were then summed. The difference between the calibrated energy of each peak and the expected value is calculated from the sum spectrum and is plotted in Figure 2.20. This plot indicates the highly non-linear behaviour of the SeGA detectors that is well known. A part of this behaviour is due to the low-energy response of detectors themselves while the remaining is associated with non-linearities in the Ortec AD413 ADCs used to digitize the shaped signals. With the present energy calibration, the energy resolution achieved is 1.8 keV (1σ) at an energy of 1 MeV.

The SeGA efficiency calibration was performed using the same SRM (^{154}Eu and ^{155}Eu) and ^{56}Co sources. Since the absolute activity of the ^{56}Co was not known very precisely, the relative intensities of γ-ray transitions were measured and a normalization factor, determined by the fit procedure, was applied relative to the SRM source. The function used to fit the efficiency data was taken from Ref. [Kis98] since it is applicable over a wide range of energies. The function can be written as:

$$\epsilon = \frac{N_{det}}{N_{em}} \tag{2.8}$$

$$= \frac{N_{det}}{A_\gamma(\Delta T)} \frac{1}{(1-\tau)} \tag{2.9}$$

$$= \exp\left(\sum_{\mathrm{i}=0}^{6} \mathrm{a_i}(\mathrm{lnE})^{\mathrm{i}}\right), \tag{2.10}$$

where N_{det} is the area of the peak deduced from the fit results obtained with *GF3 RadWare*, N_{em} is the number of emitted γ rays, $A_\gamma(\Delta T)$ is the activity of the source multiplied by the branching ratio of the γ-ray transitions, ΔT is the total acquisition time and τ is the dead time of the data-acquisition system. Table 2.7 summarizes the efficiency calibration coefficients (a_i) deduced in the present work. This results give an array photopeak efficiency of 10.5% at 662 keV and 6.8% at 1.3 MeV.

Two independent data acquisition systems were used to verify the efficiency calibration of the HPGe array. In addition to the standard NSCL data acquisition system, a single-channel Canberra data acquisition system was also used. Contrary to the standard acquisition system, for which the trigger signal is common and given by any HPGe detector (called the *OR trigger*), the Canberra system used only the individual trigger signals and calibrations were performed on a detector-by-detector basis. Figure 2.21 shows the efficiency curve using the standard acquisition system with the *OR trigger*. In Figure 2.22, the efficiency curves of the two acquisition systems are compared for a single detector using the ^{155}Eu/^{154}Eu mixed source. The difference in efficiency between both data acquisition reaches a maximum of $\simeq$2% of the

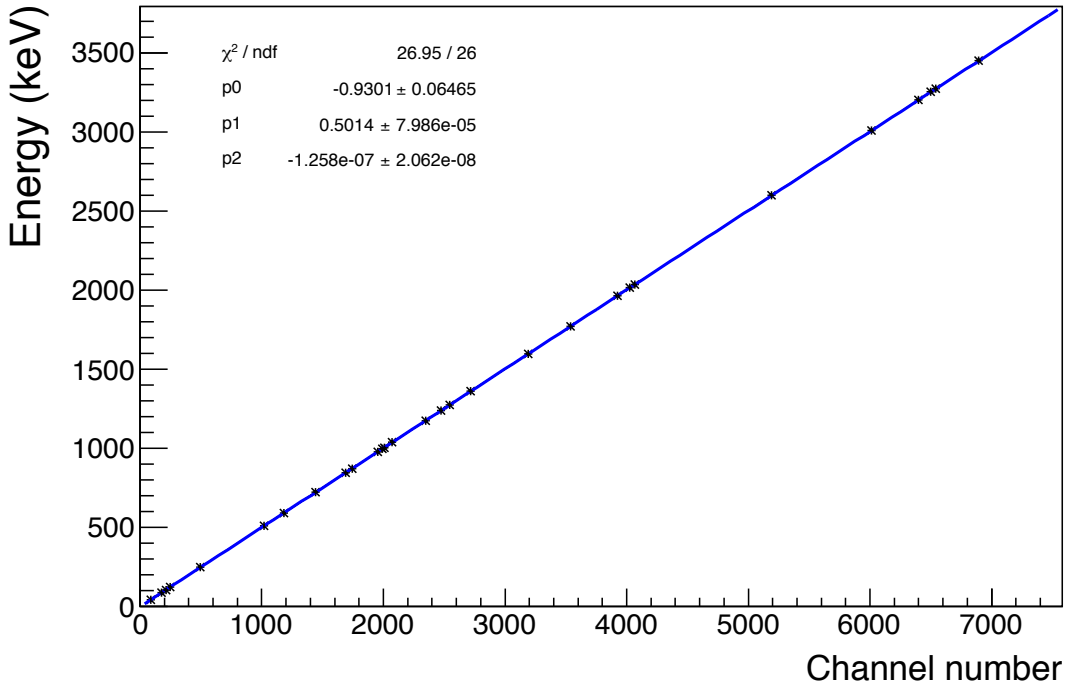

Figure 2.19 – Energy calibration of one of the 16 HPGe detectors performed using the mixed ^{155}Eu/^{154}Eu and the ^{56}Co sources with a quadratic fit function (in blue).

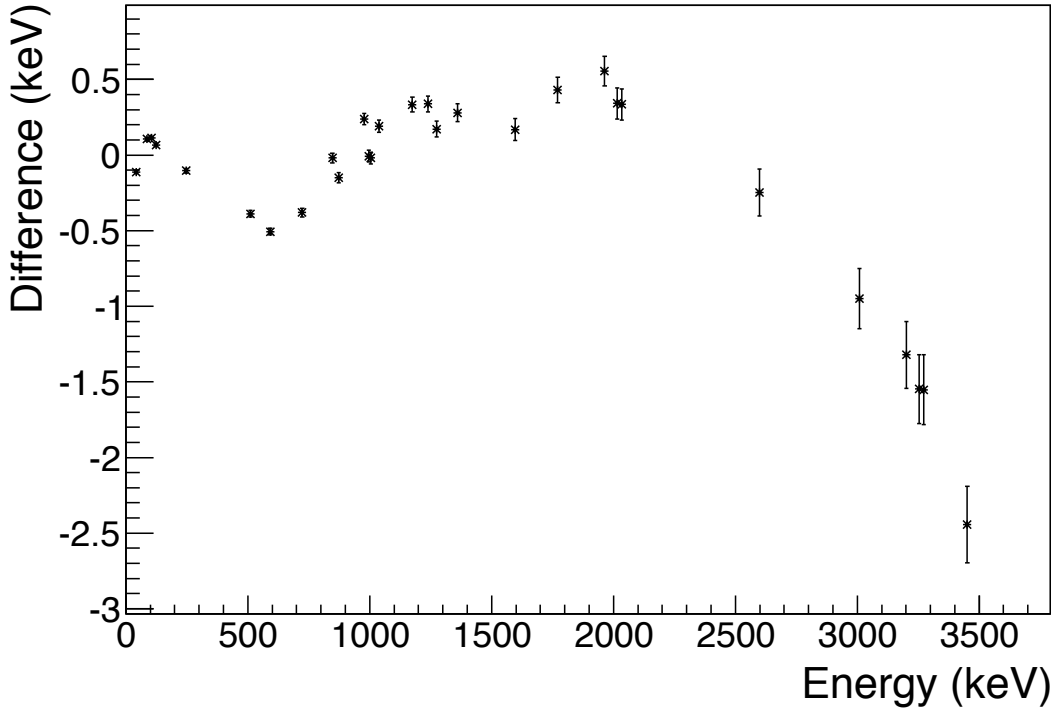

Figure 2.20 – Difference between the energy from the calibration and the previously measured γ-ray energies after summing the 16 HPGe detectors.

Coefficient results	
a_0 = -776 (261)	a_4 = -6.5 (24)
a_1 = 725 (248)	a_5 = 0.40 (15)
a_2 = -279 (98)	a_6 = -0.010 (4)
a_3 = 57 (20)	

Table 2.7 – Calibration coefficients obtained by fitting the ^{155}Eu/^{154}Eu and the ^{56}Co data with the function of Eqn. 2.10.

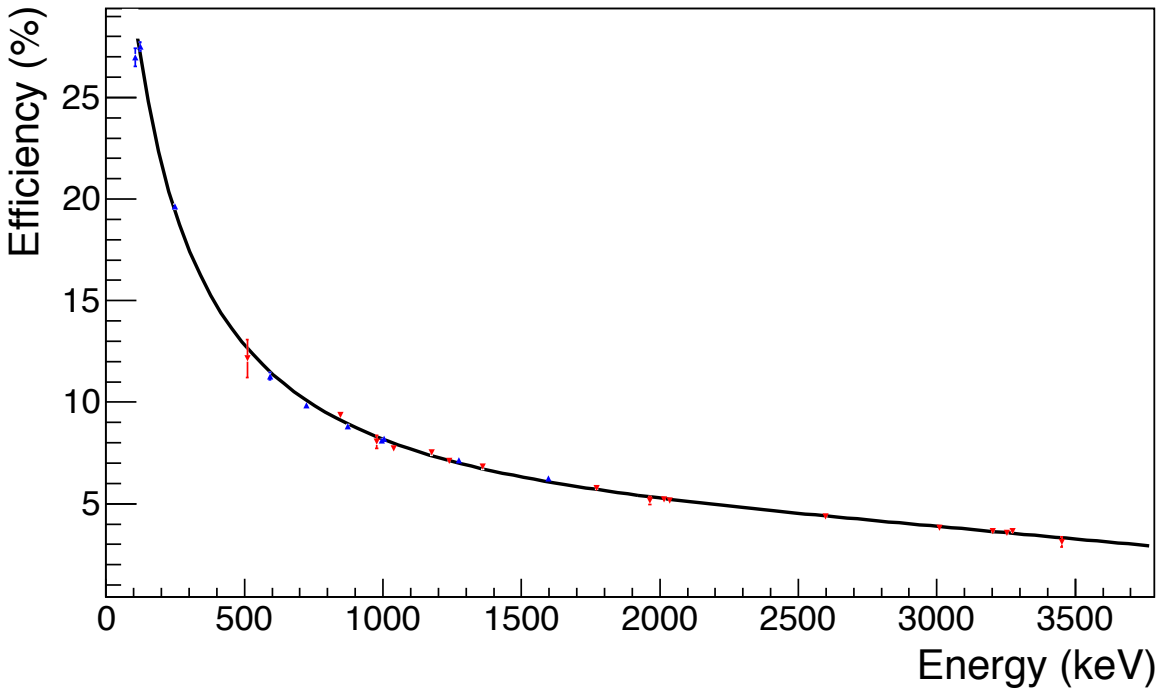

Figure 2.21 – Efficiency curve for SeGA in the *OR*-trigger mode was performed using the ^{155}Eu/^{154}Eu source (in blue) and the ^{56}Co source (in red). In black, the fit function is used to determine the fit coefficients (Eqn.2.10). The reduce χ^2 value of this fit is 5.73.

efficiency value itself in the energy range of the calibration. This Canberra acquisition was not used during the experiment, but it provided an independent means with which to verify the accuracy of the efficiency calibration. The final efficiency values are thus taken from the NSCL data acquisition as presented in Fig. 2.21 and in Table 2.7.

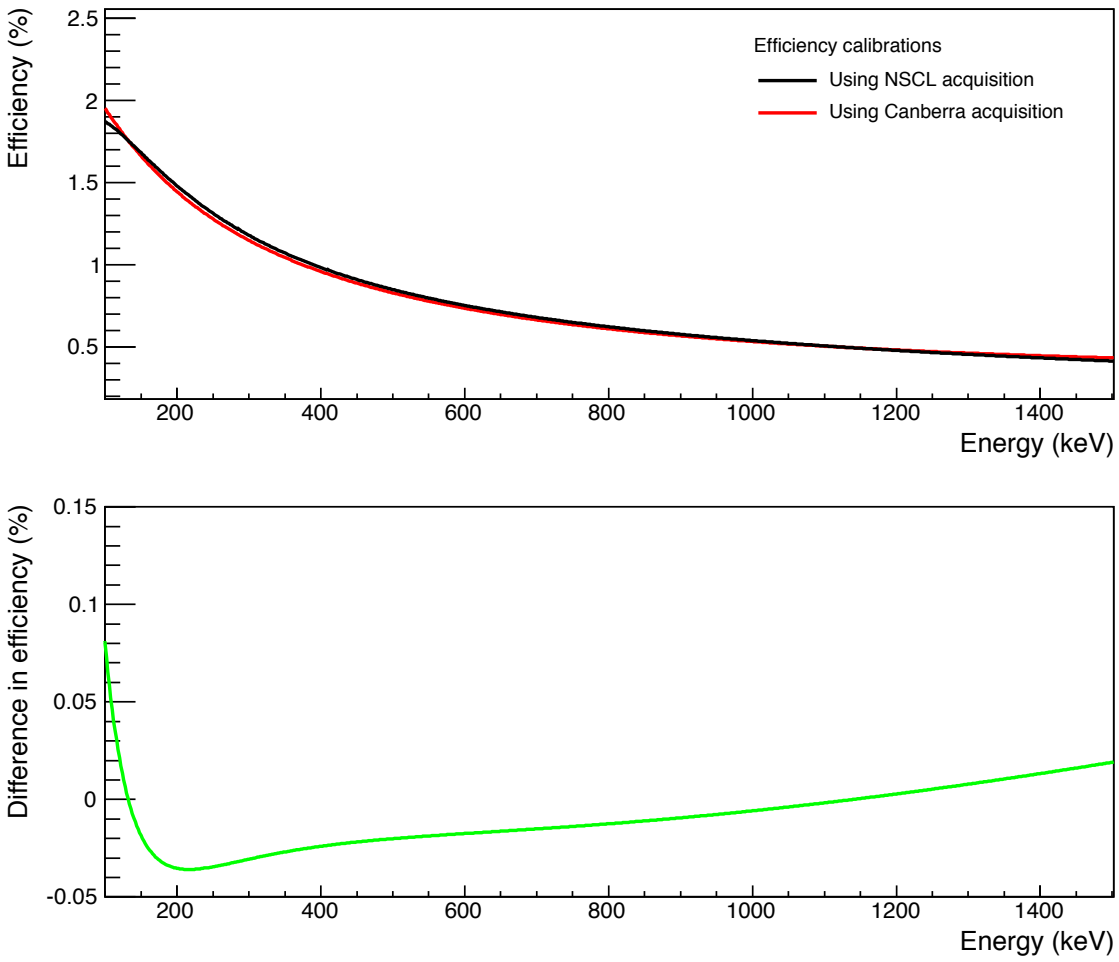

Figure 2.22 – Comparison between the two data acquisition systems for the same HPGe detector, SeGA 0. Top: the efficiency calculated using the standard NSCL data acquisition system (black line) and the Canberra system are slightly different. Bottom: the green line shows the difference between the efficiencies derived from these two systems.

2.3 Conclusion

In the present chapter, the production, selection and purification of the secondary cocktail beams at NSCL using the A1900 fragment separator were presented. An ^{36}Ar beam was accelerated by the coupled cyclotron facility at NSCL and impinged a ^{nat}Be target. The cocktail beam was selected, and purified in a first step using the A1900 fragment separator. A second stage of purification was achieved using the RFFS device. This was essential as it provided a lower overall intensity and a higher beam purity before implantation into the second DSSD of the Beta Counting System.

The implant-and-decay detection station was described and calibrations of the DSSD detectors were presented using a ^{228}Th α-decay source for the gain matching of the individual strips. The absolute energy calibration used known proton and α particles that were emitted following the β decays of both ^{20}Mg, ^{20}Na and ^{23}Si that were delivered in same settings of the separator. Surrounding the DSSDs, 16 HPGe detectors of the SeGA array were calibrated in energy and in efficiency to provide coincident γ-ray detection.

The software logic was also presented for the implant-and-decay correlation process in the analysis. The particle identification of the implanted ions utilized the ΔE-ToF method, and the γ-ray and the charged particles detected in coincidence will be used to build the decay level schemes, including the proton-unbound excited states in the daughter nuclei. In the next chapter, the analysis method will be described using the well-known β-delayed proton decay of ^{20}Mg. The spectroscopy performed in this work will be compared to previous experiments to validate both the calibration and the analysis processes.

Chapter 3

β-delayed proton decay of ^{20}Mg

The decay-implantation correlation analysis program that was introduced in the previous chapter will be presented in detail in the present chapter using the well-known decay of ^{20}Mg. A secondary beam of ^{20}Mg ions was produced as one of the contaminants in the cocktail beam that was delivered for the ^{22}Si part of the experiment (described in Chapter 5). The presence of this well known βp emitter in the beam provided an excellent opportunity to test the accuracy of the energy calibration, tune the decay-implant correlation algorithm, and verify the analysis method. For 17 hours, the A1900 spectrometer and the RFFS separator were optimized for ^{20}Mg ions, which provided sufficient statistics for these tests.

The decay of ^{20}Mg follows two distinct pathways that both result in the emission of charged particles:

- $^{20}\mathrm{Mg} \xrightarrow{\beta} {}^{20}\mathrm{Na}^{*} \xrightarrow{p} {}^{19}\mathrm{Ne}^{*}$ or
- $^{20}\mathrm{Mg} \xrightarrow{\beta} {}^{20}\mathrm{Na} \xrightarrow{\beta} {}^{20}\mathrm{Ne}^{*} \xrightarrow{\alpha} {}^{16}\mathrm{O}$

Both of these decay pathways (βp and $\beta\alpha$) are well known and have been previously measured with high statistics [Pie95, Wal12]. In the present work, protons and α particles detected following the decays of ^{20}Mg ions implanted in the central DSSD combined with coincident γ rays detected in SeGA were used to construct the ^{20}Mg decay level scheme and compare to previous studies. Measurements of the β decay branching ratios and the ^{20}Mg half-life were also performed and are compared to previous measurements.

3.1 ^{20}Mg: a well known βp emitter

The study of ^{20}Mg β decay and β-delayed proton decay has been the focus of several previous experiments [Pie95, Wal12, Gor92] that were motivated by astrophysical interests. The average half-life of ^{20}Mg is 90.8±2.4 ms [Wan12] and the decay level scheme derived from these measurements is presented in Figure 3.1. Approximately 70% of ^{20}Mg β decays proceed to the daughter, ^{20}Na, while ∼30% populate unbound levels in ^{20}Na that decay by β-delayed proton emission to states in ^{19}Ne [Pie95]. Virtually all of the 1^+ states above the proton separation threshold at $Sp = 2190.4$ keV that can be populated by β decay are known. The isobaric analogue to the ^{20}Mg 0^+ ground state is the 0^+ state located at 6521 keV excitation in ^{20}Na. From the β-decay selection rules, decay from the ^{20}Mg ground state to the ^{20}Na ground state (2^+) is second forbidden and is therefore highly suppressed.

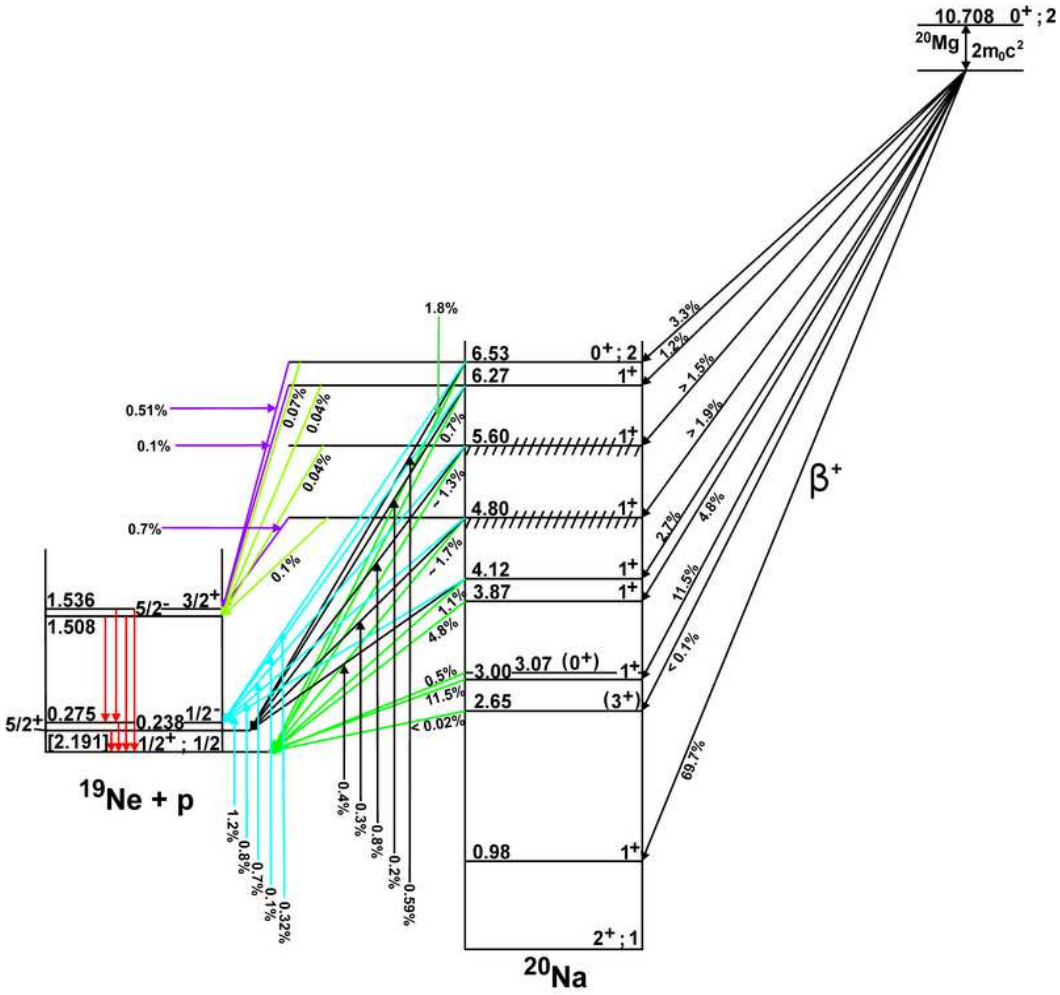

Figure 3.1 – Decay scheme of ^{20}Mg (figure from the TUNL website [TUN]).

The β-decay of the daughter ^{20}Na has also been the subject of many studies [Cli89, Fre77, Lau13] and the energies of the β-delayed α particles are known with high precision.

Taking advantage of the presence of ^{20}Mg as a contaminant in the cocktail beam, this well-known βp emitter was used to validate the analysis procedure and test the correlation algorithm. The A1900 and RFFS separator were optimized on a ^{20}Mg secondary beam setting for a total of 17 hours. The decay station was not completely optimized for ^{20}Mg as the Si detector (PIN) thicknesses were chosen for the higher energy beams of ^{22,23}Si. Nonetheless, based on the magnetic rigidity of the ^{20}Mg beam, the implantation depth of the ^{20}Mg ions into DSSD2 was deduced to be 27 μm out of the 525 μm total. The fact that the ions were implanted near the surface of DSSD2 (or very deeply into DSSD1 and did not reach DSSD2) resulted in a decrease to the overall efficiency for proton detection (high-energy protons may escape if they are emitted towards this nearest surface) and the overall size of the β summing effect. As ^{20}Mg decay offers an ideal calibration, these conditions were considered to be acceptable.

Identification of ^{20}Mg decays was performed by applying a contour to the PID spectrum that was obtained using the ΔE-ToF method. After the correlation process, 1.75×10^5 events were assigned to the implant and decay of ^{20}Mg over 17 hours of run time. For the analysis of ^{20}Mg, the correlation time and area were fixed at T_{max} = 1 s and 3x3 pixels, respectively. Figure 3.2 shows the PID spectrum after the correlation process.

In the most recent work of Wallace *et al.* [Wal12], a beam of ^{20}Mg was produced at Texas A&M University and implanted into a very thin 45 μm DSSD. The resulting charged-particle spectrum is presented in Figure 3.3 where it is compared to the spectrum obtained in the present work. At low energies, our spectrum is dominated by a large β background that prevents the identification of many of the transitions observed in Ref. [Wal12] that have the smallest branching ratios. High-energy tails observed on each of the peaks in the present work clearly show the effect of β summing in the thick (525 μm) implantation detector. The resolution in our experiment is approximately 90 keV for the proton group at 1 MeV. The high resolution obtained in Ref. [Wal12] was thus primarily due to their use of a much thinner detector that minimizes this effect.

The shapes of the peaks are characteristic of β-delayed charged-particle emission. For fitting purposes, their shapes were described using the convolution of a Gaussian distribution, for the proton or α-particle emission, with a Landau distribution, for the high-energy tail caused by β summing. Peak shapes were fit using the ROOT [Bru97] program from CERN, in order to extract the position and the area of the peaks. The width of the Gaussian distribution was fixed according to the intrinsic resolution of the detector (extrapolated from the ^{228}Th analysis) and was $\sim$ 64 keV for an α particle with an energy of 1 MeV. The width of the Landau distribution was treated as a free parameter.

The energies obtained for the proton groups observed in Figure 3.3 are compared in Table 3.1 to the results of Ref. [Wal12]. For the 4 most intense proton groups observed between

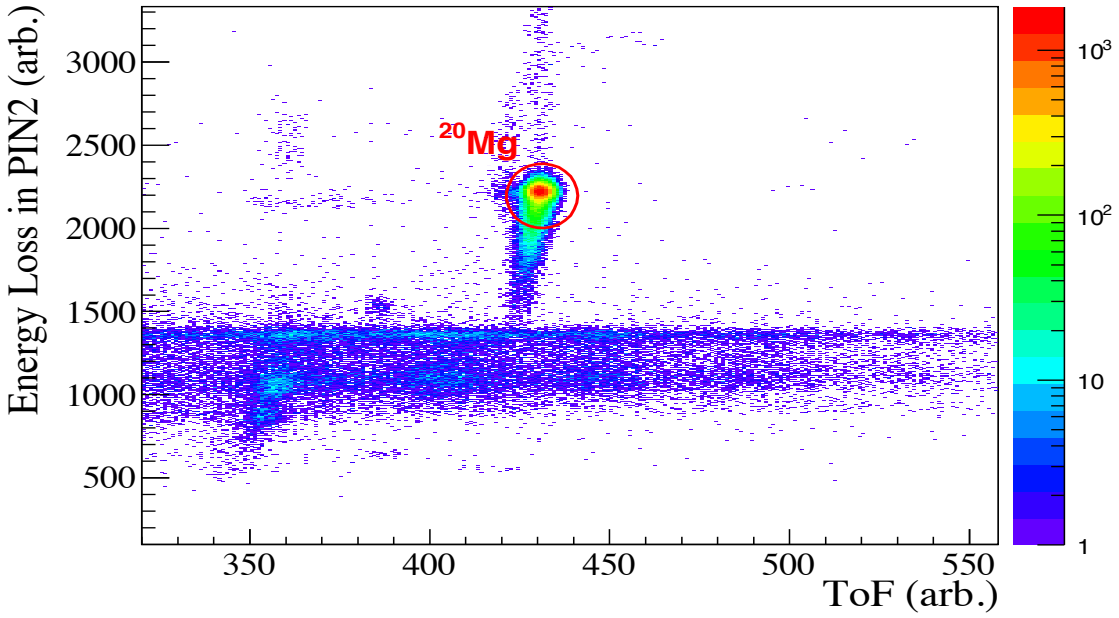

Figure 3.2 – PID spectrum of the ^{20}Mg secondary beam at the exit of the RFFS. The counts below the ^{20}Mg are due to the presence of the contaminant ^{16}O that was produced with very high intensity and scattered by the slits of the RFFS. Since this is a stable nucleus, its presence does not affect the ^{20}Mg measurement. No other contaminants were present in the beam.

800 keV and 4332 keV, there is excellent agreement between the derived energies. Although the experiment of Wallace did not use γ-ray detection, the level energies in the β-decay daughter ^{20}Na and the states they feed in the ^{19}Ne βp daughter are known from Ref. [Pie95].

#	E_{proton} (keV) (This work)	E_{proton} (keV) [Wal12]	$E_i^*(^{20}\mathrm{Na})$ (keV) [Wal12]	Final state in ^{19}Ne (keV)
1	800 (2)	797 (2)	2987 (2)	g.s.
		885 (15)	3075 (15)	g.s.
		∼1050	∼4780	238, 275
2	1675 (2)	1670 (10)	3860 (10)	g.s.
		1903 (5)	4093 (5)	g.s.
		∼2340	∼4780	1508, 1536
3	4054 (11)	∼4080	∼6270	g.s.
			6522	238, 275
4	4326 (11)	4332 (16)	6522 (16)	g.s.

Table 3.1 – Proton groups from the ungated spectrum are compared to the most recent study of Ref. [Wal12]. Only the four most intense groups were observed in the present study. The energies preceded by the approximate (∼) sign correspond to the average energy of unresolved groups of proton transitions. Energies of the final states fed by the proton transitions are derived from Ref. [Pie95].

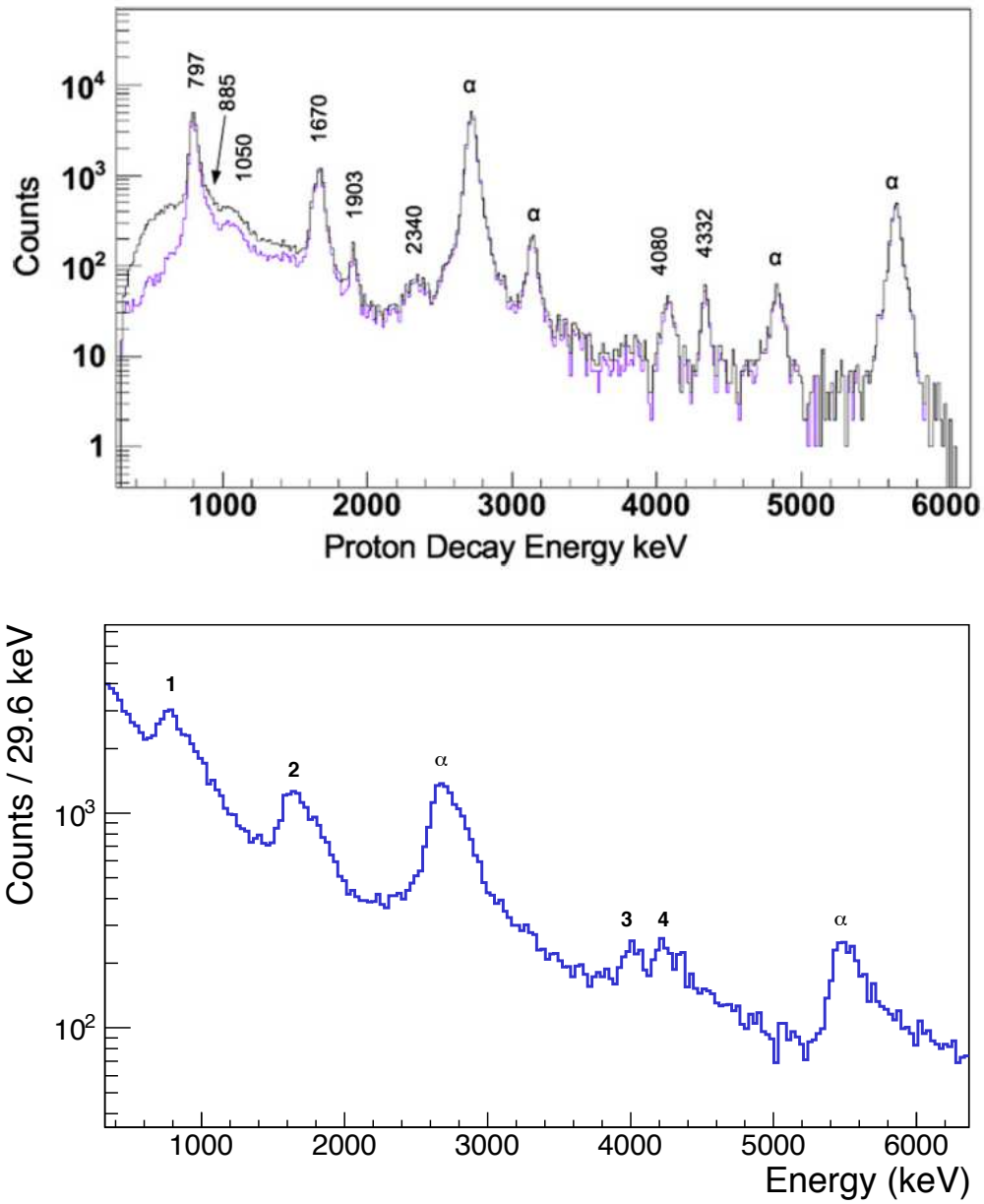

Figure 3.3 – Comparison of the β-delayed proton and α particle spectra obtained by Wallace [Wal12] (top, black spectrum - before background subtraction and purple - after background subtraction) and the present study (bottom).

An even older ^{20}Mg decay experiment was performed by Piechaczek *et* al. [Pie95] at GANIL. The secondary beam of ^{20}Mg was produced and purified with the LISE fragment separator before being implanted into a 300 μm thick position-sensitive silicon strip detector. This implantation detector was mounted between 2 thicker (500 μm) silicon detectors that were used to detect the β particles in order to reduce some of the β-summing effects in the proton detector. Three HPGe detectors surrounded the Si array to provide γ-ray detection from the de-excitation of the daughter nuclei. In the very same way as described below in the present work, γ-ray gates were applied to the proton spectrum to identify the energies of the coincident proton groups and build the decay level scheme. The corresponding γ-ray gated proton spectra obtained by Piechaczek [Pie95] are presented in Figure 3.6. The excitation energies of the excited states in ^{20}Na were deduced with relatively high precision. The energy of the IAS to the ^{20}Mg ground state was measured to be 6522(16) keV with a β branching ratio of 3.3%. From Table 3.1 above, the measurement of the proton at 4326(11) keV in the present work, combined with the proton separation energy of $Sp = 2190.4$ keV, yields the value 6516(11) keV for the energy of the IAS, which is in excellent agreement with the previous measurement [Pie95]. The energy of the IAS has recently been measured with high precision to be 6498.4±0.4 keV [Gla15] using the low-intensity γ-ray de-excitation of the IAS to the ground state.

3.2 γ-ray spectra from ^{20}Mg decay

The γ-ray spectra obtained from the 16 HPGe detectors and correlated to decays of ^{20}Mg is presented in Figure 3.4. Table 3.2 presents a summary of the 5 γ-ray transitions that were identified. This allows us to unambiguously determine which excited states in the daughter nuclei were populated, and therefore which decay pathway was followed:

- The measured γ-rays at 236±1.2 keV, 273±1.3 keV and 1299±3.7 keV correspond to known γ-ray transitions at 238 keV, 275 keV and 1298 keV that are emitted by the first three excited states in ^{19}Ne. Both the 238-keV and 275-keV transitions feed the ground state. The γ-ray at 1298 keV is the de-excitation from the third excited state at 1536 keV ($3/2^+$) to the $5/2^+$ state at 238 keV. All three transitions are due to βp decay from ^{20}Mg.

- The γ-ray at 984 keV comes from the de-excitation of the first 1^+ excited state in ^{20}Na at 984 keV. The energy of this state is below the proton separation threshold and thus cannot decay to ^{19}Ne via delayed proton emission. The β branching ratio to this state is known to be 69.7% [Pie95].

- The γ-ray transition at 1633 keV is the de-excitation of the first excited 2^+ state in ^{20}Ne at 1633 keV. This nucleus is the β-decay daughter of ^{20}Na and is populated in the present experiment by the sequential β decay from ^{20}Mg to ^{20}Na to ^{20}Ne. This γ ray was observed

because the correlation time of 1 s used in the ^{20}Mg analysis is sufficiently long enough that some false correlations with decays of ^{20}Na ($T_{1/2}$ = 448 ms) can occur.

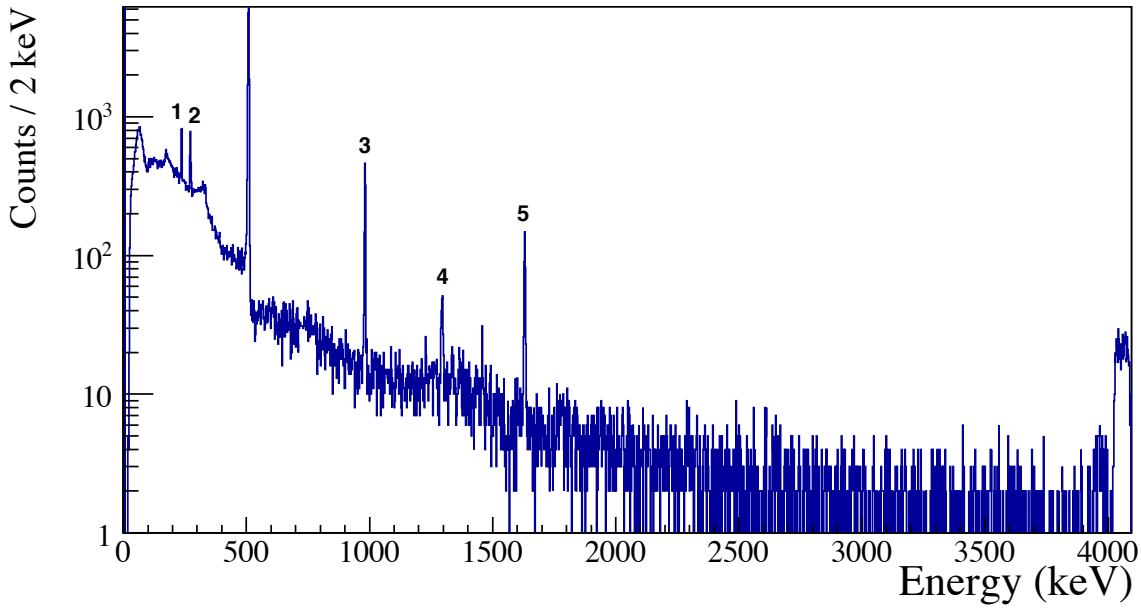

Figure 3.4 – Summed γ-ray spectrum correlated to ^{20}Mg β decays. In addition to the 511 keV created from positron decay, three transitions were identified (1,2, and 4) following the well known βp decay channel. The 984-keV transition (3) arises from β decay to the first 1^+ excited state in ^{20}Na. The 1633-keV transition (5) from the first excited state in ^{20}Ne was also observed.

#	Energy (keV)	$E_i(J^\pi) \rightarrow E_f(J^\pi)$	Daughter nucleus
1	236.0 (12)	$238(5/2^+) \rightarrow$ g.s.$(1/2^+)$	^{19}Ne (βp)
2	272.8 (13)	$275(1^-/2) \rightarrow$ g.s.$(1/2^+)$	^{19}Ne (βp)
3	983.1 (11)	$984(1^+) \rightarrow$ g.s.(2^+)	^{20}Na (β)
4	1299.4 (37)	$1536(3/2^+) \rightarrow 238(1^-/2)$	^{19}Ne (βp)
5	1630.5 (18)	$1633(2^+) \rightarrow$ g.s.(0^+)	^{20}Ne (2β)

Table 3.2 – Table of observed γ-ray transitions correlated with β decays of ^{20}Mg.

3.3 γ-ray gated proton spectra

Proton spectra in coincidence with the above γ-rays were obtained by applying a gate that was centred on the γ-ray transition of interest. In addition, two other gates were applied

immediately below and above the principal gate that were used to perform a background subtraction. An example of this procedure is presented in Figure 3.5 where the width of the background gates are normalized so that the number of channels in the γ-ray gate is identical to the number of channels in the background gate.

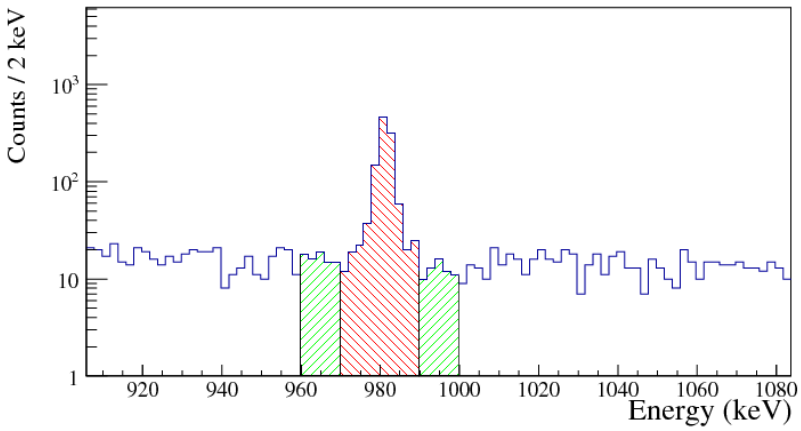

Figure 3.5 – The background from random coincidences and Compton scattering has to be subtracted from the γ-ray gated proton spectra. The range of the γ-ray gate was taken to be 4σ, with σ being the standard deviation of the γ-ray transition. Two γ-ray gates just below and just above (in green) the transition of interest were normalized to the number of bins in the central gate (in red) in order to perform the subtraction.

When using γ-ray gated spectra, the excitation energy of the level above the one-proton separation threshold in ^{20}Na was calculated according to:

$$E^*(^{20}\mathrm{Na}) = E_p + S_p + E_f^*(^{19}\mathrm{Ne}) \tag{3.1}$$

where E_p is the proton group energy, S_p is the proton separation energy in the daughter ($S_p = 2190$ (1) keV for ^{20}Na) and E_f^* is the energy of the excited state in the ^{19}Ne βp daughter. In the tables presented below, the measured excitation energies are compared to known values found in the literature. The uncertainties on the experimental values are the quadratic sum of the statistical uncertainties obtained from the fitting procedure (uncertainty on the peak centroids) combined with the uncertainties associated with the calibration of the DSSD detector.

It should be emphasized that γ-ray gated spectra for ^{20}Mg decay were obtained previously in Ref. [Pie95]. This provides another crucial test of the present experiment as it was used to test and confirm the particle-γ coincidence logic of the correlation algorithm. A summary of the previous work is presented in Figure 3.6. As the statistics in the present experiment were limited, we see only the 3 most intense γ-rays at 238 keV, 275 keV, and 1298 keV. A fourth γ ray at 1232 keV was observed in Ref. [Pie95] that corresponds to the de-excitation of the

$1508(3/2^+) \rightarrow 275(1/2^-)$ in ^{19}Ne that was not observed. In the following section, the gated proton spectra for these 3 primary γ rays will be described in detail and compared to those of Ref. [Pie95].

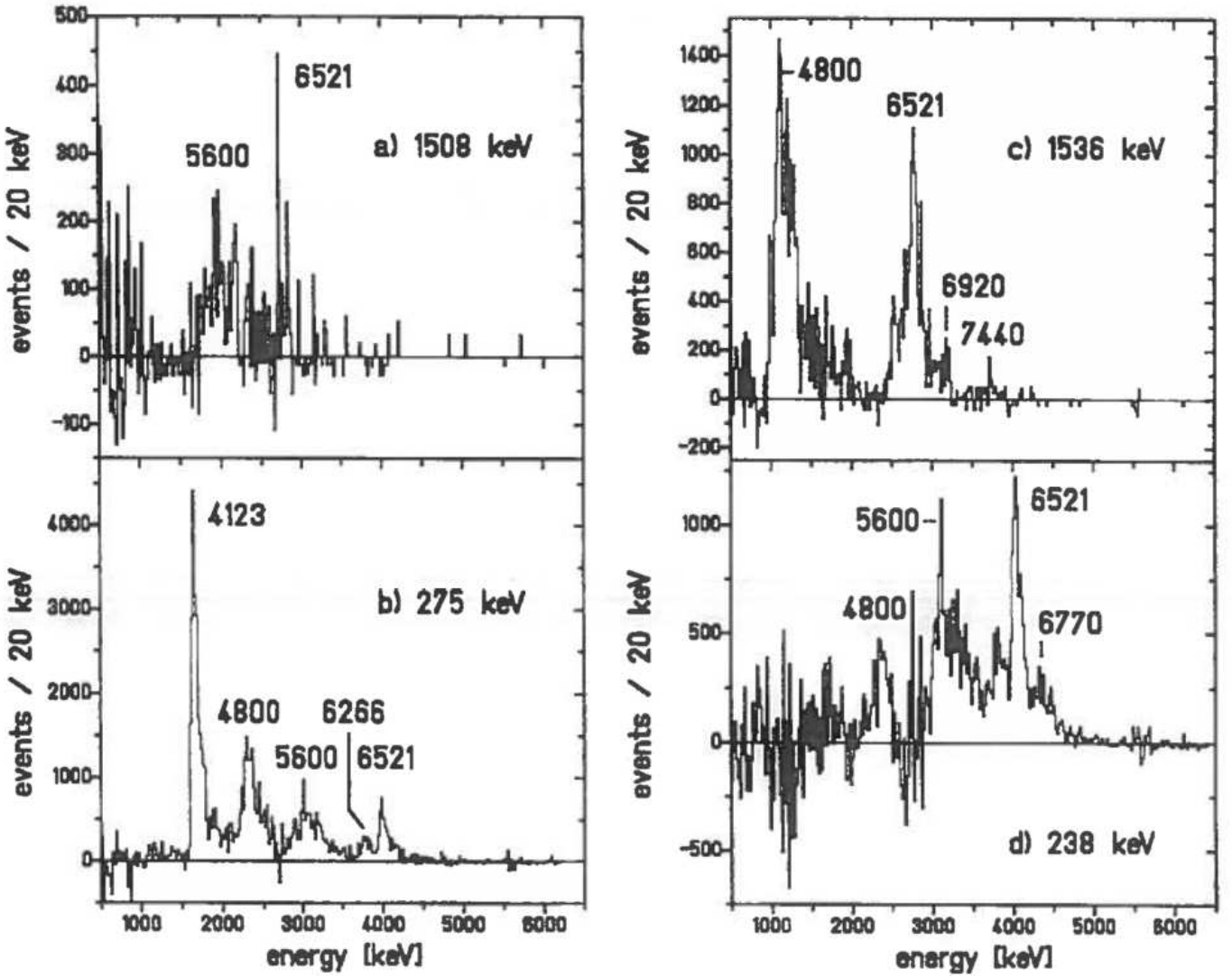

Figure 3.6 – Spectrum of charged particles in coincidence with different γ-ray gates, after background subtraction, in the previous experiment performed in Ref. [Pie95]. The numbers in the figures stand for the energy of the corresponding resonance above the proton threshold in ^{20}Na.

3.3.1 $E_\gamma = 275$ keV

The 275 keV γ-ray transition is from the de-excitation of ^{19}Ne from the first excited $1/2^-$ state at 275.09(13) keV to the ground state. The spectrum of charged particles emitted in coincidence with 275-keV γ rays, and after performing a background subtraction, is presented in Figure 3.7. Four proton transitions were observed, and the corresponding proton group and level energies are summarized in Table 3.3. In that fit procedure, the fit function was defined as the sum of four proton transition, as previously identified in Ref. [Pie95]. Most of the bins below 1.5 MeV have very high uncertainties due to the background subtraction process and thus won't be considered as belonging to a proton-transition candidate.

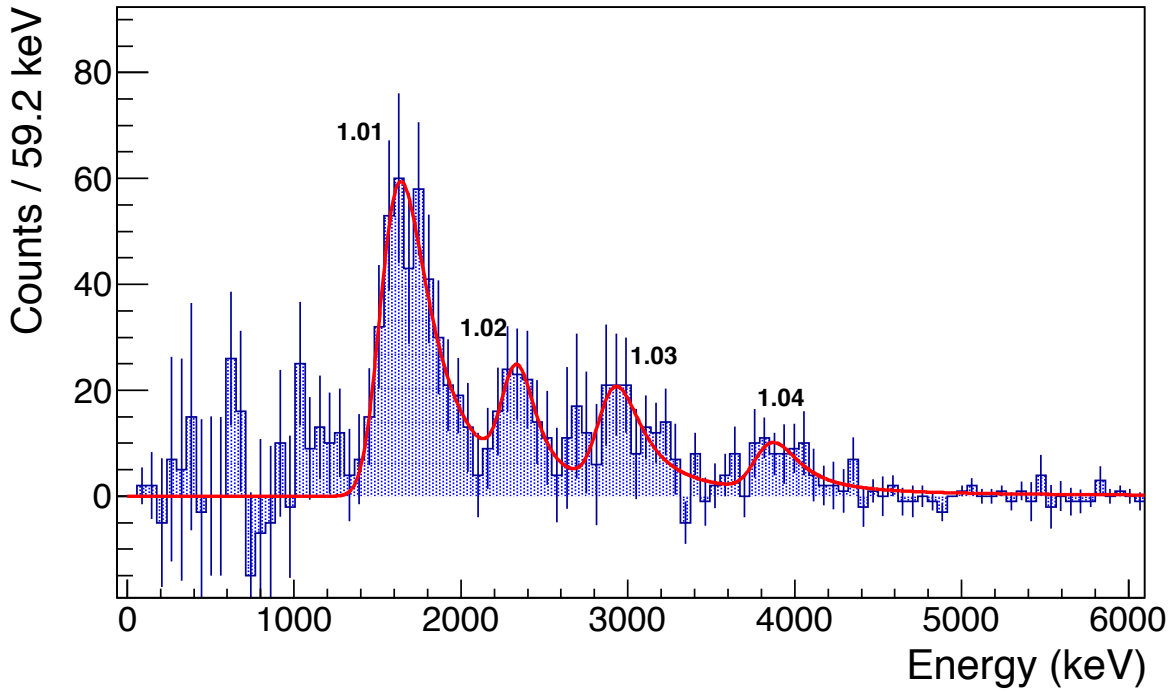

Figure 3.7 – Spectrum of charged particles in coincidence with $E_\gamma = 275$ keV, after background subtraction.

Comparing the present data of Figure 3.7 with that of Figure 3.6 .b), there is in general very good agreement. Despite having less statistics, one clearly sees the 4 main proton groups in coincidence with the 275 keV transition and the deduced proton energies are in very good agreement. In the previous work, an additional weak transition was observed, that led the authors to identify a level in ^{20}Na at 6226 keV. In the present work, this proton was not observed due to the limited statistics combined with the experimental resolution.

#	$E_{centroid}$	E_{proton} (keV)	E*(^{20}Na)	E*[Pie95]
1.01	1620 (21)	1689 (43)	4152 (43)	4123 (16)
1.02	2305 (38)	2385 (47)	4850 (47)	≈ 4800
1.03	2919 (55)	3006 (59)	5471 (59)	≈ 5600
1.04	3853 (64)	3939 (66)	6404 (66)	6521 (30)

Table 3.3 – Energies of the proton groups in the 275-keV γ-ray gated spectrum and their associated levels in ^{20}Na. In blue, the level energies obtained from Figure 3.6 .b) [Pie95] are indicated.

3.3.2 $E_\gamma = 1298$ keV

The 1298 keV γ-ray transition arises from the de-excitation of ^{19}Ne, from the state at 1536 keV ($3/2^+$) to the 238 keV ($5/2^+$) state. The background-subtracted spectrum of charged particles emitted in coincidence with 1298-keV γ rays is presented in Figure 3.8. This figure can be compared to the previous work in Figure 3.6 .c). In Table 3.4, the energies of the four proton groups that were observed are provided. In the following, these energies are compared to the previous measurements:

- The first and most intense transition (2.01 in Figure 3.8) is proton emission from what was described in Ref. [Pie95] as a group of states centred at $\sim$ 4800 keV.
- A second group (2.02) that could also come from several near-degenerate levels was not identified in Figure 3.6 .c) although the present measurement of the level energy gives a central value of 5528 keV that is in good agreement with the 5600 keV level that they obtained from other gates. It is proposed therefore to add this weak proton transition to the decay scheme that connects the 5600 keV level in ^{20}Na to the 1536 keV level in ^{19}Ne.
- Proton group 2.03 was also not identified on Figure 3.6 .c), although a value for the branching ratio of this transition was given in Table 2 of Ref [Pie95]. It is possible that the small unlabelled peak in Figure 3.6.c) that is just below the large transition labelled 6521 is this very same transition. Based on the shape of the spectrum in this region, a fit to these few counts was used to deduce a proton group energy that resulted a value of 2513(82) keV. This proton energy corresponds to a ^{20}Na excited state level energy of 6239(82) keV. This value is in very good agreement with a previously known 1^+ state at 6266 keV. It is therefore quite likely that this transition is the proton decay of the level at 6266 keV in ^{20}Na through the 1536 keV excited state in ^{19}Ne.
- The proton group 2.04 was observed in Figure 3.6 .c) and a proton energy of 2848(44) keV was deduced that corresponds to a ^{20}Na level energy of 6574(44) keV. This is in good agreement with the level previously identified at 6522 keV from Table 3.1. This level is the 0^+ isobaric analogue state to the ^{20}Mg ground state.

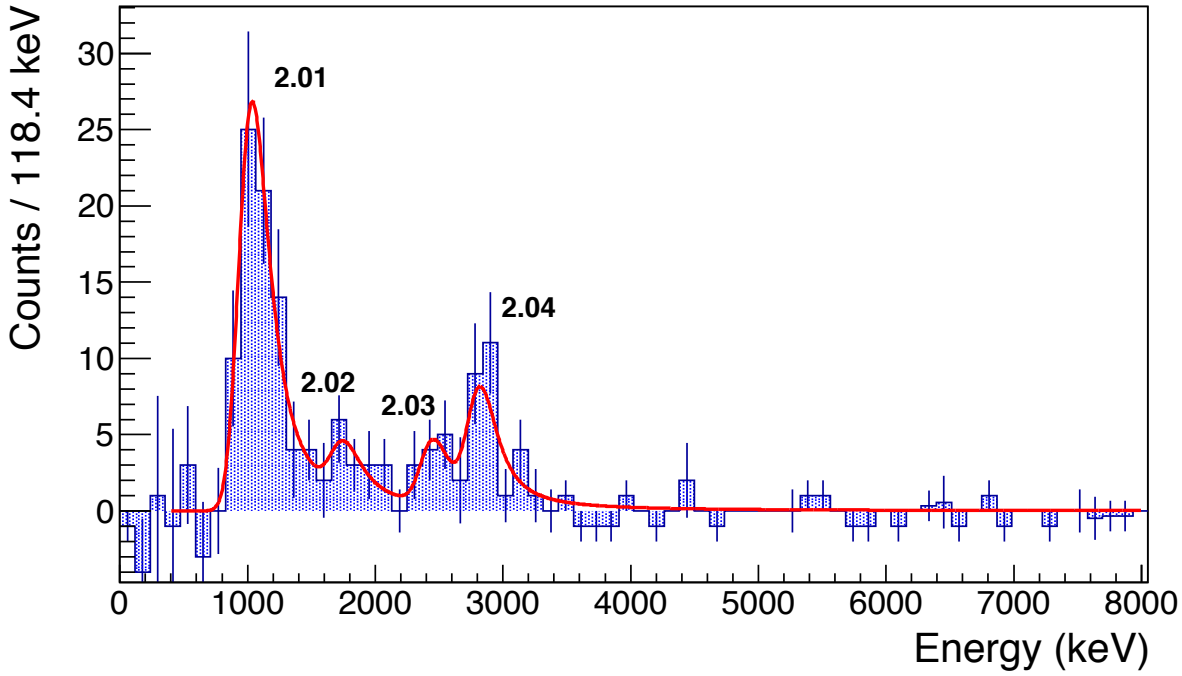

Figure 3.8 – Background subtracted spectrum of charged particles in coincidence with the 1298-keV γ rays.

#	$E_{centroid}$	E_{proton} (keV)	$E^*(^{20}Na)$	E^*[Pie95]
2.01	1010 (23)	1059 (52)	4785 (52)	4800
2.02	1733 (80)	1769 (87)	5528 (87)	–
2.03	2432 (78)	2513 (82)	6239 (82)	6266 (30)
2.04	2799 (38)	2848 (44)	6574 (44)	6521 (30)

Table 3.4 – Energies of the proton groups and ^{20}Na level energies in the 1298-keV gated spectrum.

3.3.3 $E_\gamma = 238$ keV

The 238-keV γ-ray transition is the first excited state in ^{19}Ne and has spin/parity $5/2^+$. It should be stressed that in this particular case, the 1298-keV γ ray described above feeds into this 238 keV level. In order to produce a γ-ray gated proton spectrum for decays to the 238-keV level, this upfeeding contribution from the 1298-keV γ ray must be subtracted. The resulting spectrum shown in Figure 3.9 was obtained from the 238-keV γ-ray gated spectrum from which a fraction of the 1298-keV γ-ray gated spectrum (Figure 3.8 above) was subtracted. This fraction is given by the ratio of the SeGA γ-ray detection efficiencies at 238 and 1298 keV. The

large uncertainties and negative counts for some channels are a result of the upfeeding subtraction. The standard γ-ray background subtraction was also applied using the same method as described above. This spectrum should be compared to Figure 3.6 .d).

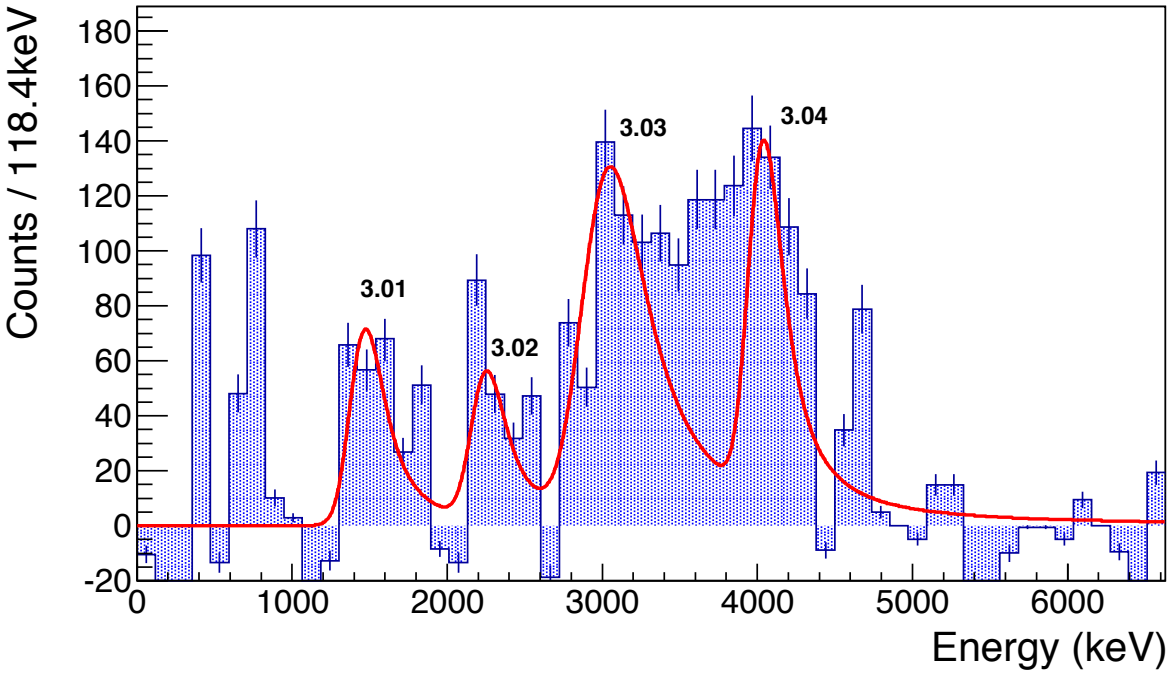

Figure 3.9 – Spectrum of charged particles in coincidence with $E_\gamma = 238$ keV after upfeeding and background subtractions. In the fit function a Gaussian distribution was added to take into account the wide and unresolved group of transitions between 3 MeV and 4 MeV that were also observed in Figure 3.6 d).

The three strongest proton groups that were observed in Ref. [Pie95] for this γ-ray gate correspond to levels in ^{20}Na at excitation energies of 4800 keV, 5600 keV and 6521 keV. Despite the low resolution and the relatively strong β-summing effects in our proton spectra, a fit of the 238-keV gated spectrum was attempted between 2.5 MeV and 4.5 MeV using two proton distributions (peak numbers 3.03 and 3.04 in Fig. 3.9). This fit gives two levels with energies of 5523 and 6527 keV. These are in good agreement with the values measured by Piechaczek [Pie95] and Wallace[Wal12].

Proton group 3.01 in Figure 3.9 was not identified in Ref. [Pie95] even though a broad group of counts is clearly observed in their spectrum. In the presents work, a transition is visible in the spectrum although the statistics are extremely limited. A fit to these counts yields a level in ^{20}Na with an excitation energy of 3908(63) keV, which could correspond to the known level at 4123 keV. The resulting fit, with a $\chi^2/\nu \approx 16$, is shown only for the purposes of comparison.

The energies of the four proton groups in coincidence with the 238 keV γ ray in ^{19}Ne and the excitation energies of the corresponding levels in ^{20}Na are presented in Table 3.5.

#	$E_{centroid}$	E_{proton} (keV)	$E^*(^{20}Na)$	E^*[Pie95]
3.01	1448 (42)	1480 (63)	3908 (63)	4123 (16)
3.02	2231 (15)	2310 (33)	4735 (33)	$\approx$ 4800
3.03	3011 (17)	3098 (27)	5523 (27)	$\approx$ 5600
3.04	4017 (38)	4105 (43)	6527 (43)	6521 (30)

Table 3.5 – Proton group energies in coincidence with the 238-keV γ ray and associated levels in ^{20}Na.

3.3.4 $E_\gamma = 984\,keV$

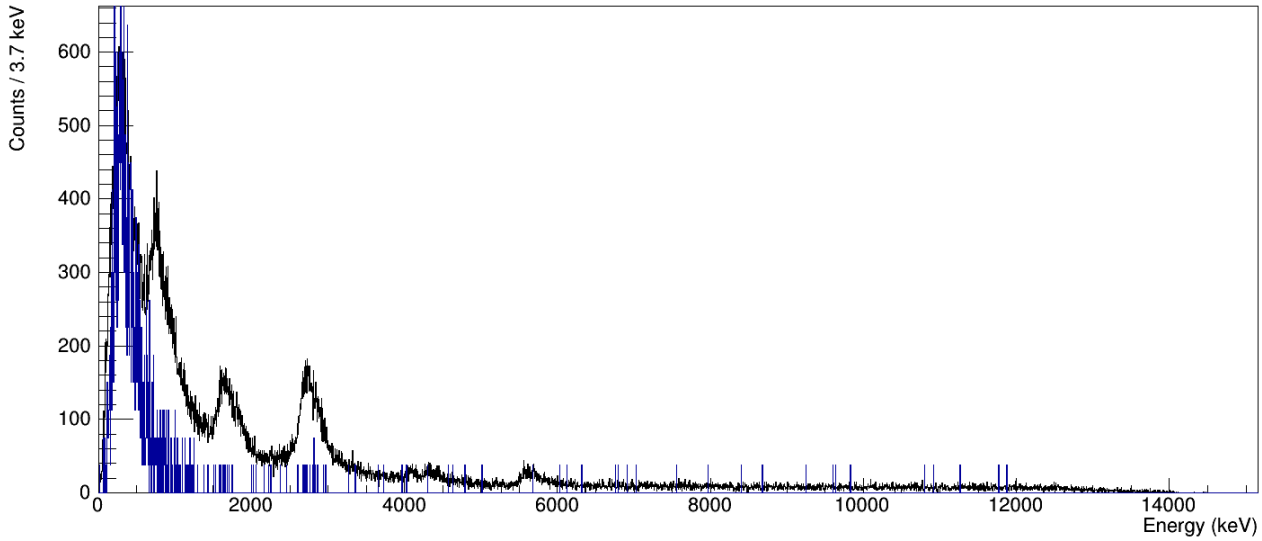

Figure 3.10 – The β-particle spectrum in coincidence with the 984 keV γ-ray transition is normalized (in blue) to emphasize the shape of the low energy β background in the ungated particle spectrum (in black).

The 984-keV γ-ray transition in Figure 3.4 was described above as the de-excitation of the first excited 1^+ level in ^{20}Na to the ground state. As this state is below the proton separation threshold, there are no β-delayed protons that will be emitted. For completeness, the corresponding γ-ray gated charged particle spectrum is shown in Figure 3.10. Overlayed with this spectrum is the ungated charged particle spectrum for all ^{20}Mg decays that was shown

previously in Figure 3.3.

From the 984-keV gated spectrum, one can see that the distribution of counts at low energy is due to β particles that leave sufficient energy in the DSSD to trigger the data acquisition. At higher energies, there are only very few random coincidences between the 984 keV and the strongest α particles from ^{20}Na decay.

3.4 ^{20}Na level energies

Based on the above analysis of the protons observed in this experiment and combined with the measured coincidences between protons and γ rays, the ^{20}Mg decay level scheme was constructed and the energies of the proton unbound levels in the daughter ^{20}Na were deduced. Five discrete levels were observed in the present work that are in very good agreement with the 1^+ states identified in the previous decay experiments [Pie95, Wal12]. The ^{20}Na excited-state energies for each of the γ-ray gates are summarized in Table 3.6. If one level decays by proton emission to several different states in ^{19}Ne, the weighted average of the energies deduced from each of these pathways was used to obtain the level energy. For the groups of nearly degenerate levels at ∼4800 keV and ∼5600 keV, only the central value is provided in Table 3.6. The ^{20}Na level energies obtained in the present work are in good agreement with the values given in Ref. [Wal12], although they are typically about a factor of 2 to 5 times less precise.

$1/2^+$, g.s.	$5/2^+$, 238 keV	$1/2^-$, 275 keV	$3/2^+$, 1536 keV	This work	Adopted value
2990 (49)				2990 (49)	3001 (2)
3865 (37)				3865 (37)	3871 (9)
		4152 (43)		4152 (43)	4123 (16)
	4735 (33)	4850 (47)	4785 (52)	4774	≈4800
	5523 (27)	5471 (59)	5528 (87)	5515	≈5600
6244 (23)			6239 (82)	6244 (22)	6266 (30)
6516 (25)	6527 (43)	6404 (66)	6574 (44)	6519 (19)	6521 (30)

Table 3.6 – Summary of the ^{20}Na level energies (in keV) deduced from the β-delayed proton groups observed in the γ-ray gated spectrum and the ungated spectrum. In the last column, the adopted values were taken from Ref. [Wal12].

3.5 Relative decay branching ratios

In the present experiment, the threshold of the DSSD was set relatively high since the goal was to trigger on protons or other charged particles that are emitted in approximately 100%

of ^{22,23}Si decays. For ^{20}Mg, that has a $\sim$ 70% β-only branch to ^{20}Na, many of these β-singles events would not have left sufficient energy in the detector to exceed the energy threshold and trigger the data acquisition. The final spectra obtained are thus dominated by the $\sim$30% of ^{20}Mg βp decay although, as was shown in Figure 3.10 for the 984 keV γ-ray gate, some fraction of the β-singles events were able to trigger the acquisition. For this reason, a measurement of the absolute β decay branching ratios in the present experiment requires an accurate evaluation of the energy threshold for the trigger that was beyond the scope of the present work. Instead, the analysis presented below focuses on the relative proton intensities for the fraction of ^{20}Mg β decays that lead to proton emission.

Relative branching ratios were deduced from the areas of the different proton groups and normalized to the largest transition observed. The most intense proton at 797(2) keV is emitted from an excited state in ^{20}Na with excitation energy of 3001 keV (2990 keV in the present work) and feeds the ground state of ^{19}Ne with a intensity I=11.5%. The relative branching ratios for the remaining states were normalized to this intensity and, if the emitted protons feed excited states in ^{19}Ne, the measured intensities were corrected according to the γ-ray detection efficiency. Relative branching ratios obtained in the present work are presented in Table 3.7 and are compared to the results obtained in Ref. [Pie95].

$E^*(^{20}\mathrm{Na})$	g.s. $(1/2^+)$	238 keV $(5/2^+)$	275 keV $(1/2^-)$	1536 keV $(3/2^+)$
2990	11.5 (2)			
3865	5.47 (7)			
4152	$\star$	0.27 (5)	1.73 (13)	
4774		0.17 (3)	0.58 (10)	0.77 (10)
5515		0.51 (39)	0.73 (12)	0.13 (9)
6244	1.32 (5)			0.19 (6)
6519	1.44 (6)	0.51 (20)	0.44 (15)	0.35 (9)
$\sum$	19.7 (2)	1.46 (44)	3.48 (25)	1.3 (2)
[Pie95]	$\geq$19.9	2.3 (3)	3.1 (4)	1.3 (2)
[Lun16]	20.35	2.23	3.69 (4)	0.83(2)

Table 3.7 – Summary of the relative proton intensities (in %) deduced from the observed proton groups. For comparison, branching ratios were normalized to the intensity of the 797 keV proton from the level at 3001 keV (11.5% from Ref. [Pie95]). The proton transition labelled with a $\star$ was not observed in the present experiment because of the β-summng in the ungated spectrum.

Proton decays to the ground state of ^{19}Ne

The branching ratio from the 3001 keV level to the ground state of ^{19}Ne, with an intensity of 11.5%, is the reference transition for our comparison. We observed that the branching ratio of 5.47(7)% from the level at 3871 keV is not in agreement with the value of 4.8(4)% obtained in previous experiment [Pie95] (and confirmed in [Lun16]). The difference of about 1.6%, matches the intensity from the level at 4.1 MeV to the ground state ($\star$) (about 1.1%) that could not be identified in the ungated spectrum (see Figure 3.3). The integral of this transition would then be included in the β-summing tail of the 1630-keV proton group in the ungated spectrum.

Proton decays to the 238 keV level in ^{19}Ne

We observed that the sum of the branching ratios to this state (1.46(44)%) is approximately 2 times less than the value 2.3(3) measured previously [Pie95]. The reason for this difference is not clear but it should be stressed that the 238 keV γ-ray gated spectrum (Figure 3.9) was one of the most complex to analyse as the statistics were very limited and the upfeeding subtraction from the 1536 keV level above had to be included.

Proton decays of the 6.3-MeV and 6.5-MeV states.

The total branching ratio of the proton transitions from the 6.3-MeV state measured in the present work (1.32%) is 2 times higher than the previous measurement (0.7%) in Ref. [Pie95]. However, the value given by Piechaczek for the path to the ground state is inconsistent: the ratio $I_{\beta p}(6266)/I_{\beta p}(6521)$ given in Ref. [Pie95] is ≈ 0.4, which is not in agreement with the qualitative appearance of the proton groups in Figure 3.3. In the recent and more precise measurement of Ref. [Lun16], this ratio was deduced to be 1.4 (6), which is in better agreement with the present measurement (0.92 (5)).

β-decay branching ratios I_β

The total β-decay branching ratios were obtained as the weighted average of all the β-delayed proton branches from the same level. In that case, we chose to use the most recent measurement of Ref. [Lun16] for the reference 800-keV branching ratio which is four times more precise than the previous one. This was due to the use of a Si box instead of the implantation in a DSSD, which significantly reduces β-summing in the charged particle spectra. In Table 3.8, we summarize and compare the normalized intensities obtained in the present work with the previous results obtained in Refs [Pie95] and [Lun16].

As described above, the β-decay branching ratio to the 3-MeV excited state is larger than the two previous experiments because of one weak transition which was included in the β tail of

	I_β	Ref. [Lun16]	Ref. [Pie95]
2990	10.9 (4)	10.9 (3)	11.5 (14)
3865	5.18 (18)	4.8 (4)	4.8 (6)
4152	1.90 (14)	2.2 (3)	2.7 (3)
4774	1.44 (13)	3.3 (3)	1.9 (2)
5515	1.30 (16)	∼1.72 (13)	1.5 (2)
6244	1.43 (11)	2.1 (4)	1.2 (1)
6519	2.60 (13)	2.2 (2)	3.3 (4)
$\sum$	24.75 (53)	27.22 (32)	26.9 (16)

Table 3.8 – Comparison between the total β strength to the proton-unbound levels in ^{20}Na with previous measurements. The absolute intensity to the 2990 keV level in the present work was normalized using the value of Ref. [Lun16].

the 1630-keV proton transition. Despite this discrepancy, most of the total branching ratios are in good agreement with the previous results [Pie95, Lun16]. One has to keep in mind that the most recent experiment [Lun16] also provided the identification of several proton transitions which populate the 1508-keV excited state in ^{19}Ne. Because no associated γ-ray transitions were observed in the present work, we could not assign any proton transitions to this state. Therefore, a 0.4% branch from the 6266-keV state was not observed in the present work, and results in a slightly lower β-decay branching ratio to this proton-unbound state.

The intensities of the decay branches to the two broad resonances in ^{20}Na at about 4800 and 5600 keV, which were unresolved in the experiment of Piechaczek *et al.* [Pie95], are also slightly lower than the new measurement of Ref. [Lun16]. In particular, the β-decay branch to the group of states centred on 4800 keV is well explained by the decay of this state to the ground state of ^{19}Ne. This transition would appear at ∼2.7 MeV in the DSSD energy spectrum, which is at the same energy as the β-delayed α particles from the decay of ^{20}Na. As a result, no proton transition was observed at this energy in the present work.

The branching ratio of the Superallowed Fermi decay of the ^{20}Mg ground state to its IAS in ^{20}Na was deduced to be 2.60(13)% in the present work. This result is in good agreement with the most recent experiment 2.2(2)% [Lun16] and is lower than the previous result of 3.3(4)% [Pie95].

3.6 Half-life measurement

As described in the previous chapter, the time standard for the data acquisition was provided by a 32-bit 50 MHz oscillator operating in VME (SIS model number 3820). Every event was time stamped, and from the time differences between correlated implantation and decay events, the β-decay activity curve was generated on an event-by-event basis. A fit to the resulting time-dependent activity curve was used to determine the half-lives of the nuclei of interest. For the case of ^{20}Mg, the decay curve was generated using a total correlation time of 2.0 s. This correlation time is a factor of 2 larger than the one used to perform the decay spectroscopy presented in the previous section and was chosen to ensure that a sufficient amount of the longer-lived ^{20}Na daughter activity ($T_{1/2}$ = 448 ms) would be present in order to better constrain the daughter and background fit parameters. The ^{20}Mg half-life analysis is presented in this section using several different proton and γ-ray gates. Results obtained are compared to previous measurements.

3.6.1 γ-ray gated decay curves

The high-purity SeGA germanium detectors were used to obtain γ-ray gated decay curves. The benefit to using this method is that the γ-ray gates are highly selective. The resulting decay curves do not contain the daughter decay components and the spectra have very little background. The main drawback is that there are significantly less statistics since the γ-ray detection efficiency is relatively low and the decay branching ratio to the γ-ray emitting state may reduce the statistics even further.

As with the γ-ray gated proton spectra described above in Section 3.3, a background subtraction was applied to the γ-ray gated decay curves. The corresponding ^{20}Mg decay curves obtained from gates on the 238-, 275-, 984-, and 1298-keV γ rays are presented in Figure 3.11. Fits to these data consisted of a single exponential function (the decay of ^{20}Mg) and a constant background.

The four independent half-life measurements obtained from the fits to the γ-ray gated decay curves are presented in Figure 3.12 and summarized in Table 4.16. As all of these results are in good agreement, their average value $T_{1/2}$ = 87.0(23) ms, with a reduced χ^2 value of 0.5, is adopted as the half-life of ^{20}Mg obtained from the γ-ray analysis. This result is in good agreement with the value of 90.8(24) ms adopted in AME2012, which was obtained from the average of several previous ^{20}Mg half-life measurements.

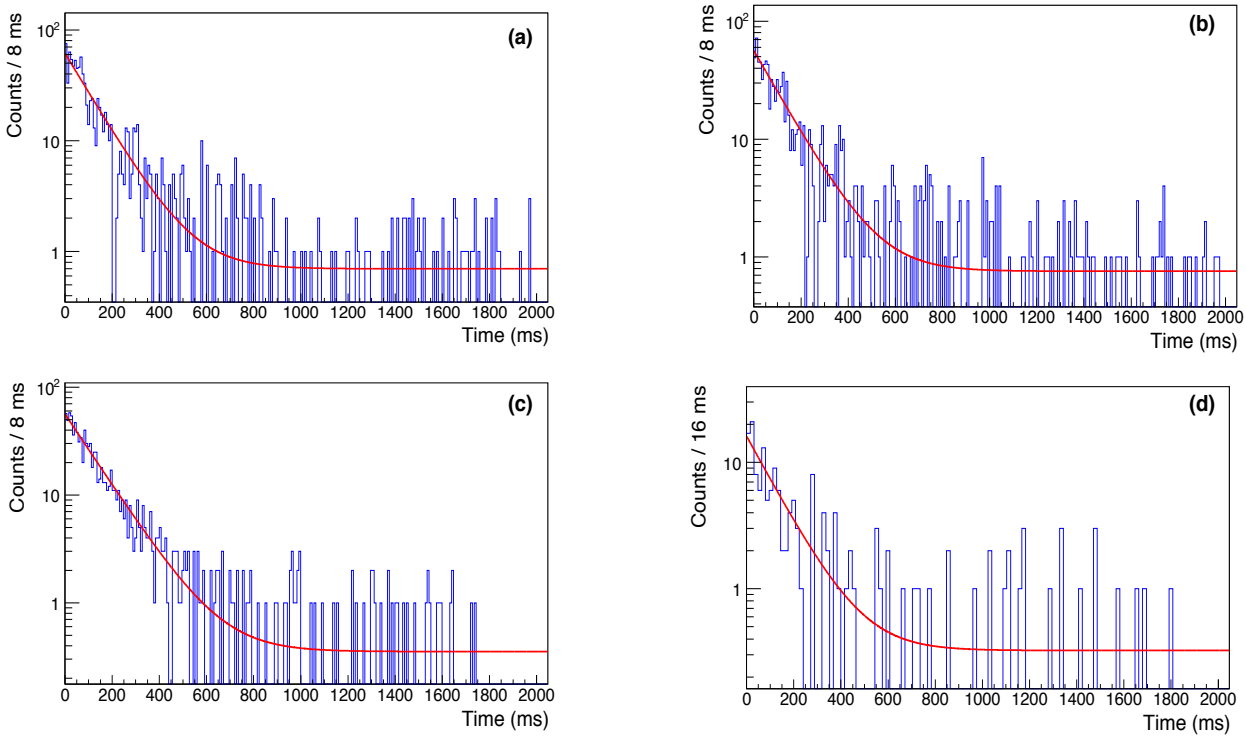

Figure 3.11 – Decay curves of correlated ^{20}Mg events with γ-ray gates on: (a) E = 238 keV, (b) E = 275 keV, (c) E = 984 keV and (d) E = 298 keV. The red solid lines indicate the best fit results that employed a single exponential decay plus a constant background parameter.

E_γ gate	Half life (ms)	χ^2/ν
238 keV	84.38 (4.10)	3.15
275 keV	85.32 (4.18)	2.77
984 keV	90.68 (3.74)	1.20
1298 keV	86.6 (11.2)	1.90
Average	87.0 (2.3)	0.5
Previous value [Wan12]	90.8 (2.4)	4.15

Table 3.9 – Half-life of ^{20}Mg deduced from the average of the γ-ray gated spectra. The reduced χ^2 values for each of the individual fits are also indicated.

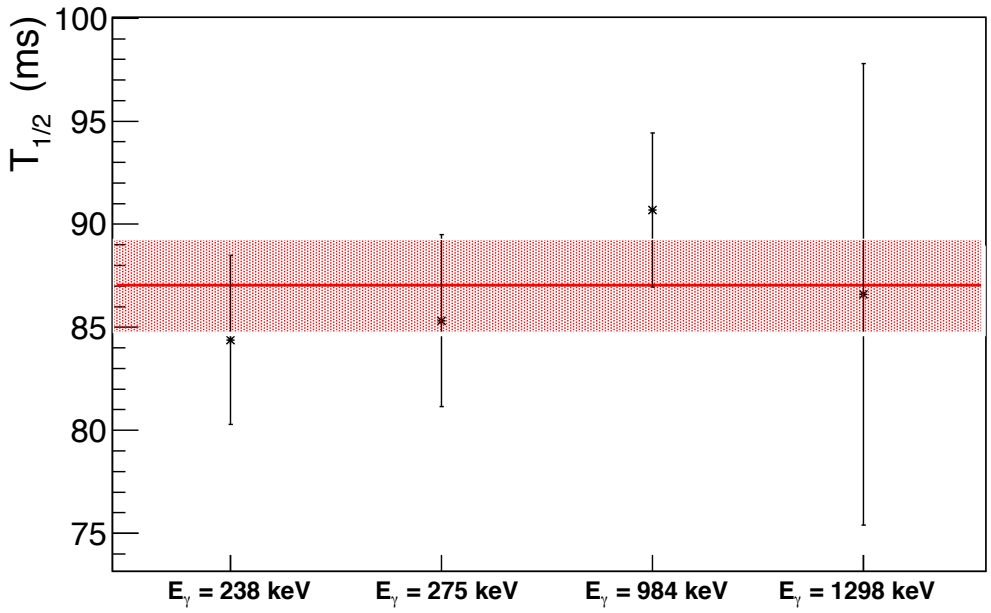

Figure 3.12 – The half-life of ^{20}Mg deduced in the present work, $T_{1/2} = 87.0(23)$ ms, with a reduced χ^2 value of 0.5, is obtained from the average of the half-life values obtained from each of the four independent γ-ray gates. This value is in good agreement with the adopted value from AME2012 $T_{1/2} = 90.8(24)$ ms.

3.6.2 Proton-gated decay curves

In the ^{20}Mg correlated proton spectrum (see Fig. 3.3), two intense protons from ^{20}Mg were observed at 797 keV and 1675 keV. Proton-gated decay curves for these two transitions were obtained by applying wide gates around these peaks in the energy spectrum. Because the proton spectrum was contaminated by both β only events (that can be produced from either ^{20}Mg decay or the decays of its daughters ^{19}Ne and ^{20}Na) and $\beta\alpha$ decays (from ^{20}Na decay), fits to these spectra had to take into account both the ^{20}Mg decay component as well as the daughter activities. Two different fit functions were employed:

- the 797 keV protons are sitting on a relatively high β background. The fit must therefore include ^{20}Mg decay as well as the decays of both of its daughters ^{19}Ne and ^{20}Na. The half-life of ^{20}Na is $T_{1/2} = 447.9$ ms while that of ^{19}Ne is much longer, $T_{1/2} = 17.22$ s. These components were included because they grow in at short times and therefore influence the resulting fit result for the half-life of ^{20}Mg. In the fit function, a constant background was also included as a free parameter. For the 797-keV proton gate, the fit function was defined as:

$$N(t) = \lambda_1 A_0 e^{(-\lambda_1 \cdot t)} \tag{3.2}$$

$$+ \varepsilon_{Na} \cdot A_0 \frac{\lambda_1 \lambda_2}{(\lambda_2 - \lambda_1)} (e^{(-\lambda_1 \cdot t)} - e^{(-\lambda_2 \cdot t)}) \tag{3.3}$$

$$+ \varepsilon_{Ne} \cdot A_0 \frac{\lambda_1 \lambda_3}{(\lambda_3 - \lambda_1)} (e^{(-\lambda_1 \cdot t)} - e^{(-\lambda_3 \cdot t)}) + C, \tag{3.4}$$

  where A_0 is the ^{20}Mg activity at $t = 0$, C is the constant background used to describe false correlations, and λ_1, λ_2 and λ_3 correspond to the decay constants for ^{20}Mg, ^{20}Na and ^{19}Ne, respectively. The half-life of ^{20}Na and ^{19}Ne were fixed at 447.9 ms and 17.22 s, respectively. Additional parameters ε_{Na} and ε_{Ne} were used to describe the overall detection efficiency for the daughter activities and the decay branching ratios of 69.7% for ^{20}Mg decays to ^{20}Na and 30.3% for decays to ^{19}Ne. In the limit of 100% detection efficiency for β particles, protons and α particles, the ε terms would just be equal to these branching ratios. In this experiment, the β detection efficiency was not accurately evaluated and the proton efficiency can only be approximately deduced using the Monte Carlo technique described in Chapter 2. It was therefore necessary to treat ε_{Na}, ε_{Ne}, and C as free parameters in the fit.

  A fit to the 797-keV proton gated decay curve is shown in Figure 3.13(a) using the fit function described above. The ^{20}Mg half-life that was obtained was 79.3(14) ms with a reduced χ^2 value of 1.4. This value is significantly lower than the reference value ($T_{1/2} = 90.8$ (24) ms from AME2012). This discrepancy is likely due to the large covariance between the free background parameter with the parameters used to describe the

daughter activities. In particular with the ^{19}Ne component as its half-life is sufficiently long enough that it could be considered as being nearly constant on the 2.0 s time scale used to generate the decay curve.

- the 1675-keV protons are sufficiently high enough in energy that the β background can be considered to be negligible. This proton is also entirely resolved from the neighbouring ^{20}Na α decays. In the decay curve presented in Fig. 3.13(b), the ^{20}Na activity and the overall background are clearly highly suppressed compared to the 797 keV proton gate. It was therefore assumed that the daughter activities in this case were negligible and any remaining background must be due only to false correlations that occur randomly in time with respect to ^{20}Mg implants. The fit function used to describe the 1675-keV gated decay curve thus employed a single exponential for ^{20}Mg decay plus a free constant background parameter. A fit to the decay curve presented in Figure 3.13(b) yields 91.4(12) ms for the ^{20}Mg half-life with a reduced χ^2 value of 1.4. This value is very good agreement with the reference value ($T_{1/2}$ = 90.8(24) ms) and the average of the fit results obtained from the γ-ray gated spectra ($T_{1/2}$ = 87.0(23) ms).

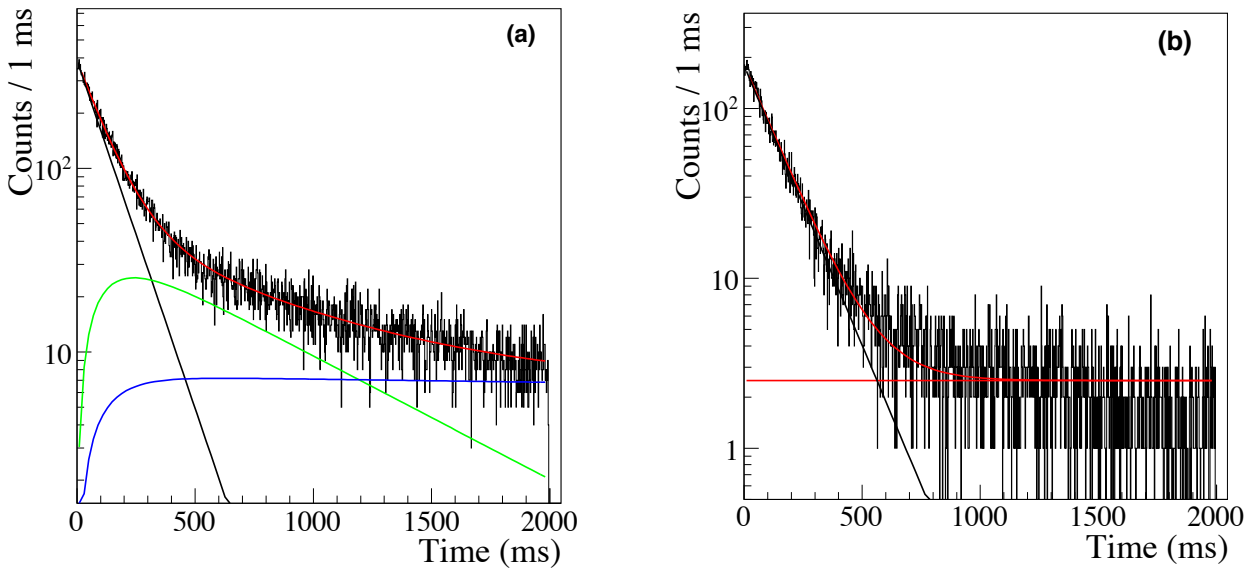

Figure 3.13 – Decay curves of correlated events gated on the two groups of protons at : (a) E = 800 keV, (b) E = 1675 keV. The red solid lines are the best fits to these data.

3.6.3 Ungated decay curve

In addition to the individual proton gated decay curves describe above, the entire ^{20}Mg correlated proton spectrum was fit without applying any particular energy gates. Because this spectrum contains β-only events from ^{20}Mg, ^{20}Na and ^{19}Ne, as well as βp decays from ^{20}Mg and $\beta\alpha$ decays from ^{20}Na, the same function as described above in Equation 3.4 was used to fit the decay curve. As with the above fit to the 797-keV protons, the detection efficiency parameters for ^{20}Na and ^{19}Ne were treated as free parameters as was the overall constant background term. The best fit to all events is presented in Figure 3.14 and resulted in a ^{20}Mg half-life of 80.1 (10) ms. This value, as with the value obtained from the 797-keV proton gate, are consistently lower than the reference value and from the results obtained above for the γ-ray gated analysis and the 1675-keV proton gate. This is likely due to the same effect described above. The covariance between the fit parameters (particularly between the ^{19}Ne component and the constant background) are too large and, as there are too many unknowns, it was not possible to fix any of these parameters to improve the overall accuracy of the fit.

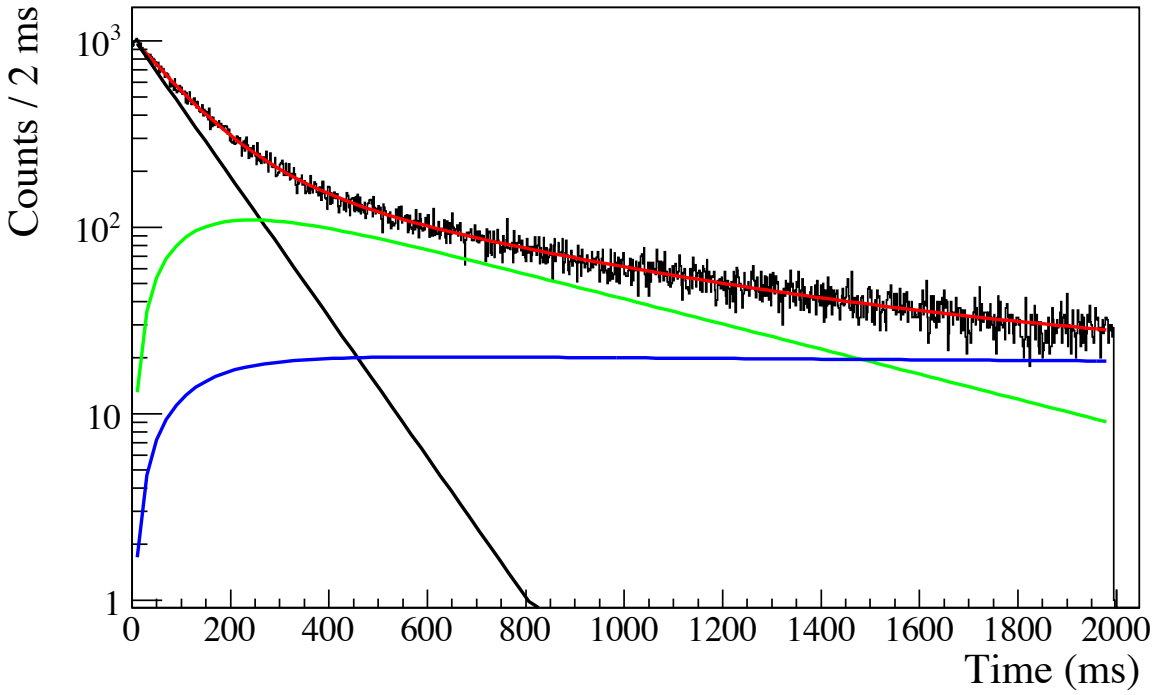

Figure 3.14 – Decay curve of all ^{20}Mg correlated events with no particle or γ-ray energy gates applied. The green and blue lines are the decay curves of the daughter s^{20}Na and ^{19}Ne with half-life fixed at 447.9 ms and 17.22 s respectively. The ^{20}Mg component is in black line, and the result of the fit (in red) gives $T_{1/2}$ = 80.1(10) ms.

An additional reason for this discrepancy might be due to the high rate of ^{20}Mg implantations that increases the probability of false correlations. When the maximum correlation time in the analysis is increased further (to 4 s for example), the half-life deduced for ^{20}Mg still disagrees with the adopted value, and is even higher. Figure 3.15 shows the decay curves obtained using correlation times of 1, 2 and 4 s for all charged-particle events. The evolution of the half-life of ^{20}Mg as a function of this maximum correlation time is provided in Table 3.10. These results were obtained by fixing the daughter intensities to $\varepsilon_{Na} = 0.7$ and $\varepsilon_{Ne} = 0.3$ (the branching ratios) and leaving the constant background parameter free. For long correlation times, the value seems to get closer to the reference value, although as shown in Fig. 3.15, the resulting fit is not able to accurately describe these data. If this hypothesis is true, that false correlations at high rates may bias the overall shape of the decay curve, it can only be caused by rate-dependent false correlations as the pure random (rate-independent) correlations should already be included in the free background parameter.

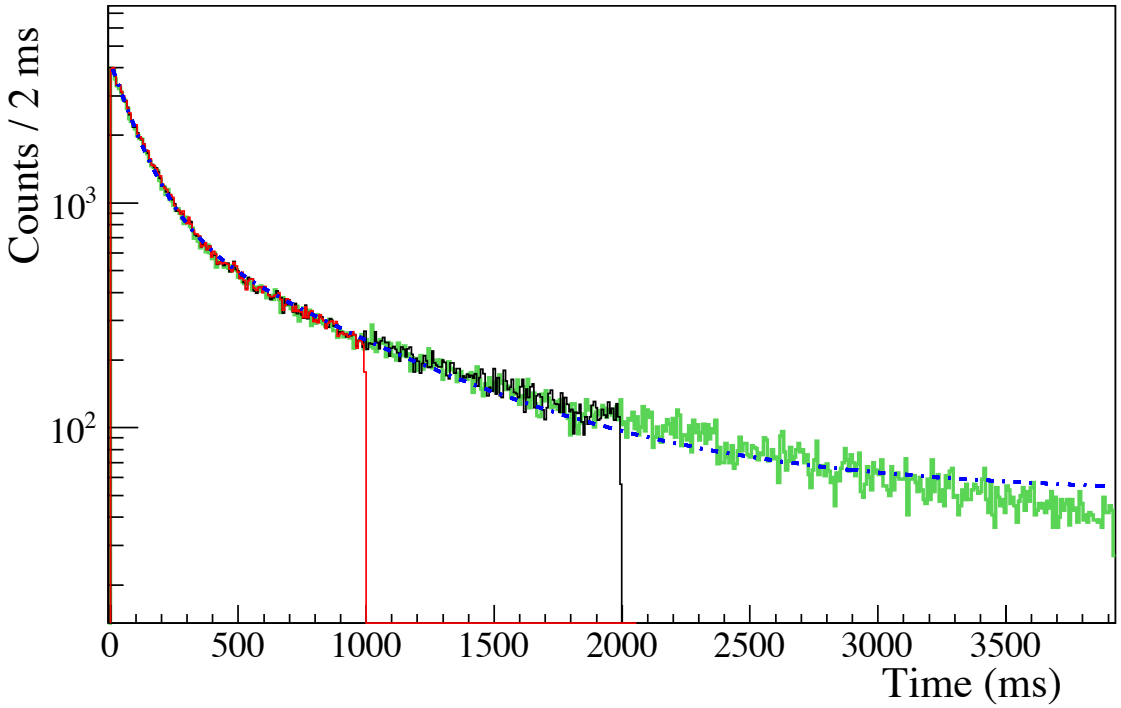

Figure 3.15 – Decay curves of the total correlated events using a correlation time of 1 (in red), 2 (in black) and 4 (in green) seconds. The blue solid lines are the best fits to the green spectrum using Equation 3.4. For a long correlation time, this fit does not accurately describe these data.

As a final test to better understand the shapes of these decay curves, the parameters that describe the efficiency and branching ratios of the daughter activities ε_{Na} and ε_{Ne} were each

Corr. time (s)	1	2	4
$T_{1/2}$ (ms)	85.1 (7)	87.7 (6)	94.0 (6)
χ^2/ν	1.15	1.32	3.76

Table 3.10 – Half-life resulting from the fit of the ungated decay curve, depending on the correlation time.

fixed between 0 and 1, their extreme values. The half-lives of ^{20}Mg obtained from several different fits and for the case of a 2 s maximum correlation time are summarized in Table 3.11. In all cases, the constant background parameter was free. The trend of these values clearly reflects the large correlation between the ^{20}Mg half-life and the daughter parameters. For example, if the ^{20}Na term is fixed to 0 or 1, and the ^{19}Ne component is free, the resulting ^{20}Mg half-life ranges from 145 ms to 75.1 ms, respectively. If both parameters are free then the resulting half-life is 80.1 ms and the fit yields $\varepsilon_{Na} = 0.85(2)$ and $\varepsilon_{Ne} = 4.23(9)$. These ε values are completely non-physical and are not in agreement with the expected values based on the decay branching ratios and the detection efficiencies.

If one further assumes an average α-particle detection efficiency of 100% and a β detection efficiency of 5% (deduced from the fraction of β-particles observed in the 984-keV γ-ray gated charged particle spectrum of Fig. 3.10) then the ε_{Na} can be fixed at its absolute maximum value of 0.17. This value is obtained from the expression $0.697\times(0.2 + 0.8\times0.05)$ where the 0.2 and 0.8 are the ^{20}Na branching ratios to β-delayed α emission and β-decay only, respectively. The resulting ^{20}Mg half-life is 125.9 (0.9) ms (with a reduced χ^2 value of 2.65) and the ϵ_{Ne} value is 5.9. This further supports the hypothesis that the parameters required to describe the complex background and daughter activities remain too correlated to yield an accurate result.

		ε_{Na}		
		free	0	1
ε_{Ne}	free	80.1 (10)	145 (1)	75.1 (6)
	0	79.8 (10)	147 (1)	75.1 (6)
	1	79.9 (10)	147 (1)	74.9 (5)

Table 3.11 – The half-life obtained by fitting the ungated decay time spectrum is very sensitive to the normalization factor ε_{Na} of the daughter with the shorter half-life, ^{20}Na.

3.6.4 Discussion on the half-life

From the above results, the half-lives obtained from the 797-keV proton gate and the ungated proton spectra must be rejected from the analysis for the reasons described above. The final result must therefore rely on the values obtained from the 1675-keV proton gated decay curve ($T_{1/2}$ = 90.8 (24) ms) and the average of the γ-ray gated analysis ($T_{1/2}$ = 87.0 (23) ms), which are independent of the contributions from the daughter activities. Because the 1675-keV proton feeds the ^{19}Ne ground state this proton cannot not be in coincidence with any of the γ rays used in the γ-ray gated analysis and thus these two results are entirely independent. Averaging both of them together yields the final result of $T_{1/2}$ = 88.8(17) ms for the half-life of ^{20}Mg derived in the present work. This value agrees within 1.2σ with the reference value from AME2012 ($T_{1/2}$ = 90.8(24) ms) and within 1.5σ with the more precise result, $T_{1/2}$ = 91.4(10) ms [Lun16], obtained in a recent ^{20}Mg half-life measurement. A comparison of the present result with previous ^{20}Mg half-life measurements is presented in Table 3.12 and in Figure 3.16.

Measurements	$T_{1/2}$ (ms)
Moltz (PRL 42, 1979)	95^{+80}_{-50}
Görres (PRC 46, 1992)	82 ± 4
Kubono (PRC 46, 1992)	144 ± 17
Dufour (unpublished)	95 ± 15
Piechaczek (NPA 584, 1995)	95 ± 3
Lund (EPJA 52, 2016)	91.4 ± 1.0
AME2012	90.8 ± 2.4
This work - average	88.8 ± 1.7

Table 3.12 – Summary of previous measurements of the ^{20}Mg half-life and comparison to the present work.

3.7 Conclusion

In the cocktail beam produced for studying ^{23}Si decay, ^{20}Mg ions were produced as a contaminant with high intensity. This provided an ideal case to test the correlation algorithm and the analysis method that will be used in the analysis of ^{22,23}Si decays that will be described in the following chapters. After properly setting the A1900 separator and the RFFS for ^{20}Mg, a total of approximately 17 hours of calibration data were obtained. From the analysis of these data, three γ-ray transitions at 238 keV, 275 keV and 1298 keV were observed in SeGA that correspond to the excited states in ^{19}Ne that are populated from the known β-delayed proton

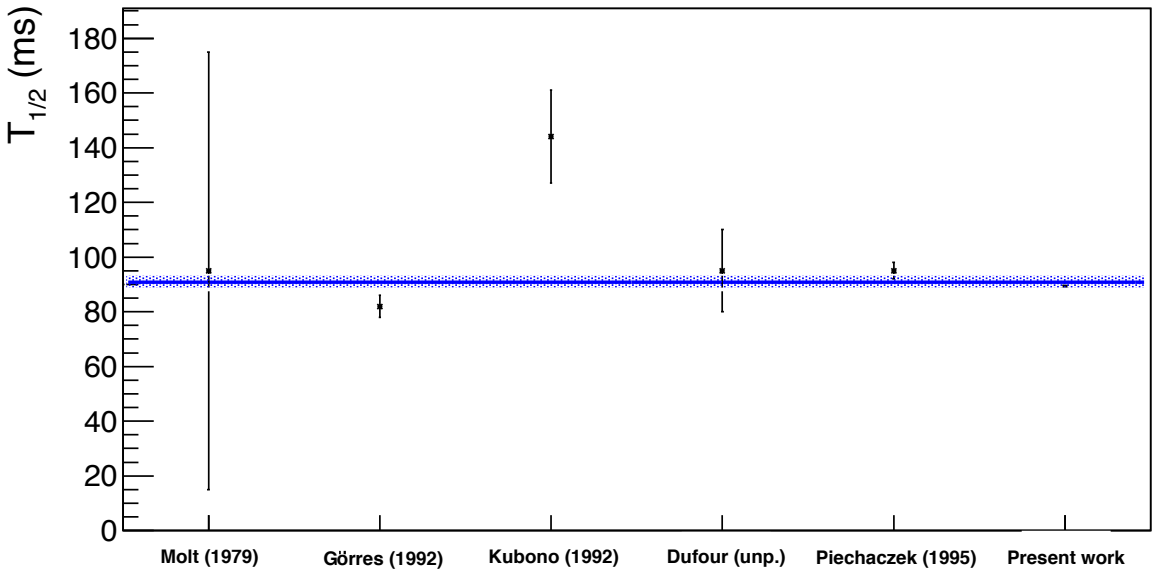

Figure 3.16 – The half-lives of ^{20}Mg deduced in the present work using the γ-gated spectra, $T_{1/2}$ = 87.0 (23) ms is compared to previous measurements. In blue, the average half-life adopted in the most recent evaluation from AME2012 and its uncertainties $T_{1/2}$ = 90.8 (24) ms.

branches from ^{20}Mg decay. The detailed study of the proton spectra in coincidence with γ rays detected in SeGA allowed us to determine the excitation energies of the levels in ^{20}Na populated above the one-proton separation threshold.

Despite having a lower resolution than in previous ^{20}Mg decay experiments and a stronger β summing, the excitation energies of five discrete levels and two unresolved groups of levels were measured. In all cases, the measured energies are in good agreement with two previous measurements [Pie95, Wal12]. In particular, the γ-ray gated spectra were used to derive the energy of the excited 0^+ state in ^{20}Na that is the isobaric analogue to the ^{20}Mg ground state. The result of the present work 6519(19) keV is in excellent agreement with the value of 6522(16) keV obtained in Ref. [Wal12].

Relative proton branching ratios were deduced from the fits to the proton groups. Results were, for the most part, in reasonable agreement with previous results although, in some cases, the statistics were extremely limited. The intensities of the proton branches deduced to the 238-keV excited state in ^{19}Ne do not agree with the values given in Ref. [Pie95].

The half-life of ^{20}Mg was also measured in the present study using both γ-ray gated and proton energy gates. The half-life obtained from the γ-ray analysis yielded $T_{1/2}$ = 87.0(6) ms, which is in good agreement with the adopted value of 90.8(24) ms from AME2012 [Wan12]. The high counting rate induces a significant amount of false correlation and thus makes the

fit difficult when using the proton-gated spectrum at low energy, as well as the total number of events. Gating on the 1675-keV transition, we obtained a half-life of 91.4 (12) ms which is closer to the reference value. We deduce a ^{20}Mg half-life of 88.8 (17) ms from the average of the fit results of the γ-ray gated spectra and the decay curve of the 1675-keV events. This value is in good agreement with the adopted value from AME2012 [Wan12] but also with the most recent and precise measurement, 91.4 ± 1.0 ms [Lun16].

The analysis protocol and methods have been thoroughly tested and validated using the known decay of ^{20}Mg. This same analysis procedure will now be applied to the decays of ^{23}Si decay and ^{22}Si where much less information is known about the decay level schemes and where several additional exotic decay pathways such as β2p are open and could, in principle, be observed.

Chapter 4

β-delayed charged particle decays of ^{23}Si

The previous chapter outlined the analysis procedure and applied this protocol to the implantation and decay of ^{20}Mg. The γ-rays emitted by the daughter nucleus were a powerful tool to identify the known decay paths of ^{20}Mg. Protons in coincidence with the daughter γ-rays were used to reconstruct the level scheme of ^{20}Na. The branching ratio and the energies of the unbound levels that were deduced were in agreement with previous experiments, and validated the experimental setup as well as the analysis procedure.

In this chapter, we present the study of the β-delayed proton emission of the more exotic nucleus ^{23}Si. The ground state of ^{23}Si ($T_Z = -5/2$) and its isobaric analogue state in the daughter ^{23}Al are part of an isobaric multiplet of 6 states (A=23, $T = 5/2$), of which 2 additional states are presently known. By measuring the energy of the IAS in ^{23}Al, the IMME can be used to provide an indirect measurement of the mass of the ^{23}Si ground state. In addition, the full decay scheme of the daughter ^{23}Al has been built using proton and γ-ray coincidences. The relatively large β-decay Q-value opens several additional exotic decay channels, as presented in Table 4.1.

Decay	Daughter	Q-value (keV)
β^+	^{23}Al	16952
βp	^{22}Mg	16811
β2p	^{21}Na	11307
β3p	^{20}Ne	8875
βpα	^{18}Ne	8669

Table 4.1 – Summary of the Q-values for the possible β delayed charged particle decays of ^{23}Si, using the adopted value of ^{23}Si mass excess from AME2012 [Wan12].

The γ-rays detected in the SeGA detectors were used to identify the states populated in the daughter nuclei and to deduce the corresponding decay paths. Several γ-ray gates were applied to the charged particle spectra and were used to identify the unbound states populated in ^{23}Al which decay by the emission of one or two protons. A total of three γ-rays were observed that correspond to the de-excitation of the first three excited states in ^{22}Mg, and confirms the βp decay channel that was already deduced from proton energy differences in the work of Ref. [Bla97]. Another γ-ray transition, coming from the de-excitation of the first excited state of ^{21}Na, confirms the β2p decay branch through the IAS which was deduced in this same study. A weak β3p decay branch was also tentatively deduced as we observed a proton group in coincidence with the 1633 keV γ-ray in the daughter ^{20}Ne.

The ungated charged particle spectrum, which gives information on the transitions going to the daughter ground states was used to complete the level scheme of ^{23}Al. This spectrum was partially contaminated due to the presence of ^{20}Na ($T_{1/2}$=447.9 ms) in the secondary beam. An estimation of this contamination and its subtraction were performed. This has led to the identification and the measurement of a β2p transition to the ground state of ^{21}Na. The energy and branching ratio of this transition was measured in the ungated spectrum, as well as 14 new levels, confirming most of the transitions that were previously observed in a decay experiment at GANIL [Bla97].

4.1 Previous measurements

During a campaign of experiments at GANIL, focusing on neutron-deficient nuclei, ^{23}Si was produced using in-flight projectile fragmentation with the LISE spectrometer, and its β-delayed charged particle decays were studied by B. Blank *et al.* [Bla97]. The ^{23}Si nuclei, but also ^{20}Na which was a contaminant in the secondary beam, were implanted into two different detection systems: a Micro-Strip Gas Counter (MSGC) used to detect the low-energy protons, and a system of three silicon detectors. The MSGC had a better efficiency and resolution at low energy and was nearly transparent to β particles thus significantly reducing the β-summing effect. Figure 4.1 presents the spectra of charged particles that were obtained with both detector setups.

The identification and the assignment of the unbound levels in ^{23}Al were performed by comparison between the energy differences between the proton groups and the values of the transition energies in the daughter nuclei. The proton groups measured by B. Blank *et al.* are presented in Table 4.2.

The IAS in Ref. [Bla97] was deduced from multiple decay paths. The energy difference between proton groups 10 and 11 was close to the previously known first excited state in ^{21}Na at 332 keV. In addition, the proton group 14 at 10.41 MeV was consistent with a proton emission from the IAS to the first excited state in ^{22}Mg at 1247 keV. The energy difference between the

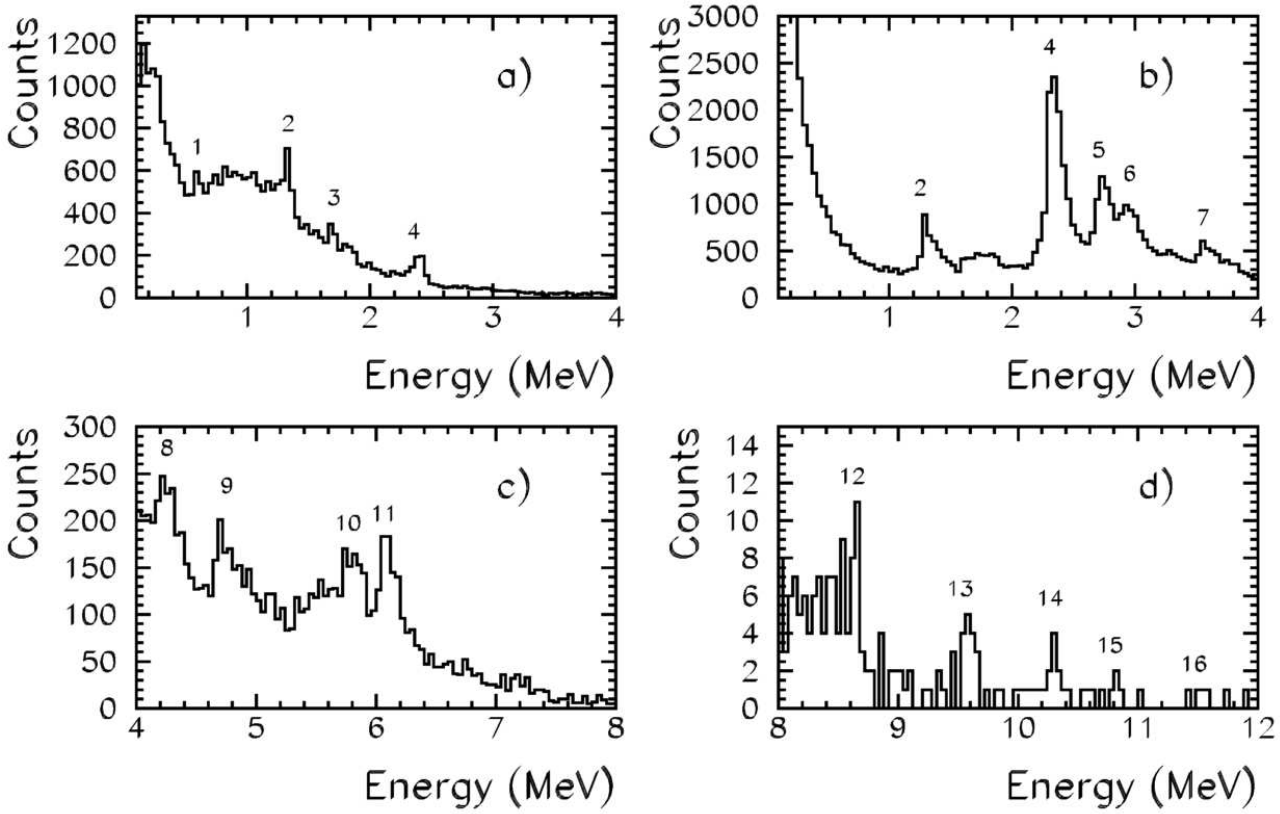

Figure 4.1 – Charged particle spectra obtained at GANIL in the previous experiment by B. Blank [Bla97]. Figure (a) presents the spectrum from the MSGC gas detector and Figures (b), (c), and (d) are the proton spectra from the DSSD.

proton group 14 and 16 is about 1.25 MeV. For this reason, the proton group 16 at 11.62 MeV was identified as a proton transition from the IAS to the ground state of ^{22}Mg. Based on these four proton transitions (groups 10, 11, 14 and 16), Blank *et al.* concluded that the energy of the IAS feeding these transitions was located at 11.78-MeV excitation energy in ^{23}Al. From the energy of the IAS, the mass excess of the ^{23}Si ground state was determined to be 23.42(10) MeV using the IMME for the (A=23, T=5/2) multiplet. During the same experiment, the half-life of ^{23}Si was deduced to be 42.3±0.4 ms [Bla97].

4.2 Experiment analysis

The secondary beam implanted in DSSD2 had an average rate of 0.70 pps after the A1900 and RFFS purification processes. A contour was applied to the ΔE-ToF PID spectrum in order to select the ^{23}Si implants. After the correlation process, a total of 1.50×10^5 events were assigned to ^{23}Si correlated implant-and-decays in this contour. The correlation time and area

#	Energy (keV) [Bla97]	#	Energy (keV) [Bla97]
1	600 (60)	9	4760 (60)
2	1320 (40)	10	5860 (100)
3	1700 (60)	11	6180 (100)
4	2400 (40)	12	8680 (70)
5	2830 (60)	13	9670 (70)
6	3040 (60)	14	10410 (70)
7	3650 (60)	15	10930 (80)
8	4370 (60)	16	11620 (100)

Table 4.2 – Proton energies as measured in the previous experiment performed by B. Blank *et al.* [Bla97] at GANIL.

were fixed at $T_{max} = 0.4$ s and 3x3 pixels around the implantation site, respectively. The purity of the implanted beam, after the A1900 and RFFS selection, and after correlation process, was approximately 19 %. Figure 4.2 presents the PID spectrum of the nuclei in the cocktail beam and after the correlation process. The rate of the contaminants in the beam are summarized in Table 4.3. The contour applied to the PID spectrum, is shown in Figure 4.2 and allows the selection of the decays identified as charged particle decays from ^{23}Si. Other conditions were applied including $|E_{front} - E_{back}| \leq 400$keV on the difference between both energies measured in the front and back strips of the DSSD2 detector. This condition conserves about 80% of the orginal set of correlated decays.

	Purity (%)	Half-life
^{23}Si	19.0	42.3 ms
^{22}Al	3.1	59 ms
^{20}Na	75.7	447.9 ms
^{19}Ne	1.1	17.22 s
^{18}F	0.7	109.7 min

Table 4.3 – Purity of the secondary cocktail beam optimized for ^{23}Si. The main contamination comes from ^{20}Na, which is a known β-delayed α emitter [Lau13].

To avoid pile-up phenomena and false correlations in a concentrated region of pixels, the beam was defocused across the surface of DSSD2. Decays of ^{20}Na, which was produced in the cocktail beam with relatively high intensity, has a half-life that is only one order of magnitude larger than ^{23}Si. This nucleus emits β-delayed α particles, which could also trigger the data-acquisition system. The presence of false correlations from ^{20}Na in the ^{23}Si correlated spectra

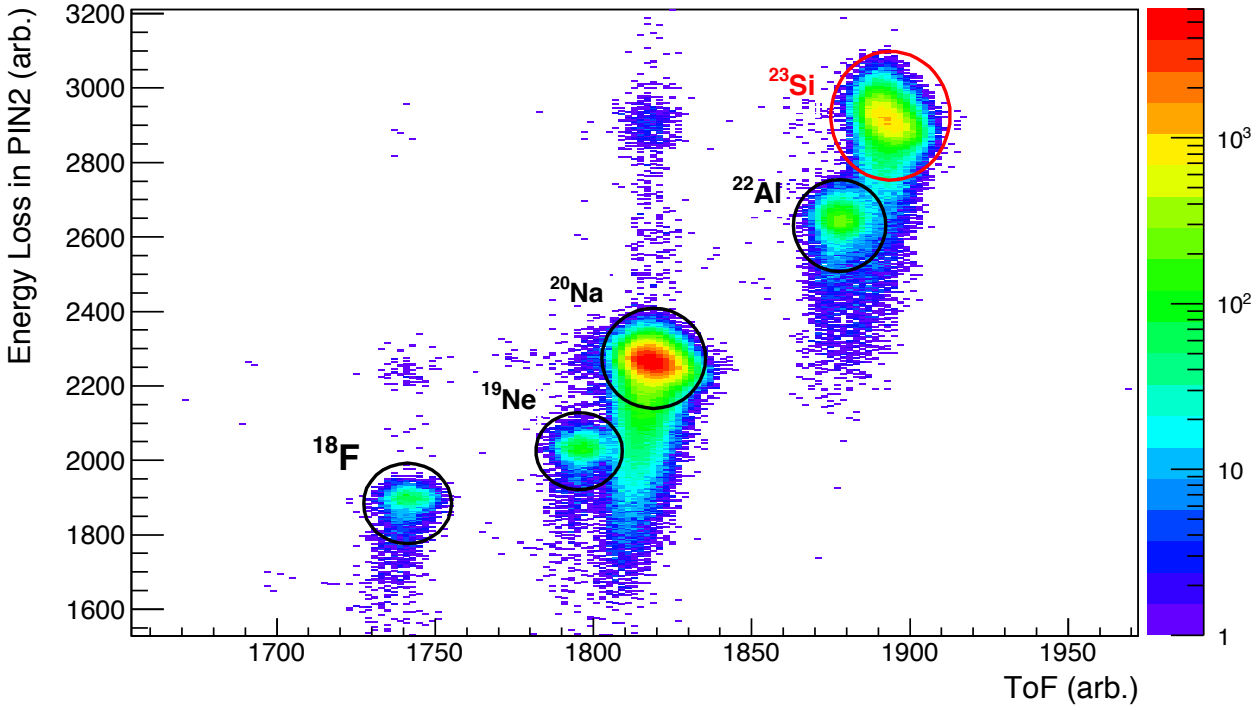

Figure 4.2 – After the correlation process, the PID was made using ΔE-ToF method. Most of the identified contaminants also decay via β-delayed charged particle emission.

was confirmed by applying a much longer correlation time window (2 s). As shown in Figure 4.3, the slope of the longer-lived component was consistent with the half-life of ^{20}Na.

4.2.1 ^{20}Na contamination

To maximize the overall statistics, the correlation time in the ^{23}Si analysis was fixed to be 400 ms, which corresponds to 10 times the half-life of ^{23}Si and approximately one half-life of ^{20}Na. This induced a contamination in the charged particle spectrum because of the β-delayed α particles emitted from ^{20}Na. Strong peaks in the energy spectrum were observed at 2.7 MeV and 5.9 MeV [Lau13]. The energy spectrum of charged particles emitted from all long-lived contaminants was obtained by increasing the maximum correlation time and using a time gate on decay events with a half-life larger than 1 s. Assuming that the contribution of the contaminants follows an exponential decay curve, the number of false correlations in the 0.4-s time range can be deduced. The normalized spectrum is compared to the total charged particle spectrum in Figure 4.4.

To quantify this contamination, we used proton groups observed in the previous experiment and presented in Table 4.2. The ratio r between the integral of particle groups 4 at 2.3 MeV ($I = 32(5)\%$) and the sum of both groups 5 and 6 ($I = 14 + 7.8 = 21.8(12)\%$) was plotted

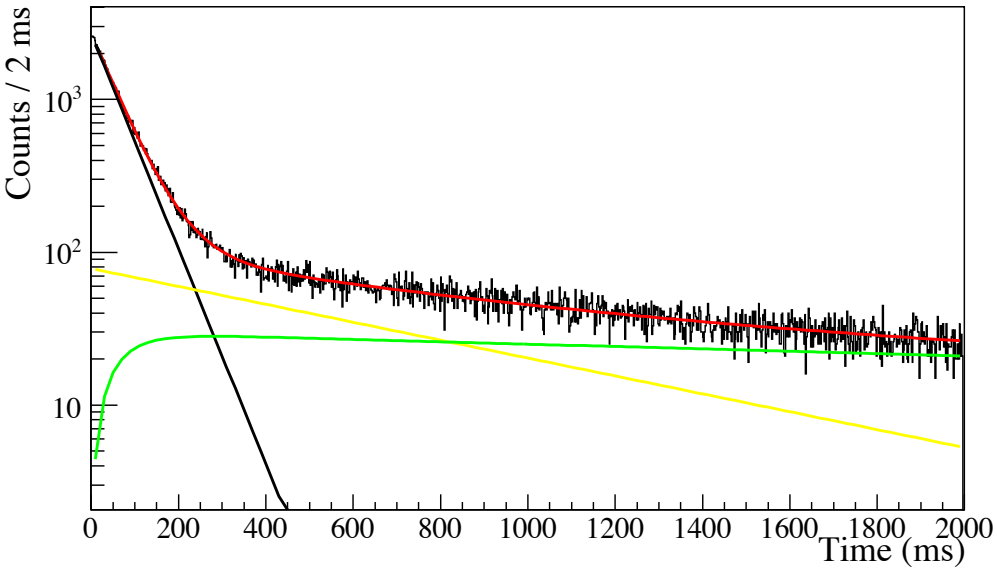

Figure 4.3 – The fit of the decay curve of all the particles detected in the DSSD was made assuming an exponential decay of the parent (in black), the successive decay of the daughter (in green), a constant background (off axis) and an exponential decay for the correlated decays from contaminants (in yellow).

as a function of the correlation time. The evolution of this ratio is presented in Figure 4.5. It decreases when the correlation time is increased, meaning that proton group at 2.8 MeV is increasingly contaminated by ^{20}Na β-delayed α particles.

The decay time spectrum of all correlated events obtained with a correlation time of 400 ms, is presented in Figure 4.6. The charged-particle spectrum from the contaminants was normalized before being subtracted from the total charged-particle spectrum. This normalization was performed using the decay time spectrum: the integral of the contaminant energy spectrum presented in Figure 4.4 was normalized to the integral of the exponential decay curve and the constant background obtained by fitting the 400-ms decay time spectrum.

The ratio of the proton groups in the energy spectrum after the subtraction of the contaminants is ($r = 1.24\,(4)$), which is in good agreement with the value deduced from B. Blank previous measurement ($r = 1.47\,(24)$) as presented in Figure 4.5.

After subtraction, Figure 4.7 shows the comparison between the resulting charged-particle spectrum and the energy spectrum previously obtained by B. Blank *et al.* in Ref. [Bla97]. In Figure 4.7.b), the absence of a low-energy β background is due to the background subtraction process just described. The width of the proton group at 2.8 MeV is the result of two peaks that could not be resolved as easily as in the previous experiment because of the lower resolution. For this same reason, the proton groups associated to the β2p decay of ^{23}Si are resolved but

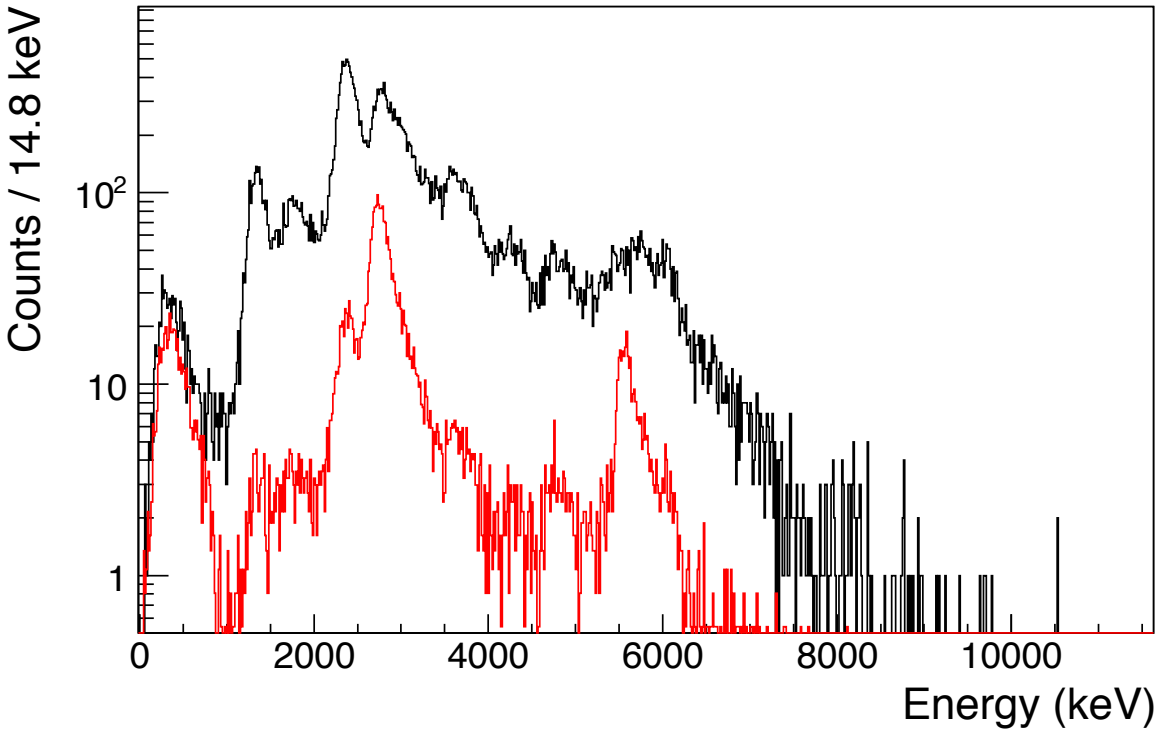

Figure 4.4 – In black, the spectrum of the charged particles identified as β-delayed emission from ^{23}Si in the second DSSD. In red, the normalized spectrum corresponding to the decay of the different contaminants in the long decay-time ($\geq$ 1000 ms) gated spectrum. The two strongest transitions are the known $\beta\alpha$ branches from ^{20}Na studied in Ref. [Lau13].

not as well defined as in the previous experiment, as shown in Figure 4.7.c).

The higher efficiency of the thick DSSDs used in the present work allows a better identification of the weak proton transitions at high energy in Figure 4.7.d). A summary of the proton group energies deduced in the present experiment is presented in Table 4.4. These energies are also compared to the previous results from Ref. [Bla97]. As expected, the energy of proton groups 2 to 9 which were used to calibrate the majority of the DSSD strips (from 0.8 MeV to 5.5 MeV) are in good agreement with Blank's results. For energies larger than 4.5 MeV, a small systematic shift is observed that increases with proton energy. This most likely due to small differences in the extrapolation of the calibration functions between the two experiments towards the highest energies.

Because of the higher efficiency in the present experiment, we were able to observe that proton group 10 is actually made up of two distinct components. A fit to this group with two peaks yielded mean energies of 5745(47) keV and 5518(48) keV. In the case of the emission of 2 protons from the IAS, the average kinematic values after PHD corrections are 5802(47)(57) keV

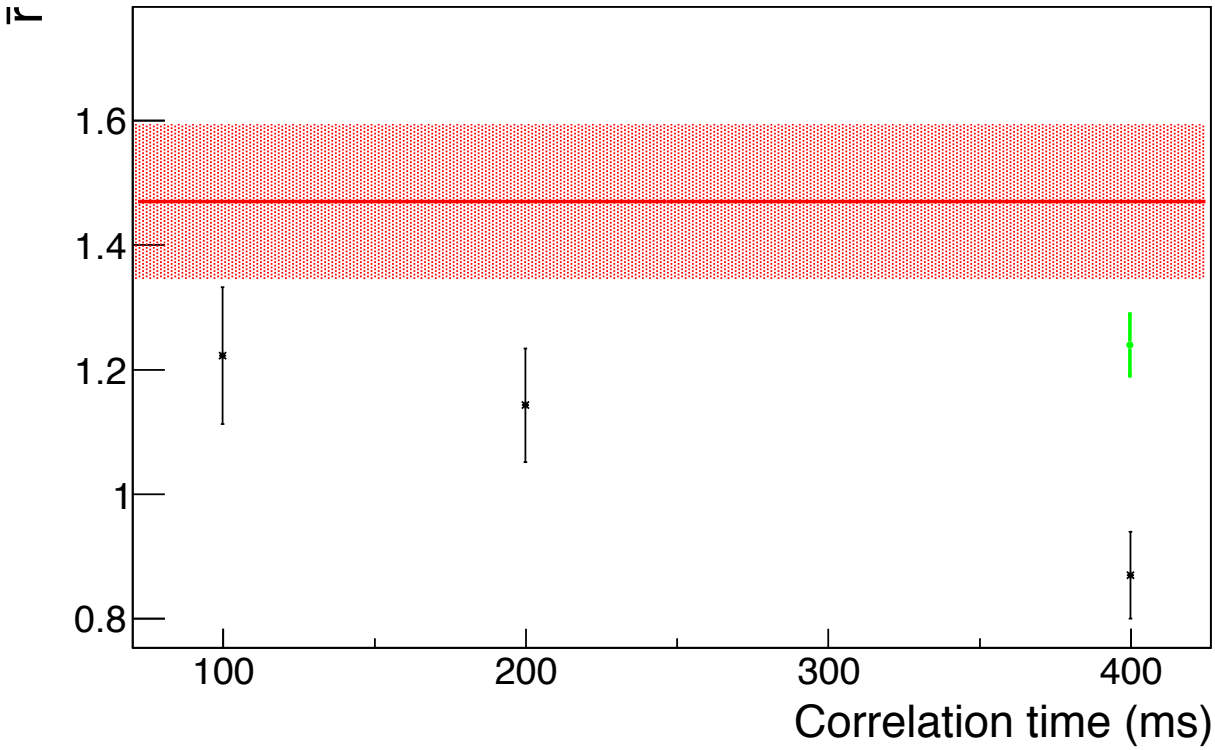

Figure 4.5 – The ratio r of protons from the βp channel of ^{23}Si and the peak with both βp from ^{23}Si and α from ^{20}Na decreases with a long correlation time (in black). This is the sign of contamination in the raw proton spectrum. After the subtraction (in green), the ratio becomes close to the one obtained with a short correlation time. For comparison purpose, the value and its uncertainties, deduced from the previous measurement [Bla97], are indicated (in red).

and 5574(48)(56) keV, respectively where the first uncertainty is from the calibration and the second kinematic. Proton group 11 was identified as the β2p branch from the IAS to the ground sate. The difference between proton groups 10 and 11 is the closest to the energy to the known first excited state in ^{21}Na at 332 keV, and so confirms the identification previously made in Ref. [Bla97].

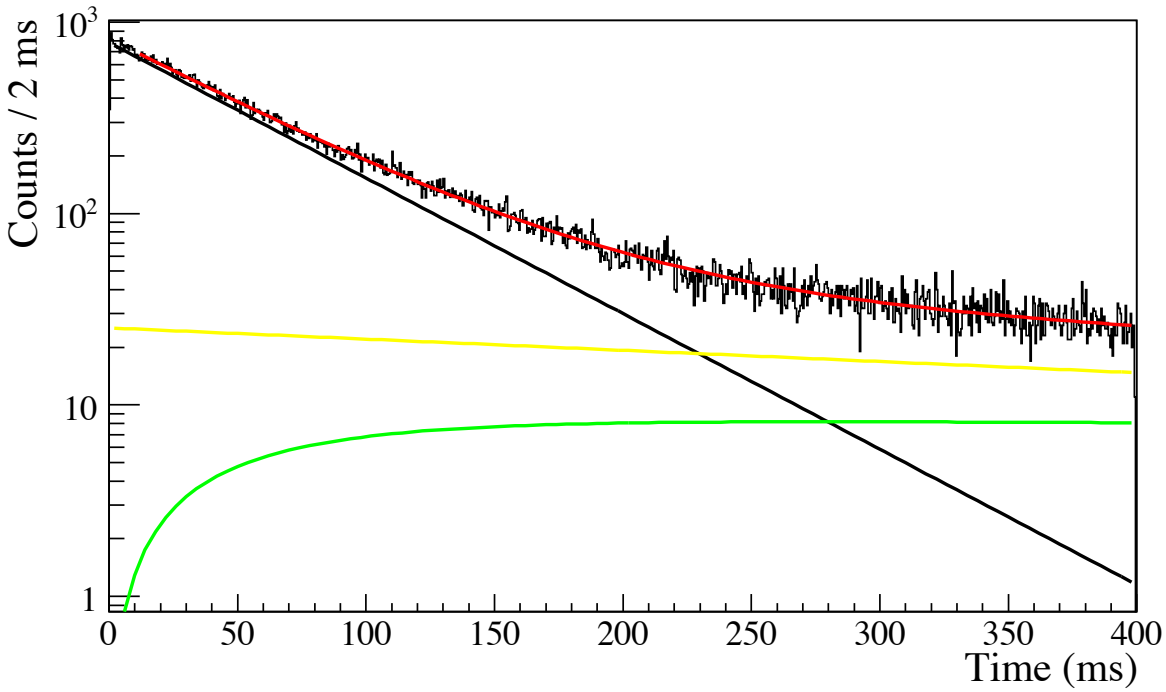

Figure 4.6 – The fit of the decay curve for all particles detected in the DSSD assuming an exponential decay of the ^{23}Si parent (in black), the ^{23}Al daughter (in green), a constant background (≤ 1 count/bin - off axis) and an exponential decay used to determine the rate of wrong correlations (in yellow). The half-life of this decay is consistent with that of ^{20}Na. The fit of this decay curve yields the half-life of ^{23}Si, $T_{1/2}$=42.5(10) ms

#	$E_{Protongroup}$ (keV)	Energy (keV) [Bla97]	#	$E_{Protongroup}$ (keV)	Energy (keV) [Bla97]
1	-	600 (60)	9	4763 (47)	4760 (60)
2	1354 (71)	1320 (40)	10	5800 (57)	5860 (100)
3	1733 (62)	1700 (60)	11	6076 (57)	6180 (100)
4	2395 (50)	2400 (40)	12	8299 (95)	8680 (70)
5	2823 (44)	2830 (60)	13	9360 (109)	9670 (70)
6	3096 (42)	3040 (60)	14	9716 (117)	10410 (70)
7	3700 (38)	3650 (60)	15	10636 (132)	10930 (80)
8	4350 (41)	4370 (60)	16	11474 (148)	11620 (100)

Table 4.4 – Proton energies determined from the ^{23}Si correlated decay spectrum and compared to the previous values of B. Blank *et al.* Proton groups from 2 to 9 were used to calibrate the DSSD. Uncertainties on the proton energies include contributions from the calibration and the fit procedure. For proton groups 10 and 11, the energy given is the energy in the average value between a static recoil ion and a diproton decay.

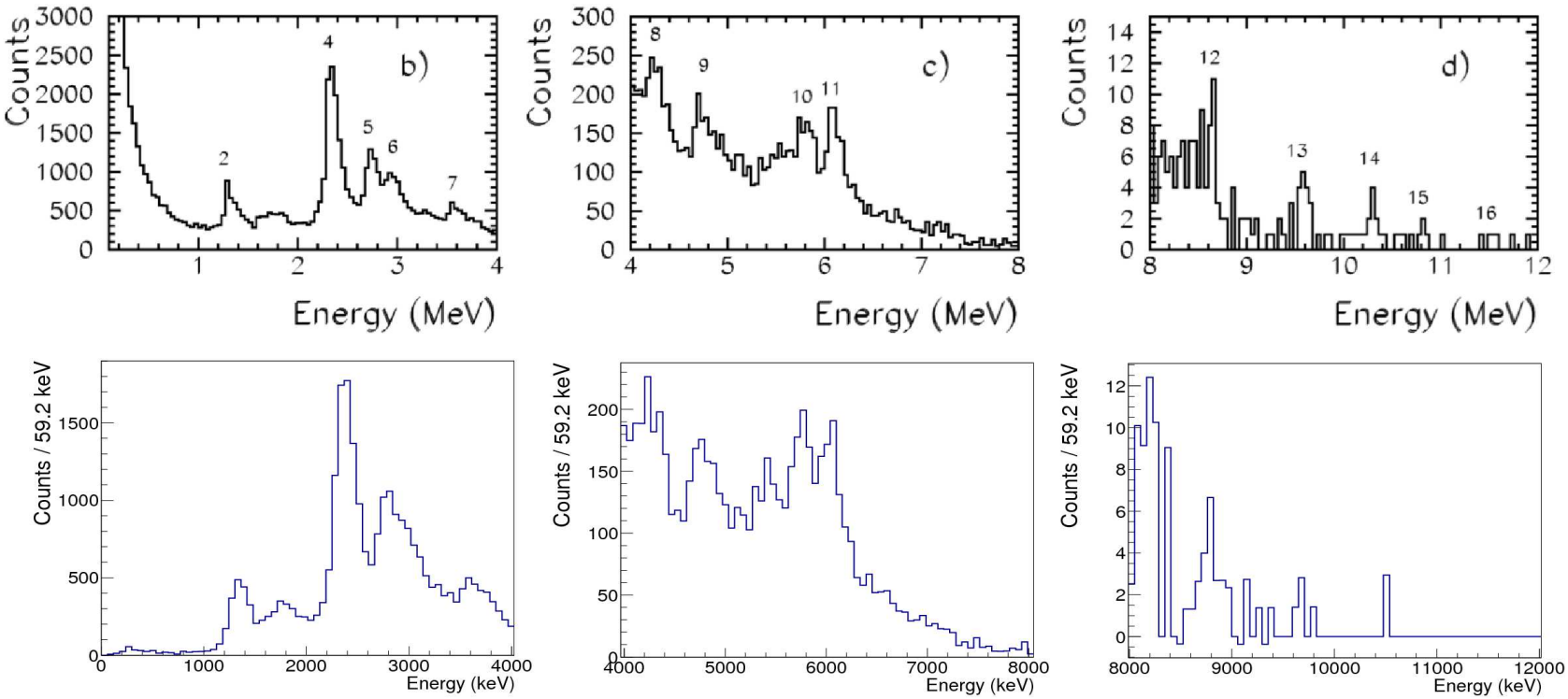

Figure 4.7 – Comparison between the present experiment (bottom row) and the previous one (top row) from Blank *et al.* [Bla97]. The energy spectra presented here are for the decays of ^{23}Si nuclei after background and contamination subtraction. A first comparison between the strong transitions allows the assessment of the same proton groups as identified in this previous work. The figure of low-energy range shows some counts under 500 keV, which are likely due to ground-state-to-ground-state β-only decays.

4.3 γ-ray spectrum from ^{23}Si decay

The 16 HPGe detectors surrounding the implantation site were used to detect β-delayed γ rays and identify the decay pathways in the corresponding daughters. In the energy spectrum of Fig. 4.8, six γ-ray transitions were observed that are summarized in Table 4.5.

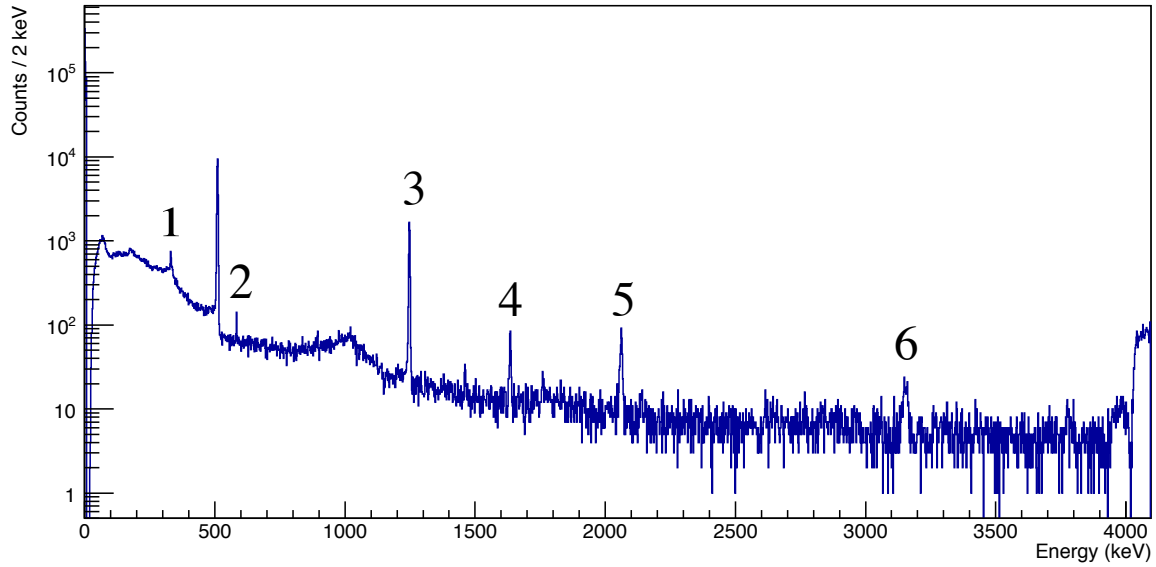

Figure 4.8 – γ-ray spectrum correlated to ^{23}Si decays.

#	Energy (keV)	$E_i(J^\pi) \rightarrow E_f(J^\pi)$	Daughter nucleus
1	331.5 (10)	$332(5/2^+) \rightarrow$ g.s.$(3/2^+)$	^{21}Na (β2p)
2	583.8 (12)	$583(1^+) \rightarrow$ g.s.(3^+)	^{22}Na ($\beta\beta$p)
3	1247.6 (11)	$1247(2^+) \rightarrow$ g.s.(0^+)	^{22}Mg (βp)
4	1634.4 (10)	$1634(2^+) \rightarrow$ g.s.(0^+)	^{20}Ne (β3p) - ^{20}Ne(β)
5	2061.9 (11)	$3307(4^+) \rightarrow 1247(2^+)$	^{22}Mg (βp)
6	3152.5 (14)	$4402(2^+) \rightarrow 1247(2^+)$	^{22}Mg (βp)

Table 4.5 – Six γ-ray transitions were observed and correspond to the βp and β2p decays of ^{23}Si. A transition at 583 keV in ^{22}Na is probably due to the ground state to ground state β decay of ^{23}Si $(5^+/2)$ to ^{23}Al $(5^+/2)$, which then decays via βp [Saa11, Iac06]. The γ-rays at 1634 keV has two possible origins: a β3p decay from ^{23}Si and a β decay from ^{20}Na.

Apart from the 511-keV γ-rays, which originate from positron annihilation following β^+ decays inside the DSSD, these γ-ray transitions provide a clear means to identify three daughter nuclei:

- γ rays at 1247 keV, 2062 keV and 3152 keV are emitted from the de-excitation of the three first excited states in ^{22}Mg. The 2062-keV and 3152-keV γ rays are from the γ decays of states at 3307 keV and 4402 keV, respectively, to the first excited 2^+ state at 1247 keV [Buc05]. Based on the SeGA efficiency at this energy, this state is the main final state of the βp channel.

- γ rays at 332 keV are due to the de-excitation of the first excited state ($5/2^+$) in ^{21}Na. Because ^{22}Al was part of the cocktail beam and was also implanted in the DSSD, ^{21}Na excited states could be populated from one of two possible decay paths:

  – $^{23}\text{Si} \xrightarrow{\beta 2p} {}^{21}\text{Na}$ or

  – $^{22}\text{Al} \xrightarrow{\beta p} {}^{21}\text{Na}$

  The β decay of ^{22}Al was recently studied by Achouri *et al* [Ach06]. This experiment also relied on proton and γ-ray coincidences and showed that the strongest proton group in coincidence with the 332 keV γ ray is expected at an energy of 1.3 MeV. The 332-keV γ-ray gated proton groups observed in the experiment of Ref. [Ach06] are summarized in Table 4.9. Since no proton group with an energy above 2 MeV was identified, we assume that the contribution from the ^{22}Al decay can be ignored, and thus that the 332-keV excited state in ^{21}Na was populated purely by the β-delayed 2p emission of ^{23}Si.

- γ rays at 584 keV appear in the spectrum that are due to the de-excitation of the first excited state in ^{22}Na. Since we have selected the events corresponding to ^{23}Si decays, two different decay paths can populate ^{22}Na with different half-lives:

  – $^{23}\text{Si} \xrightarrow{\beta p} {}^{22}\text{Mg} \xrightarrow{\beta} {}^{22}\text{Na}$ or

  – $^{23}\text{Si} \xrightarrow{\beta} {}^{23}\text{Al} \xrightarrow{\beta p} {}^{22}\text{Na}$.

  The two different effective half-lives of these two pathways will be limited by the half-life of the second β emitter, either $T_{1/2}(^{22}\text{Mg}) = 3.86$ s or $T_{1/2}(^{23}\text{Al}) = 470$ ms. After fitting the decay curve with all of the low-energy events in coincidence with this transition, we obtain a half-life of $T_{1/2} = 164(90)$ ms with a reduced χ^2 value of $= 323/170$. This value is of the same order of magnitude as the half-life of ^{23}Al. From this analysis it is concluded that the 584 keV γ rays are probably the signature of the β decay of ^{23}Si to the ^{23}Al ground state that is then followed by a βp decay to ^{22}Na. This branch was previously observed in other experiments focused on the decay of ^{23}Al [Saa11, Iac06] and [Per00] and would also confirm the spin-parity assignment of ^{23}Si ground state as a $5/2^+$ [Cza97, Bla97].

- γ rays at 1633 keV also have two possible origins, which will be discussed later in this chapter in Subsection 4.3.3.

4.3.1 βp decay channel in coincidence with γ rays.

In this section, we present the analysis method to deduce the excitation energies of the levels populated in ^{23}Al. Several γ-ray gates were applied to the charged particle spectrum in order to identify, and measure, the energy of the proton groups. The same background subtraction process as detailed in the βp decay of ^{20}Mg was applied to deduce the proton emission from excited levels above the one-proton and two-proton separation thresholds of ^{23}Al, at S_p=141.0(5) keV and S_{2p}=5645.2(6) keV respectively.

Since the background-subtraction process can result in channels with zero or negative counts, the fitting procedure was performed using the maximum likelihood method in ROOT. For all fit functions, the width parameter (σ) was fixed according to the energy resolution previously obtained (see Section 2.2.1). The value of the tail parameter due to β summing was deduced from a fit to the most intense proton group (peak number 1.15 in Figure 4.13), and was bound to be within $\pm$0.2% of this value. In the following analysis, the assessment of the proton peaks labelled with an $*$ is tentative, due to particluraly low statistics or huge uncertainties on the bin contents after being background subtracted.

$E_\gamma = 3155$ **keV**

The E_γ = 3155 keV transition arises from the de-excitation of the second 2^+ (at 4402 keV) to the first 2^+ excited state (at 1247 keV) of ^{22}Mg. The spectrum of charged particles emitted in coincidence with the 3155-keV γ rays, and after background subtraction, is presented in Figure 4.9. A total of five proton groups were observed. From the reduced χ^2 value to the fitted data, one additional group at high energy is tentatively proposed despite the relatively poor statistics for this transition. The energy of the proton groups are summarized in Table 4.6.

The particles in this spectrum were emitted from an excited state in ^{23}Al above the proton threshold. The energy of the associated initial proton-unbound levels in ^{23}Al, calculated as the sum of the proton threshold (S_p=141.0(5) keV), plus the energy of the γ-ray and the energy of the protons, are also given in this table. The corresponding decay scheme from the unbound levels in ^{23}Al is presented in Figure 4.10.

#	$E_{centroid}$ (keV)	E_p (keV)	E^*_{level} (^{23}Al)	Intensity (%)
1.01∗	1648 (85)	1683 (92)	6226 (92)	0.30 (25)
1.02	2300 (52)	2345 (59)	6888 (59)	0.66 (24)
1.03	2766 (83)	2817 (86)	7360 (86)	0.82 (36)
1.04	3171 (65)	3227 (68)	7770 (68)	0.55 (23)
1.05	3643 (73)	3705 (75)	8248 (75)	0.44 (20)
1.06∗	6218 (151)	6303 (158)	10846 (158)	0.053 (11)

Table 4.6 – Proton energies in the 3155-keV gated spectrum and their associated levels in ^{23}Al. The uncertainties on the proton energies are deduced from the fit and the calibration uncertainties. Intensities are calculated from the ratio of the area of the peaks over the total number of decays, corrected of the efficiency of the Ge array.

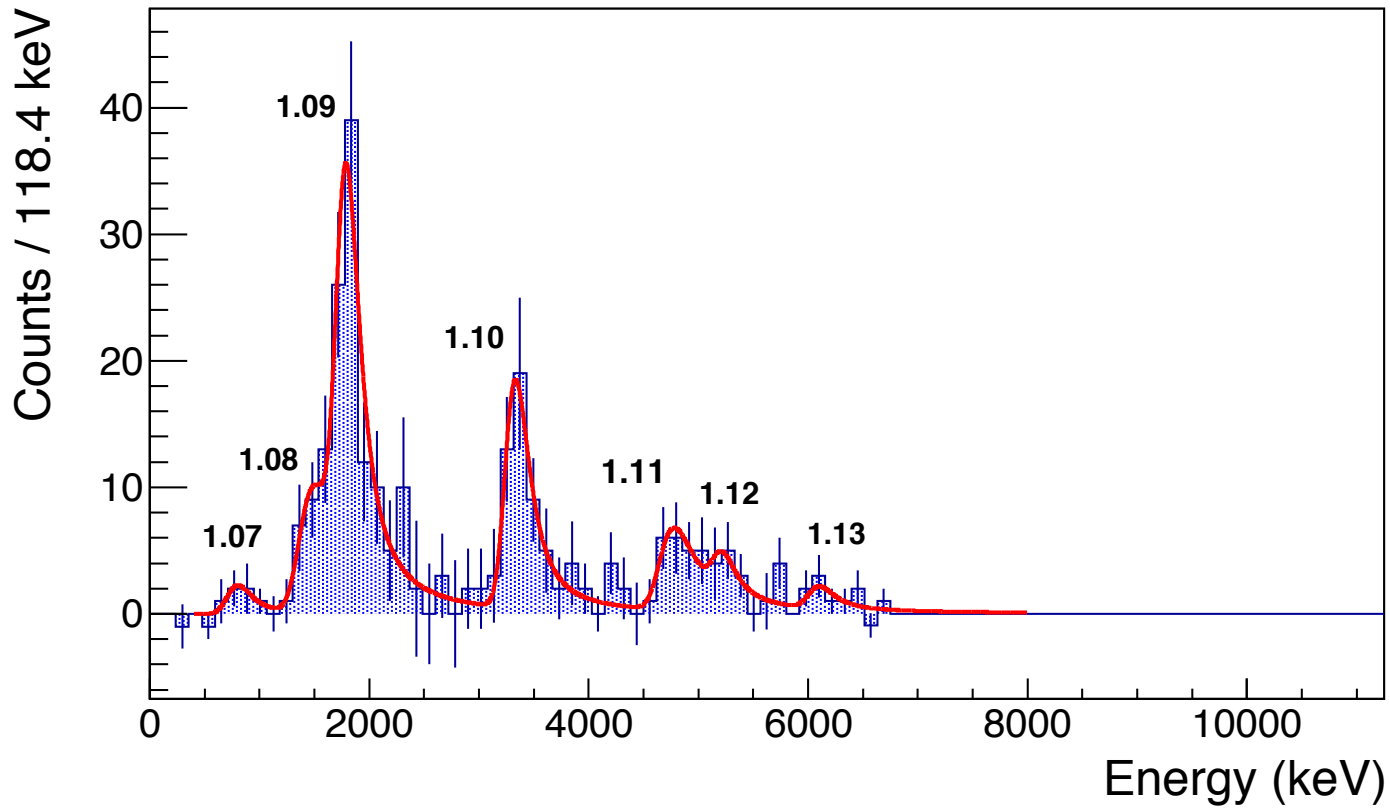

Figure 4.9 – Because of the low statistics in this γ-ray gated spectrum (the SeGa efficiency at 3155 keV is around 3.6 %), the spectrum has very low statistics and the identification of low-intensity transition is difficult. However, and according to the resolution at this energy ($\sigma \approx 64$ keV), the fit function made of 6 proton groups gives the best overall reduced χ^2.

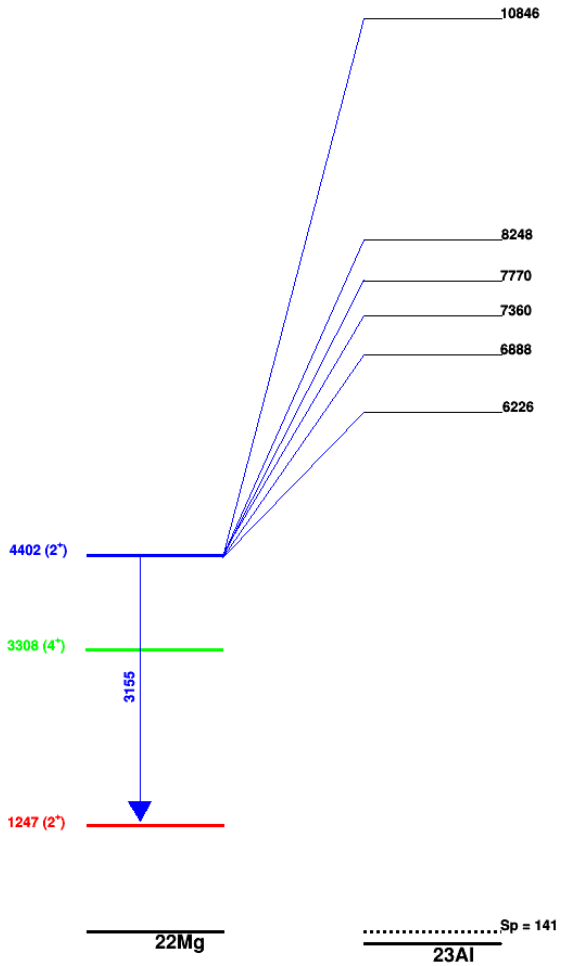

Figure 4.10 – Decay scheme of ^{23}Si built on the basis of the proton groups in coincidence with the γ rays emitted by the de-excitation of the 4402-keV excited state of ^{22}Mg.

$E_\gamma = 2061$ **keV**

The transition at $E_\gamma = 2061$ keV is due to the de-excitation of the first 4^+ (at 3308 keV) to the first 2^+ state (at 1247 keV) in ^{22}Mg. In Figure 4.11, which presents the background-subtracted spectrum of protons in coincidence with this transition, we observed at least three strong transitions. Based on the resolution of the DSSD detector at this energy, and comparing with the broadness of the counts, the structure between 4.2 MeV and 5.6 MeV was fitted with a doublet. The resulting uncertainty on the centroids are larger than any of the other proton groups. The energies of the proton transitions, the energies of the excited states and their associated uncertainties and branching ratios were calculated in the same way as in the previous case for ^{20}Mg. These results are summarized in Table 4.7. Figure 4.12 presents the partial decay scheme of the proton-unbound levels in ^{23}Al which decay to the 4^+ excited state in ^{22}Mg. By adding the proton group 1.08 at 1432 keV, the reduced χ^2 improves from 32/40 to 21/40. Despite the low branching ratio associated with this transition, we assume that this confirms the existence of this transition.

#	$E_{centroid}$ (keV)	E_p (keV)	E^*_{level} (^{23}Al)	Intensity (%)
1.07	785 (84)	806 (97)	4255 (97)	0.13 (6)
1.08∗	1432 (49)	1463 (63)	4912 (63)	0.50 (13)
1.09	1761 (21)	1798 (41)	5247 (41)	1.72 (22)
1.10	3309 (28)	3367 (34)	6816 (34)	0.93 (17)
1.11	4734 (44)	4809 (51)	8258 (51)	0.38 (10)
1.12	5151 (125)	5230 (128)	8679 (128)	0.23 (11)
1.13∗	6084 (76)	5230 (93)	9533 (93)	0.12 (5)

Table 4.7 – Proton energies in the 2061-keV gated spectrum and their associated levels in ^{23}Al. The uncertainties on the proton energies are deduced from the fit and the calibration uncertainties. Intensities were calculated from the ratio of the area of the peaks over the total number of decays, corrected of the efficiency of the Ge array.

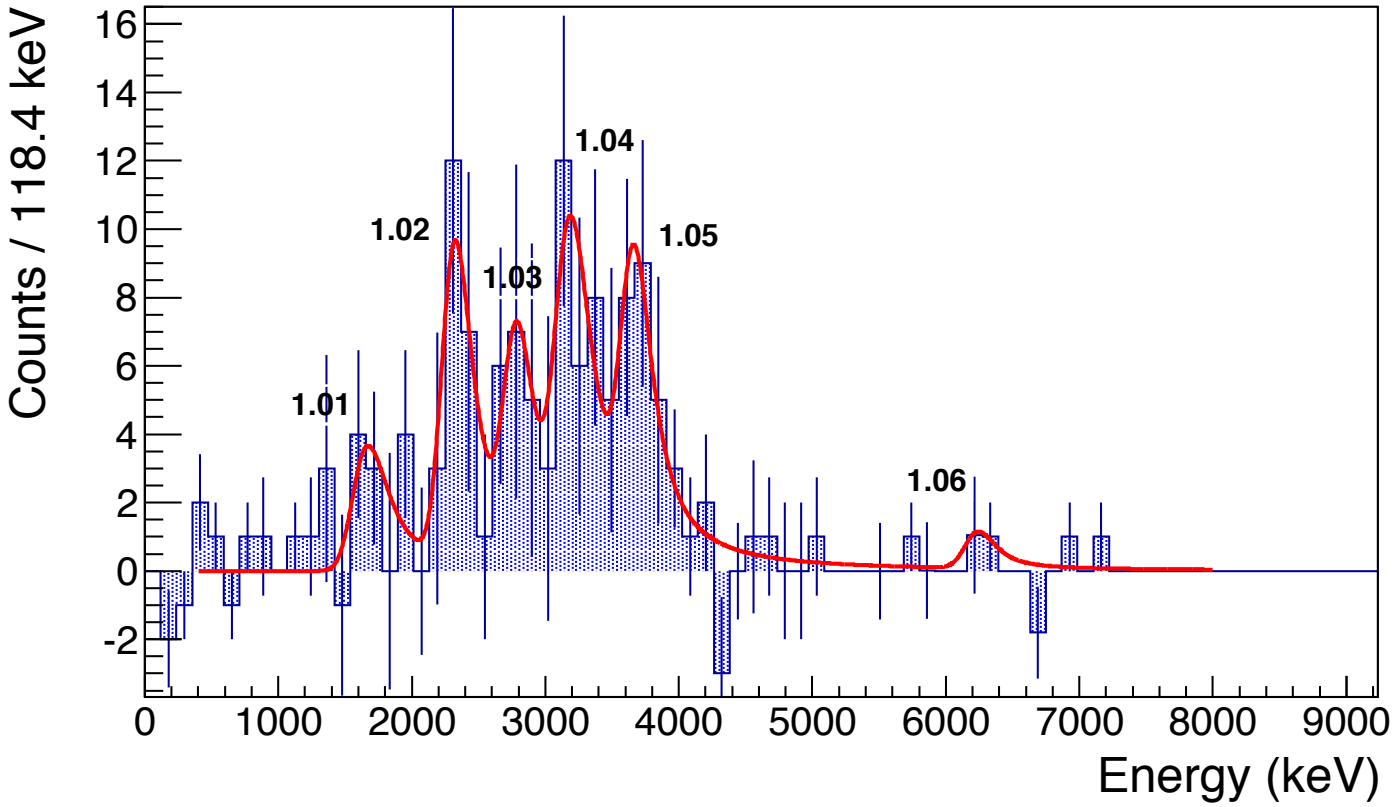

Figure 4.11 – Spectrum of charged particles in coincidence with $E_\gamma = 2061$ keV, after background subtraction. Six transitions were identified, and allows the identification of several unbound levels in ^{23}Al. Using a fit function made of seven distributions gives a reduced χ^2 value of 32.2/30.

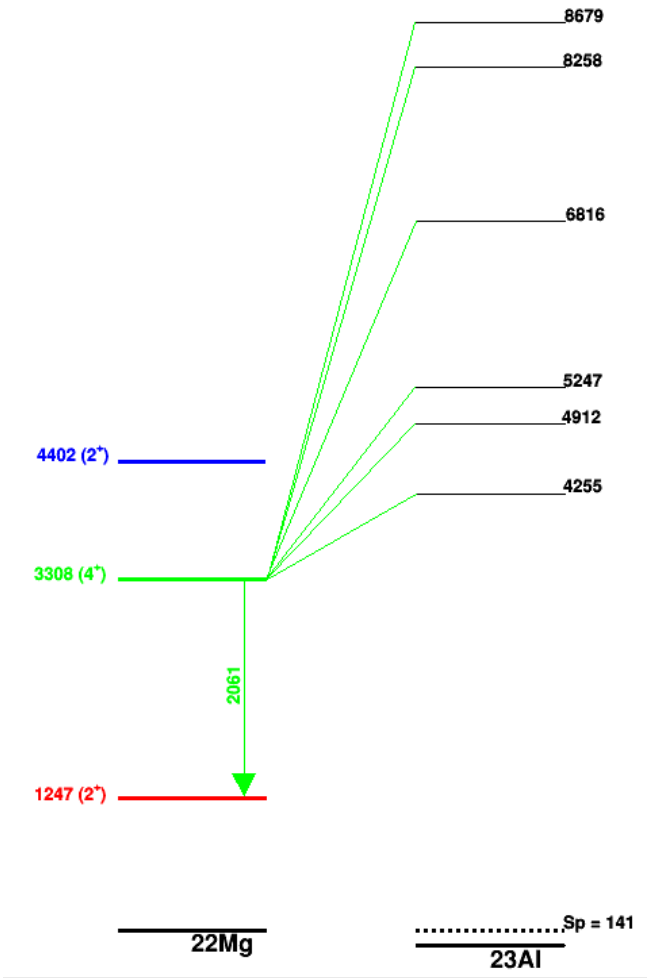

Figure 4.12 – Partial decay scheme of ^{23}Al built on the basis of the proton groups in coincidence with γ rays emitted from the de-excitation of the 3308 keV excited state of ^{22}Mg.

$E_\gamma = 1247$ **keV**

The γ-ray transition at 1247 keV is the signature of the de-excitation of the first excited 2^+ state in ^{22}Mg to its ground state. Protons detected in coincidence with the 1247-keV γ ray correspond to those protons emitted following the decay of a highly excited unbound level in ^{23}Al to this state. However, since the two more energetic states feed this first 2^+ excited state from above (the 2061 keV and the 3155 keV γ rays described above feed this state), their contribution in the proton spectrum must also be subtracted. The two spectra, from both the E_γ=2061 keV and the E_γ=3155 keV gates were subtracted after being normalized for their respective γ-ray efficiencies. The energies of the remaining transitions were deduced from the energies of the proton groups, and results are summarized in Table 4.8. Based on the previous measurement in coincidence with the 3155-keV γ-ray transition, we conclude that the last proton group 1.27 at 8.18 MeV does not correspond to β-delayed proton emission from the IAS but from a state at lower energy in ^{23}Al. The corresponding partial decay scheme from the unbound levels in ^{23}Al to the first excited state in ^{22}Mg at 1247 keV is provided in Figure 4.13.

#	$E_{centroid}$ (keV)	E_p (keV)	E^*_{level} (^{23}Al)	Intensity (%)
1.13∗	1137 (48)	1164 (65)	2551 (65)	0.40 (16)
1.14	1880 (46)	1918 (51)	3306 (51)	2.24 (39)
1.15	2334 (4)	2376 (28)	3764 (28)	18.68 (85)
1.16	2776 (9)	2834 (25)	4222 (25)	5.33 (60)
1.17	3398 (37)	3510 (41)	4898 (41)	0.83 (34)
1.18	3753 (22)	3863 (29)	5251 (29)	1.75 (35)
1.19	4156 (30)	4264 (36)	5652 (36)	0.92 (31)
1.20	4778 (21)	4864 (34)	6252 (34)	0.91 (42)
1.21∗	5064 (52)	5142 (59)	6530 (59)	0.48 (36)
1.22	5441 (21)	5523 (41)	6910 (41)	0.69 (23)
1.23	5843 (21)	5943 (46)	7331 (46)	0.59 (23)
1.24∗	6272 (60)	6361 (76)	7748 (76)	0.298 (117)
1.25	6680 (36)	6772 (64)	8160 (64)	0.225 (101)
1.26∗	7408 (27)	7505 (70)	8893 (70)	0.145 (87)
1.27	8282 (77)	8384 (110)	9772 (110)	0.126 (75)

Table 4.8 – Energies of the proton peaks in the 1247-keV gated spectrum and their associated levels in ^{23}Al. Peaks labelled with an $*$ are tentative because of the poor resolution and the high density of proton groups between 3 and 7 MeV. If we include these peaks in the fit function, it gives a reduced χ^2 value of 80/81.

The first nine proton groups in the energy spectrum are presented in Figure 4.14. Two

proton groups 1.15 and 1.16 were clearly identified. Proton group 1.15 at 2.4 MeV is the strongest transition in this spectrum, and appears to be the main component of the proton group 4 in the ungated spectrum. Above 3.5 MeV, the proton groups are less resolved and have much lower intensities. Figure 4.15 presents the energy spectrum from 3 to 9 MeV.

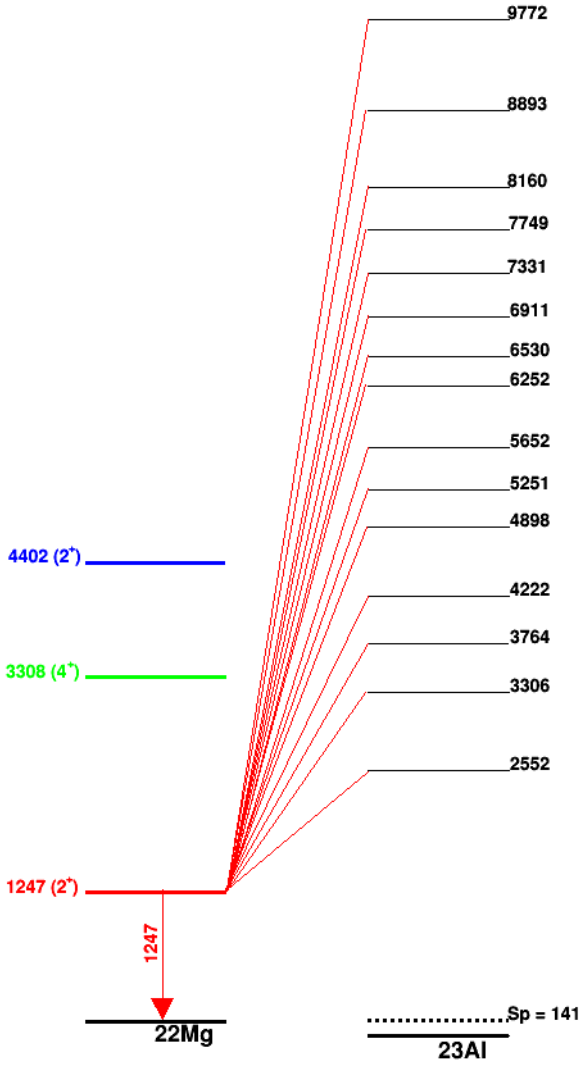

Figure 4.13 – Decay scheme of ^{23}Al based on the proton groups in coincidence with the γ-rays emitted by the first excited state at 1247 keV in ^{22}Mg.

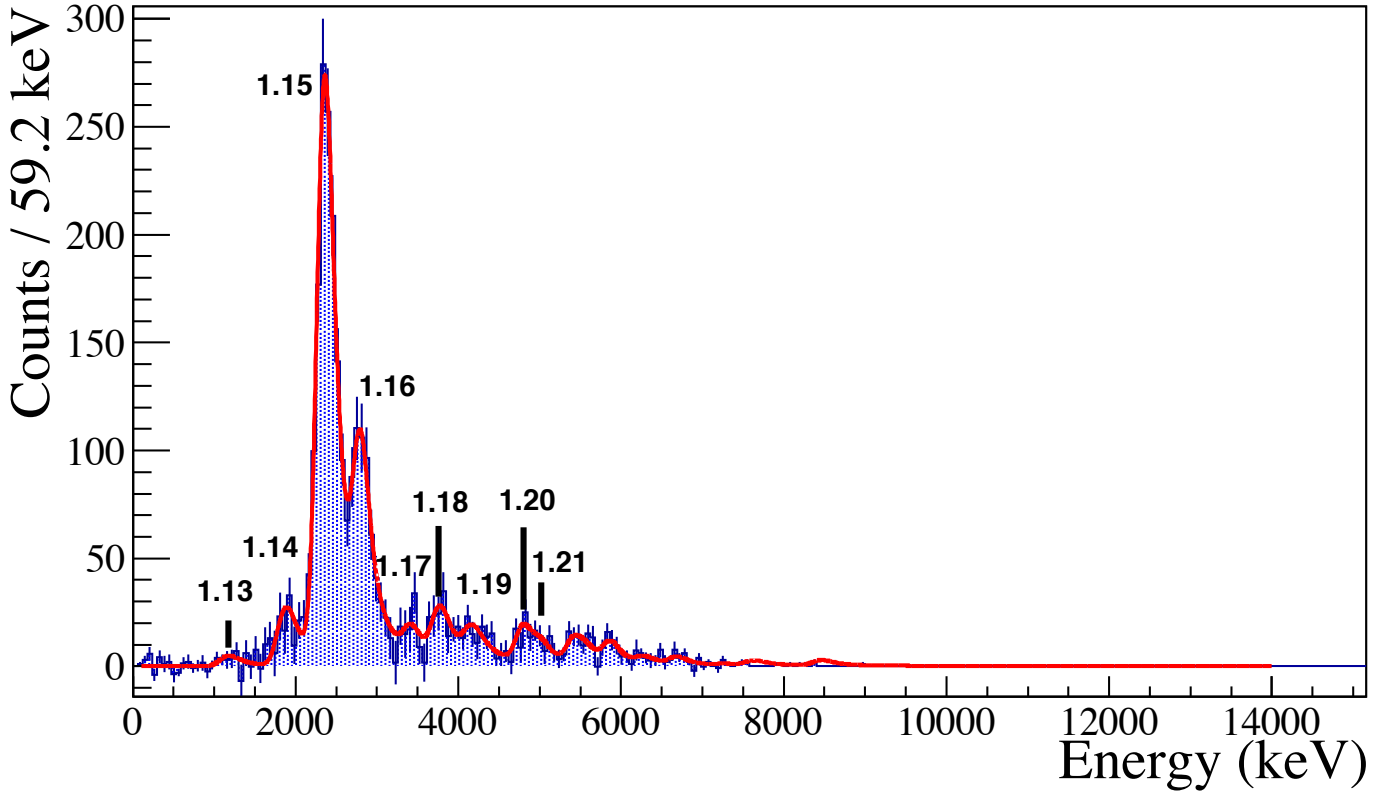

Figure 4.14 – Zoom in on the low energy part of the charged-particle energy spectrum emitted in coincidence with the 1247-keV γ rays after background and γ-ray up-feeding subtraction. In red, the fit function.

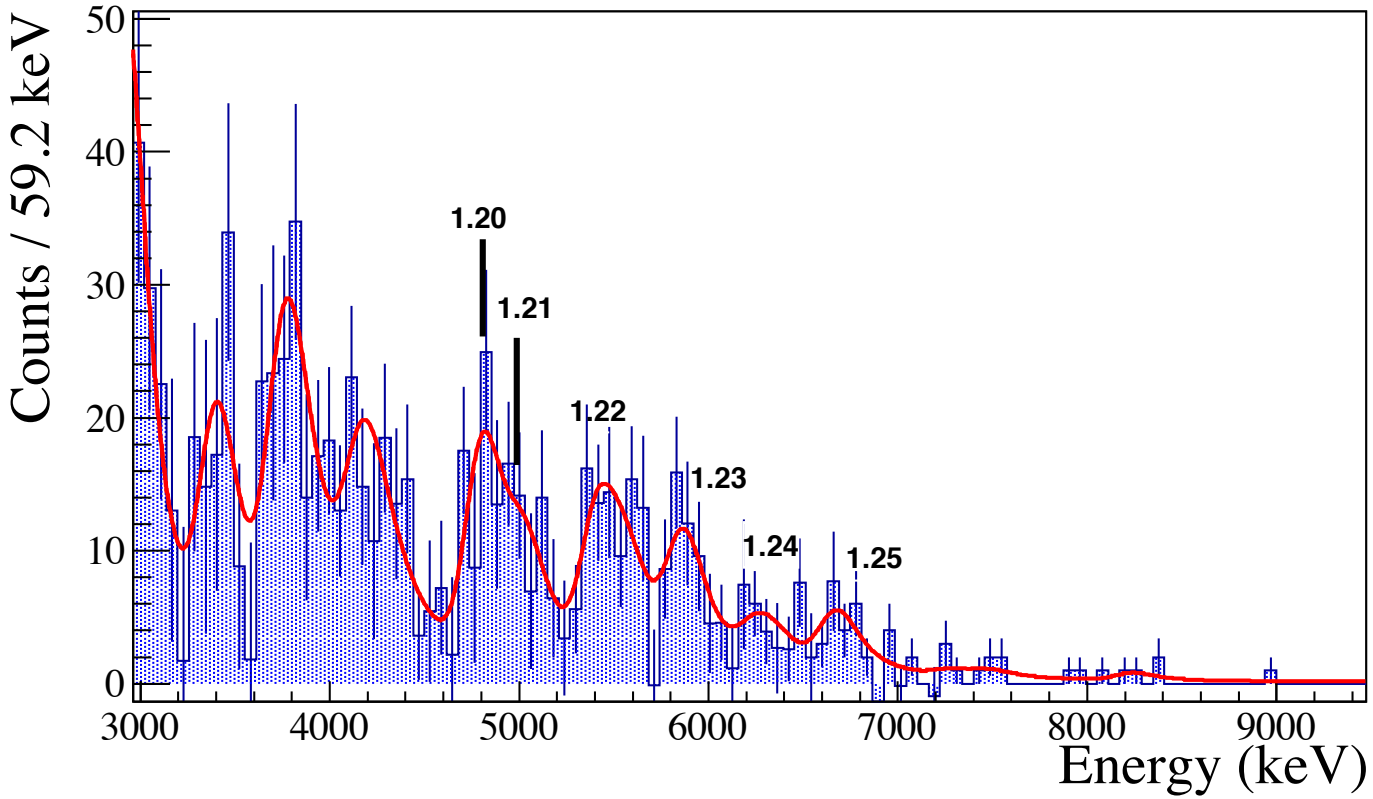

Figure 4.15 – The parameters corresponding to the β-summing tail and the width of the proton component of the fit function were bound and fixed respectively to allow the identification of the proton groups in this wide structure.

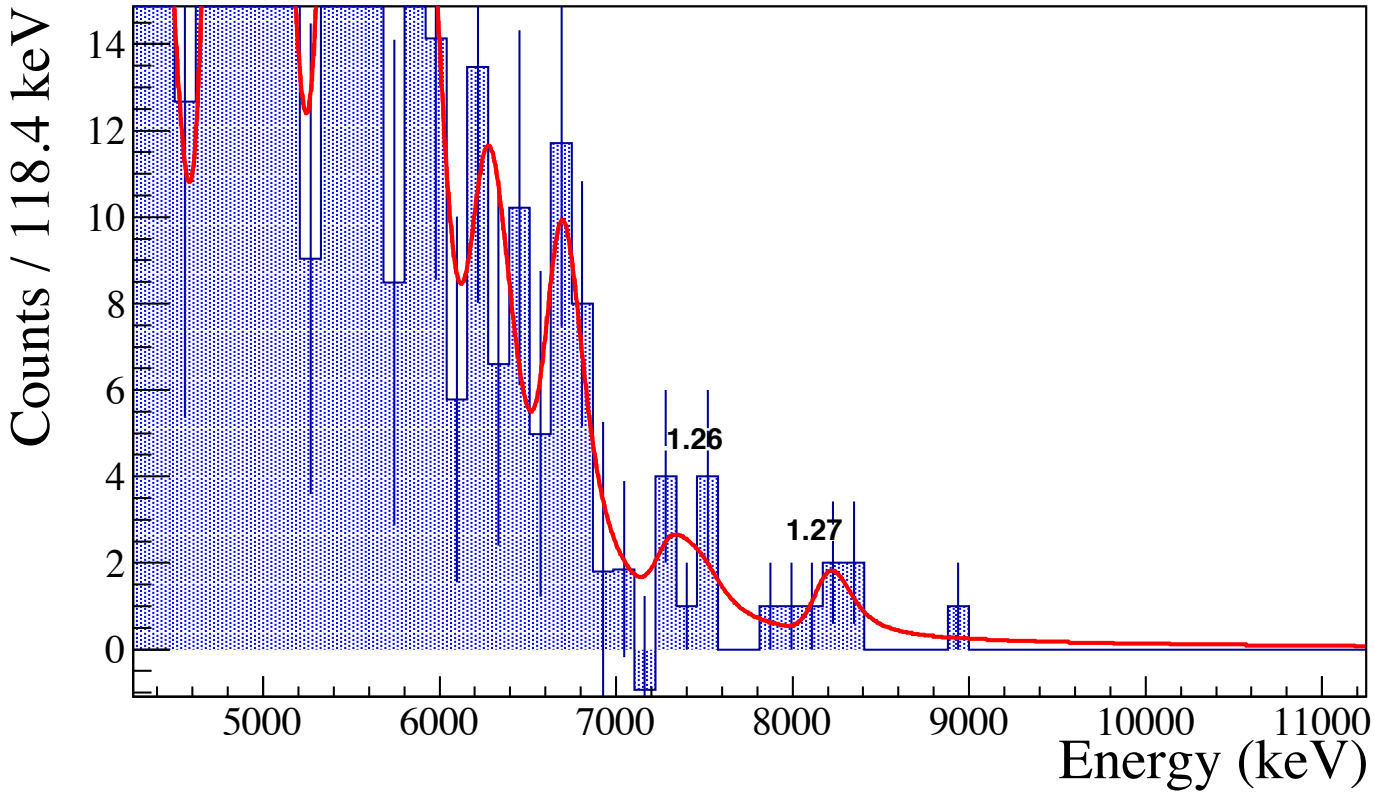

Figure 4.16 – Zoom in of the previous spectrum on the high energy part. In red, the function is fitted with the maximum likelihood method.

4.3.2 β2p decay channel in coincidence with $E_\gamma = 332$ keV

The presence of the E_γ=332 keV transition in the γ-ray spectrum correlated to ^{23}Si decays is a clear signature of the β2p channel. This transition is due to the de-excitation of the first excited state in ^{21}Na. The gated and subtracted spectrum is shown in Figure 4.17. Table 4.9 summarizes the energy of the proton groups. The PHD corrections are, in this case, calculated as the average between the two extremes, when the two protons are emitted in the same direction and when they are emitted in opposite directions (the recoil ion is static). The difference between these two cases was then included as an uncertainty in addition to the uncertainties from the fit and calibration processes. The two-proton separation energy is $S_{2p} = 5645$ keV (deduced from AME2012 [Wan12]) and this was added to the energy of the proton groups to determine the excitation energies.

As explained above (see Section 4.3), this particular γ ray at 332 keV could also be the signature of βp decay of ^{22}Al, a known contaminant in the secondary cocktail beam. In this case, the most intense proton group in coincidence with the 332-keV γ-ray transition has an energy of 1.3 MeV [Ach06], with a branching ratio of $\sim$18.5%. In this work, a total of 17(16) events were observed in the energy range between 1.0 and 1.6 MeV which could be evidence for this group. This value and its uncertainty are compatible with zero, and thus any possible contamination that arise from false correlations of ^{22}Al decay in the ^{23}Si decay spectra can be considered negligible.

The most intense proton group in the 332-keV γ-ray gated proton spectrum is due to the β-delayed two-proton emission from the IAS in ^{23}Al to the first excited state in ^{21}Na. In the present work, the corresponding excitation energy of the IAS is 11.71(6) MeV, which is in very good agreement with the previous measurement from Blank *et al.* [Bla97] who deduced an IAS energy of 11.78(6) MeV. The decay scheme corresponding to the two-proton emission from unbound excited states in ^{23}Al is presented in Figure 4.18.

#	$E_{centroid}$ (keV)	E_{kin} (keV)	E^*_{level} (^{23}Al) (keV)	Intensity (%)
2.01$\star$	2137 (87)	2169 (45)(87)	8147 (98)	0.26% (14)
2.02	3789 (79)	3835 (48)(79)	9812 (91)	0.51% (16)
2.03	5145 (76)	5200 (55)(76)	11177 (94)	0.24% (8)
2.04	5683 (28)	5740 (57)(28)	11717 (64)	0.91% (16)

Table 4.9 – Energies of the proton groups in the 332-keV gated spectrum and their associated levels in ^{23}Al. In the column E_{kin}, the energy of the proton group takes into account the uncertainty of the emission angle between the two protons.

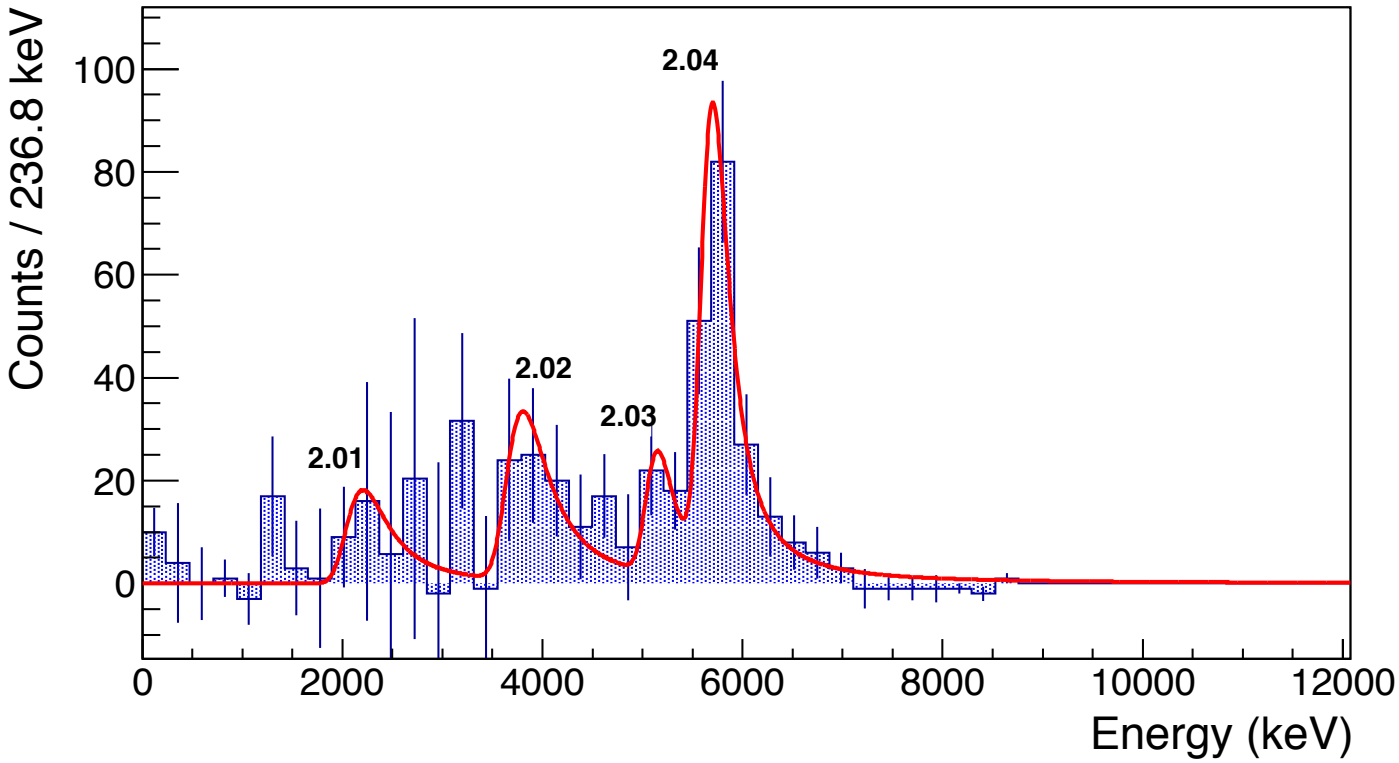

Figure 4.17 – Spectrum in coincidence with the E_γ=332 keV transition in ^{21}Na. In red, the fit function.

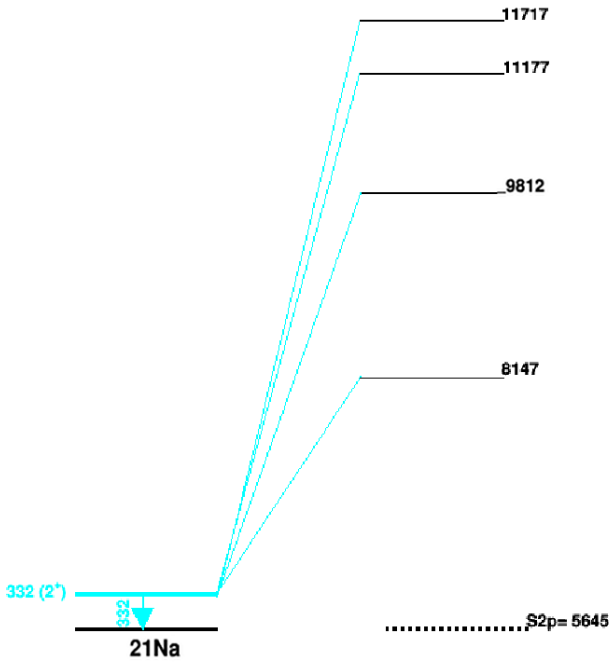

Figure 4.18 – Decay scheme of ^{23}Al based on the proton groups in coincidence with the γ rays emitted by the first excited state at 332 keV in ^{21}Na.

4.3.3 β3p decay channel in coincidence with $E_\gamma = 1633$ keV

This γ-ray transition at $E_\gamma = 1633$ keV rises from the de-excitation of the first excited 2^+ state in ^{20}Ne. This is the daughter nucleus of the β3p decay of ^{23}Si and this rare decay channel is, in principle, possible based on Q-value arguments. However, this 1633-keV state in ^{20}Ne can also be populated from the β decay of ^{20}Na [Cli89, AS87] that is the most intense contaminant in the secondary cocktail beam. The spectrum of charged particles in coincidence with this γ-ray transition obtained for a maximum correlation time of 400 ms is presented in Figure 4.19.

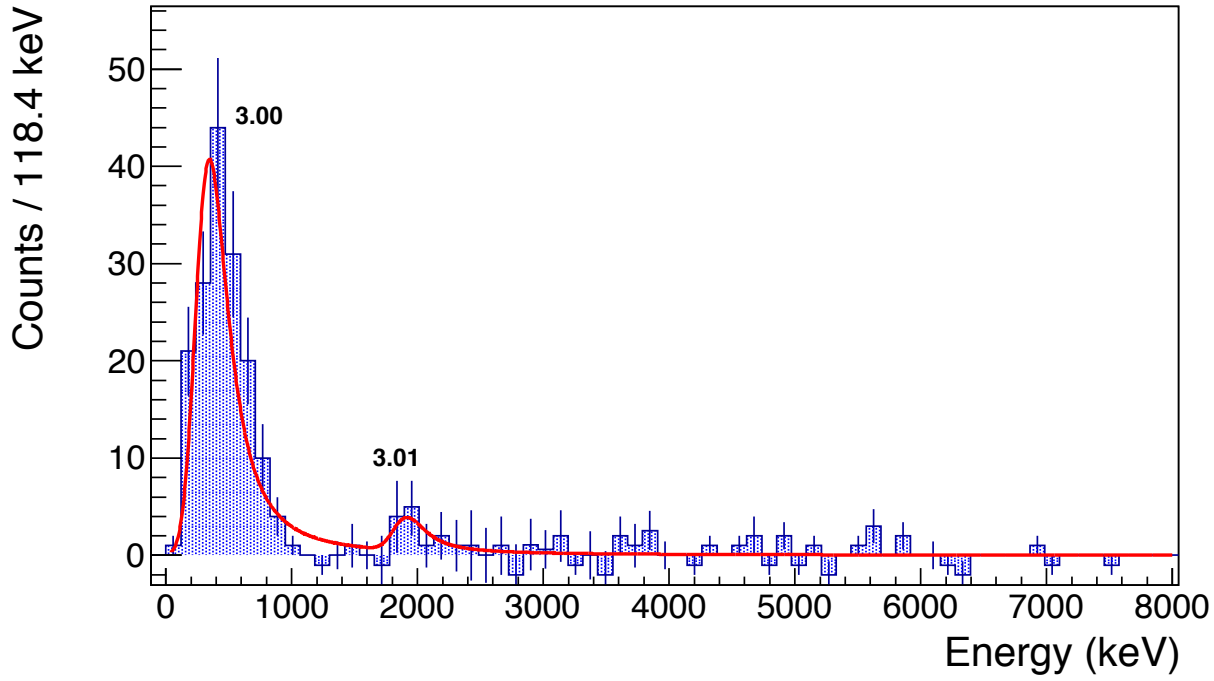

Figure 4.19 – Charged-particle spectrum in coincidence with the $E_\gamma = 1633$ keV transition in ^{20}Ne. In red, the fit function.

The charged particle group 3.00, at low energy, dominates the spectrum. The decay curve obtained from a gate on this group can be compared to the decay curve from high-energy events. The decay curves were fitted for a longer correlation time (2 s), as shown on Figure 4.20 and 4.21, in order to better constrain the fit. The resulting half-life obtained for the low-energy events has the same order of magnitude as the half-life of ^{20}Na. These events are thus identified as false correlations within the analysis process, and based on the energy recorded in DSSD2, correspond primarily to β particles from ^{20}Na decay in false coincidence with implants of ^{23}Si.

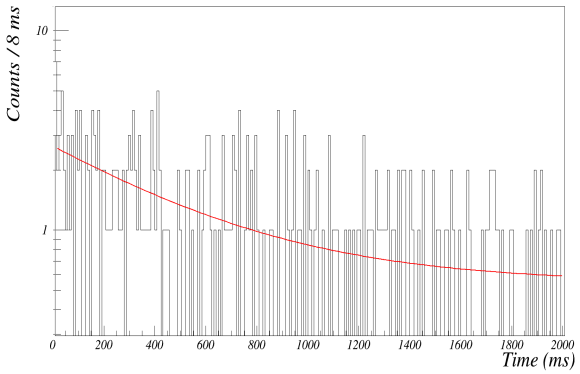

Figure 4.20 – Decay curve of the events in the group of particles with an energy lower than 1 MeV. The fit of the decay curve is giving a half-life of 355 (148) ms, which is consistant with the half-life of ^{20}Na.

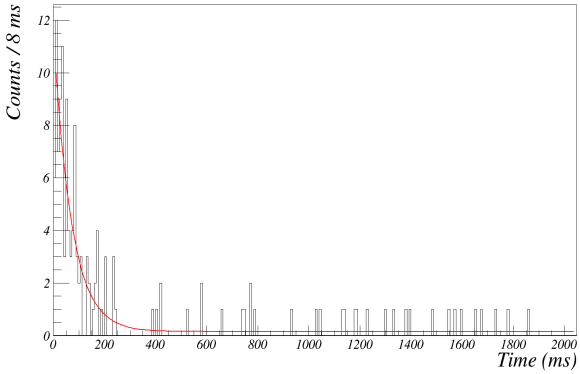

Figure 4.21 – Decay curve of the events with an energy higher than 1.1 MeV. The fit of the decay curve is giving a half-life of 41.0 (55) ms, which is close to the adopted value of the half-life of ^{23}Si.

The half-life deduced for proton group 3.01, $T_{1/2}$=41.0(55) ms, is much shorter that deduced for the low-energy β particle events. Although this result is ten times less precise, its magnitude is in good agreement with the previously measured ^{23}Si half-life of $T_{1/2}$=42.3(4) ms . If we assume that these events are three-proton decays to the 1633-keV excited state in ^{20}Na, the corresponding excitation energy of the parent state in ^{23}Al is deduced to be 11.71(11) MeV, as presented in Table 4.10. This value is in good agreement with the previous measurement of the excitation energy of the IAS in ^{23}Al. The large uncertainties on the centroids and the level energies are due to the PHD corrections in both extreme cases: when the recoil energy is zero, and when it is maximal (meaning that the 3 protons are correlated). We propose that this proton group is a candidate for the first observation of β3p decay from ^{23}Si.

	$E_{centroid}$	E_{proton} (keV)	E^*_{level} (^{23}Al)	Intensity (%)
3.00	320 (29)	-	-	-
3.01	1890 (99)	1998 (100)(105)	11707 (111)	0.16% (12)

Table 4.10 – Energies of the proton peaks in the 1633-keV gated spectrum and their associated levels in ^{23}Al. The first proton group is identified as β particles from ^{20}Na decays. Only the second charged particle group at 1.9 MeV is identified as protons, and the corresponding excitation energy is in agreement with the IAS energy in ^{23}Al as determined from the γ-ray gated proton spectra.

4.4 The ungated charged particle spectrum

All of the γ-ray gated particle spectra presented above were normalized (according the HPGe detection efficiency at each γ-ray energy), summed and subtracted from the total charged-particle energy spectrum. The resulting spectrum are only those particle decays that proceed from excited states in ^{23}Al to the ground states of the daughter nuclei. This spectrum is presented in Figures 4.22, 4.23 and 4.24. The energy of the proton groups identified in this complicated spectrum are presented in Table 4.11, as well as the corresponding excitation energies. The proton group 0.17 at 5.97 MeV is in good agreement with the energy expected for the β2p channel to the ground state of ^{21}Na and corresponds to an excited level at 11679(72) keV.

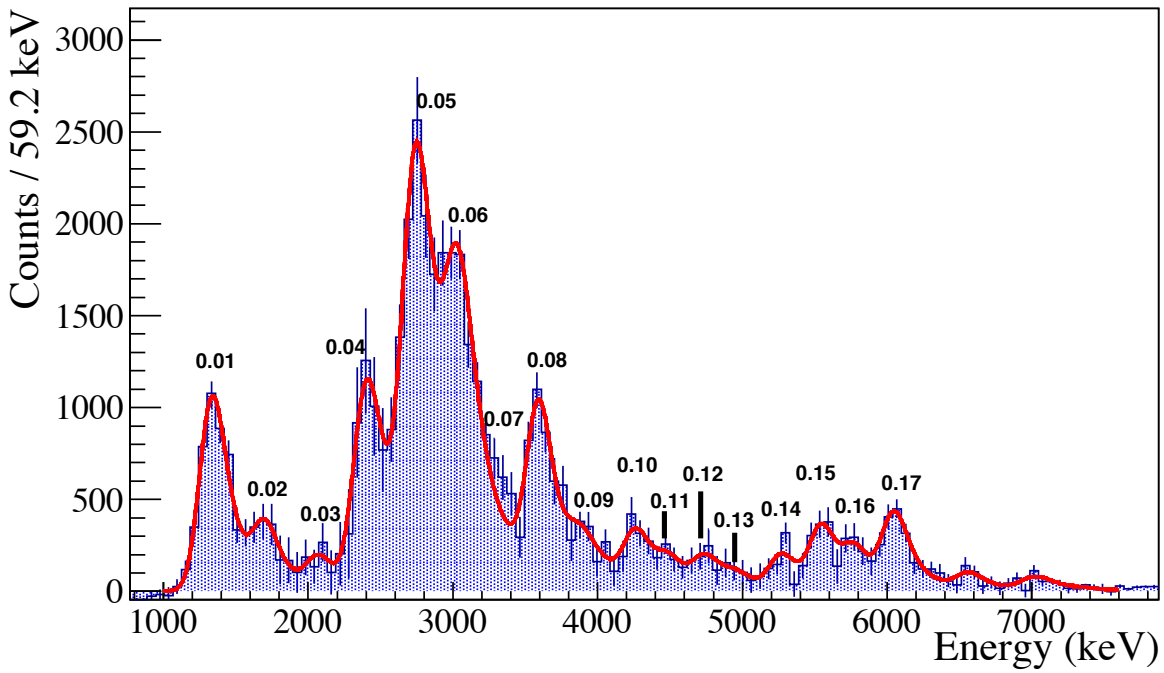

Figure 4.22 – Zoom in on the low-energy part of the ungated ground-state charged-particle spectrum. Because of the β background at low energies, the fit function (in red) begins at 1 MeV.

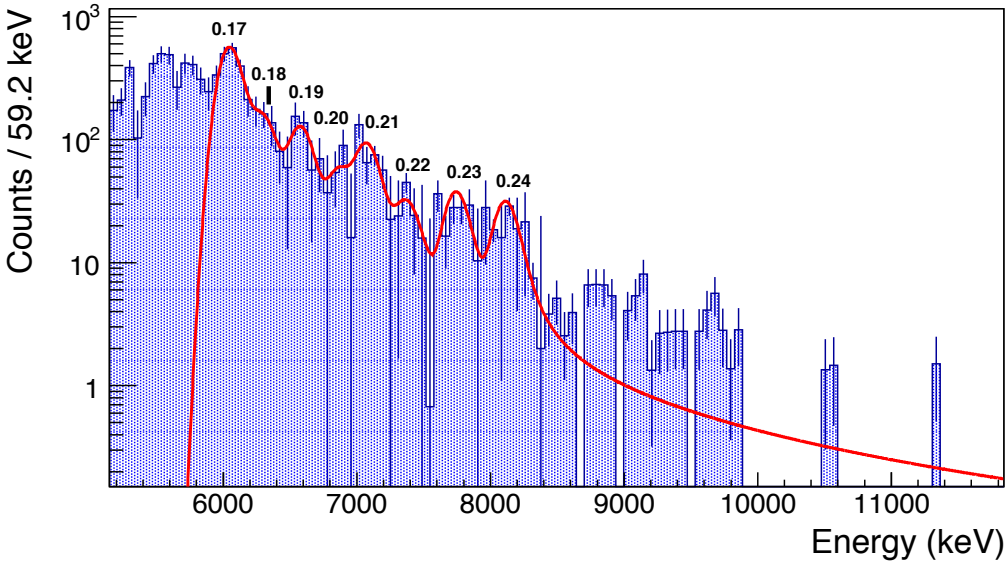

Figure 4.23 – Zoom in on the ungated ground-state charged-particle spectrum. In red, the fit function.

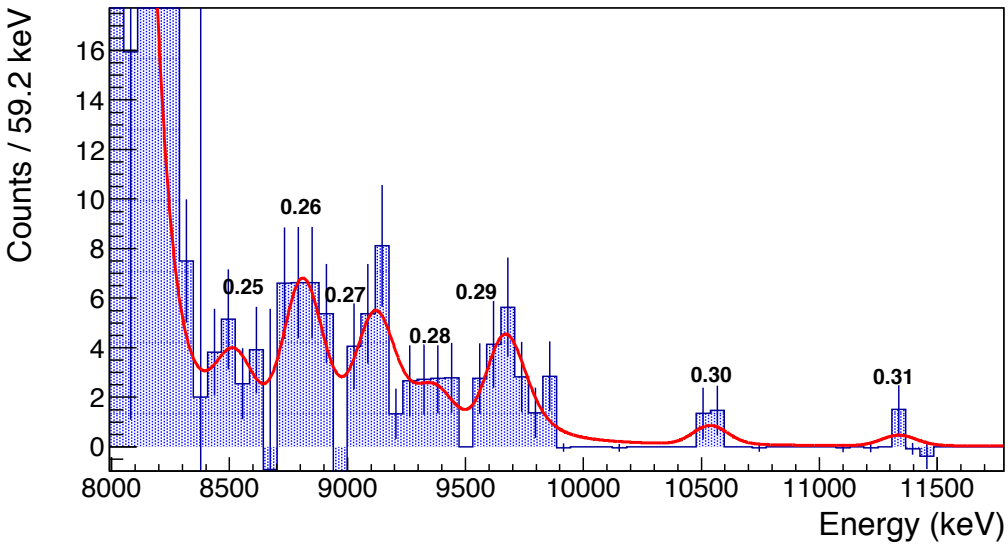

Figure 4.24 – Zoom in on the ungated ground-state charged-particle spectrum. In red, the fit function. The last proton group (0.31) in the spectrum is a possible candidate for proton decay of the IAS in ^{23}Al to the ground state of ^{22}Mg.

#	$E_{centroid}$	E_{proton} (keV)	E^*_{level} (^{23}Al)	Intensity (%)
0.01	1312 (5)	1342 (37)	1483 (37)	5.78% (28)
0.02	1698 (21)	1733 (38)	1874 (38)	2.03% (54)
0.03	2054 (51)	2095 (58)	2236 (58)	1.32% (38)
0.04	2369 (11)	2415 (27)	2556 (27)	8.4% (12)
0.05	2730 (8)	2780 (24)	2921 (24)	15.67% (84)
0.06	3016 (12)	3070 (25)	3211 (25)	7.68% (51)
0.07⋆	3306 (35)	3364 (41)	3505 (41)	1.21% (31)
0.08	3580 (10)	3642 (25)	3783 (25)	4.02% (27)
0.09⋆	3862 (31)	3927 (40)	4068 (40)	1.55% (26)
0.10	4242 (21)	4311 (36)	4452 (36)	1.28% (20)
0.11⋆	4478 (36)	4549 (48)	4690 (48)	0.65% (15)
0.12	4716 (36)	4791 (50)	4932 (50)	0.78% (22)
0.13⋆	4929 (53)	5006 (65)	5147 (65)	0.46% (19)
0.14	5243 (21)	5323 (47)	5464 (47)	0.91% (14)
0.15	5518 (15)	5601 (48)	5742 (48)	1.69% (20)
0.16	5745 (24)	5829 (54)	5970 (54)	1.06% (20)
0.17	6026 (11)	6084 (54)	**11729 (79)**	2.10% (10)
0.18⋆	6284 (10)	6373 (58)	6514 (58)	0.39% (3)
0.19	6558 (7)	6649 (61)	6790 (61)	0.42% (2)
0.20⋆	6852 (16)	6945 (68)	7086 (68)	0.17% (2)
0.21	7052 (9)	7147 (69)	7288 (69)	0.33% (2)
0.22	7355 (16)	7451 (75)	7592 (75)	0.10% (1)
0.23	7720 (14)	7818 (80)	7959 (80)	0.16% (1)
0.24	8089 (18)	8190 (87)	8331 (87)	0.14% (1)
0.25⋆	8492 (46)	8595 (102)	8736 (102)	0.013% (6)
0.26	8779 (32)	8882 (101)	9023 (101)	0.03% (15)
0.27	9057 (35)	9162 (106)	9303 (106)	0.026% (8)
0.28	9345 (49)	9450 (116)	9591 (116)	0.011% (5)
0.29	9591 (31)	9697 (113)	9838 (113)	0.023% (3)
0.30	10526(47)	10634 (132)	10775 (132)	0.004% (2)
0.31	11365(54)	11474 (148)	**11615 (148)**	0.002% (1)

Table 4.11 – Energies of the proton peaks in the ungated ground-state charged-particle spectrum and their associated levels in ^{23}Al. The proton group at 5977 keV corresponds to the expected energy for β-delayed 2-proton emission from the IAS to the ^{21}Na ground state. Adding those proton groups labelled with an $*$ does not significantly improve the reduced χ^2 and so the corresponding excited states in ^{23}Al are considered to be tentative.

4.5 Discussion on the excitation energies

Based on the above charged-particle spectra, an updated decay scheme of ^{23}Si can be constructed that is presented here. A total of 14 proton-unbound levels were identified in ^{23}Al, compared to only 5 levels that were known previously [Bla97]. The criteria that were used to propose a new level in ^{23}Al was to have at least two independent decay pathways that originated from the same energy level within an uncertainty of $\pm$ 90 keV. When several transitions were identified as originating from the same unbound excited state in ^{23}Al, the excitation energy of this state was determined using the weighted average of the different pathways. If two distinct decay pathways could not be established from the same state, a new level was proposed in ^{23}Al only if the single proton group had a sufficient branching ratio ($\geq$ 0.2%) and whose fit yielded an area whose confidence threshold was larger than 3σ (proton peaks that do not satisfy this condition are labelled with a $\star$ in the analysis presented below). Table 4.12 summarizes all of the proton groups that were identified in the present study, and present the weighted average excitation energies for each level in ^{23}Al. The branching ratios were calculated with respect to the total number of particles detected in the DSSD2 and corrected using the efficiency distribution described in Section 2.2.1.

In the following section, a comparison of the excitation energies and branching ratios of the already know from the previous measurement [Bla97] is also provided.

Discussion about the level at 1483 (37) keV

In the previous study of the β-delayed proton decay of ^{23}Si [Bla97], the proton group 2 at 1.32(40) MeV in Table 4.2 was assigned to the proton decay from a state at 1.45 MeV excitation energy in ^{23}Al to the ground state of ^{22}Mg with a branching ratio of $\approx$ 7.8% [Bla97]. Using the 2061-keV γ-ray gate, we observed that the main component in this proton group corresponds to charged particle decay to the 3308-keV states in ^{22}Mg. In the ungated spectrum, and after the upfeeding subtraction, we still observed a proton transition at 1.34 keV. Thus, we confirm the energy of the level but propose a lower branching ratio for this level ($\approx$ 5.8%).

Discussion about the level at 1874 (38) keV

In the previous measurement, the energy of this level was deduced from proton group 3 in Table 4.2. In the present work, we observed that this peak is in fact a doublet, made of proton groups 0.02 and 1.09, which correspond to a proton emission to the ground state and to the 3308-keV excited state in ^{22}Mg, respectively. Therefore, we measured a lower β-decay branching ratio to the 1874-keV state ($\sim$2 %).

Confirmation of the level at 3226 (23) keV

A proton group at 3.04 MeV was previously observed by Blank [Bla97] without any γ-gates. In the present work, we confirm the energy of this proton and that it is a transition to the ^{22}Mg ground state. A small component is also a transition to the first excited state in ^{22}Mg as confirmed by the existence of proton group 1.14 in the 1247-keV γ-ray gated spectrum.

Confirmation of the level at 3775 (19) keV

In the previous experiment [Bla97], this level was identified based on two protons that decay to the ground state of ^{22}Mg and the first excited state at 1247 keV. In the present work, we observed a proton group at 2.38 MeV (group 1.15) in coincidence with the 1247 keV γ-ray transition and a proton group at 3.64 MeV in the ungated ground-state spectrum. We confirm the energy of this level at 3.78 MeV, in good agreement with the energy previously measured at 3.77 MeV [Bla97]. We deduced a branching ratio for this state of 22.7% which is lower than the previous measurement (39.4%). This difference is due to the fact that the proton group 7 (in Table 4.2) observed by Blank *et al.* [Bla97] is made of a transition in coincidence with a 3155-keV γ ray in addition to the transition to the ground state.

Confirmation of the level at 4224 (24) keV

This level was deduced by Blank *et al.* [Bla97] from the observation of the strong proton group at 2.83 MeV. Using the γ-ray gates, we observed that this proton group is a doublet. Two decay paths corresponds to this energy: from a previously unobserved level at 2921-keV to the ground state, and from the previously known 4222-keV level to the first excited state in ^{22}Mg at 1247 keV.

Identification of the IAS at 11710 (43) keV

The energy of the Isobaric Analogue State was deduced from the spectrum gated on the γ-ray transition at 332 keV. This was the signature of a β-delayed 2-proton emission from the IAS to the first excited state of ^{21}Na. The 332-keV γ-ray gate applied to the proton spectrum also reveals the strong proton group 2.04 at 5683 keV. The identification of the proton group 0.17 in the ungated and subtracted ground-state spectrum, at 5977 keV, also confirms the two-proton decay from the IAS to the ground state of ^{21}Na. From these results, the IAS energy deduced in the present work is 11710(43) keV and is in good agreement with the value 11.78(6) MeV obtained previously.

In the ungated spectrum, two counts were observed in proton group 0.31 and correspond to an excitation energy of 11615(148) keV which in agreement with our estimation of the IAS energy.

A possible 3-proton emission from the IAS to the first excited state of ^{20}Ne, in coincidence with γ-rays at 1633 keV was identified in the spectrum presented in Figure 4.10. Because of the very low statistics, the uncertainties on the energy are large (111 keV). Adding this excitation energy to the set of data does not shift the average value.

The branching ratio for β decay of ^{23}Si to its IAS in ^{23}Al was determined to be 3.18 (25)%. Using the deduced half-life of $T_{1/2}$ = 42.80(27) ms (see below), we obtain a log ft value of 3.16 (13) which is in good agreement with the expected range of log ft values for allowed Fermi decays [Sin98].

3-proton decay to ^{20}Ne ground state

A weak transition from the IAS to the first excited state in ^{20}Ne was observed in the 1633-keV gated spectrum. We also expect a transition going to the ground state, and according to the energy of the IAS, the energy of this transition should be around 3.6 MeV. In this work, we are unable to conclude on a possible β3p decay to the ground state of ^{20}Ne due to the high intensity βp protons that decay with a similar energy. Figure 4.25 presents the range of energies where such a β3p proton group would be expected.

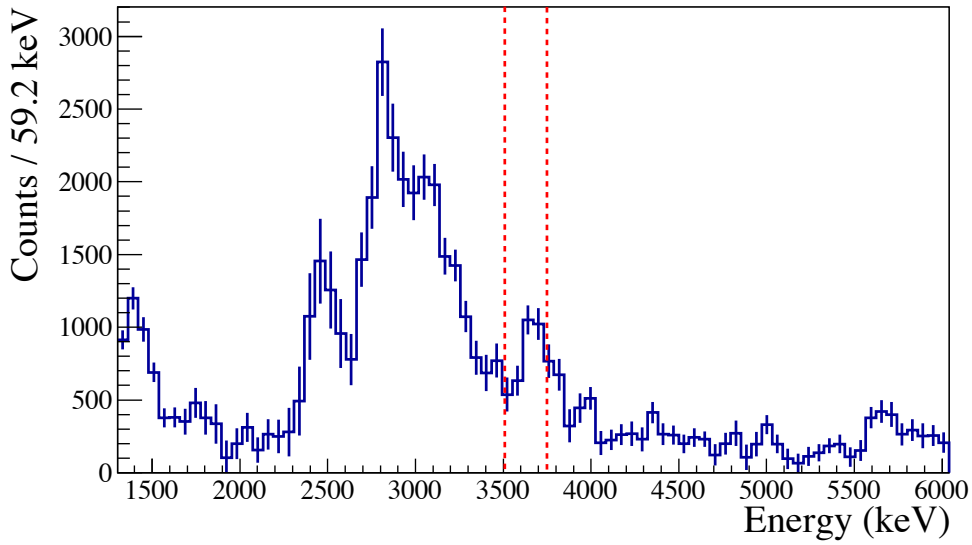

Figure 4.25 – The red dashed line indicates the energy range of a proton groups correspondig to the β3p decay from the IAS to the ^{20}Ne ground state. Due to significant amounts of βp decays with similar energies, we could not conclude on this β3p transition.

Level scheme of ^{23}Si

In this work, 14 levels were identified, including 9 new levels above the one- and two-proton thresholds. The ^{23}Si decay level scheme obtained in the present work is presented in Figure 4.26. Many of the levels presented in Figure 4.26 were only tentatively identified and some of the weakest proton groups could be the result of an incomplete background subtraction. This subtraction was particularly difficult because of the shape of the contribution of the contaminant, ^{20}Na, and the proton groups appearing in the energy range of the α-particle energy are ambiguous.

The final ^{23}Si decay level scheme used a strict set of criteria. Only those levels with branching ratios that exceeded 1% were included and of those, only those proton groups whose fits yielded a confidence interval that was larger than 3σ. The final level scheme, which includes a total of 12 levels (7 levels are newly proposed), is presented in Figure 4.27 and is compared to the previous measurements as well as a theoretical calculation using the USDB interaction [Bro].

#	4402 keV	332 keV	3308 keV	1247 keV	^{22}Mg g.s.	^{21}Na g.s.	1633 keV	E^*_{level}	BR (%)
1					1483 (37)			1483 (37)	5.78 (28)
2					1874 (38)			1874 (38)	2.03 (54)
3					2236 (58)			2236 (58)	1.32 (38)
4				2551 (65)	2556 (27)			2555 (25)	8.80 (20)
5					2921 (24)			2921 (24)	15.67 (84)
6				3306 (51)	3211 (25)			3226 (23)	9.92 (54)
7					3505 (41)			3505 (41)	1.21 (31)
8				3764 (28)	3783 (25)			3775 (19)	22.7 (85)
9					4068 (40)			4068 (40)	1.55 (26)
10			4255 (97)	4222 (25)				4224 (24)	5.46 (60)
11					4452 (36)			4455 (42)	1.28 (20)
12					4690 (48)			4690 (48)	0.65 (15)
13			4912 (63)	4898 (41)	4932 (50)			4912 (28)	2.11 (43)
14			5247 (41)	5251 (29)	5147 (65)			5238 (22)	3.93 (45)
15					5464 (47)			5464 (47)	0.91 (14)
16				5652 (36)	5742 (48)			5684 (29)	2.61 (37)
17					5970 (54)			5970 (54)	1.06 (20)
18	6226 (92)			6252 (34)				6249 (32)	1.21 (49)
19				6530 (59)	6514 (58)			6521 (41)	0.88 (37)
20			6816 (34)		6790 (61)			6810 (30)	1.35 (17)
21	6888 (59)			6910 (41)	7086 (68)			6933 (27)	1.55 (33)
22	7360 (86)			7331 (46)	7288 (69)			7325 (35)	1.74 (43)
23					7592 (75)			7592 (75)	0.099 (12)
24	7770 (68)			7748 (76)	7959 (80)			7817 (43)	1.02 (26)
25		8147 (98)		8160 (64)				8156 (54)	0.49 (16)
26	8248 (75)		8258 (58)		8331 (87)			8270 (41)	0.96 (22)
27			8679 (128)	8893 (70)	8736 (102)			8815 (53)	0.40 (13)
28					9023 (101)			9023 (101)	0.030 (15)
29					9303 (106)			9303 (106)	0.026 (10)
30			9533 (93)		9591 (116)			9556 (73)	0.144 (61)
31		9812 (91)		9772 (110)	9838 (113)			9807 (60)	0.65 (16)
32	10846 (158)				10775 (113)			10799 (92)	0.057 (10)
33		11177 (94)						11177 (94)	0.24 (8)
34		11717 (64)			11615 (148)	11729 (79)	11707 (111)	11710 (43)	3.18 (25)

Table 4.12 – Energies of the unbound levels in ^{23}Al populated by the β decay of ^{23}Si deduced from the γ-ray gated spectra and the ungated ground-state spectrum. This table includes the three identified channels to ^{22}Mg, ^{21}Na and ^{20}Ne ground states. A weighted average was used to calculate the energies of the excited levels in ^{23}Al when more than one pathway was observed.)

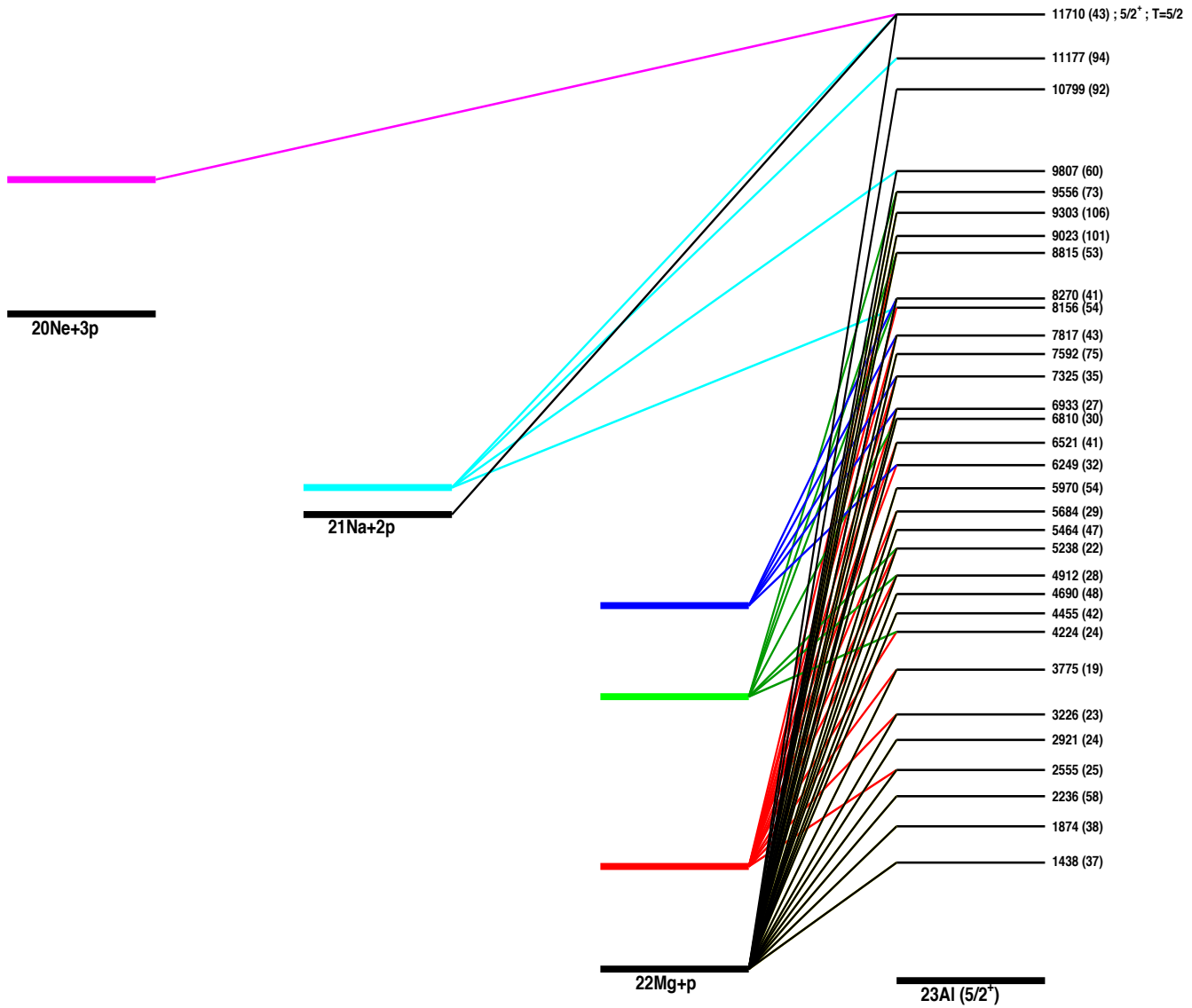

Figure 4.26 – Decay scheme of ^{23}Si identified in the present work. The βp and β2p decay branches were identified and the excitation energy of the levels in ^{23}Al measured. A possible β3p decay through the IAS at 11.71 MeV was tentatively observed.

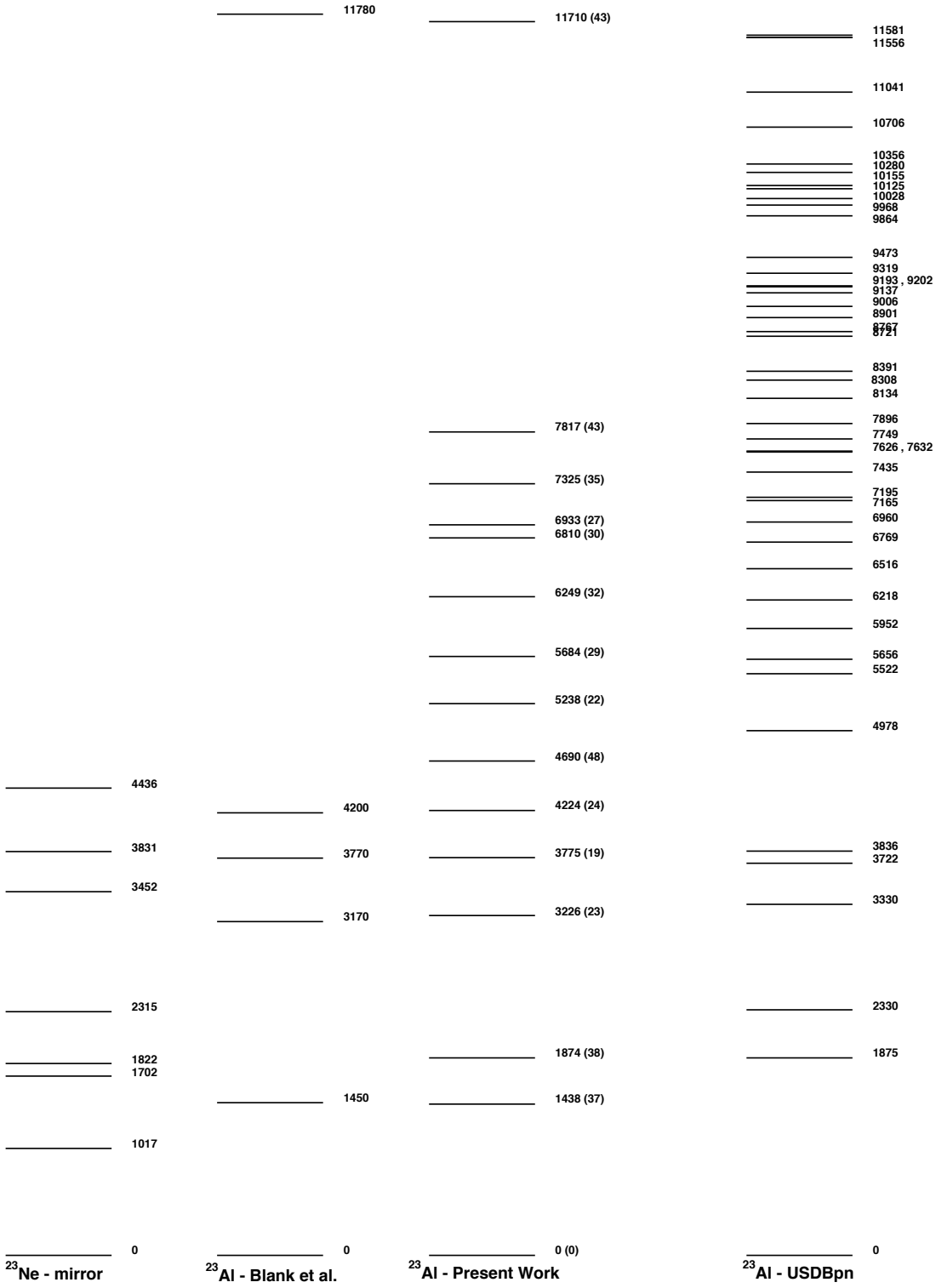

Figure 4.27 – The level scheme of ^{23}Al obtained in the present work is compared to the previous measurement performed by Blank *et al.* [Bla97] and to the USDB shell-model calculation of B.A. Brown [Bro]. On the left side, the decay level scheme of the mirror nucleus, ^{23}F.

4.6 The IMME for T = 5/2 and the mass of ^{23}Si

The Isobaric Analogue State that was identified in this work at 11710(43) keV belongs to the same isospin multiplet as the ground state of ^{23}Si. Two other states in this multiplet, the ground state of ^{23}F and a level at 19.6 MeV excitation energy in ^{23}Na are also known from previous measurements. The mass excess of the ground states of these nuclei, and the excitation energies of these states, are summarized in Table 4.13. These values were used to determine the coefficients of the IMME and that were, in turn, used to deduce the mass excess of the ^{23}Si ground state.

The coefficients of the IMME quadratic function describing the A=23, T=5/2 multiplet were derived to be: a = 12005.5(8.4) keV, b = −3993(17) keV and c = 205.9(8.3) keV. Extrapolation of these results leads to an estimate for the mass excess of the ^{23}Si ground state to be 23274(68) keV. This value is in very good agreement with the previous measurement [Bla97] and the most recent AME2012 [Wan12] estimation, as presented in Table 4.14. This new indirect mass measurement was used to deduce the one-proton and two-proton separation thresholds, as well as a new β-decay Q-value, whose energies are presented in Table 4.15.

Based on the theory of the IMME described in Chapter 1, coefficients b and c can be calculated analytically using Equations 1.56 and 1.57, respectively. For the A = 23 multiplet, we obtain b = -3892.7 keV and c = 215.15 keV, which are in good agreement with the coefficients deduced in the fit. The ratio of the b and c coefficients is $|b/c|$ = 19.4, which is also in good agreement with the value of 18.3 that was obtained using Equation 1.58.

Nucleus	T_Z	Mass excess (keV)	Excited state (keV)
^{23}Al	-3/2	6478.1 (0.3)	11710 (43)
^{23}Na	1/2	-9529.8525 (18)	19590.404 (2.000) [Mac]
^{23}F	5/2	3310 (30)	0

Table 4.13 – Set of isobaric analogue states from the (A=23, T=5/2) multiplet used to determine the coefficients of the IMME.

	Mass excess (MeV)
B. Bank *et al.* [Bla97]	23.42 (10)
Audi (AME2012) [Wan12]	23.70 (50)
This work	23.27 (7)

Table 4.14 – The mass determined in this work is in good agreement with the previous measurement by B. Blank *et al.*, and the AME2012 extrapolation from Audi *et al.*

$Q(\beta^+) =$	15504 (70) keV
$S_p =$	2195 (114) keV
$S_{2p} =$	2218 (72) keV

Table 4.15 – Updated S_{2p} and Q_β-value determined using the ^{23}Si ground-state mass excess deduced in the present work. In the case of S_p, the mass of the daughter ^{22}Al is taken from [Ach06].

4.7 Half-life measurement

The half-life of ^{23}Si was deduced using the same analysis techniques as described above for ^{20}Mg decay. Several decay time spectra were generated both with and without γ-ray gates applied. Results obtained are described below and are compared to the previous measurement $T_{1/2} = 42.3(4)$ ms in the previous experiment of Ref. [Bla97].

4.7.1 Using γ-ray gates

Application of a γ-ray gate to generate the decay curve provides a nearly pure and background free spectrum because of the distinct energies and origins of each individual γ ray. A summary of the ^{23}Si γ-ray gated decay curves obtained from the present experiment are presented in Figure 4.28. A background subtraction was performed, as described above, using gates placed just below and above the γ-ray gate of interest and normalized to the same number of channels. Table 4.16 presents the results of the fit for the γ-ray gated and background subtracted spectra. The fit function used a single exponential decay and a constant background. The half-life of the decay events in coincidence with 1633-keV γ rays considered only charged-particle events that deposited more than 1 MeV in DSSD2 to avoid contamination from the low-energy β particles from ^{20}Na decay. The half-lives from each of the five γ-ray gates are in very good agreement (reduced χ^2 value of 0.98 for 4 degrees of freedom) and thus the average half-life, $T_{1/2} = 41.7(9)$ ms, is adopted as the final result of the γ-ray analysis. This result is in good agreement with the value $T_{1/2} = 42.3(4)$ ms obtained in Ref. [Bla97] but is approximately two times less precise. A summary of the results of Table 4.16 and the weighted average is presented in Figure 4.30.

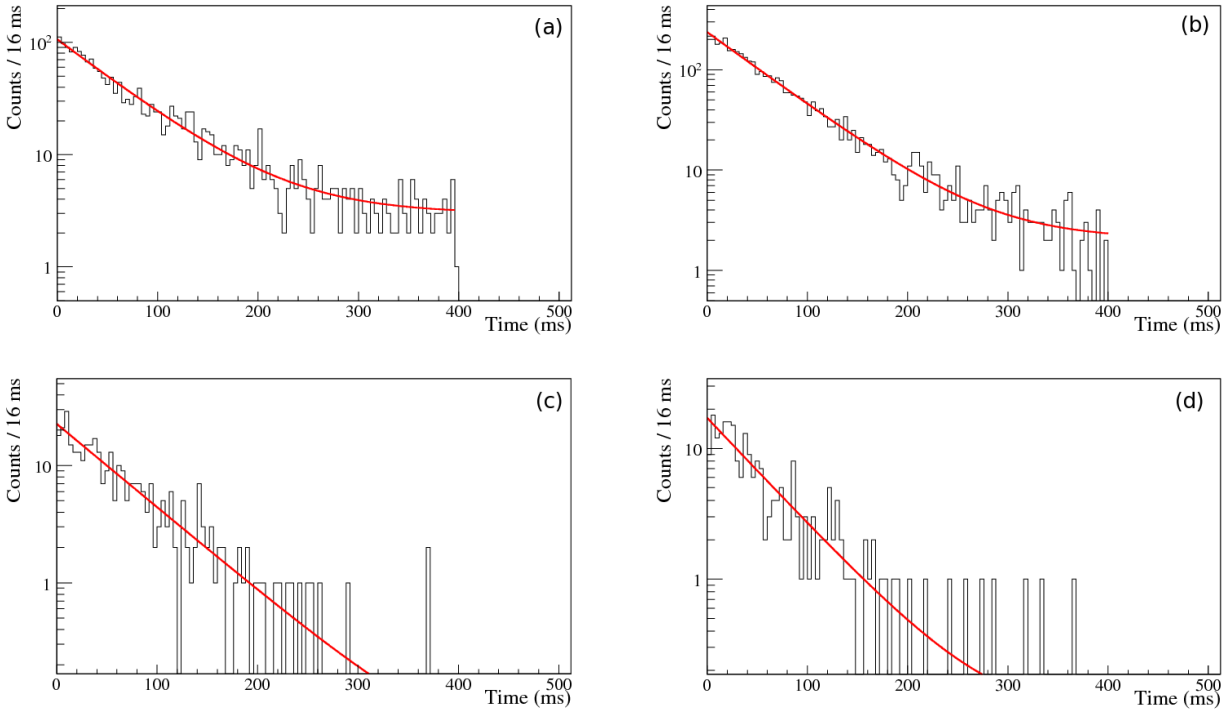

Figure 4.28 – Decay curves of ^{23}Si corresponding to the 332-keV (a), the 1247-keV (b), the 2061-keV (c) and the 3155-keV (d) γ-ray gates. In red, the fit function, which used an exponential decay and a constant background. The fit included all data up to and including the maximum correlation time range of 400 ms.

E_γ gate	Half life (ms)
332 keV	44.2 (19)
1247 keV	41.3 (11)
2061 keV	42.2 (29)
3155 keV	37.0 (33)
1633 keV	41.0 (55)
Average	41.7 (9)
Previous value [Bla97]	42.3 (4)

Table 4.16 – Half-life determined as the average of the γ-gated spectra with a reduced χ^2 of 0.96.

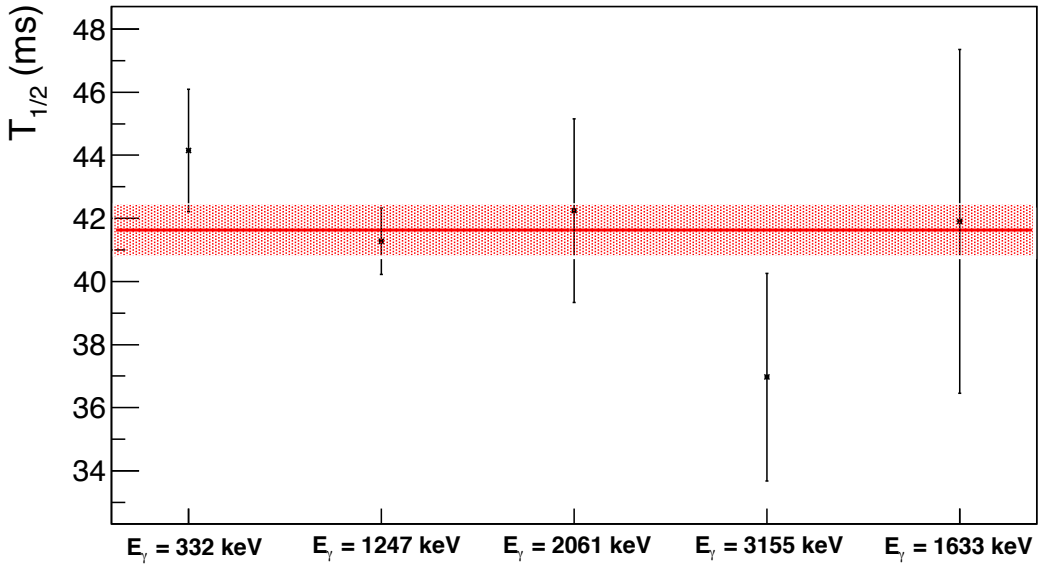

Figure 4.29 – The weighted average of the different γ-gated spectra gives 41.7 (9) ms, which is in good agreement with the previous measurement from [Bla97]. In red, the average half-life and its uncertainties.

4.7.2 Using proton gates

The other method used to deduce the half-life of ^{23}Si was to perform several different proton gates and to fit the corresponding decay curves. Proton gates were applied on an energy range which was chosen to include only one of both decay branches, βp or β2p. Some gates were also made to isolate proton groups that were contaminated by ^{20}Na, in order to properly include this component in the fit function. The energy gate applied in this analysis are described in Table 4.17.

The grow-in and decay activity of the βp daughter, ^{22}Mg, must also be taken into account in the fit function. The half-life of ^{22}Mg, $T_{1/2} = 3.88$ s [Wan12], was treated as a fixed parameter. The contribution of the β2p daughter, ^{21}Na ($T_{1/2} = 22.5$ s [Wan12]) was assumed to be sufficiently long compared to the 400 ms time scale of the measurement that its contribution would be included in the free constant background parameter. Decay curves gated on the proton gates 1, 2, 4 and 6 were fitted with the following function:

$$N(t) = \lambda_1 A_0 e^{(-\lambda_1 \cdot t)} + \varepsilon \cdot A_0 \frac{\lambda_1 \lambda_2}{(\lambda_2 - \lambda_1)} (e^{(-\lambda_1 \cdot t)} - e^{(-\lambda_2 \cdot t)}) + C \tag{4.1}$$

where $\lambda_1 = \frac{1}{T_{1/2}(^{23}Si)}$ was a free parameter, and $T_{1/2}(^{22}Mg)$ was fixed at 3.88 s. The activity at $t = 0$ is denoted A_0, C is the constant background parameter and ε is a free parameter used to describe the β-only efficiency.

In addition, the primary contaminant in the secondary beam was ^{20}Na whose half-life is $T_{1/2} = 447.9$ ms. Based on the spectrum of charged particles emitted by ^{20}Na (see Figure 4.4), an additional exponential decay was added to the fit function for the particular case of the decay curves generated from proton gates 3 and 5 (corresponding to the energy range where the $\beta\alpha$ particles would be recorded). The results of the fit to the proton-gated decay time spectra are summarized in Table 4.17. The average value of the proton-gated decay spectra is 42.67(23) ms with a reduced χ^2 value of 1.13 for 5 degrees of freedom. This result is in excellent agreement with the value obtained above $T_{1/2} = 41.7(9)$ ms from the γ-ray analysis and is nearly four times more precise. Figure 4.30 presents the half-life results and the average half-life with its statistical uncertainties.

Proton division	Energy (keV)	Half life (ms)
1	[1135 ; 1570] keV	42.87 (77)
2	[2150 ; 2635] keV	42.94 (30)
3	[2640 ; 3310] keV	41.92 (58)
4	[3520 ; 4105] keV	41.91 (62)
5	[6035 ; 6365] keV	44.34 (139)
6	$\geq$ 8000 keV	44.09 (390)
	Average	42.67 (23)
	Previous value [Bla97]	42.3 (4)

Table 4.17 – Half-life determined from the average of the proton-gated spectra. The decay curve of proton groups 3 and 5 were fitted with two exponential decays to take into account the possibility of false correlations from ^{20}Na β-delayed α decays. The average half-life is $T_{1/2}$ = 42.67(23) ms with a reduced χ^2 of 1.13.

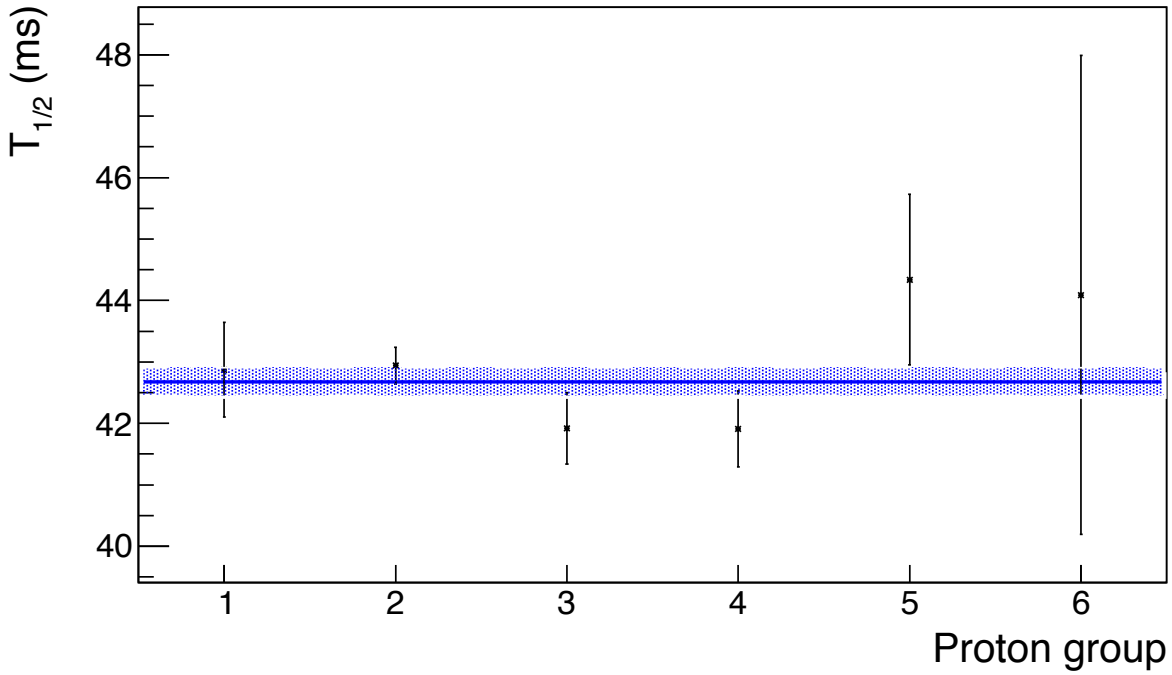

Figure 4.30 – The weighted average of the half-life results gated on several different proton groups gives a value in good agreement with the previous average from the γ-ray gated spectra and has a reduced χ^2 value of 1.1. In blue, the average half-life of ^{23}Si is 42.67(23) ms.

4.7.3 Conclusion on the half-life

As presented in Figure 4.31, the ^{23}Si decay curve obtained from all charged particles (with no energy gates applied) was also fitted, assuming four components:

- one exponential decay curve describing the β decay of ^{23}Si,
- a function describing the grow-in and decay of the ^{22}Mg daughter, with its half-life fixed to $T_{1/2}(^{22}\mathrm{Mg}) = 3.88$ s, and ε satisfying the boundary conditions as described in the ^{20}Mg analysis,
- a second exponential decay to describe false correlations with ^{20}Na decay but with a free half-life $T_{1/2} \approx T_{1/2}(^{20}\mathrm{Na}) = 447.9$ ms,
- a constant background.

The half-life obtained with this fit (see Figure 4.31) is $T_{1/2} = 42.80(27)$ ms. This value is slightly less precise than the average of the proton-gated spectra due to the presence of several additional free parameters but the result is in excellent agreement with the proton-gated and γ-ray gated measurements presented above.

We therefore adopt the value $T_{1/2} = 42.67(23)$ ms, obtained from the average of the proton group gates, as the half-life of ^{23}Si deduced in the present experiment. This result is in good agreement with the previous value 42.3(4) ms [Bla97] and is nearly a factor of two times more precise.

4.8 Conclusion

Because of a large β Q-value, several β-delayed charged particle decays of the $T_Z = -5/2$ nucleus ^{23}Si were studied to perform detailed spectroscopy of the daughter ^{23}Al. Five excited states in the daughter ^{23}Al were previously measured by B.Blank *et al.* in Ref. [Bla97], including the IAS at ~ 11.8 MeV. This energy was deduced from two proton groups which were observed in the charged particle spectrum and identified as the β2p decay of ^{23}Si.

In the present work, the addition of HPGe detectors to the implant-and-decay station were used to detect γ-rays coming from the electromagnetic decay of excited states in the daughter nuclei. We observed three γ-ray transitions corresponding to the first excited states of ^{22}Mg, as well as the 332-keV transition in ^{21}Na, confirming the β2p decay path of ^{23}Si via the IAS and measuring its β2p branching ratio. By applying γ-ray gates to the proton spectra, we performed the spectroscopy of ^{23}Al, measuring excitation energies, and β branching ratios. As

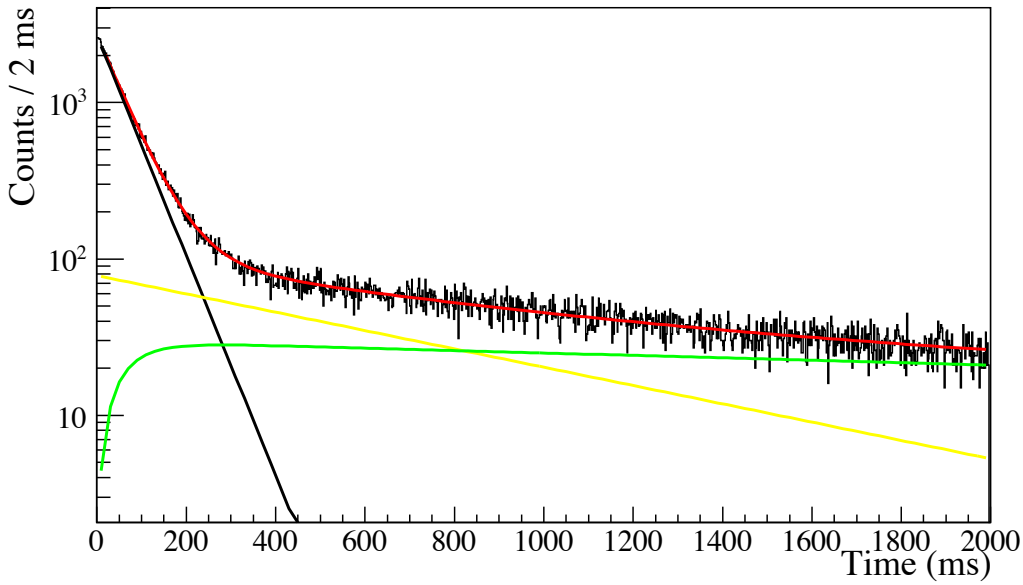

Figure 4.31 – The fit to the decay curve for all particles detected in DSSD2 was performed assuming an exponential decay of the parent (in black), the successive decay of the daughter (in green), an exponential decay for false correlations (^{20}Na) and a constant background (in red). The constant background parameter was consistent with zero and does not appear on the figure.

a result of this work, 9 additional levels in ^{23}Al were observed for the first time. In addition, the half-life of ^{23}Si was determined to be $T_{1/2} = 42.67(23)$ ms, a result that is two times more precise than the previous measurement of Ref. [Bla97].

The energy of the IAS to ^{23}Si was measured at an excitation energy of 11710(43) keV in ^{23}Al. The mass excess of the ^{23}Si ground state was estimated using the IMME for the (A=23, T=5/2) multiplet, and the value obtained is in good agreement with both the previous measurement of Ref. [Bla97] and the recommended value from AME2012 [Wan12]. Because of the value of the one-proton and two-proton separation thresholds, the ^{23}Si ground state cannot be a 1-proton or 2-proton emitter. However, the more exotic isotope of ^{22}Si, with $T_Z = -3$, is a candidate for 2-proton radioactivity. In the next chapter, we follow the same analysis as presented above but focus on decays of ^{22}Si to its daughter ^{22}Al.

Chapter 5

β-delayed charged particle decays of ^{22}Si

In the previous chapter, β-delayed charged particle decays of ^{23}Si were used to probe the structure of the exotic nucleus ^{23}Al near the proton drip-line. The level scheme consisting of several previously unobserved excited was built and the energy of the IAS to the ^{23}Si ground state was deduced. The excitation energy of the IAS was then used to derive an indirect mass measurement of the ^{23}Si ground state using the IMME. The β-delayed proton decay of the even more neutron deficient nucleus ^{22}Si will be presented in this Chapter. Using the SeGA array, two γ rays corresponding to the de-excitation of the first two excited states in the βp daughter ^{22}Mg were observed. One weak γ-ray transition was also observed that led to the identification of β2p decay from this nucleus for the first time. The level scheme of the daughter ^{22}Al was constructed using the γ-ray gated spectra and the ungated proton spectrum using the same methods as described in previous chapters. The identification and measurement of both the energy and the partial half-life of the IAS in ^{22}Al was performed.

Based on a parametrization of the statistical rate function for known superallowed Fermi transitions, a new method is proposed to determine the Q-value of the decay from the 0^+ ground state of ^{22}Si to its IAS in ^{22}Al from the partial half-life measured in this work. Results of this method were used to determine the mass excess of ^{22}Si and the one- and two-proton separation thresholds. Results will be presented and compared to several model predictions.

5.1 Discussion on the particle thresholds

Very early, ^{22}Si was predicted to be a ground-state two-proton emitter [Gol61, Gol60]. Its discovery at GANIL in 1987 [SL87] proved that this nucleus is bound, despite it being extremely neutron deficient as it is the lightest known $T_Z = -3$ nucleus. The ^{22}Si nucleus has a $N = 8$ neutron closed shell configuration and 6 protons in the *sd* shell that could gain additional sta-

bility if there were an appreciable subshell closure at $Z = 14$. This semi-double shell closure would imply a spherical shape [Lal98] and therefore an even stronger binding energy than in neighbouring nuclei. Recent predictions suggest a very weakly-bound ground state with respect to two proton emission [Hol13] and have stressed that three-body forces may play a key role.

The search for two-proton radioactivity in ^{22}Si is motivated by the fact that its mass excess and S_{2p} values have never been determined experimentally and several mass predictions suggest a very small or even negative S_{2p} threshold. Table 5.1 presents the different values of the mass excess and the associated S_p and S_{2p} values obtained from various models. These values clearly span a wide range and carry significant uncertainties thus offering very little in the way of predicting whether or not ^{22}Si is a candidate to decay by 2p radioactivity. With the exception of the NL-SH [Ren96] and the Hartree-Fock [Col98] models, most predictions suggest that ^{22}Si could decay by 2p radioactivity despite the fact that it is already known to β decay [Bla96]. It is therefore crucial to provide an experimental measurement of the mass of the ground state before definitive conclusions about the structure and decay modes of this nucleus can be reached.

Model	Mass excess of ^{22}Si (keV)	Sp (keV)	S_{2p} (keV)
NL-SH [Ren96]	31016 (2000)	3263 (2000)	1121 (2000)
NL1 [Ren96]	33066 (2000)	1213 (2000)	-929 (2000)
Coulomb-shift syst. [Col98]	32166 (90)	1450 (64) (90)	-18 (63)
Hartree-Fock [Col98]	32916	220	700
AME03 [Aud03]	32160 (200)	2119 (200)	-23 (200)
AME12 [Wan12]	33340 (400)	940 (400)	-1200 (400)

Table 5.1 – Mass excess, single and two-proton separation values of ^{22}Si deduced from non-linear relativistic mean-field (NL-SH, NL1) and Hartree-Fock models. These are compared to the Coulomb-shift systematics and the most recent atomic mass evaluations (AME03, AME12).

In the previous chapter on ^{23}Si, the excitation energies of the resonances in the ^{23}Al daughter were deduced using the sum of the measured decay energy and the proton separation threshold. In the case of ^{22}Si, the ground state of the daughter ^{22}Al that would be required to determine the excitation energies of the proton-emitting states has not yet been measured experimentally. Estimations of the ^{22}Al mass excess presented in the latest atomic mass evaluations (AME03 and AME12) are both entirely consistent (see Table 5.2) although they differ by from a recent determination using the IMME by approximately 200 keV [Ach06]. As part of this thesis work, the mass excess of the ^{22}Al ground state has been investigated and updated using the IMME and the most recent experimental data.

The isospin projection of the ^{22}Al ground state is T_Z=-−2. Application of the IMME

across the A=22, T=2 isospin multiplet was recently performed by Achouri *et al* [Ach06]. The coefficients of the IMME equation were determined using the three known isobaric analogue states of the multiplet:

- the ground state of the ^{22}Si mirror nucleus ^{22}F ($T_Z = +2$), with a mass excess of 2793(12) keV,
- an excited state at 14011.7(35) keV in ^{22}Mg ($T_Z = -1$), with a mass excess of $-399.9(3)$ keV, and
- the excited state at 14070(40) keV in ^{22}Ne ($T_Z = +1$), with a mass excess of -8024.714 (18) keV.

It should be stressed that the spin of this latter state is not definitively known. It is therefore only an hypothesis that this state belongs to the isospin multiplet. Several reaction experiments were performed to probe low-energy excited states in ^{22}Ne [G83]. Spectroscopy of high-energy states was also performed in Ref. [Wil87] but the assignment of spins and parities (1^+ or 2^-) was incompatible with the IAS that must be $J^\pi = 4^+$. Other experiments including (p, p') and (t, t') inelastic scattering reactions[Sza83] were used to populate higher-spin excited states in ^{22}Ne. Although no spin and parity assignment was provided, they observed a state at 14.07(40) MeV that was later identified in [Sto69] as a part of the $T = 2$ multiplet. Another state at slightly lower energy was populated via the (α, α') reaction [Gol04]. This state was measured to be 13.88(10) MeV and its spin and parity were firmly established to be 4^+. This excited state could therefore also be a potential candidate for the $T = 2$ IAS in ^{22}Ne. However, according to Ref. [Sto69], $T = 2$ states cannot be below 14.07 MeV and thus the state found in Ref. [Gol04] at 13.88(10) MeV is more than likely a 4^+ state with $T = 1$.

Coefficients of the IMME for the ($A = 22$, $T = 2$) multiplet were obtained using both of these candidate states at 13.88(10) MeV and 14.07(40) MeV. The resulting mass excesses derived for ^{22}Al are summarized in Table 5.2 along with the AME predictions.

E_{IAS} in ^{22}Ne (keV)	Mass excess of ^{22}Al (keV)	S_p (keV)	$S2p$ (keV)
AME03 [Aud03]	18180 (90)	20 (100)	3240 (90)
AME12 [Wan12]	18200 (400)	0 (400)	3230 (400)
14070 (40)	17932 (99)	271 (100)	3496 (100)
13880 (100)	18312 (30)	-109 (34)	3116 (34)

Table 5.2 – Mass excess, proton and two proton separation threshold as calculated using the IMME and compared to the previous mass evaluations. For comparison, the value used in the previous ^{22}Si decay experiment[Bla96] was $S_p = 18$ keV.

Using the excited state from Ref. [Gol04] at 13.88(10) MeV leads to a mass excess for ^{22}Al that would be proton unbound ($S_p = -109(34)$ keV). As a result, this state was discarded from the analysis and the discussion below. This is perhaps additional confirmation that this state is probably not part of the $T = 2$ multiplet but rather an excited 4^+ state with $T = 1$. The two values from the atomic mass evaluations are nearly identical but these are not independent results. Both are estimated using the same analysis protocol that is based on trends in neighbouring nuclei. In the present work, we therefore adopt the mass excess of 17932(99) keV from the IMME as this value is better constrained using experimentally measured states from the same multiplet. This value is also in agreement with the value of 18200(400) keV from the latest mass evaluation [Wan12].

Using the IMME mass excess for ^{22}Al, the corresponding one- and two-proton thresholds are S_p =271(100) keV and S_{2p} = 3496(100) keV, respectively. These are also summarized in Table 5.2. These low-energy separation energies combined with the relatively large Q_β value of ^{22}Si imply that several β-delayed charged particle channels are potentially open. The daughter nuclei and the Q-values are summarized in Table 5.3.

Decay path	Daughter	Q-value (keV)
β^+	^{22}Al	14387
βp	^{21}Mg	14115
β2p	^{20}Na	10889
β3p	^{19}Ne	8699
βpα	^{17}Ne	6104

Table 5.3 – Summary of the update Q-values for the possible β-delayed decay branches of ^{22}Si.

5.2 Previous study of ^{22}Si decay

First decay spectroscopy of β-delayed proton emission from ^{22}Si was performed by Blank *et al.* at the LISE facility of GANIL [Cza97, Bla96]. A secondary beam of ^{22}Si was implanted into a Si detector and a MSGC. This was the same setup that they used to study ^{23}Si decay [Bla97] and that was described above in Chapter 4. The two spectra obtained in this experiment are presented in Figure 5.1. Four proton groups were observed, at 1.63(5) MeV, 1.99(5) MeV, 2.10(5) MeV and 2.17(5) MeV. A total of three proton transitions from two excited states proposed in ^{22}Al at 1.85 MeV and 2.21 MeV (see Fig. 5.1). The fourth proton group at 2.17(5) MeV could not be placed in the decay scheme. No candidate for the IAS of the ^{22}Si ground state was observed. The half-life of ^{22}Si was also measured in this work and was determined to be $T_{1/2}$ = 29(2) ms [Bla96].

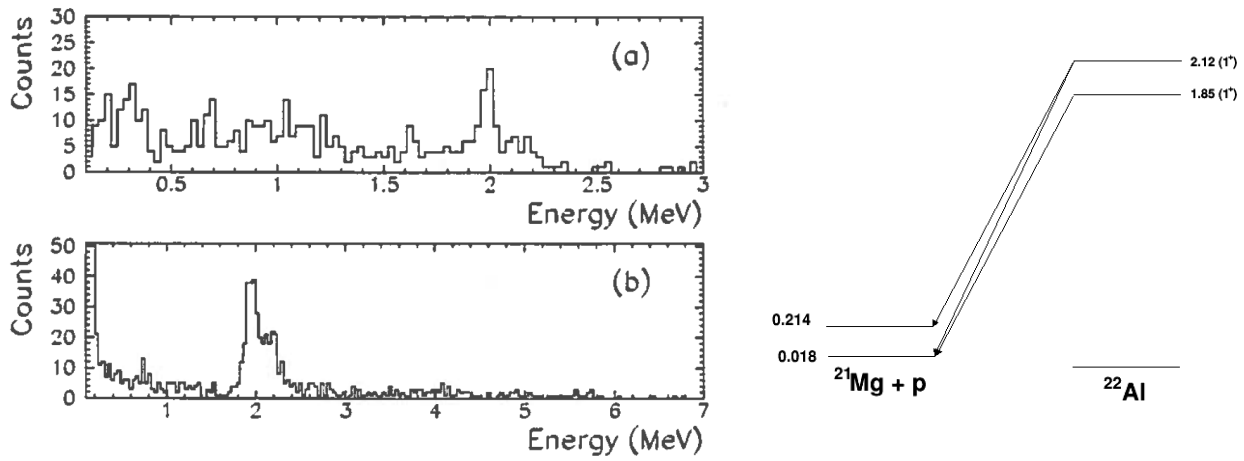

Figure 5.1 – (Left) The spectrum of the β-delayed protons emitted after the implantation of ^{22}Si in a MSGC (a) and a Si detector (b). (Right) The level scheme deduced from the energy of the observed proton groups[Cza97, Bla96].

In his recent review [Bla08], Blank calculated the Coulomb displacement of ^{22}Si with respect to ^{22}O under the hypothesis of a uniform charged sphere. An energy of the IAS in ^{22}Al was deduced, at 8840(220) keV above the one-proton separation threshold. Using the IMME prediction for S_p as described above, this leads to an excitation energy of the IAS to the ^{22}Si ground state of 9111±242 keV in ^{22}Al.

5.3 Present experiment

In the present work, a ^{22}Si secondary beam was produced and purified at NSCL using the A1900 and the RFFS devices. The production rate of ^{22}Si at the exit of the RFFS was 15 ions per minute, which represented approximately 0.03% of the total cocktail beam. As shown in the PID spectrum presented in Figure 5.2, the only β-delayed proton emitter implanted into DSSD2 at this setting was ^{22}Si. In particular, the known βp emitter ^{20}Mg, which was present in the secondary fragmentation beam at the exit of the A1900, does not appear in the spectrum. This is because it was essentially fully suppressed by the RFFS. The ^{20}Mg data that was presented in Chapter 3 of this thesis was obtained using the ^{22}Si setting shown here with the only difference being the position of the vertical slits at the end of the RFFS. All lighter nuclei that were present in the beam are either stable or they decay by β^+ decay only and have relatively long half-lives. These are listed in Table 5.4. In the analysis, the maximum correlation time used for the implantation-and-decay events was 300 ms (approximately 10 half-lives of ^{22}Si). The correlation area was fixed to a 3x3-pixel area centred around the implantation site in DSSD2.

A total of 7.16×10^4 decay-and-implant events were identified as β-delayed charged particles emitted from ^{22}Si. This represents 4.2% of the beam purity after the correlation process.

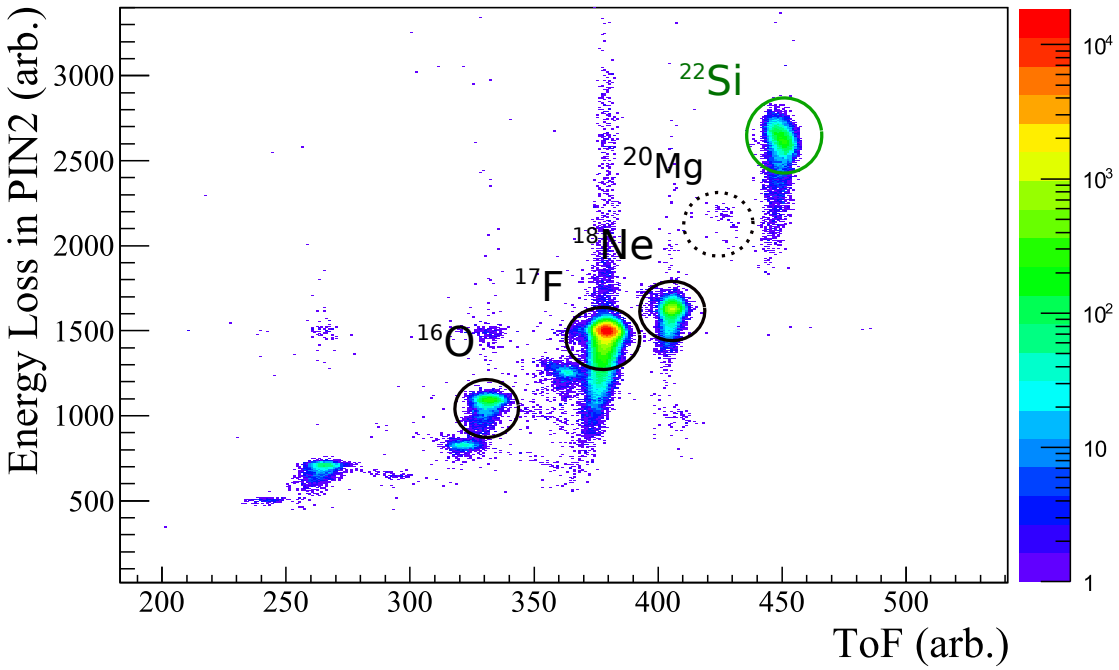

Figure 5.2 – Particle identification spectrum of all implant-and-decay events identified after the correlation process. As with the analysis presented for the previous nuclei ^{20}Mg and ^{23}Si, the identification of the implants was performed using the ΔE-TOF method.

Parents	Decay path	Purity (%)	Half-life
^{22}Si	βp, β2p	4.2	29 ms
^{20}Mg	β^+,βp	0.003	91 s
^{18}Ne	β^+	0.7	1.67 s
^{17}F	β^+	94.0	64.49 s
^{16}O	β^+	0.48	stable

Table 5.4 – Purity of the secondary cocktail beam with A1900 settings optimized for ^{22}Si after the implant-and-decay correlation process. In this work, the contaminants in the beam are either stable or emit only β particles and have relatively long half-lives compared to that of ^{22}Si.

The charged-particle spectrum obtained was corrected for the efficiency of the DSSD and is shown in Figure 5.3 where it is compared to the previous study of Blank *et al.* [Bla96]. A

detailed description of each of the four proton groups observed previously and their comparison to the present experiment can be summarized as follows:

- A first proton group at 1.63(5) MeV was identified in the previous measurement. In the present work, we confirm this proton group and measure its energy to 1.69(8) MeV, in good agreement. The uncertainty of 80 keV on the energy of this centroid is limited by the statistics of this transition due to its low branching ratio. The energy difference between proton groups 2 and 4 is close to the energy of the first excited state in ^{21}Mg, at 201(4) keV[Dig08]. For this reason, the two main groups were identified by Blank *et al.* as coming from the same excited level in ^{22}Al and populating either the ground or first excited state in ^{21}Mg. The energies in the ungated proton spectrum are presented in Table 5.5 and these are in very good agreement with the previous measurement.

- Proton group 3 could not be resolved in the present work. The Si detector used for the implantation in the present experiment was almost two times more thick (525 μm rather than 300 μm) than used in the previous experiment. This implies more β-summing in the present work that hid any possible evidence for this small proton group.

- In the previous experiment, several counts between 2.5 and 6.0 MeV were observed but no information as to their possible origin could be deduced. In addition to having more statistics in the present experiment along with a higher detection efficiency, a very strong transition was observed at 5.5 MeV that will be discussed in detail below.

#	E_{proton} (keV)	E_{proton} (MeV) [Bla96]
1	1.69 (8)	1.63 (5)
2	1.95 (4)	1.99 (5)
3	–	2.10 (5)
4	2.16 (5)	2.17 (5)

Table 5.5 – Comparison between the four main proton groups observed in Ref. [Bla96] and the present work.

5.4 γ-ray spectrum from ^{22}Si decay

From the correlated γ-ray spectrum presented in Figure 5.4, a total of five γ-ray transitions (in addition to the 511 keV) were observed. The energy and the origin of these γ rays are described below and summarized in Table 5.6:

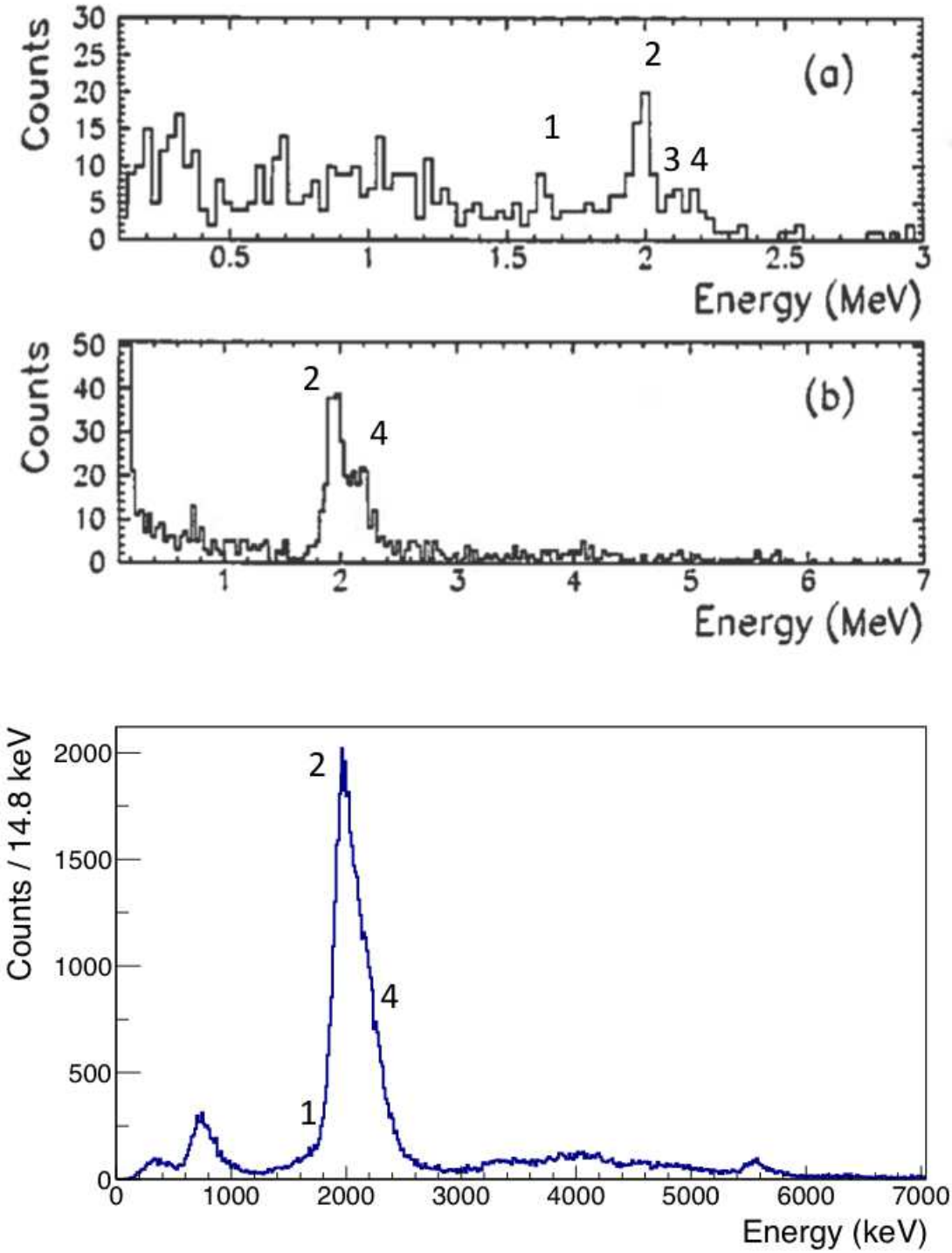

Figure 5.3 – The energy spectra obtained in Ref. [Bla96] (top) are compared to the ungated proton spectrum in the present experiment (bottom). In the bottom spectrum, the three proton groups determined via the fit procedure have been labelled to ease comparison with the previous measurement.

- The first γ ray (1) at $E_\gamma = 203.8$ (5) keV arises from the de-excitation of the first $1/2^+$ excited state of ^{21}Mg. This level is populated after the β-delayed one-proton emission of the ^{22}Si ground state with high intensity.

- The third γ ray (3) at $E_\gamma = 713.7$ (8) keV is the sum of this 204-keV γ ray with the 511-keV γ ray from positron annihilation.

- A weak γ-ray transition was observed at $E_4 = 880$ (1) keV. This transition was observed in Ref. [Dig08], and is the signature of the de-excitation of the second excited state in ^{21}Mg at 1084(4) keV that decays into the 204-keV excited state.

- The second γ-ray transition (2) at 596(1) keV corresponds to the de-excitation of the first excited state (3^+) in ^{20}Na to its ground state (2^+). Since virtually all of the ^{20}Mg ions from the beam were suppressed by the RFFS, and given that ^{20}Mg decay does not populate this state in ^{20}Na, this nucleus must have been populated from the decay of ^{22}Si or one of its daughters. This state furthermore not populated in the βp decay of the daughter ^{21}Mg [Lun] and therefore we propose that this γ-ray transition is emitted following the β-delayed two-proton emission of ^{22}Si through proton unbound levels populated above the S_{2p} threshold in ^{22}Al.

- The γ-ray 5 at 1631(1) keV arises from the de-excitation of the first excited 2^+ state at 1633 keV in ^{20}Ne. This state could be populated following the β2p decay from the ^{22}Al ground state [Ach06]. However, because the ^{22}Al ground state is 4^+ this cannot be populated via a direct branch from the β decay of the 0^+ ground state of ^{22}Si. Given the very low one-proton separation threshold in ^{22}Al we further assume that there are no proton-bound states in ^{22}Al that could decay via γ-ray emission to the ^{22}Al ground state. The only decay path that could lead to this daughter nucleus must therefore be a two-step βp decay: $^{22}\text{Si} \xrightarrow{\beta p} {}^{21}\text{Mg} \xrightarrow{\beta p} {}^{20}\text{Ne}^*$.

#	Energy (keV)	$E_i(J^\pi) \rightarrow E_f(J^\pi)$	Daughter
1	203.8 (5)	$201\,(1^+/2) \rightarrow$ g.s. $(5^+/2)$	^{21}Mg (βp)
2	596.2 (10)	$596\,(3^+) \rightarrow$ g.s. (2^+)	^{20}Na (β2p)
3	713.7 (8)	Sum of 511-keV and 204-keV γ-rays	^{21}Mg (βp)
4	879.6 (10)	$1081\,(1^-/2) \rightarrow 201\,(1^+/2)$	^{21}Mg (βp)
5	1631.4 (14)	$1633\,(2^+) \rightarrow$ g.s. (0^+)	^{20}Ne (β)

Table 5.6 – Five γ-ray transitions were observed following βp and β2p decays of ^{22}Si. The transition at 1631 keV is due to a sequential set of βp decays that populate the first excited state in ^{20}Ne (see text).

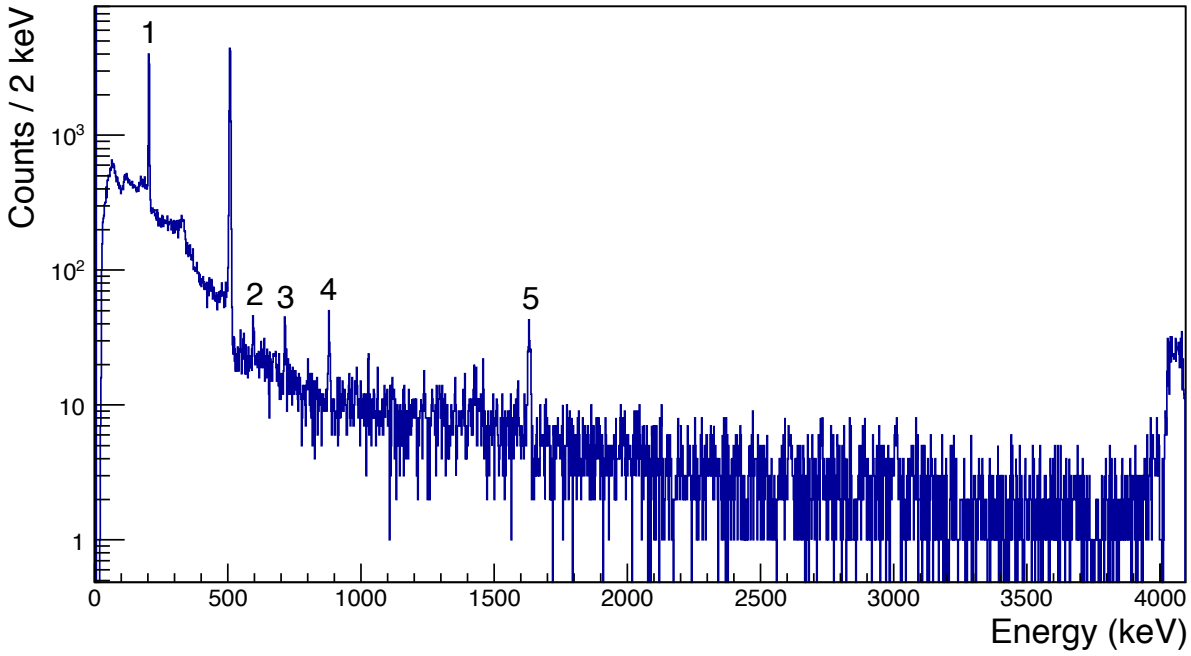

Figure 5.4 – Correlated ^{22}Si decay γ-ray spectrum. A summary of the γ-ray energies are presented in Table 5.6.

5.5 βp decay channel with γ-ray coincidence

The γ rays at 204 keV (peak 1 in Fig. 5.4) and 880 keV (peak 4) are emitted from excited states in ^{21}Mg, and correspond to the β-delayed one-proton decay channel. In this case, the excitation energy of the initial level in ^{22}Al can be derived using the expression:

$$E_l^* = S_p + E_{level} + E_{proton}, \tag{5.1}$$

where S_p = 271(100) keV for ^{22}Al (from the IMME analysis described above), E_{level} is the excited state level energy in ^{21}Mg and E_{proton} is the energy of the proton group detected in DSSD2. In order to facilitate the comparison of the levels from different gated spectra, the 100-keV uncertainties on the one-proton or two proton separation thresholds are not propagated to the excitation energy, but in the final summary (see Table 5.12).

In the following analysis, the tail parameter used in the fit function for the proton groups was determined by fitting proton group 1.06, which was assumed to consist of a single proton transition. A fit to this proton group yielded a value of ∼30 for the tail parameter, which is about two times lower than the value deduced in the analysis of ^{23}Si decays.

The relatively high-statistics spectra obtained for the ungated proton spectrum as well as the 204-keV γ-ray gated proton spectrum permitted the use of the β-particle coincidence procedure

from DSSD1 and DSSD3 that was described in Section 2.2.1. This procedure suppresses the β-summing tails on the high-energy side of the proton transitions, improves the overall energy resolution thus simplifying the identification of the proton transitions. The results of the fit procedure for these particular cases are described in detail below.

5.5.1 γ-ray at $E = 880$ keV

The 880-keV γ-ray transition is the de-excitation of the second excited state in ^{21}Mg at 1084(4) keV to the first excited state at 201(4) keV [Dig08]. The proton groups detected in coincidence with this γ ray were used to identify levels in ^{22}Al that were populated above the one-proton separation threshold. Figure 5.5 presents the energy spectrum of these protons after background subtraction. Fits to these proton transitions were particularly challenging because of the low statistics. The branching ratio to this state is of the order $BR_{\beta p} \sim 1.2$ %.

A total of five transitions have been tentatively identified in this spectrum. However, as in the previous analyses of ^{20}Mg and ^{23}Si, a confidence threshold of 3σ has been applied as a condition to identify the existence of a proton group. Proton groups 1.02 and 1.03 do not satisfy this confidence criterion. In addition, the energy of the proton group 1.02 is very close to 2 MeV, which is the highest intensity proton observed in the ungated proton energy spectrum. The few counts observed at this energy in the 880-keV γ-ray gated spectrum could be false correlation with this intense transition.

#	$E_{centroid}$	E_{proton} (keV)	E^*_{level} (^{22}Al)	Intensity (%)
1.01	1080 (66)	1106 (101)	2461 (101)	0.20 (7)
1.02	2363 (100)	2409 (112)	3764 (112)	0.21 (10)
1.03	4291 (47)	4363 (62)	5718 (62)	0.10 (5)
1.04	4798 (60)	4876 (76)	6238 (76)	0.10 (6)
1.05	5637 (28)	5723 (68)	7078 (68)	0.35 (9)
$\sum$				0.97 (17)

Table 5.7 – Energies and intensities of the proton groups emitted in coincidence with γ rays at $E = 880$ keV. The branching ratios are given with respect to the total implant-and-decay events and corrected for the γ-ray efficiency.

5.5.2 γ-ray at $E = 204$ keV

In the previous experiment of Ref. [Dig08], a γ-ray transition was measured at 201(4) keV that was identified as the de-excitation of the first excited $1/2^+$ state in ^{21}Mg to its $5/2^+$ ground

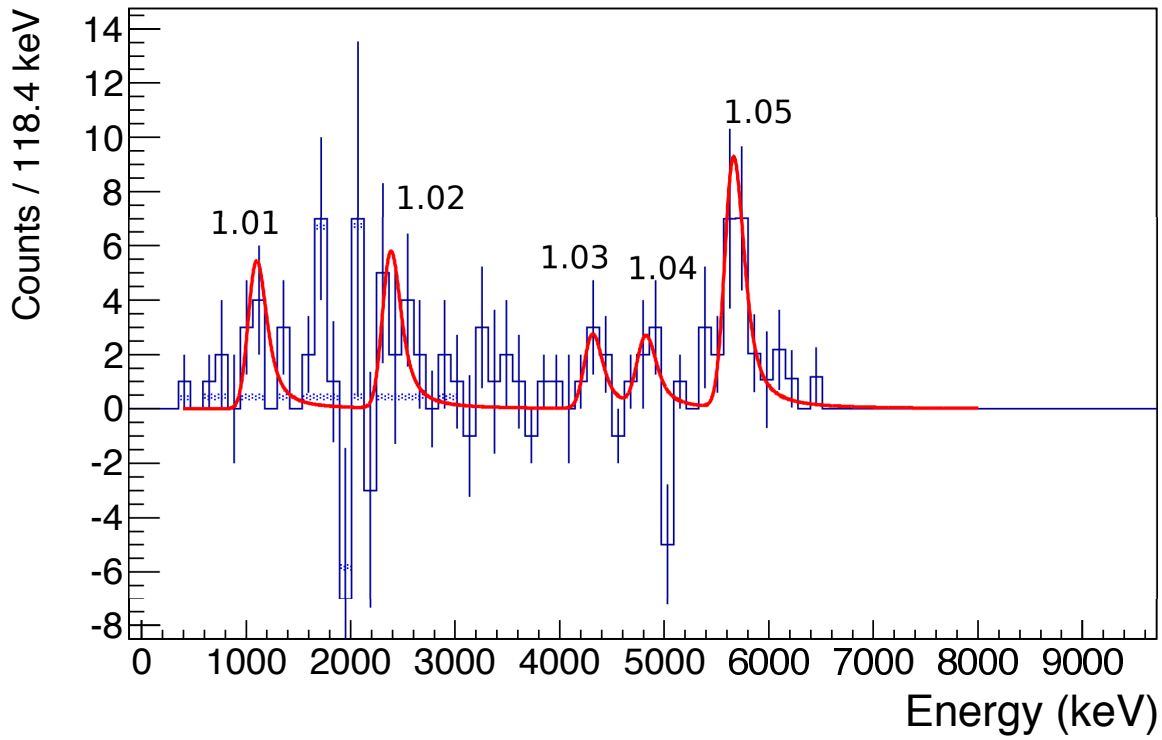

Figure 5.5 – Spectrum of β-delayed protons emitted in coincidence with 880-keV γ rays. This spectrum includes corrections for the DSSD and SeGA detection efficiency.

state. In this work, the energy of this γ ray was determined to be 203.8(5) keV, in good agreement with the previous work. Population of the 204-keV state in ^{21}Mg is the signature of β-delayed proton emission from resonances in ^{22}Al.

Figure 5.6 presents the low-energy part of the 204-keV γ-ray gated proton spectrum and following a background and up-feeding subtraction. A proton group at 2 MeV was observed with a branching ratio of 18.4%, which corresponds to the main proton group observed by Blank *et al.* [Bla96]. Another strong proton group at 0.75 MeV is likely emitted from a state with an excitation energy of 1234(59) keV in ^{22}Al. From the protons identified in Table 5.8, 8 proton groups are tentatively identified in the broad structure between 3.2 and 8.0 MeV.

The energies and the branching ratios are summarized in Table 5.8. The results of the fitting procedure are presented in Figure 5.7 and give an overall reduced χ^2 value of 13.1. This value is dominated by several bins between 2.5 and 3.0 MeV that have very few counts. At high energy ($\sim$ 7 MeV), the very weak branching ratios and the low backgrounds allowed a tentative fit to be performed on the last few counts at 7.5 MeV and 8.1 MeV. The last few counts above 8.1 Mev, and assuming this is a proton emitted from an excited state in ^{22}Al to

the ground state in ^{21}Mg, yields an excitation energy of ≈8735 keV. This is lower than the expected energy of the IAS, 9111 ± 228 keV that was deduced in Ref. [Bla08].

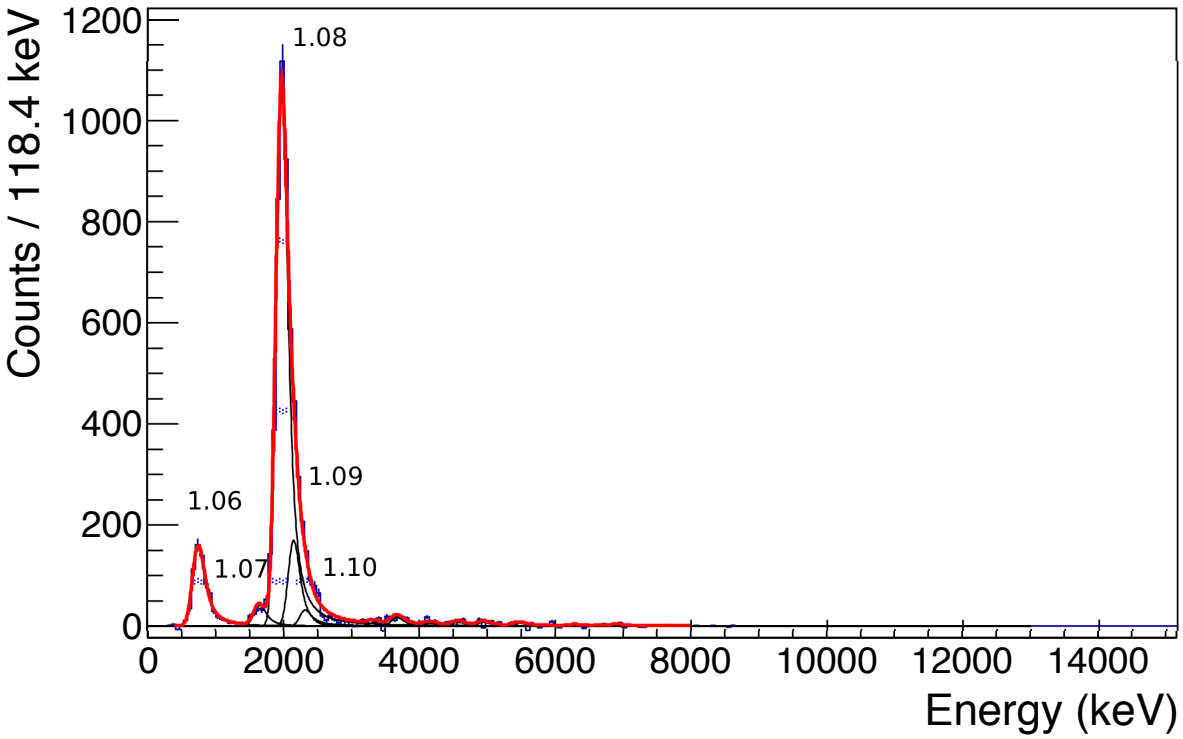

Figure 5.6 – Spectrum of β-delayed protons emitted in coincidence with 204-keV γ rays.

The use of a coincidence gate with β particles detected in DSSD 1 and 3 is a powerful tool for the identification of the strongest transitions. As described above, the efficiency for this procedure is relatively low (about 3%) and thus this analysis does not allow the weakest transitions above 3.5 MeV to be clearly identified. Nevertheless the two main transitions are visible on a negligible background. The analysis of this spectrum presented in Figure 5.8 and confirms the identification of proton groups 1.10 and 1.13. In addition, the energies of the events selected by this procedure are only the proton-decay group energies that are nearly free of the β-particle summing effect. Thus, the energy distribution can be described as a simple Gaussian distribution, with a fixed σ parameter to reflect the resolution of the detector. Based on this argument, we identify 4 additional proton groups, whose energies $E_{proton}\prime$ are summarized in Table 5.9 and are compared to the transitions previously measured in Table 5.8.

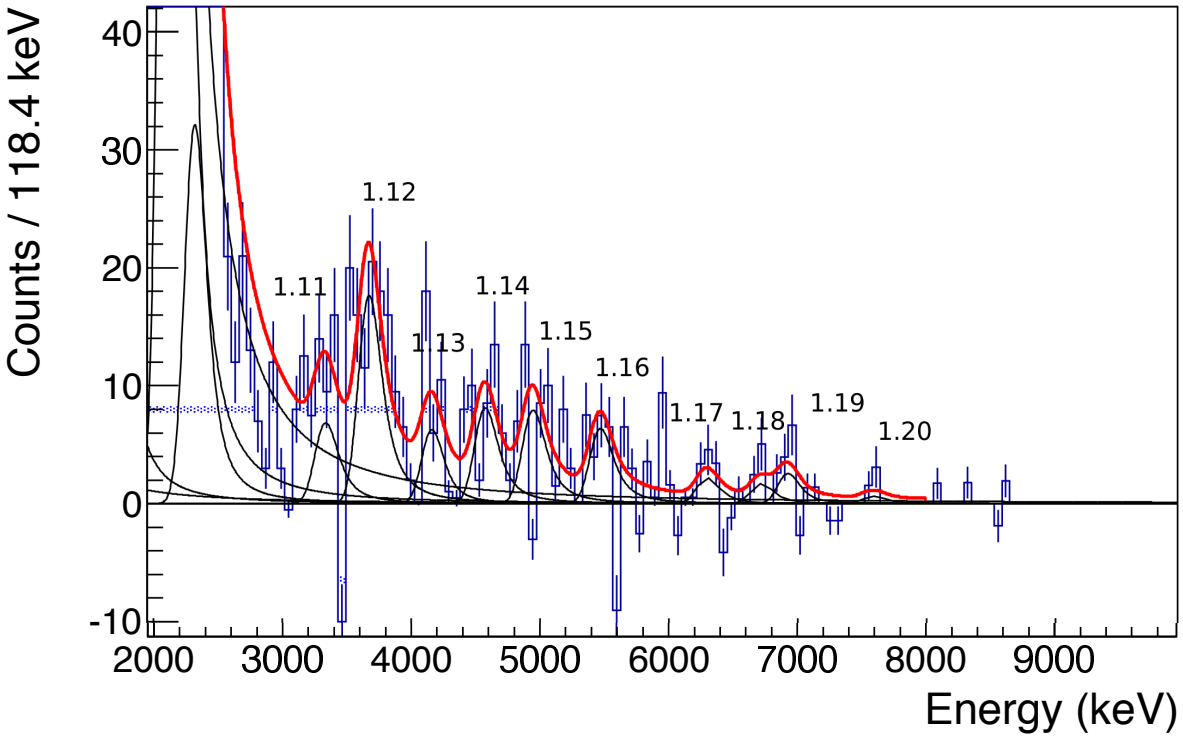

Figure 5.7 – High-energy part of the spectrum of β-delayed protons emitted in coincidence with 204-keV γ rays.

5.6 β2p decay channel with γ-ray coincidence

A γ-ray transition was observed at 596 keV that is due to the de-excitation of the first excited 3^+ state in ^{20}Na to its ground state. This observation provides the first confirmation for β-delayed 2 proton decay from ^{22}Si. The spectrum of charged particles emitted in coincidence with the 596-keV γ-ray transition and after background subtraction is presented in Figure 5.9. This low-statistics spectrum and weak peak-to-background ratios do not permit any conclusive evidence as to the initial levels in ^{22}Al that were populated.

At higher energy, tentative proton groups were identified for four weak transitions. The energy and the branching ratios for each proton group are summarized in Table 5.10 along with the corresponding excited states in ^{22}Al. Although these proton groups suffer from very low statistics, the maximum excitation energy of 8984(91) keV was derived from the highest-energy proton group. This result is in good agreement with the expected value of the IAS 9111 $\pm$ 228 keV that was deduced from systematic trends in Ref. [Bla08].

#	$E_{centroid}$	E_{proton} (keV)	E^*_{level} (^{22}Al)	Intensity (%)
1.06	722 (4)	742 (85)	1218 (85)	4.89 (20)
1.07	1616 (12)	1651 (66)	2127 (66)	1.25 (12)
1.08	1936 (3)	1976 (59)	2452 (59)	26.3 (10)
1.09	2086 (10)	2128 (56)	2604 (56)	8.35 (86)
1.10	2297 (4)	2342 (52)	2818 (52)	1.11 (24)
1.11	3297 (32)	3357 (50)	3833 (50)	0.18 (6)
1.12	3670 (26)	3734 (46)	4210 (46)	0.52 (7)
1.13	4105 (27)	4175 (47)	4651 (47)	0.16 (5)
1.14	4621 (31)	4697 (54)	5175 (54)	0.27 (5
1.15	4989 (25)	5069 (55)	5545 (55)	0.21 (4)
1.16	5419 (21)	5503 (61)	5979 (61)	0.15 (4)
1.17	6271 (35)	6363 (83)	6839 (83)	0.06 (2)
1.18	6679 (40)	6774 (93)	7250 (93)	0.06 (3)
1.19	6887 (32)	6984 (94)	7460 (94)	0.06 (2)
1.20	7573 (69)	7675 (125)	8151 (125)	0.02 (2)
$\sum$				43.6 (14)

Table 5.8 – Proton group energies in coincidence with γ rays at $E = 204$ keV. As in the previous chapter, the uncertainties on the energy of the proton groups are the quadratic sum of the fit uncertainties and systematic uncertainties in the DSSD calibratio. Branching ratios are provided in percentage, with respect with the total number of decay events, and corrected for the SeGA HPGe γ-ray detection efficiency.

#	$E_{proton}\prime$	E_{proton} (keV)
1.05	781 (34)	728 (4)
1.07	1982 (12)	1935 (3)
1.09	2165 (18)	2086 (10)
-	2447 (55)	-
1.11	3543 (150)	3670 (26)
1.14	4785 (153)	4621 (31)

Table 5.9 – Proton group energies in coincidence with γ rays at $E = 204$ keV. As in the previous chapter, the uncertainties on the energy of the proton groups are the quadratic sum of the fit uncertainties, and the systematic uncertainties in the DSSD calibration. Branching ratios are given in percentage, with respect with the total number of decay events, and corrected form the SeGA efficiency.

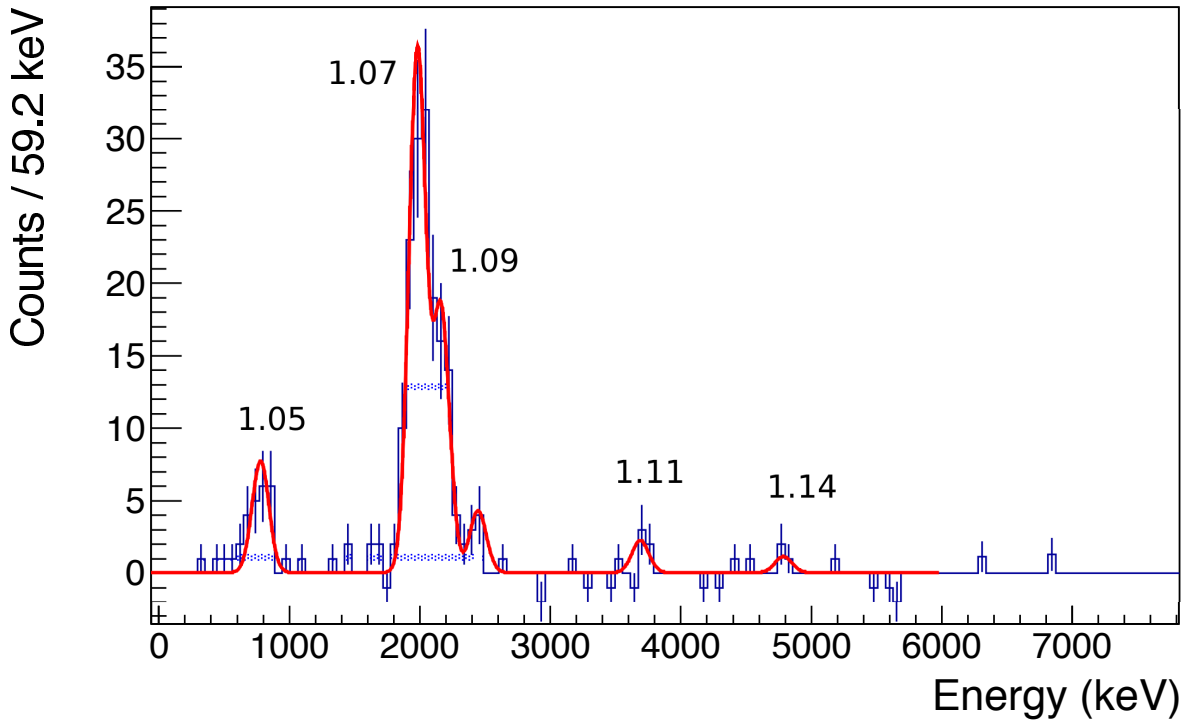

Figure 5.8 – Energy spectrum of the β-delayed protons in coincidence with 204-keV γ rays. A veto condition was also applied when a β particle was detected in coincidence in DSSD 1 and 3.

#	$E_{centroid}$	E_{proton} (keV)	E^*_{level} (^{23}Al)	Intensity (%)
2.01	3785 (49)	3833 (62)(48)	7925 (78)	0.17 (7)
2.02	3417 (51)	3462 (64)(45)	7554 (78)	0.10 (6)
2.03	4384 (50)	4437 (65)(53)	8529 (84)	0.10 (5)
2.04	4837 (55)	4892 (72)(55)	8984 (91)	0.11 (4)
$\sum$				0.48 (11)

Table 5.10 – Energy of the proton groups emitted in coincidence with γ-rays at $E = 596$ keV. In the second column the systematic uncertainties due to calibration are presented separately from the uncertainties on the angular distribution of the two protons.

5.7 Ungated proton spectrum with γ-ray subtraction

As for the case of ^{23}Si describe in Chapter 4, an ungated ground-state proton spectrum was constructed by taking the sum of all γ-ray coincident proton spectra, normalizing each of them by their respective γ-ray detection efficiency and subtracting their sum from the ungated proton spectrum. The resulting spectrum, presented in Figs. 5.10 and 5.11, corresponds to only those

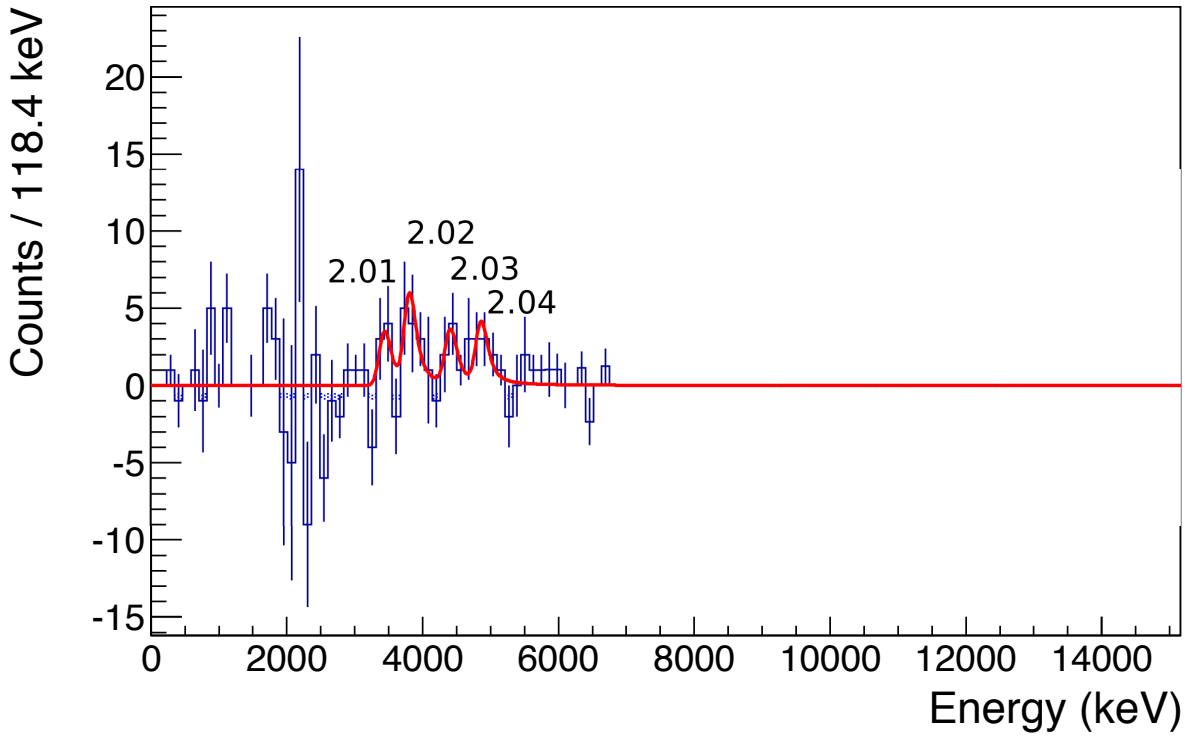

Figure 5.9 – Spectrum of β-delayed protons emitted in coincidence with 596-keV γ-rays.

transitions from unbound states in ^{22}Al to the ground states of the daughter nuclei.

Gating on events in the ground-state proton spectrum with energies below 500 keV and looking at their decay time yields a half-life of $\sim$ 500 ms. These were therefore identified as β-particles coming from false correlations with the beam contaminants. The strong proton group (0.01) yields an excitation energy of 993(59) keV in ^{22}Al which does not correspond to any other state observed in the previous γ-ray gated spectra.

The two main transitions at 1.9 MeV and 2.2 MeV observed by Blank *et al.* [Bla96] are confirmed although they are not resolved in our detector. Adding the updated proton separation energy S_p = 271(100) keV from the IMME analysis leads to excited-state energies of 2298(60) keV and 2488(59) keV, respectively. In coincidence with 204-keV γ rays, a proton group was observed from a level at 2467(59) keV, which agrees with the value of 2488(59) keV. Although they had no γ-ray information, Blank *et al.* relied on energy differences and decay patterns in the mirror nucleus to correctly assign this proton as populating the 204 keV state in ^{21}Mg. The γ-ray gate in the present experiment unambiguously confirms this assignment.

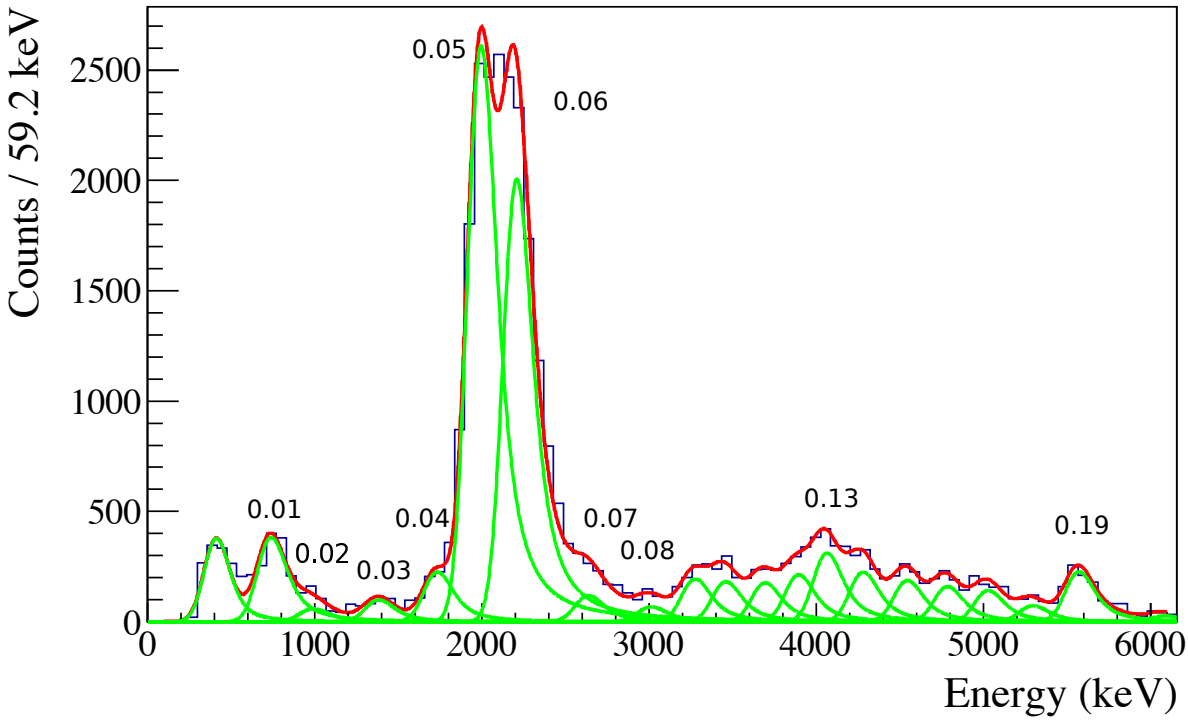

Figure 5.10 – Low-energy part of the spectrum of β-delayed protons emitted to the ground states of the daughter nuclei ^{21}Mg and ^{20}Na. Events measured with an energy below 500 keV are identified as β particles from contaminants in the secondary beam falsely correlated to ^{22}Si implants.

The very broad structure of counts observed between 3 and 6 MeV is consistent with a high density of states. The width of the proton component in the fit function was fixed at $\approx$ 70 keV for the average resolution. In the fit procedure, the minimization of the reduced χ^2 value was performed with a free parameter describing the area of the proton group. This was done in order to optimize the number of individual proton components in this distribution . The energy of the proton groups and the energy of the initial levels derived from this analysis are summarized in Table 5.11. The proton group 0.15 at 5596(84) MeV is in good agreement with the expected decay energy of 5614(228) keV for two-proton decay from the IAS that was evaluated in Ref. [Bla08]. Using the mass excess of ^{20}Na = 6850.6(11) keV, the excitation energy of the IAS to the ^{22}Si ground state in ^{22}Al is determined to be 9092(84) keV.

Assuming that the highest-energy proton group is βp to the ground state of ^{21}Mg, it is emitted from a state in ^{22}Al with an excitation energy of 8803 (126) keV. This result is in good agreement with the previous energy of approximately 8.7 MeV obtained for the last excited state in the βp branch.

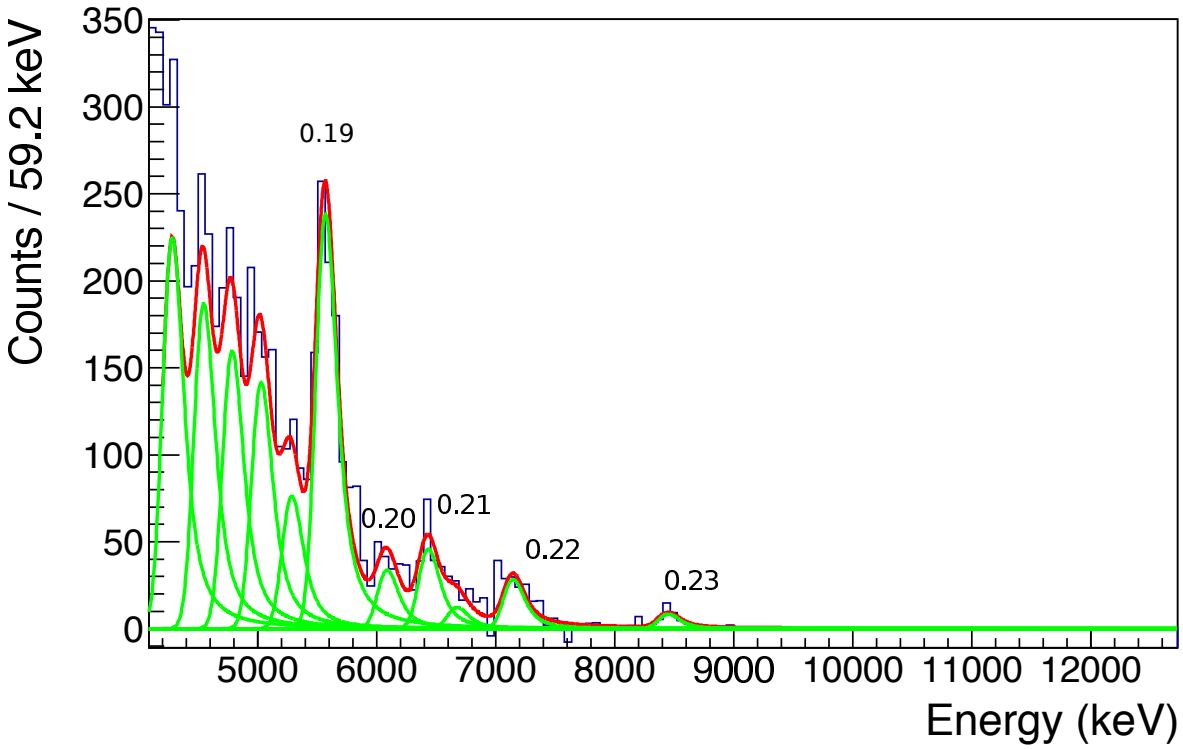

Figure 5.11 – High-energy part of the spectrum of β-delayed protons emitted to the ground states of the daughter nuclei ^{21}Mg and ^{20}Na. Proton group 0.15 corresponds to the β2p decay branch from the IAS in ^{22}Al to the ground state of ^{20}Na.

#	$E_{centroid}$	E_{proton} (keV)	E^*_{level} (^{23}Al)	Intensity (%)
0.01	713 (4)	734 (85)	1006 (85)	2.50 (8)
0.02	964 (14)	989 (80)	1261 (80)	0.39 (5)
0.03	1357 (10)	1389 (71)	1661 (71)	0.65 (4)
0.04	1708 (6)	1744 (63)	2016 (63)	1.47 (8)
0.05	1969 (1)	2010 (58)	2282 (58)	17.08 (26)
0.06	2182 (2)	2226 (54)	2498 (54)	13.13 (26)
0.07	2612 (3)	2662 (47)	2934 (47)	0.77 (6)
0.08	2987 (15)	3043 (44)	3315 (44)	0.44 (5)
0.09	3250 (10)	3309 (41)	3581 (41)	1.27 (9)
0.10	3433 (12)	3495 (40)	3767 (40)	1.19 (9)
0.11	3668 (11)	3733 (39)	4005 (39)	1.16 (9)
0.12	3869 (7)	3937 (38)	4209 (38)	1.39 (15)
0.13	4038 (6)	4108 (39)	4380 (39)	2.04 (14)
0.14	4255 (8)	4327 (41)	4599 (41)	1.47 (9)
0.15	4519 (8)	4595 (43)	4867 (43)	1.22 (7)
0.16	4759 (9)	4837 (47)	5109 (47)	1.05 (7)
0.17	5003 (10)	5083 (51)	5355 (51)	0.93 (6)
0.18	5271 (6)	5354 (55)	5626 (55)	0.48 (4)
0.19	5545 (4)	5575 (60)(30)	**9071 (67)**	1.53 (15)
0.20	6060 (28)	6151 (76)	6423 (76)	0.20 (2)
0.21	6407 (10)	6501 (79)	6773 (79)	0.30 (3)
0.22	6650 (227)	6745 (242)	7017 (242)	0.08 (2)
0.23	7120 (12)	7219 (95)	7491 (95)	0.19 (2)
0.24	8424 (17)	8531 (126)	8803 (126)	0.06 (1)
$\sum$				51.0(5)

Table 5.11 – Energy of the proton groups in the ungated ground-state spectrum after subtracting the upfeeding contributions from the γ-ray transitions. We conclude that proton group 0.15 at E_{proton} = 5596 keV corresponds to the β2p decay from the IAS in ^{22}Al to the ground state of ^{20}Na.

5.8 Decay level scheme of ^{22}Si

To build the final decay scheme, level energies were obtained from the weighted average of the excitation energies in the event that several decay branches orginate from the same excited state. In case of large uncertainties on the energies, for example the 596-keV and 880-keV γ-ray gated proton spectra, the level energy is assumed to be the value obtained from the branches that have higher statistics. In the final level scheme, we apply the rule of a double confirmation, meaning that each level requires two independent decay branches to have been observed. Otherwise, when only one transition is observed, there must be a minimum amount of statistics associated with this transition. A minimum threshold on the branching ratio of $\geq 0.4\%$ was therefore applied. The final excitation energies of the proton-unbound levels in ^{22}Al that were deduced in this work are summarized in Table 5.12 and in the decay scheme of Figure 5.12. From this analysis, a total of 13 new levels were observed. Level energies and β-decay branching ratios are compared to the USDBpn predictions and the mirror nucleus 22F [Hub89, Wei05] in Figure 5.13.

It should be emphasized that there is, in general, very good agreement between the proton energies measured by Blank *et al.* in Ref. [Bla96] and those of the present work. However, the resulting level energies are different because Blank used an ^{22}Al one-proton separation energy of $S_p = 18$ keV (deduced from the 1993 atomic mass evaluation) while the value of $S_p = 272(100)$ keV was adopted in the present work. This leads to a systematic shift of ~ 250 keV between how the level energies are presented between the two experiments.

5.8.1 Discussion on $\mathbf{E^*_{level} = 2181\ (44)\ keV}$

In the previous study of Ref. [Bla96], a level in ^{22}Al was at 1.85 MeV was deduced from a weak proton group that was measured in the MSGC at 1.63 MeV. This transition was not convincingly observed in the Si detector. Nonetheless, this transition was tentatively identified as a proton decay to the first excited state in ^{21}Mg and a branching ratio of 6(2) % was obtained.

In this work, applying a gate to the 204-keV γ-ray transition was performed and a weak transition was observed at 1717(60) keV. This energy agrees reasonably well with the previous measurement and yields an excitation energy of 2181(44) keV. A branching ratio of 2.1(2)% was derived for this transition which is about a factor of 3 smaller than, but in agreement with, the previous work. Another proton transition from the decay of this level at 2181(44) keV in ^{22}Al to the ground state of ^{21}Mg was also observed. The total β-decay branching ratio for this state is 5.9(13) %.

5.8.2 Discussion on $E^*_{level} = 2466$ (38) keV

Evidence for a level at 2466(38) keV was deduced from both the 204-keV γ-ray gated spectrum and the ungated ground-state proton spectrum. These two proton transitions were already observed by Blank *et al.* [Bla96], and the total β-decay branching ratio was predicted to be >22 %. In the present work, a β-decay branching ratio of 47.5(10)% was derived for this state.

5.8.3 Discussion on the IAS

In the ungated proton spectrum obtained following decays of ^{22}Si that was presented in Figure 5.16, we observed a strong transition at 5545 (4) keV and with an intensity that is larger than expected when considering simple β-decay Q-value arguments. In the ^{23}Si decay presented in Chapter 4 and again in Fig. 5.16, a similar intense structure was also observed at $\sim$ 6 MeV and this was unambiguously attributed to β-delayed two-proton decays from the IAS in ^{23}Al. Similar structures have also been observed from decays of ^{22}Al [Ach06], ^{43}Cr and ^{50}Ni [Dos07] and these have all been identified as β2p decay branch through the IAS. In the ^{22}Si spectrum obtained in the present work, proton group 0.15 in the ungated spectrum is therefore identified as β-delayed two-proton decay from the IAS in ^{22}Al to the ground state of the daughter ^{20}Na. The excitation energy of the IAS derived from this hypothesis is in good agreement with the value obtained from a few counts observed in the proton spectrum that was gated on the 596-keV γ ray. This γ-ray corresponds to the de-excitation of the first excited state in ^{20}Na to its ground state and provides additional confirmation for the existence of the previously unobserved β2p decay branch from ^{22}Si.

The alternative hypothesis was also considered, namely that the intense proton group at 5545 keV is simply a one-proton emission process from an excited level in the ^{22}Al that populates the ground state of ^{21}Mg. Such a level would be situated at 5816(60) keV excitation energy in ^{22}Al. One could also reasonably expect that this state should also decay by the emission of a 5341 keV proton to the 204-keV excited state in ^{21}Mg. However, analysis of the 204-keV γ-ray gated proton spectrum does not provide any evidence for such a transition. In addition, there are no strong theoretical arguments as to why a particular state at mid excitation energy would be much more strongly populated than any of the the neighbouring 1^+ states. Given these considerations, this βp hypothesis was ruled out.

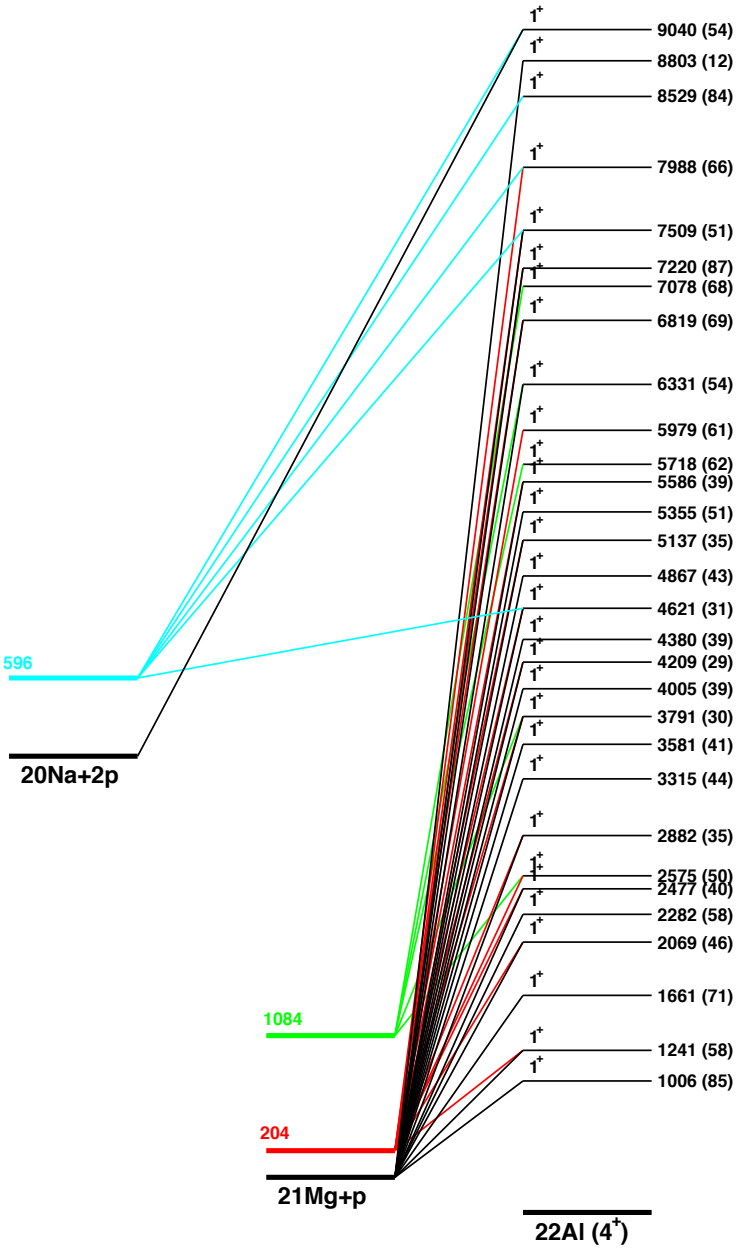

Figure 5.12 – Decay scheme of ^{22}Si summarizing all the transitions observed in the present work. The βp and β2p decay branches have been identified and the excitation energy of the levels in ^{22}Al have been deduced using $S_p = 271(100)$ keV (see text). However only 13 levels were unambiguously identified based the sufficient statistics in the corresponding proton groups (see text).

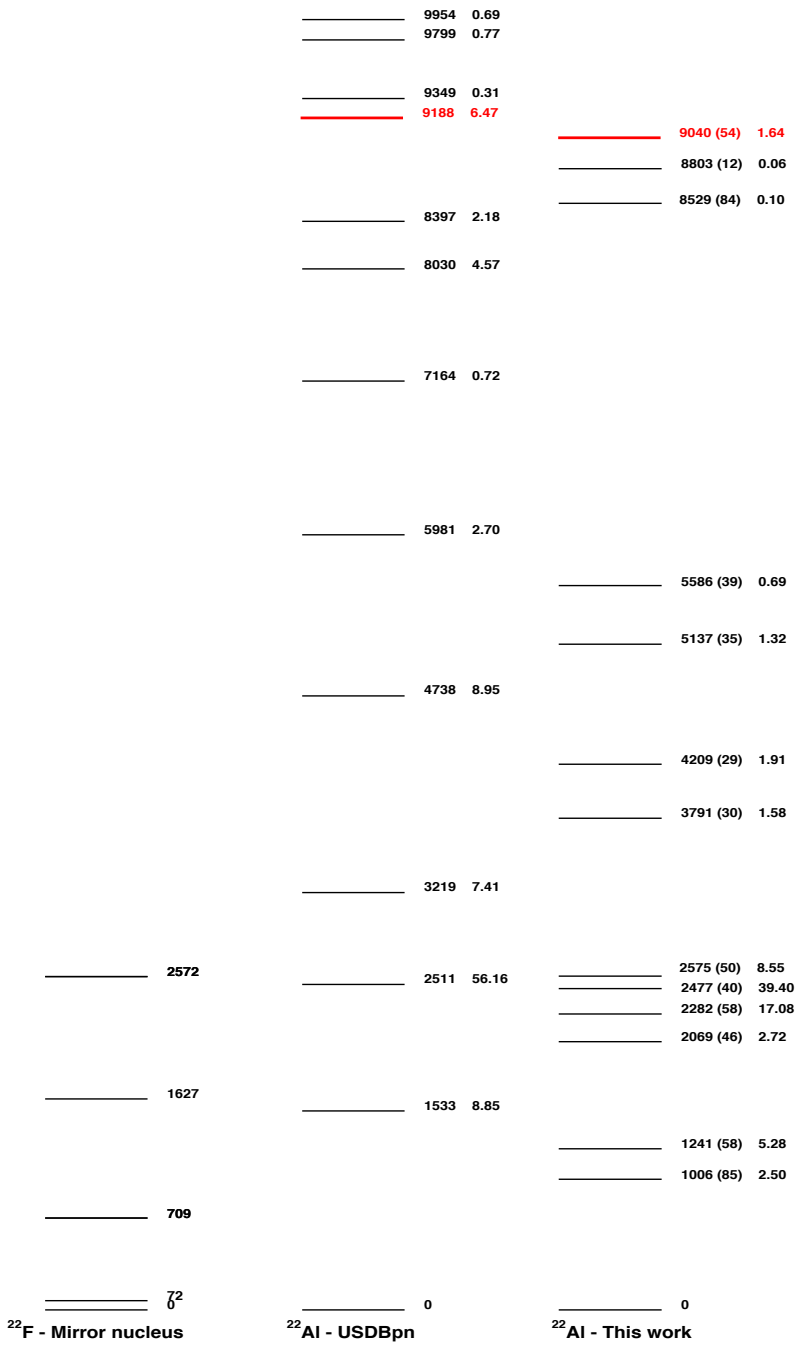

Figure 5.13 – Level scheme of ^{22}Al derived in the present study using $S_p = 271(100)$ keV (see text). The excitation energies of the proton-unbound levels are compared to the USBBpn model [Bro] and the mirror ^{22}F. One has to keep in mind that a systematic uncertainty of 100 keV, associated with the mass of ^{22}Al ground state, has to be added to the uncertainties of the levels determined in this work. In red, the IAS was deduced to be 9040(54) keV, in good agreement with the predictions.

#	204 keV	1084 keV	596 keV	^{21}Mg g.s.	^{20}Na g.s.	E^*_{level}	BR (%)
1				1006 (85)		1006 (85)	2.50 (8)
2	1218 (85)			1261 (80)		1241 (58)	5.28 (21)
3				1661 (71)		1661 (71)	0.65 (4)
4	2127 (66)			2016 (63)		2069 (46)	2.72 (14)
5				2282 (58)		2282 (58)	17.08 (26)
6	2452 (59)			2498 (54)		2477 (40)	39.4 (10)
7	2604 (56)	2461 (11)				2575 (50)	8.55 (86)
8	2818 (52)			2934 (47)		2882 (35)	1.88 (25)
9				3315 (44)		3315 (44)	0.44 (5)
10				3581 (41)		3581 (41)	1.27 (9)
11	3833 (50)	3764 (11)		3767 (40)		3791 (30)	1.58 (15)
12				4005 (39)		4005 (39)	1.16 (9)
13	4210 (46)			4209 (38)		4209 (29)	1.91 (17)
14				4380 (39)		4380 (39)	2.04 (14)
15	4651 (47)			4599 (41)		4621 (31)	1.63 (10)
16				4867 (43)		4867 (43)	1.22 (7)
17	5175 (54)			5109 (47)		5137 (35)	1.32 (9)
18				5355 (51)		5355 (51)	0.93 (6)
19	5545 (55)			5626 (55)		5586 (39)	0.69 (6)
20		5718 (62)				5718 (62)	0.1 (5)
21	5979 (61)					5979 (61)	0.15 (4)
22		6238 (76)		6423 (76)		6331 (54)	0.3 (6)
23	6839 (83)			6773 (12)		6819 (69)	0.36 (4)
24		7078 (68)				7078 (68)	0.35 (9)
25	7250 (93)			7017 (24)		7220 (87)	0.14 (4)
26	7460 (94)		7554 (78)	7491 (95)		7509 (51)	0.35 (7)
27	8151 (12)		7925 (78)			7988 (66)	0.19 (7)
28			8529 (84)			8529 (84)	0.1 (5)
29				8803 (12)		8803 (12)	0.06 (1)
30			8984 (91)		9071 (67)	9040 (54)	1.64 (16)

Table 5.12 – Energies of the unbound levels in ^{22}Al populated by the β decay of ^{22}Si. The method of the weighted average was used to calculate the energies of the excited levels in ^{22}Al. The sum of β strength emitting a proton with a least 500 keV is $\geq 98\%$.

When applying the β coincidence on DSSD1 and 3, the shape of the proton group is defined by a Gaussian distribution as the beta background is removed/eliminated. Figure 5.14 shows the superposition of the fit to the proton group 0.19 and a Gaussian function with a width fixed by the resolution of the Si detector for single protons (≈65 keV). The result of the fit to the data gives a σ of 154 (23) keV, which is larger than the expected resolution for single proton emission at this energy. This discrepancy would suggest two-proton emission due to the kinematics and angular distribution between the two protons.

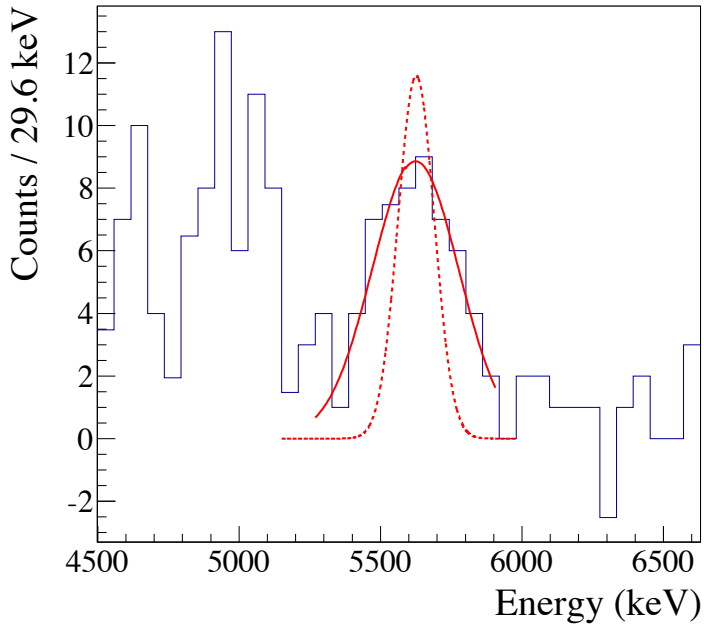

Figure 5.14 – The width of the proton group identified as an IAS is larger than expected for a single proton emission. This wider distribution would be expected for a two-proton distribution, due to the angular distribution between the two protons. In red, the best fit function gives a resolution of σ = 154 (23) keV, while the expected one-proton resolution at this energy is ≈65 keV, as shown by the dashed line.

The 5545 (4) keV transition is therefore proposed to be β-delayed two-proton emission from the IAS in ^{22}Al. From the proton decay energy and the S_{2p} value of 3496(100) keV, the IAS excitation energy is E^*_{level} = 9071(60)(30) keV where 100 keV are due to the uncertainty on the S_p value as explained in Section 5.1. This value is in good agreement with the predicted value of 8840(220) keV from Ref. [Bla08].

As observed in the decay of ^{23}Si, the branching ratio for one-proton decay from the IAS to the ^{22}Mg ground state was extremely low (≈ 0.002%). In Figure 5.15 an emphasis on the energy range above 8 MeV in both the ungated and the 204-keV γ-ray gated spectrum is presented.

Assuming an IAS energy of 9092 keV, one would expect to observe a similarly weak proton group at the energy marked by the arrow around 8.8 MeV in the ungated spectrum. In the γ-ray gated spectrum, this energy would be shifted to 8.6 MeV, but the number of events would be reduced by an order of magnitude due to the SeGA efficiency for this γ-ray energy (approximately 11%). Based on the branching ratio deduced for the βp decay from the IAS in ^{23}Al to the ^{22}Mg ground state (and correcting for the DSSD efficiency) approximately 2 counts are expected in the ungated proton spectrum around 8.8 MeV while less than one count would appear in the 204-keV γ-gated spectrum around 8.6 MeV. Although there are relatively very few counts in both spectra that seem to be close to this energy, it should be emphasized that not a single count was observed in either spectra above these energies. This is consistent with the fact that the total β-decay strength is almost entirely exhausted above the IAS.

The total β-decay branching ratio to the IAS of was deduced to be 1.64(16)%. This was obtained from the sum of the β-delayed two-proton decay branches that populate the ground state ($BR = 1.53(15)\%$) and first excited state ($BR = 0.11(4)\%$) of ^{20}Na. As described above, β-delayed proton decay branches from the IAS to the ground and first excited state at 204-keV in the ^{21}Mg daughter can be considered negligible. However, it could be possible for several additional weak βp transitions to feed higher lying states in ^{21}Mg. These protons would be lower in energy and could therefore be potentially missed in the analysis as they would lie underneath the signals produced from the higher intensity protons. Although each branch may itself be negligible, the sum of all of these undetected transitions may not be. Without considering this possibility, the branching ratio to the IAS obtained from the observed transitions can therefore only be considered as a lower limit. To estimate the amount of βp feeding that was potentially missed in the experiment, the theoretical work of Detraz [Dét91] is used to provide estimates for the ratio of β2p/βp decays from the IAS. These theoretical predictions have been verified for decays of several proton-rich nuclei including ^{35}Ca [Tri99] and ^{23}Si [Bla97]. The ratio of β2p/βp for the case of ^{22}Si is predicted to be 2.0. Assuming this theoretical prediction, it would imply that a total of 0.82(8) % of βp strength from the IAS was potentially missed in the experiment. To be conservative, we adopt half of this total and assign a relative uncertainty of 100% on its value and add the result $BR_{\beta p} = 0.41(41)$ % to the overall branching ratio to the IAS. The total decay branching ratio from the IAS is therefore evaluated in this work to be $BR_{IAS} = 2.05(44)\%$.

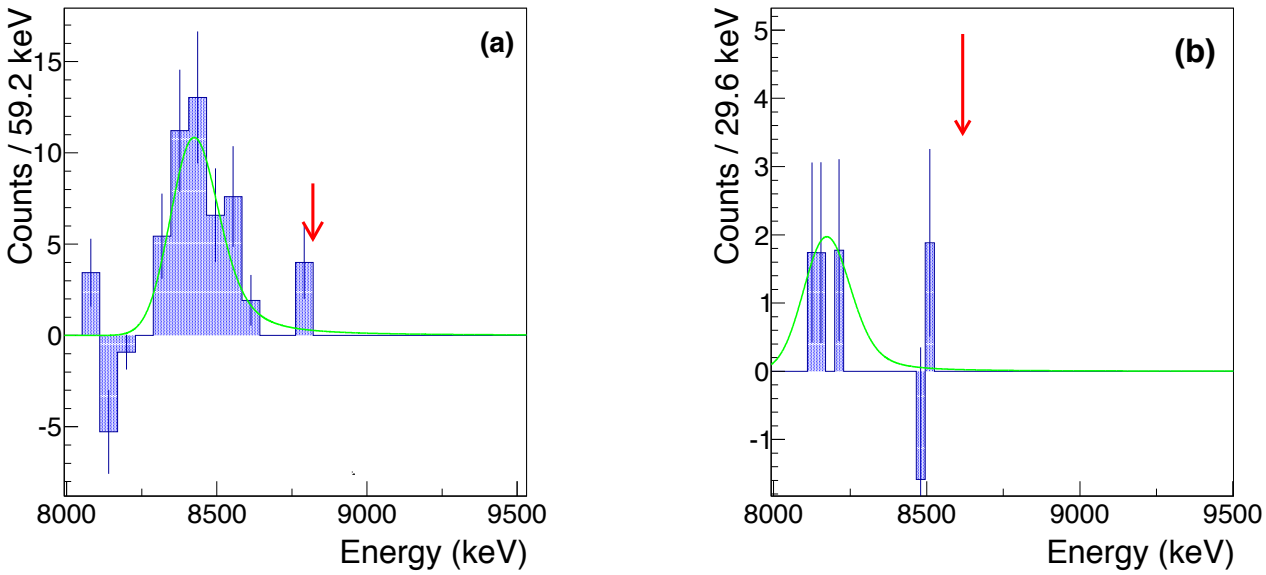

Figure 5.15 – The β-delayed one-proton decay channel from the IAS in ^{22}Si is expected to have a very low branching ratio. In both the ungated spectrum (a) and 204-keV γ-ray gated spectrum (b), the expected energies of the proton groups from the IAS are marked with an arrow. Only a few counts are observed and do not allow a firm conclusion as to the existence of this decay branch.

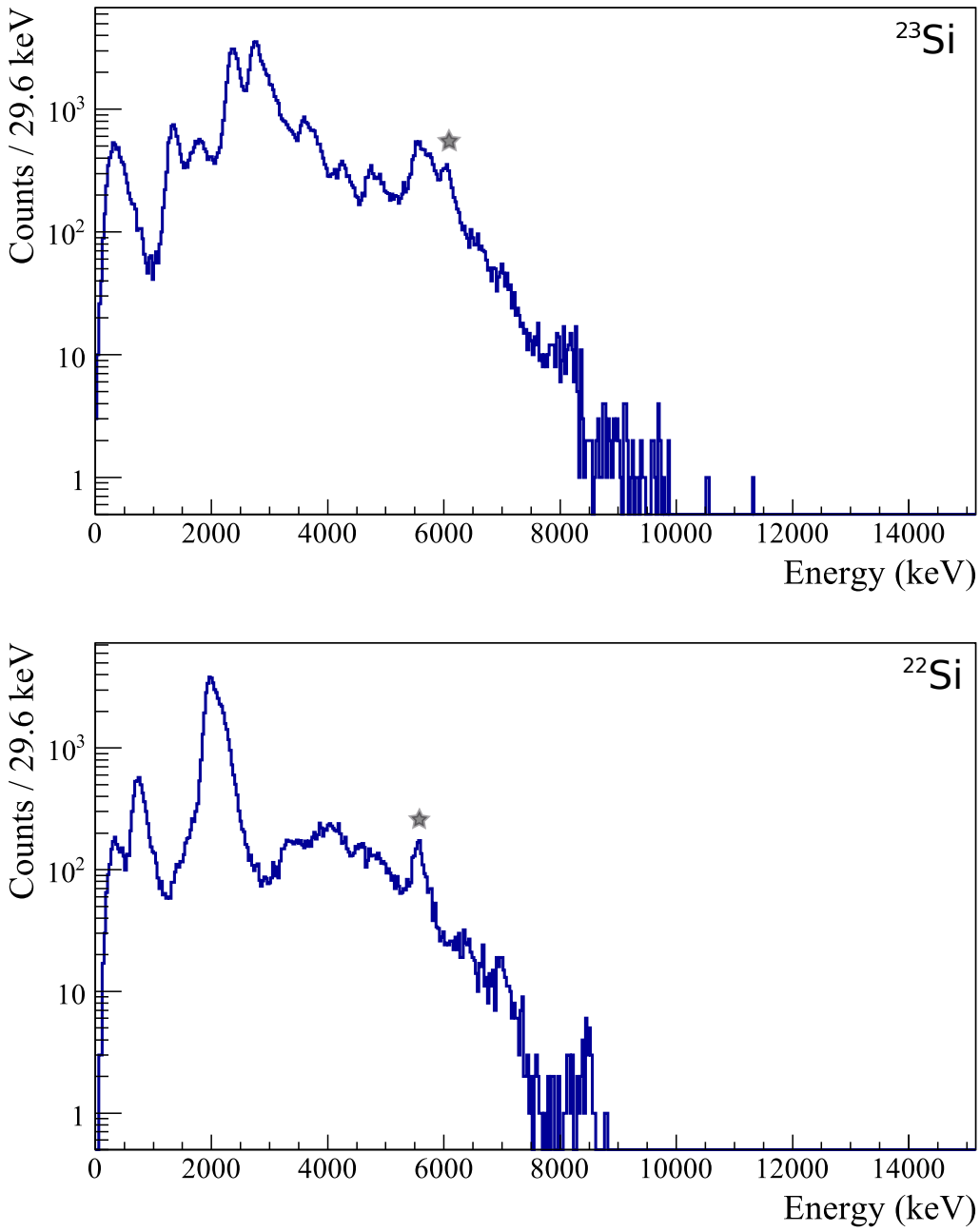

Figure 5.16 – In the ungated and subtracted proton spectrum of ^{22}Si decay (bottom), a strong proton transition was observed at 5.5 MeV, labelled with a star. Based on the similarities with the proton spectrum from ^{23}Si decay (top), we propose that the charged particle group in ^{22}Si is due to β-delayed two-proton decay from the IAS whose excitation energy was derived to be 9092(84) keV.

5.9 Half-life measurement of ^{22}Si

A precise measurement of the half-life of ^{22}Si is necessary to obtain a precise value for the partial half-life t. Two methods were applied, using the same methods as described above for ^{23}Si. In the PID spectrum, ^{22}Si was the only β-delayed proton emitter in the secondary beam, which simplifies the analysis significantly compared to the case of ^{23}Si that was contaminated by decays of ^{20}Na. Fits to the decay curves were performed over the time range from 10 ms to 290 ms and used the maximum likelihood method.

5.9.1 Using proton gates

The energy spectrum of charged particles was divided into six energy ranges. All ranges considered only those energies above 500 keV to avoid contamination from low-energy β particles emitted from the decays of long-lived nuclei that were present in the secondary cocktail beam. The corresponding decay curves were fit using a single decay exponential with a constant background and examples are presented in Figure 5.18. The fit results are summarized in Table 5.13. A weighted average of the results presented in Figure 5.21 yields a ^{22}Si half-life of $T_{1/2} = 31.88(29)$ ms with a reduced χ^2 of 2.35 for 5 degrees of freedom.

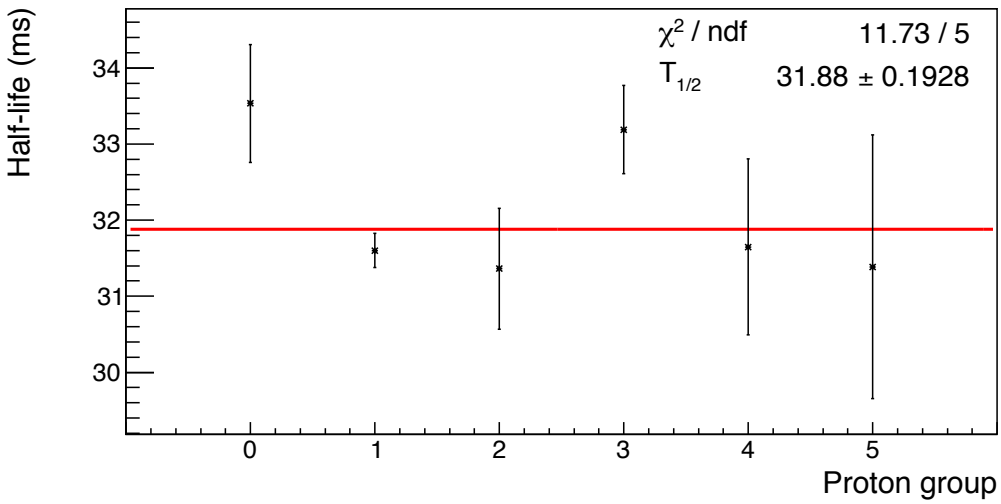

Figure 5.17 – The weighted average of the ^{22}Si half-lives obtained by fitting the proton-gated spectra yields $T_{1/2} = 31.88(19)$ ms with a reduced χ^2 value of 11.73/5.

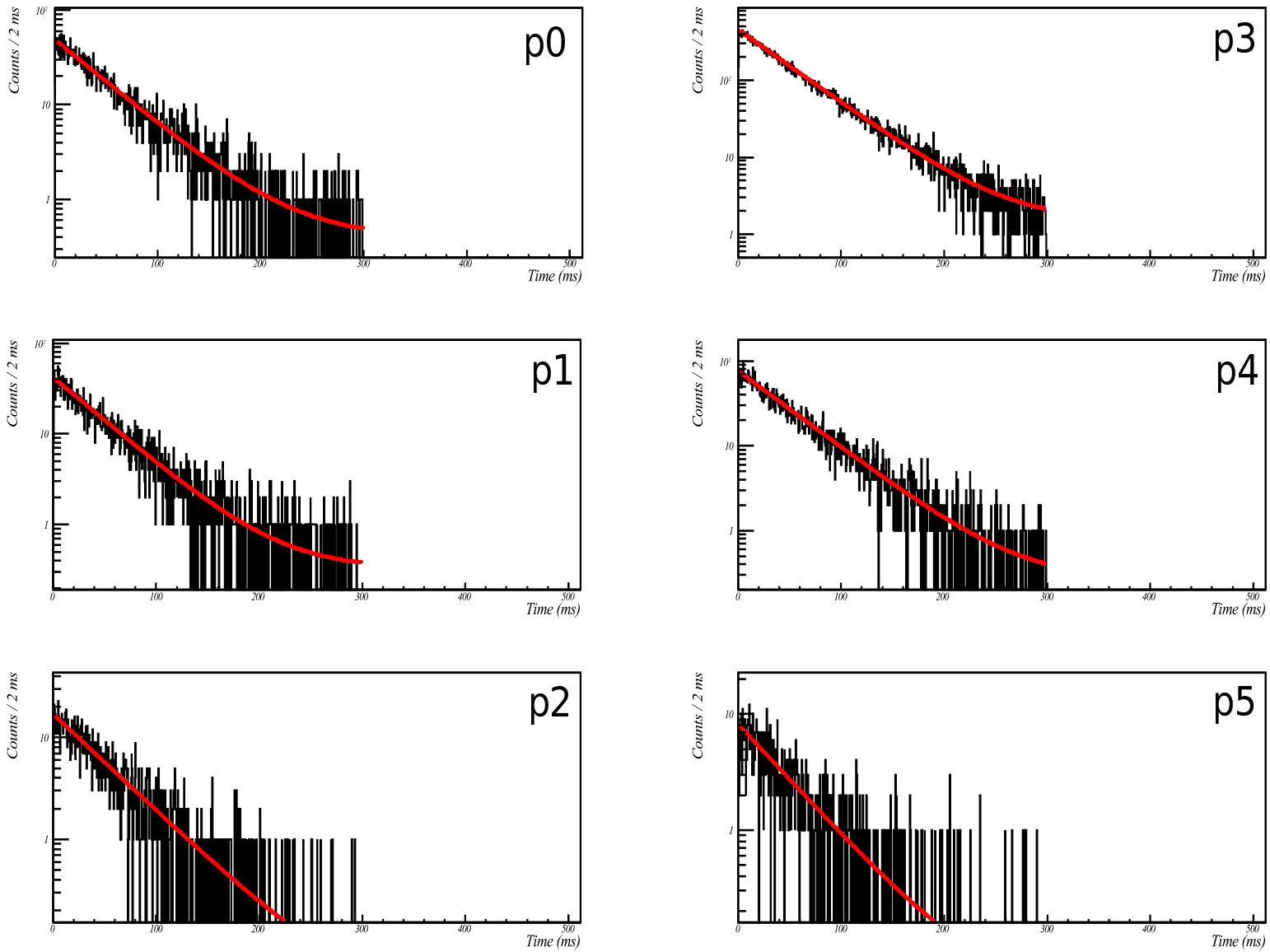

Figure 5.18 – Decay curves corresponding to the different energy gates applied to the proton spectrum. In red, the fit function, using an exponential decay and a constant background. The fit extends to 300 ms, which was the maximum correlation time used in the analysis program. Energies of the proton gates are given in Table 5.13.

Energy range (keV)	p0 [1135;1570]	p1 [2150;2640]	p2 [2645;3310]	p3 [9520;4105]	p4 [5387;6330]	p5 [8000;10490]
Half-life (ms)	33.53 (78)	31.60 (23)	31.36 (79)	33.19 (58)	31.6 (12)	31.4 (17)

Table 5.13 – Half-life determined by fitting the decay curves of different proton groups with an exponential decay and a constant background.

5.9.2 Using γ-ray gates

In addition to the proton gates, two γ-ray gated decay curves were generated using the $E = 204$ keV and $E = 880$ keV γ rays. The use of a γ-ray gate provides a clean decay curve that is essentially free of all contaminants and false correlation events. The decay time spectra obtained with this method does however suffer from low statistics due to the γ-ray detection efficiency.

The decay time spectrum gated on the most intense γ ray at 204 keV is presented in Figure 5.19. A fit to these data yields a ^{22}Si half-life of 31.13(41) ms with χ^2 value of 2.7.

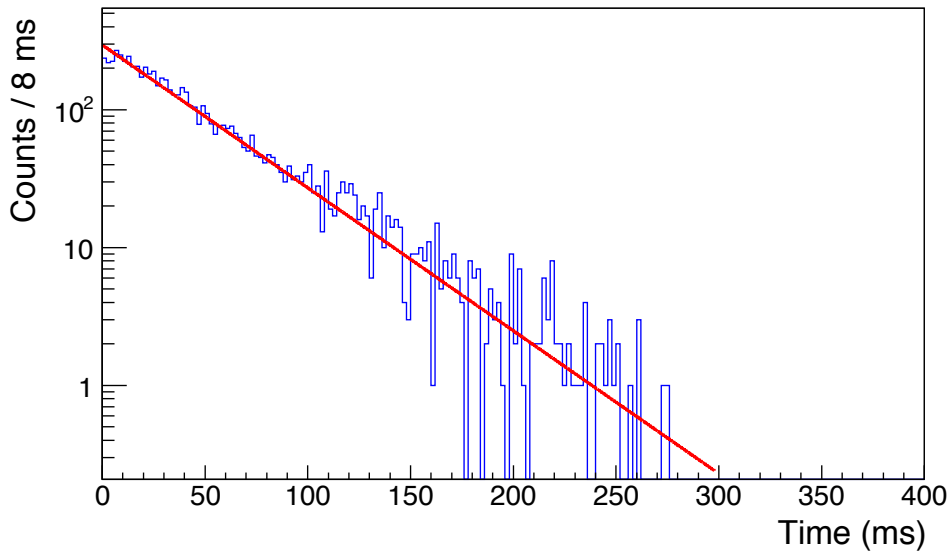

Figure 5.19 – Decay curves corresponding to the 204-keV γ-ray gate. In red, the fit function, that used an exponential decay and a constant background. The half-life obtained from this fit is $T_{1/2} = 31.13(41)$ ms with a reduced χ^2 value of 370/136.

Figure 5.20 presents the time spectrum obtained while applying the second γ-ray gate centred on the γ-ray transition at 880 keV. The result of the fit to this decay curve yields a half-life

of 30.4(34) ms for ^{22}Si, which is in agreement with the previous values but is significantly less precise due to statistical limitations.

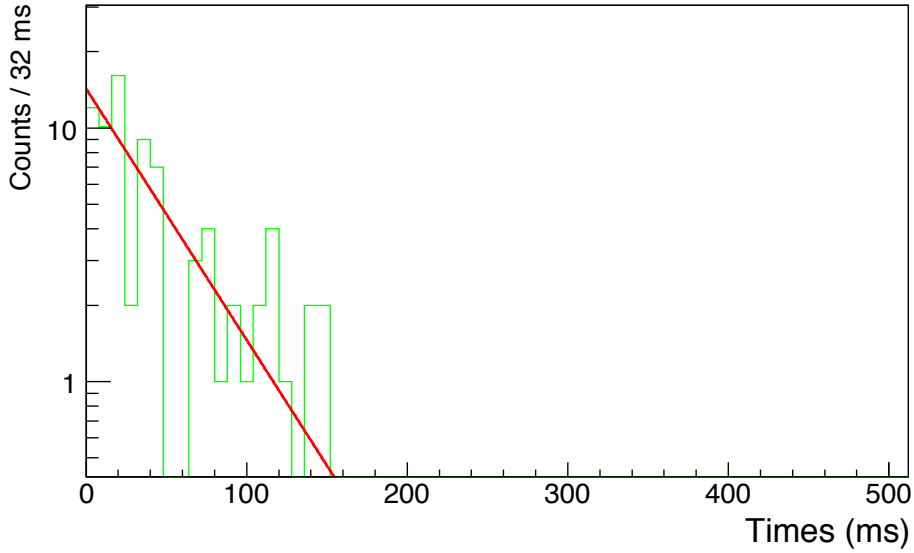

Figure 5.20 – Decay curves corresponding to the 880-keV γ-gate. Due to the low statistics, we obtain a half-life with high uncertainties, $T_{1/2}$ = 30.4 (34) ms, but in agreement with the previous measurements

5.9.3 Final result: the half-life of ^{22}Si

The total decay curve obtained from all of the implant-and-decay events detected in DSSD2 was also fitted. Because the half-life of daughter, $T_{1/2}(^{21}Mg)$ = 122.5 ms, is about 4 times longer than ^{22}Si and because the correlation time extended to only 300 ms, the fit function included only a single exponential decay plus a constant background parameter. An energy condition of E > 500 keV was applied to reject β-particles from the decays of the other implanted nuclei. The half-life obtained from the fit to the data shown in Fig. 5.21 was $T_{1/2}$ = 31.79(20) ms with a reduced χ^2 value of 1.20. If the ^{21}Mg daughter is included in the fit function and the data refit, the result was $T_{1/2}$ = 30.38(45) ms with a reduced χ^2 value of 1.18. Both of these values are in reasonably good agreement with both the average of $T_{1/2}$ = 31.88(19) ms from the average of the individually gated proton time spectra and $T_{1/2}$ = 31.13(41) ms from the 204-keV γ-gated spectrum. The half-life of ^{22}Si obtained in this present work is therefore adopted to be $T_{1/2}$ = 30.38(45) ms from the proton analysis, which is in very good agreement with the previous measurement of $T_{1/2}$ = 29(2) ms measured by Blank *et al.* in Ref. [Bla96].

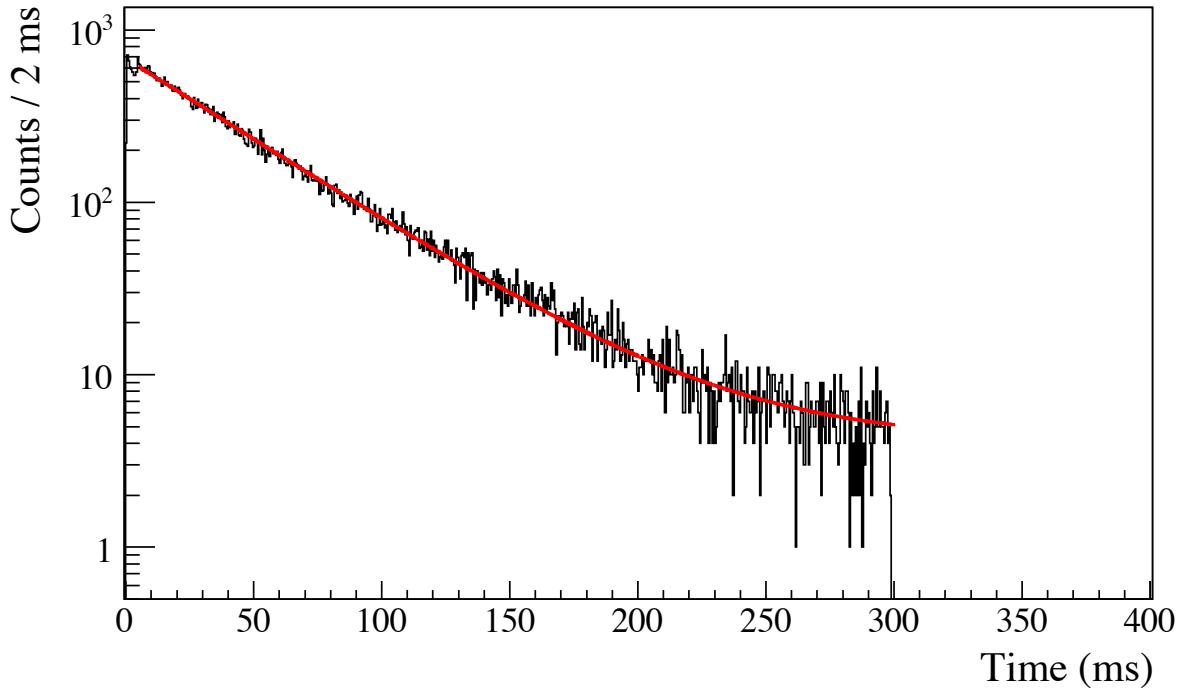

Figure 5.21 – Decay curves of all the correlated implant-and-decay events. The fit gives a half-life of $T_{1/2} = 30.38(45)$ ms (45) ms, with a reduced χ^2 of 692/575.

5.10 Mass excess of ^{22}Si ground state

The β-decay of the ^{22}Si ground state to its IAS in ^{22}Al is a superallowed Fermi decay, since the transition occurs between 0^+ isobaric analogue states. As previously described in Section 1.1.4, the weak interaction formalism leads to an expression of the ft value, which for all superallowed Fermi decays can be expressed as a constant. The most precise and up-to-date value measured for $T = 1$ superallowed Fermi decays is $\overline{\mathcal{F}t}_{T=1} = 3072.27 \pm 0.72$ s[Har15]. For $T = 3$ states, the matrix element is modified to 6 (from 2 in the $T = 1$ case) and thus, we obtain a ft value given by:

$$ft = \frac{1}{g^2|M'_{fi}|^2}\frac{2\pi^3\hbar^7\ln 2}{m_e^5c^4} = \frac{1}{6\cdot g^2}\frac{2\pi^3\hbar^7\ln 2}{m_e^5c^4} \tag{5.2}$$

$$= \frac{\overline{\mathcal{F}t}_{T=1}}{3} = 1024.2\ s. \tag{5.3}$$

where t is the partial half-life, defined as $BR_{IAS}/T_{1/2}$, and f is the statistical rate function. To deduce the mass excess of ^{22}Si, the strategy is then to use the experimentally deduced half-life and branching ratio to the IAS in ^{22}Al at 9092 keV and compare this result to the constant of Equation 5.3 in order to deduce the f value. From the f value, the β-decay Q-value can be be derived and hence the mass excess ΔE along with the one- and two-proton separation energies.

5.10.1 Statistical rate function for $T = 3$

In order to extract the ft value from the half-life, branching ratio and Q-value measurements, a parametrization of the statistical rate function for the set of $T = 1$ superallowed Fermi β decays was presented by Towner and Hardy in Ref. [Tow15]. In their work, f was divided into two parts in order to treat the shape corrections as an overall small effect δ_s, such as:

$$f = f_0(1 + \delta_s) \tag{5.4}$$

where δ_s stands for small shape corrections and f_0 was fitted with the form:

$$f_0 = a_0{Q_0}^4 p_0 + a_1{Q_0}^2 p_0 + a_2 p_0 + a_3 Q_0 \ln(Q_0 + p_0) \tag{5.5}$$

where a_0, a_1, a_2 and a_3 are the parametrization parameters provided by Towner and Hardy in this same study. The constant p_0 is defined as $p_0 = \sqrt{({Q_0}^2) - 1)}$ where Q_0 is the maximum of the total positron energy in electron-mass units. This function gives the direct link between the Q_β-value and the statistical rate function. This parametrization is not what Towner and Hardy actually use to calculate their final f value that are presented in their review articles. They instead use a master code that takes into account all possible effects and numerically evaluate the full expression of the f value. In the present, the fit parameters a_i were fixed to

the values derived from the limit that $Z = 0$, giving $a_0 = 1/30$, $a_1 = -3/20$, $a_2 = -2/15$ and $a_3 = 1/4$. This convenient parametrization is, however, valid at the level of 0.1% precision and allows the evaluation of f values without complicated computing [Tow15].

In this approximation, the δ_s correction factors provided by Towner and Hardy are no longer valid and therefore need to be recalculated. The ratio of the f values provided in Ref. [Har15] (that use their full calculation) divided by the f_0 values calculated using Equation 5.5 are plotted in Fig. 5.22 as a function of the number of protons Z in the parent nucleus. These values follow a very smooth trend that was approximated using a quadratic function to parametrize $(1 + \delta_s)$ as

$$(1 + \delta_s) = 0.9566 - 0.016Z + 0.0001Z^2. \tag{5.6}$$

Thus, one can calculate f_0 for any nucleus using Equation 5.5 and apply the correction factor from above to deduce the final f value as if the full Towner and Hardy calculation had been performed.

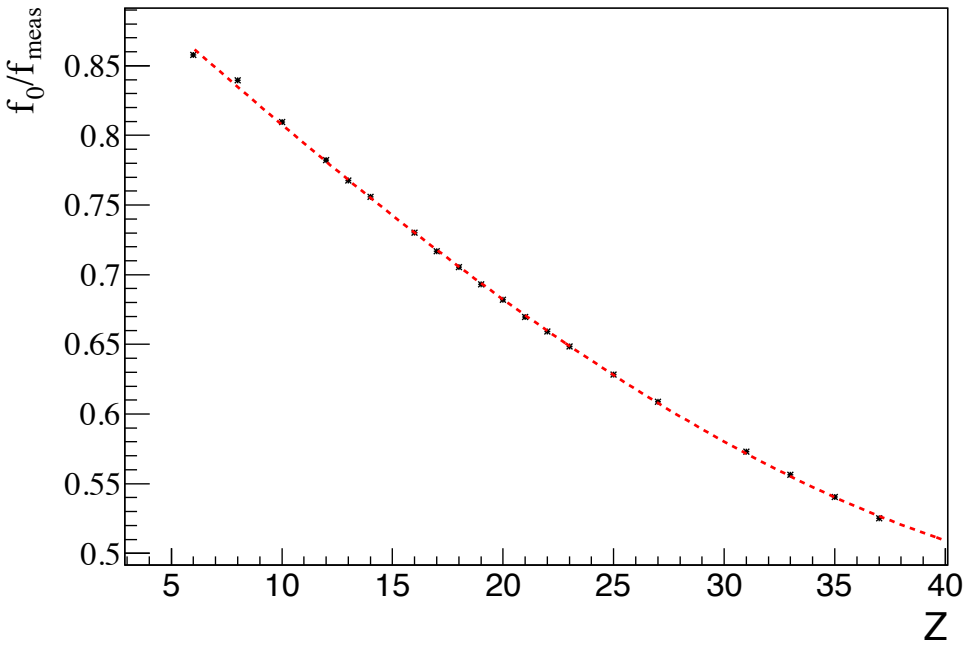

Figure 5.22 – The ratio of f_0/f_{meas} can be plotted as a function of the charge Z of the parent. In dashed red line, the quadratic fit used to calculate the corrections.

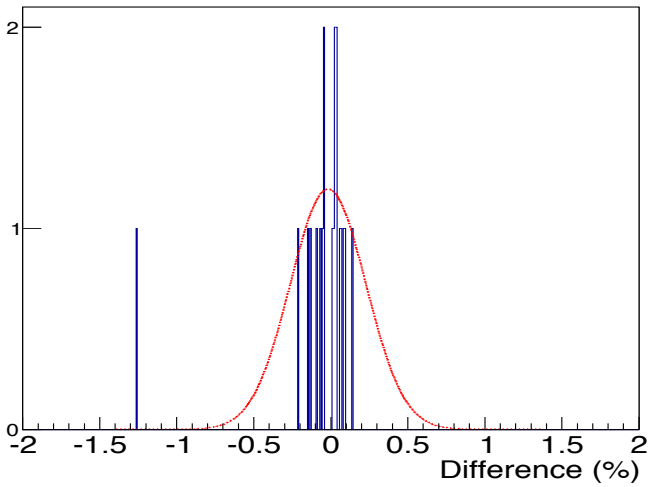

Figure 5.23 – Distribution of the differences between the parametrized f values and the f value obtained from the full calculation of Towner and Hardy [Har15]. Most values are significantly below 0.5% and only ^{10}C exhibits a difference that exceeds 1%.

Parametrization for known T=1 β decays

For a few of the known superallowed Fermi decays, the accuracy of this procedure was tested. Table 5.14 presents the $T_Z = -1$ and $T_Z = 0$ nuclei studied in Ref. [Har15] and that were used to parametrize the statistical function in this work. The Q_{EC}-value as well as the f value from Towner and Hardy's full calculation are compared to the f_0 parametrization procedure described above. In Figure 5.23, the differences between these two methods are presented. They indicate that for the 20 nuclei considered, the difference between the full calculation and the parametrized values are typically below 0.5%, with only value (^{10}C) that exceeds 1%. The mean of this distribution is consistent with 0 and the standard deviation is $\sigma = 0.25\%$. Uncertainties on the f values obtained from this approximation are given by

$$\Delta f = \sigma_Q \cdot \left[\frac{2}{15} W_0^3 p_0 + \frac{W_0^5}{30 p_0} - \frac{3}{10} W_0 p_0 - \frac{3W_0^3}{20 p_0} - \frac{2W_0}{15 p_0} + \frac{W_0 (1 + \frac{W_0}{p_0})}{4(W_0 + p_0)} + \frac{1}{4} \ln(W_0 + p_0) \right] \tag{5.7}$$

where σ_Q is the uncertainty on the Q_{EC}-value in electron-mass units.

Given measurements of the branching ratio of the superallowed Fermi β-decay to the IAS and the corresponding half-life of the parent of $T = 1$ nuclei, one can calculate the expected f value for ^{22}Si using Equation 5.3. By applying the correction factor $(1+\delta_s)$ that we parametrize in Equation 5.6, we can provide an approximate Q-value between the IAS in the daughter and the ground state of the parent. Figure 5.24 presents the difference between this calculated Q-

Parent	Q_{EC} (keV)	Adopted f [Har15]	f value (this work)
^{10}C	1907.87 (0.11)	2.3004 (0.0012)	2.32946 (0.0056)
^{14}O	2831.24 (0.23)	42.772 (0.023)	42.742 (0.064)
^{18}Ne	3401.99 (0.6)	134.47 (0.15)	134.529 (0.36)
^{22}Mg	4124.55 (0.28)	418.39 (0.17)	418.255 (0.37)
^{26}Si	4842 (1.8)	1029.4 (2.2)	1028.81 (4.6)
^{30}S	5459.5 (3.9)	1966.9 (3)	1966.22 (16)
^{34}Ar	6062.98 (0.48)	3414.5 (1.5)	3414.16 (3.0)
^{38}Ca	6611.75 (0.41)	5327.2 (1.8)	5325.5 (3.7)
^{42}Ti	7000.5 (5.4)	7040 (30)	7042.84 (61)
^{26m}Al	4232.66 (0.12)	478.237 (0.08)	478.95 (0.18)
^{34}Cl	5491.64 (0.23)	1995.96 (0.47)	1997.73 (0.98)
^{38m}K	6044.4 (0.11)	3297.88 (0.34)	3300.05 (0.69)
^{42}Sc	6426.28 (0.3)	4472.24 (1.15)	4478.21 (2.4)
^{46}V	7052.49 (0.16)	7209.47 (0.9)	7213.21 (1.9)
^{50}Mn	7634.45 (0.07)	10746 (0.51)	10742.8 (1.12)
^{54}Co	8244.37 (0.28)	15766.6 (2.9)	15752.8 (6.1)
^{62}Ga	9181.07 (0.54)	26400.2 (8.3)	26362.4 (18.2)
^{66}As	9579 (26)	32125 (470)	32094 (1038)
^{70}Br	9970 (170)	38600 (3600)	38592 (7973)
^{74}Rb	10417.3 (4.4)	47300 (110)	47400 (246)

Table 5.14 – Comparison of the f value determined by the parametrization in the present work with the adopted values from the full calculations of Towner and Hardy [Har15].

value and the ones in the literature for the superallowed Fermi β-decays used to parametrized our statistical Fermi function, as a function of the Q-value. The dispersion is about 1.6 keV. For the decay of ^{22}Si, one does not require such a high-precision evaluation of the Q-value and thus this parametrization can be safely applied to convert between the f value and the Q-value.

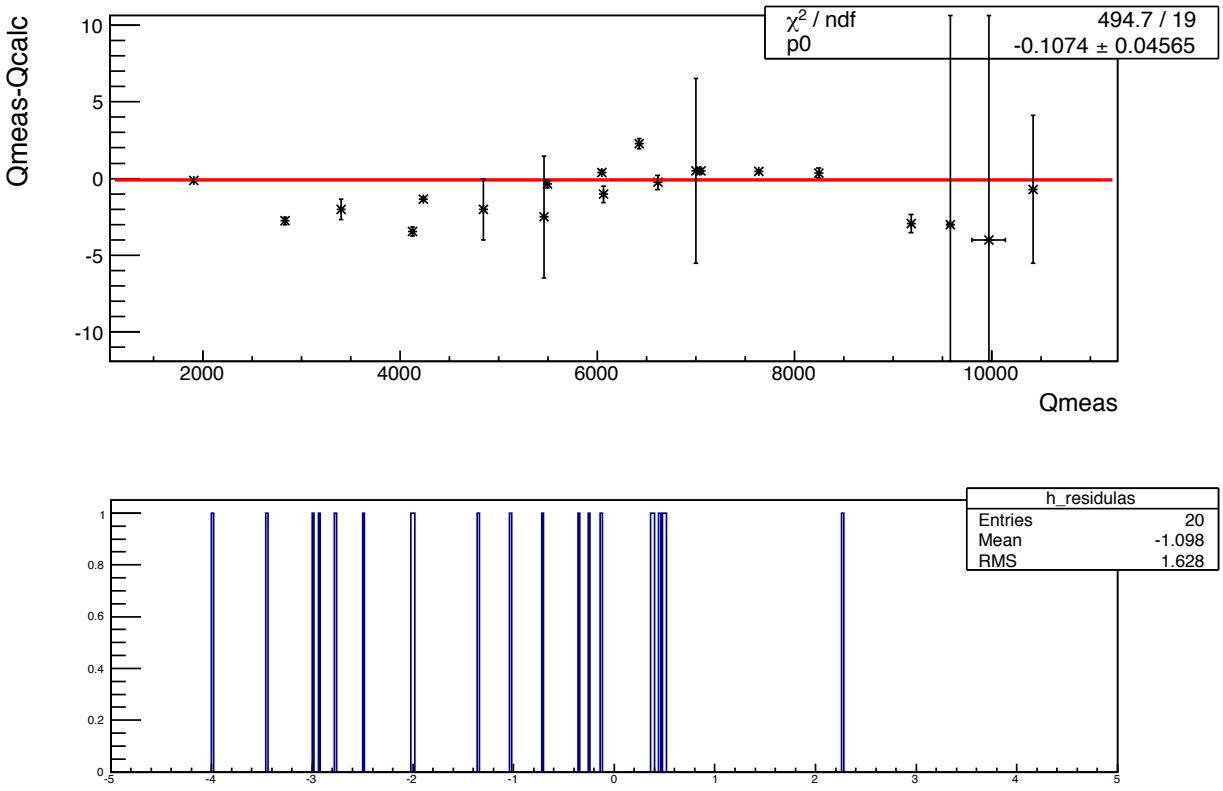

Figure 5.24 – Top: the difference between the Q-value that we determined with our parametrization and the very precise measurement for $T = 1$ nuclei is below 5 keV and doesn't diverge with high decay energies. Bottom: the dispersion is about 1.6 keV and will be included as a systematic uncertainty.

Predictive power for $T \geq 1$

The accuracy of using a superallowed ft value to derive the Q value and mass excess will now be tested using several cases where the mass excess is already known. This is also done to ensure that accuracy of the method with larger isospin as all of the Towner and Hardy nuclei are $T = 1$ cases. The Q-values for several $T = 2$ and $T = 3$ nuclei were calculated using the average $\mathcal{F}$t value from Ref. [Har15] and the experimental partial half-life measured in several β-delayed proton decay experiments. The mass excess of the parent, defined as the sum of the Q-value, the energy of the IAS and the mass excess of the daughter ground state (from [Wan12]), is compared to the value from the latest mass evaluation [Wan12] or determined using the IMME as described in Ref. [Dos07].

- **Mass excess of ^{20}Mg**

  In a recent experiment [Lun16] that focused on the β-delayed proton emission of the $T_Z = -2$ nucleus ^{20}Mg, new measurements of the half-life ($T_{1/2} = 91.4(12)$ ms) and β-decay branching ratios were performed. Some new β-delayed proton transitions were identified, and the IAS was measured, with an energy of 6298.4(5) keV [Gla15]. The absolute branching ratio for the β decay from ^{20}Mg ground state to its IAS in ^{20}Na was measured to be 2.2 (2)%, which is higher than the value of 3.3(4)% [Pie95] obtained in the previous measurement.

  With a partial half-life of $t = 2.18(11)$ s deduced from [Lun16], the corresponding f value is 370(34). Using the parametrization described above, we calculate a Q-value of 4042(27) keV. Adding the energy of the IAS, we determine the mass excess of ^{20}Mg to be $\Delta\, M = 17391(28)$ keV. This value can be compared with the adopted value from [Wan12], which is $\Delta\, M = 17559(27)$ keV. The difference is therefore about 150 keV. Using the previous partial half-life t= 2.75(34) s [Pie95], we find a mass excess of $\Delta\, M = 17680(42)$ keV which is in a similar agreement with this AME adopted value.

- **Mass excess of ^{24}Si**

  The half-life of ^{24}Si is $T_{1/2} = 140.5(15)$ ms, and its IAS in the daughter ^{24}Al was measured with an energy of 5953(8) keV [Ich09]. A measurement of the β branching ratio to the IAS yielded 9.9(9) %.

  The partial half-life for the decay to the IAS is thefore $t = 1.42$ (13) s, and the corresponding f value for this ($T = 2$,$T_Z = -2$) transition is 1085(99). The Q-value for this decay is calculated to be 4888 (37) keV and the mass excess of ^{24}Si is deduced to be $\Delta\, M = 10793$ (40) keV, which is in very good agreement with the adopted value in the most recent mass evaluation [Wan12], $\Delta\, M = 10744$ (19) keV. The difference in this case is only $\sim$ 50 keV.

- **Mass excess of ^{32}Ar**

  A precise measurement of the partial half-life of the superallowed Fermi β decay of ^{32}Ar to its IAS was performed in Ref. [Bha08] to quantify isospin symmetry breaking. Using the measured half-life ($T_{1/2}$ = 100.5 (3) ms) and branching ratio (22.71 (16) %) to the IAS, we calculate the corresponding f value for this transition which is f = 3475 (27). Using the parametrization of the f value, we determine a decay energy of Q = 6082 (4) keV for the transition from the ^{32}Ar ground state to its IAS in ^{32}Cl.

  Using the 5046-keV energy of the IAS and the mass excess of the daughter, we determine a mass excess of Δ M = −2206 (4) keV for the ^{32}Ar ground state, which is only 6 keV different from the adopted value in [Wan12], ΔM = −2200.4 (18) keV.

- **Mass excess of ^{36}Ca**

  The partial half-life of the decay of ^{36}Ca to its IAS was deduced in Ref. [Dos07]. With a half-life of $T_{1/2}$ = 100.1 (23) ms and a branching ratio of 37.9(8)% for this transition, the partial half-life is t = 0.264(1) s. The resulting Q-value is then 6718(21) keV.

  Adding the average energy of the IAS in ^{36}K (4281.9(8) keV) and the mass excess of the daughter, we determine the mass excess of ^{36}Ca ground state, ΔM = −6417 (21) keV which differs from the AME value, ΔM = −6450(40) keV [Wan12] by only 32 keV.

- **Mass excess of ^{40}Ti**

  With an average half-life of $T_{1/2}$ = 52.4(3) ms and a branching ratio of 25.2(6) % measured in Ref. [Dos07], the partial half-life for the superallowed Fermi β decay of ^{40}Ti to its IAS at 4367.7(60) keV is t = 0.208(5) s. For this (T = 2, T_Z = −2) transition, the corresponding value of f is therefore 7395(181).

  Using the present parametrization, a decay energy of Q = 7062 (15) keV is deduced, which leads to a mass excess of ΔM = −9094 (17) keV for the ^{40}Ti ground state. This value is in very good agreement with the value derived from the IMME [Dos07], ΔM = −9059.7 (78) keV but does not agree (within 1σ) with the evaluated mass in Ref. [Wan12], ΔM = −8850 (160) keV. The difference between AME12 and the value obtained in this work is $\sim$ 250 keV.

- **Mass excess of ^{44}Cr**

  From the measurements of the half-life ($T_{1/2}$ = 43.1 (17) ms) and the branching ratio (1.7(3) %) performed in Ref. [Dos07], we calculate an f value of 7395(181). Using the parametrization and the correction factor for Z = 22, we find a decay energy of Q = 4548 (56) keV. If we consider the energy of the IAS at 9298 (20) keV, this leads to a mass excess of ΔM = −10274 (189) keV for the ^{44}Cr ground state.

This value is not in agreement with both the most recent mass evaluation [Wan12], $\Delta M = -13640$ (300) keV, and the value deduced from the IMME [Dos07], $\Delta M = -13644$ (21) keV. However, in Ref.[Dos07], it was mentioned that the experimental branching ratio of 1.7(3) % deduced for this decay is in a clear disagreement with the theoretical value of 28 %. Using the corresponding theoretical half-life, we obtain a mass excess of $\Delta M = -7314$ (183) keV that disagrees even further.

Due to the lack of a precise experimental branching ratio, the mass excess of ^{44}Cr cannot be evaluated.

- **Mass excess of ^{48}Fe**

  Using the half-life ($T_{1/2} = 45.3(5)$ ms) and branching ratio (31.9(5) %) measured for the β decay of ^{48}Fe to its IAS [Dos07], we can calculate the partial half-life and the value of the corresponding statistical rate function, $f = 10826.5$ (1700) for this transition.

  Using the energy of the IAS, measured at 3036.7 (9) keV, and the mass excess of ^{48}Mn, we deduce a mass excess of $\Delta M = -18617$ (199) keV. This value is in good agreement with the value proposed by Dossat *et al.* [Dos07], $\Delta M = -18049$ (56) keV, using the IMME.

  However, it is also mentioned that the measured branching ratio is slightly lower than the theoretical prediction (45 %) for this Superallowed Fermi decay. Using the value from theory, we find a mass excess of about $\Delta M = -18113.3$ (170) keV, in better agreement with our calculation and within 1σ.

- **Mass excess of ^{52}Ni**

  Using the experimental half-life of $T_{1/2} = 40.8$ (2) ms and branching ratio of 48.3 (5) %, we determine that the f value for the superallowed Fermi β decay of ^{52}Ni to its IAS in ^{52}Co is $f = 18204$ (1884). This value leads to a Q-value of 8492 (77) keV for this branch.

  Adding the mass excess of the IAS in ^{52}Co as determined in [Dos07], we find a mass excess of $\Delta M = -22568$ (216) keV. The IMME for the ($A = 52$,$T = 2$) multiplet, composed by 4 analogue states, gives a mass excess in very good agreement, $\Delta M = -22639$ (33) keV [Dos07], as well as the most recent mass evaluation, $\Delta M = -22654$ (84) keV [Wan12]. The maximum difference in this case is only ~ 15 keV.

  In [Dos07], it was mentioned that a part of the β feeding of the IAS could have been undetected due to γ-ray de-excitation. The measured branching ratio may be compared to the theoretical one, about 66 %, which leads to a mass excess of $\Delta M = -22058$ (202) keV.

- **Mass excess of ^{56}Zn**

  For this high-Z nucleus, an IAS was identified in its daughter ^{56}Cu with an energy of 2929(31) keV [Dos07] above the proton threshold $S_p = 190$ (200) keV [Wan12]. The

measurements of the half-life ($T_{1/2}$ = 30.06 (17) ms) and branching ratio (20 (5) %) allow us to calculate the partial half-life of this decay, $t = 0.15(4)$ s.

This leads to a decay energy of Q = 7674(160) keV using the parametrization of the statistical rate function. Thus, we determine the mass excess of ^{56}Zn ground state to be ΔM = −27447 (326) keV.

For the decay to its IAS, a theoretical branching ratio is predicted to be 54%. Using this value, we find a lower mass excess of ΔM = −25887 (288) keV, which is in better agreement with the value obtained by from a Coulomb displacement calculation, ΔM = −25927 (65) keV.

- **Mass excess of ^{50}Ni, a $T_Z = -3$ nucleus**

  The decay of ^{50}Ni is the only $T_Z = -3$ nucleus measured with enough statistics to allow precise measurements of both the branching ratio and the excitation energy of the IAS. Its half-life is already well known, and the average value is $T_{1/2}$ = 17.2 (13) ms.

  In [Dos07], the IAS was identified with an energy of 4835 (47) keV and a β strength of 14 (5)% was measured. Using the $\mathcal{F}$t value corrected for the (T = 3,T_Z = −3) superallowed Fermi β decay and the parametrization described above, we find a decay energy of Q = 7346 (230) keV. The mass excess of the IAS in ^{50}Co was determined in Ref. [Dos07] at ΔM = −12750 (67) keV.

  Added to the Q-value determined in the present work, this yields a mass excess for ^{50}Ni ground state of ΔM = −5402 (230) keV, which is in about 4 standard deviations larger than the value determined with the IMME, ΔM = −4136 (25) keV.

- **Other $T = 3$ nuclei**

  The β-delayed proton emissions of ^{42}Cr and ^{46}Fe, two other $T_Z = -3$ nuclei, were studied [Gio01, Dos07] and the accuracy of our method was investigated for these proton-rich nuclei. Their respective half-lives are known with sufficient precision, but the low statistics and the β-summing present in the decay energy spectra did not allow the identification of the transition corresponding to the decays of the IAS. For these reasons, comparisons cannot be made between the mass excesses for these nuclei.

  For the decay from the ^{46}Fe to its IAS, a branching ratio of 7.9 (32) % was measured in Ref. [Gio01]. This value does not agree with the theoretical value which is about 20 % [Dos07]. Using the experimental value, the mass excess derived from the corresponding partial half-lives gives a mass excess of ΔM = −641 (248) keV, which is in good agreement with the mass deduced from the IMME applied in [Dos07], ΔM = −759 (96) keV. Using the theoritical value, we obtain a mass excess of 663 keV.

Mass excesses determined in the present work based on the measured branching ratio and half-lives for each transitions are summarized in Table 5.15. These values are also compared to the adopted values obtained by calculating the Coulomb displacement or the IMME when at least three analogue states are known.

Parent	Mass excess (keV) - adopted value -	Mass excess (keV) - this work -
^{20}Mg⋆	17559 (27)	17391 (28)
^{24}Si	10744 (19)	10793 (40)
^{32}Ar	-2200 (18)	-2206 (4)
^{36}Ca	-6450 (40)	-6417 (21)
^{40}Ti	-9095 (78)	-9094 (17)
^{44}Cr⋆	-13644 (21)	-10274 (189)
^{48}Fe⋆	-18049 (56)	-18617 (199)
^{52}Ni	-22639 (33)	-22568 (216)
^{56}Zn⋆	-25927 (65)	-27447 (326)
^{50}Ni⋆, $T_Z = -3$	-4136 (25)	-5402 (230)

Table 5.15 – Mass excesses of $T_Z = -2$ nuclei determined using our parametrization (see Equation 5.5) and the measured partial half-life are compared to the adopted values, from the AME2012 [Wan12] or [Dos07]. When the branching ratios have not been measured with enough confidence, the nucleus is labelled with a star. For comparison purpose, the mass excess of the $T_Z = -3$ nucleus ^{50}Ni is also presented.

Figure 5.25 presents the values calculated in this work as a function of the adopted mass excesses. When all the decay branches have been unambiguously identified, and the complete branching ratios have been measured with good accuracy (in red), the difference is lower than 100 keV over the whole energy range. In three cases, theoretical predictions of the branching ratio allow us to calculate a different mass excess, which is also compared in this figure. The trend of these values for a wide energy range shows a very good agreement with the adopted value but with bigger uncertainties. The case of ^{20}Mg is still debated since the two branching ratio measurements lead to mass measurements which vary with more than 5σ. The mass excess calculated for the $T_Z = -3$ nucleus ^{50}Ni is also plotted (black star in Figure 5.25) and agrees with the general trend of our calculations.

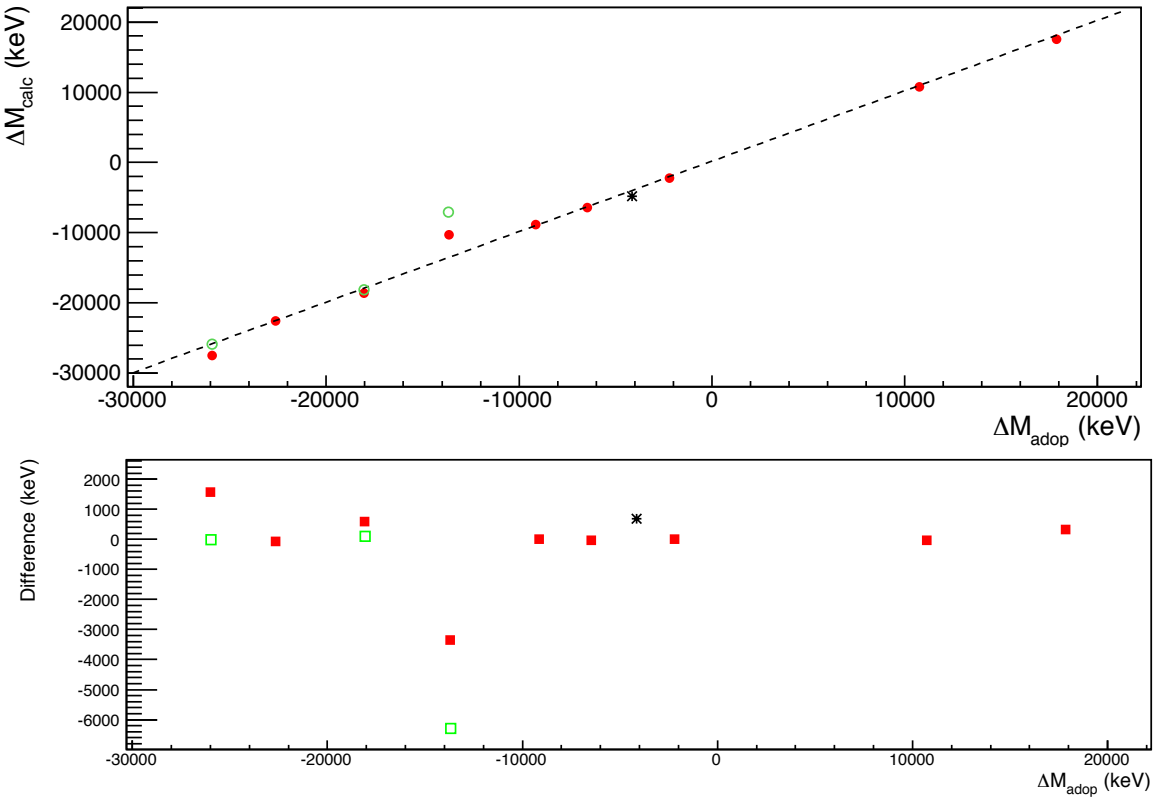

Figure 5.25 – Top: Mass excesses as determined using our parametrization, and based on the branching ratio and half-life measurements (in red) are in good agreement with adopted values. Mass excesses calculated with the theoretical branching ratios (in green) are displayed when they differ from the measured one. Bottom: Differences between the adopted and the calculated mass excesses. The mass excess calculated for ^{50}Ni (black star) also seems in good agreement with the adopted mass excess. The only nucleus with a significant difference between the calculated and the adopted masses is ^{44}Cr.

5.10.2 Mass excess of ^{22}Si ground state

In this work, the β-decay half-life of the $T_z = -3$ nucleus ^{22}Si and the branching ratio to its IAS in ^{22}Al were measured to be $T_{1/2} = 30.38\ (45)$ ms and $BR = 2.05\ (44)$ %, respectively. These measurements allow us to calculate the partial half-life for this superallowed Fermi transition, $t = 1.48\ (32)$ s. As this nucleus is part of the $T = 3$ multiplet, we expect the f value to be

$$f = \frac{1024.2}{1.48} = 692\ (150) \tag{5.8}$$

Using the approximation defined by Equation 5.7 for the Si isotopes ($Z = 14$), and after applying the correction factor obtained from the fit of the measured statistical function, we

obtain a Q-value for the decay of the ground state to the IAS of $Q_\beta = 4580\ (91)$ keV.

In Section 5.1, the IMME applied to the multiplet ($A = 22$,$T = 5/2$) allowed us to determine the mass excess of ^{22}Al that is 17932(99) keV. With this result, we obtain the mass excess of ^{22}Si ground state

$$\Delta M = 9040\,(54) + 4520\,(78) + 17932\,(99) = 31492\,(137)\ \text{keV}. \tag{5.9}$$

This value is about 2 MeV below the estimation from AME2012 which predicted a mass excess of 33340(500) keV. Using our result, new values for the Q_β-value, S_p and S_{2p} energies are presented in Table 5.16. The use of the mass excesses of ^{22}Al as provided by the AME03 and AME12 leads to an identical conclusion about the particle threshold, although the uncertainties are significantly larger.

	Present work
$Q(\beta^+)$	12350 (95) keV
S_p	2787 (429) keV
S_{2p}	645 (140) keV

Table 5.16 – Updated S_p, S_{2p} and Q_β-value determined with the mass measurement performed in the present work. One has to keep in mind that the mass excesses of the daughters ^{21,22}Al are still unknown, and so this value is given using the AME12 estimation.

As expected from many models, we deduced a S_p energy that is larger than 2 MeV and therefore single-proton radioactivity to the unbound ^{21}Al nucleus is forbidden. The decay process of ^{22}Si is dominated by the large β^+-decay Q-value. The S_{2p} obtained in this work is positive, and larger than expected. With a value of 645(140) keV, this threshold implies a bound ground state with respect to two-proton emission. In Figure 5.26, we compare this measurement with the previous predictions from Table 5.1 which were all consistent with a two-proton radioactive nucleus.

5.11 Conclusion

The study of the β-delayed proton emission of the even-even nucleus ^{22}Si was performed by measuring the energy of the proton groups emitted by proton-unbound excited states in ^{22}Al. Two γ-ray transitions arise from the de-excitation of the first two excited states in the daughter ^{21}Mg, and have allowed for the identification and the measurement of the branching ratio of

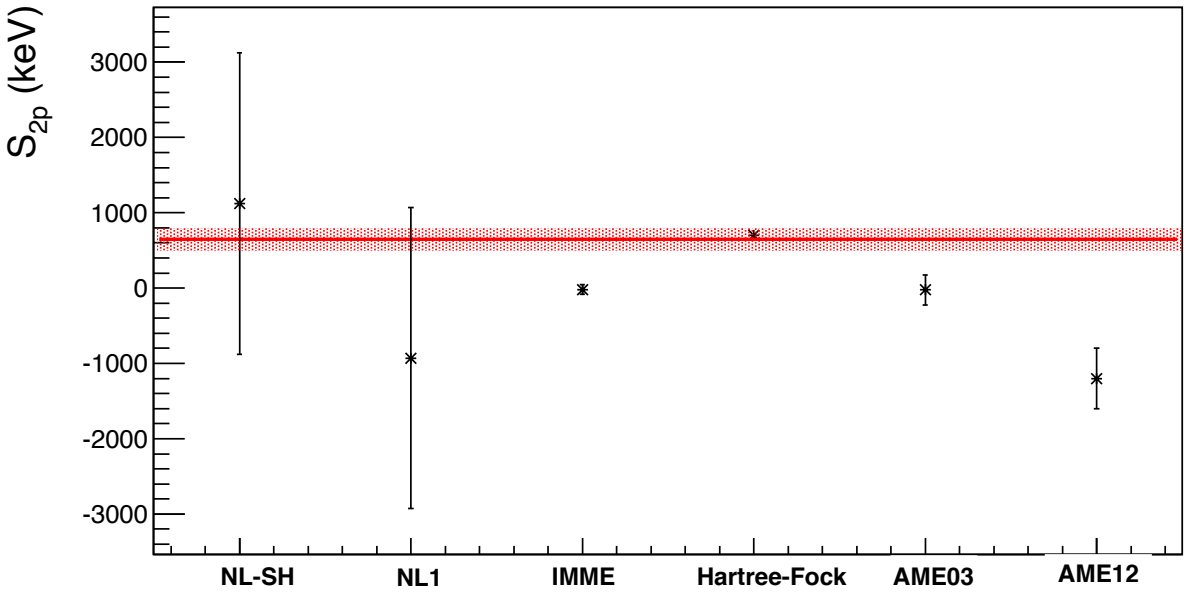

Figure 5.26 – Comparison between the S_{2p} value determined in this work and the previous predictions using different models. In red, the two-proton separation threshold as determined in the present work (645 (140) keV).

more than 13 new states.

The ungated spectrum confirmed the excitation energies, and we observed a proton group at 5596(84) keV which was identified as the β-delayed two-proton emission of the IAS to the ground state of ^{20}Na. The branching ratio of this transition has been measured and is lower than expected from shell-model calculations. The γ rays corresponding to the first excited state in ^{20}Na at 596 keV were also observed, but we were unable to draw a conclusion on the decay of the IAS to this state. The β-decay branching ratio to the IAS is 1.54 (38), which is several times lower than the USDBpn predictions. One has to keep in mind that this theoretical value is very sensitive to the mass excess defined as an input: a decrease by 2 MeV of the β-decay Q-value induces a factor-2 decrease of the branching ratio to the IAS.

A precise measurement of the half-life has been performed using γ-ray and proton gates, and we propose $T_{1/2} = 30.38$ (45) ms as the new half-life measurement, which is a factor of ten times more precise than the presently adopted value. Using this half-life and the branching ratio measured in the current work, we calculated the expected Q-value in the case of a superallowed Fermi decay to the $T = 3$ IAS in ^{22}Al. Added to the energy of the IAS and the mass excess of the daughter, we provide the first indirect mass measurement of ^{22}Si. With a mass excess of

31604 (155) keV and a two-proton separation threshold of S_{2p} = 645 (140) keV, we conclude that the ground state of ^{22}Si is bound with respect to the two-proton emission.

Chapter 6

Conclusion and Future work

The knowledge of the masses of neutron-deficient nuclei is one of the keys to understand the behaviour of weakly bound nuclei near or at the proton drip-line. β-delayed one-proton emission favored by an increasing Q_β-value has been used to perform detailed the spectroscopy of proton-unbound excited states in the daughter nuclei. Depending on the position of the particle separation energies with respect to the Q-value of the β-decay, several exotic decay paths such as β2p and β3p can also occur. The latter was predicted to occur in ^{23}Si, but has thus far never been observed.

These rare decay processes result in a large branching ratio when decays occur between Isobaric Analogue States. The mass excesses of these IAS are linked by the Isobaric Mass Multiplet Equation. This relation treats the Coulomb displacement as a perturbation and allows the prediction of one state if at least three other members of the same multiplet have been previously measured.

When the mass excess of the ground state allows it, particle decay from the ground state can also occur. At the proton drip-line, the more exotic two-proton ground state radioactivity was observed when the S_{2p} is negative, but when single proton emission is forbidden. The measurement of angular correlations and the energy sharing between the two protons can be used to identify the orbital in the parent nucleus. This decay was predicted in several light proton-rich nuclei and ^{22}Si is one of the lightest candidates to decay via two-proton radioactivity. However, discrepancies in the models predicting its binding energy did not yet allow to assess whether or not it is a two-proton emitter.

At the National Superconducting Cyclotron Laboratory, a primary fragmentation beam of ^{36}Ar was used to produce beams of the neutron-deficient nuclei ^{20}Mg, ^{23}Si and ^{22}Si. Purification of the beam and reduction of the beam intensity were required to avoid contamination and false correlations from other β-delayed charged particle emitters. This was achieved using the A1900 Fragment Separator and the Radio Frequency Fragment Separator. The cocktail beam

was implanted in the Beta Counting System, made of an arrangement of 3 Double-Sided Si Strip detectors to provide time and energy signals. An analysis program allowed the correlated the implant-and-decay events based on the energies, times sequences and spatial coordinates. An array of 16 HPGe surrounding the BCS was used to detect the γ rays emitted in coincidence with the decays of interest.

6.1 Conclusion

The presence of ^{20}Mg in the cocktail beam was used to test the analysis program and the calibration of the detectors by studying its β-delayed proton decay. Three γ rays arising from the de-excitation of the βp daughter were observed. The proton spectra in coincidence with these transitions allowed us to deduce the excitation energies of the levels above the one-proton separation threshold in the daughter ^{20}Na. The level scheme built by measuring the decay energy was in good agreement with previous measurements. In particular, the IAS in ^{20}Na was measured at 6519 (19) keV, that is in excellent agreement with the value 6522 (16) keV obtained in a previous experiment[Pie95]. We also performed the measurement of the relative β-decay branching ratios. The efficiency of the central DSSD2 was particularly low, due to an implantation depth very near to the surface. However, for most of the branches, results after efficiency correction are in good agreement the previous measurements. Uncertainties on low branching ratios were mainly due to a lack of statistics in the γ-gated spectra. The decay-and-implant correlation process provided the decay time spectrum. Several proton and γ-ray gates were applied to measure the half-life of ^{20}Mg. The fit of these data as well as the overall statistics, was particularly difficult. The contributions of the long half-life daughters as well as wrong correlations were investigated. We propose a half-life of 88.8(17) ms, as the average of the 1675-keV proton-gated and the γ-gated spectra. This value is in agreement with the previous adopted value 90.8 (24) ms [Wan12], and the most recent measurement 91.4 (10) ms [Lun16].

The β-delayed spectroscopy of the $T_Z = -5/2$ nucleus ^{23}Si was performed using the same method. Three γ rays, corresponding to the de-excitation of the three first excited states in the βp daughter ^{21}Mg were observed. One γ-ray transition at 332 keV, corresponding to the first excited state in ^{21}Na, confirmed the β2p decay channel. The energy of the IAS was deduced from the 332-keV γ-gated spectrum. A proton group in the ungated spectrum corresponding to the two-proton emission of the IAS to the ground state of ^{21}Na was also measured. We measured an excitation energy of 11710 (43) keV that is in good agreement with the previous measurement, 11.78 MeV[Bla97]. More than 25 new proton-unbound levels were measured in ^{23}Al.

The energy of the IAS was added to the set of analogue states in the ($A = 23$,$T = -5/2$) multiplet to determine the mass excess of the ^{23}Si ground state. In this work, we deduced a

value of 23.24 (7) MeV, a few hundred keV less than the previous measurement[Bla97] and the adopted value in the AME2012[Wan12]. The corresponding particle emission thresholds are $S_p = 2195$ (114) keV and $S_{2p} = 2218$ (72) keV. Based on this new measurement, the β3p decay is allowed by its high Q-value $Q_{\beta 3p} \approx 7.4$ MeV. This decay may have been observed in the present experiment because of the presence of a proton group in the 1633-keV γ-gated spectrum.

The half-life of ^{23}Si was measured by applying γ-ray and proton gates on the decay time spectrum. We propose a half-life of 42.67 (23) ms, a result that is twice more precise than the previous measurement of 42.3 (4) ms[Bla97].

The level scheme of ^{22}Al was built by studying the β-delayed proton decay of the lighest $T_z = -3$ nucleus, ^{22}Si. Two γ rays were observed, corresponding to the de-excitation of the first two excited states in the βp daughter ^{21}Mg. In addition, the ungated proton spectrum allowed us to determine the energy of 13 proton-unbound states in ^{22}Al and confirmed the two levels observed in the previous measurement of Blank *et al.*[Bla96].

The presence of γ rays at 596 keV, that corresponds to the de-excitation of the first excited state in ^{20}Na, supports the identification of the β2p decay channel. Based on the similarities with the other proton-rich nuclei, we measured the energy of the two-proton emission from the IAS to the ground state at 5596 keV, which corresponds to an IAS energy of 9040 (54)(100) keV. In this work, the measurements of the β-decay branching ratios were also performed. In particular, the branching ratio of the β decay from ^{22}Si to the IAS in ^{22}Al was measured to be $BR_{IAS} = 2.06(56)\%$. The half-life of ^{22}Al was also measured at 30.38 (45) ms, using both proton ang γ-ray gates. This value is in good agreement with the previous measurement, 29 (2) ms[Bla96].

We proposed a new method based on the β-decay theory to determine the mass excess of the 0^+ ground state of ^{22}Si, for which the ft value is predicted to be a constant. Following the work of Towner and Hardy [Tow15], the statistical rate function f was parametrized using the precise measurements of superallowed Fermi β decays of $T = 1$ nuclei. Since the statistical rate function depends on the Q-value, we were able to test these estimations on more exotic nuclei with a relatively good accuracy. This method allowed us to calculate the Q-value of the superallowed Fermi decay from the ^{22}Si ground state to its IAS. The mass excess was determined as the sum of energy of the IAS (9040 (54)(100) keV), the mass excess of the daughter as determined from the IMME in this work (17932 (99) KeV), and the Q-value (4520 (85) keV).

We propose the first indirect mass measurement of the ^{22}Si ground state, $\Delta M = 31492$ (137) keV. In agreement with all the predictions, we conclude that ^{22}Si is bound with respect to the one-proton decay. However, contrary to most of the recent predictions, we deduce a S_{2p} value of 645 (140) keV which prohibits two-proton radioactivity from the ground state.

6.2 Future Work

6.2.1 New measurement of ^{20}Mg decay

In 2015, an experiment focusing on the β-delayed charged particle decays of ^{21}Mg and ^{20}Mg was performed at the ISOLDE Decay Station [Lun16]. A new measurement of the energy and the branching ratio of the $T = 2$ IAS in ^{20}Na was performed. With an energy of 6496 (3) keV, this measurement is in good agreement with this work 6519 (19) keV but about six times more precise. The energy of the proton transtions were measured using a gas detector which was not sensitive to the β particles. In addition to the absence of β-summing, the discrimination between proton and α particles hitting the Si detector allowed the identification of excited states in ^{20}Na without contamination from the decay of the ^{20}Na ground state. A new half-life was also provided by measuring the protons and yields to $T_{1/2} = 88.8$ (17) ms, which is in agreement with the previous measurements, but suffers of uncertainties due to the normalization of the long half-life components.

Therefore, to provide a confident half-life measurement from the present work, an estimation of the false correlations would be necessary. A full simulation of the setup, taking into account the implantation pile-up phenomenon and the $\beta\alpha$ decay of ^{20}Na would be needed to constrain the fit parameters of the events with a long decay time.

Also, in Section 5.10.1, we calculated the mass excess of ^{20}Mg ground state using the partial half-life measured in [Lun16]. We noticed a difference of about 150 keV, more than 5σ, between the adopted value of the mass excess of ^{20}Mg and the one calculated using the parametrization described above. The value of the Q-value between the ground state and its IAS is highly dependant of the branching ratio of this superallowed Fermi transition. One could therefore detemined a theoritical branching by using the reverse logic: if we consider that the half-life measured in [Lun16] is correct, the branching ratio should be $\approx$2.8%. For future experiments of β-decay of proton-rich nuclei, this method could be used to expose irregularities in the measurement of the partial half-life, and determined if some β-delayed charged particle branches from the IAS were missed.

6.2.2 Observing the β3p channel in ^{23}Si

In the study of the β-delayed charged particle decays of ^{23}Si, we observed the emission of γ rays at 1633 keV. That transition arises from the de-excitation of the first excited state in ^{20}Ne. Because the secondary beam was contaminated by ^{20}Na, we identified that this level can be populated by two different decay paths:

- $^{23}\mathrm{Si} \xrightarrow{\beta} {}^{23}\mathrm{Al}^{*} \xrightarrow{3p} {}^{20}\mathrm{Ne}^{*}$ or

- $^{20}\mathrm{Na} \xrightarrow{\beta} {}^{20}\mathrm{Ne}^{*}$

As we expressed above, the Q-value corresponding to the $\beta 3p$ decay channel is quite high. The total decay energy from the IAS would be around $\approx$ 4.3 MeV, which makes it impossible to observe in our DSSD because of the high density of βp transitions. Up to now, only three $\beta 3p$ emitter have been observed(^{31}Ar[Kol14], ^{45}Fe[Mie07] and ^{43}Cr[Pom11a, Aud12]) with various branching ratios.

The observation of such a decay proces is very challenging because its weak branching ratio never exceeds a few percent. Thus, a detector with a high luminosity and a high detection efficiency is required. The recent development in Time Projection Chamber (TPC) have enlightened the possibility to observe this rare decay path: the parent is implanted in the gas volume which acts as a thick Si detector. After a certain decay time, the three protons are emitted and observed separately. The reconstruction of the full kinematics allows the determination of the decay energy. Because this detector is transparent to the β-particles, the use of the TPC in studying the β-delayed proton decay is even more appropriate. The lack of β-summing allows the measurement of transitions with low branching ratios, and with a better precision on the decay energy. High-efficiency γ-ray detectors can also be coupled to TPC's in order to observing the de-excitation of low-energy bound states, and to identify the daughters.

6.2.3 The spectroscopy of ^{22}Al

Although the study of the β-delayed charged particle decay of ^{22}Si was performed in this work with a good accuracy, the energy resolution was limited because of β-summing. In the ungated spectrum, the broad structure between 3.2 and 8 MeV was tentitavely fitted with 8 proton groups. The uncertainties on the branching ratio and the energy of the corresponding transitions are mainly due to the low resolution, which barely allows us to resolve these groups. As described above, the β particles are not detected in the TPC volume and would guarantee a better resolution in this high-density region. Such a detection setup would also enable the identification of the decay paths in the case of two proton emission from the IAS, providing informations about the unbound states populated in ^{21}Mg.

The mass excess of the ^{22}Si ground state was determined with respect to the mass excess of its IAS in ^{22}Al. As discussed in Section 5.1, the direct mass measurement of the ground state of ^{22}Al has not yet been performed and the current uncertainties on the estimation is 400 keV[Wan12]. In this work, an updated value of the IMME prediction was determined by the mean of the IAS in 22Mg whom the spin and parity remain unknown and so another way to provide a direct measurement of the mass of ^{22}Al has been investigated. In a transfer experiment, the mass of the neutron-rich ^{11}Li was performed by measuring the Q-value of the ^{11}Li(^{1}H,^{3}H)^{9}Li reaction in an active target[Rog09]. The uncertainties on the mass obtained

with this method is about 20 keV, which is 5 times better than the IMME prediction used in this work. In the same way, the mass measurement of ^{22}Al could be performed by measuring the Q-value of the reaction ^{21}Mg(^{4}He,t)^{22}Al using the novel active target ACTAR TPC developped at GANIL, where a ^{21}Mg beam with suitable intensity and energy for this kind of experiment are planned to be delivered in the near future following the upgrade to SPIRAL1.

Bibliography

[Ach06] N. L. Achouri, F. de Oliveira Santos, B. Lewitowicz, M .and Blank, J. Äystö, G. Canchel, S. Czajkowski, P. Dendooven, A. Emsallem, J. Giovinazzo, N. Guillet, A. Jokinen, A. M. Laird, C. Longour, K. Peräjärvi, N. Smirnova, M. Stanoiu and J. C. Thomas. The β-decay of ^{22}Al. *The European Physical Journal A - Hadrons and Nuclei*, **27 3**: (2006) 287–300. ISSN 1434-601X. doi:10.1140/epja/i2005-10274-0.
URL `http://dx.doi.org/10.1140/epja/i2005-10274-0`

[AS87] F. Ajzenberg-Selove. Energy levels of light nuclei $A = 1820$. *Nuclear Physics A*, **475 1**: (1987) 1 – 198. ISSN 0375-9474. doi:http://dx.doi.org/10.1016/0375-9474(87)90205-3.
URL `http://www.sciencedirect.com/science/article/pii/0375947487902053`

[Asc11] P. Ascher, L. Audirac, N. Adimi, B. Blank, C. Borcea, B. A. Brown, I. Companis, F. Delalee, C. E. Demonchy, F. de Oliveira Santos, J. Giovinazzo, S. Grévy, L. V. Grigorenko, T. Kurtukian-Nieto, S. Leblanc, J.-L. Pedroza, L. Perrot, J. Pibernat, L. Serani, P. C. Srivastava and J.-C. Thomas. Direct observation of two protons in the decay of ^{54}Zn. *Phys. Rev. Lett.*, **107**: (2011) 102502. doi:10.1103/PhysRevLett.107.102502.
URL `http://link.aps.org/doi/10.1103/PhysRevLett.107.102502`

[Aud03] G. Audi, O. Bersillon, J. Blachot and a. H. Wapstra. The NUBASE evaluation of nuclear and decay properties. *Nuclear Physics A*, **729**: (2003) 3–128. ISSN 03759474. doi:10.1016/j.nuclphysa.2003.11.001.

[Aud12] L. Audirac, P. Ascher, B. Blank, C. Borcea, B. A. Brown, G. Canchel, C. E. Demonchy, F. de Oliveira Santos, C. Dossat, J. Giovinazzo, S. Grévy, L. Hay, J. Huikari, S. Leblanc, I. Matea, J. L. Pedroza, L. Perrot, J. Pibernat, L. Serani, C. Stodel and J. C. Thomas. Direct and β-delayed multi-proton emission from atomic nuclei with a time projection chamber: the cases of ^{43}Cr, ^{45}Fe, and ^{51}Ni. *The European Physical Journal A*, **48 12**: (2012) 1–12. ISSN 1434-601X. doi:10.1140/epja/i2012-12179-1.
URL `http://dx.doi.org/10.1140/epja/i2012-12179-1`

[Baz02] D. Bazin, O. Tarasov, M. Lewitowicz and O. Sorlin. The program LISE: a simulation of fragment separators. *Nuclear Instruments and Methods in Physics Research Section A: Accelerators, Spectrometers, Detectors and Associated Equipment*, **482 12**: (2002) 307 – 327. ISSN 0168-9002. doi:http://dx.doi.org/10.1016/S0168-9002(01)01504-2.
URL `http://www.sciencedirect.com/science/article/pii/S0168900201015042`

[Baz09] D. Bazin, V. Andreev, A. Becerril, M. Dolans, P. Mantica, J. Ottarson, H. Schatz, J. Stoker and J. Vincent. Radio Frequency Fragment Separator at NSCL. *Nuclear Instruments and Methods in Physics Research Section A: Accelerators, Spectrometers, Detectors and Associated Equipment*, **606 3**: (2009) 314 – 319. ISSN 0168-9002. doi:http://dx.doi.org/10.1016/j.nima.2009.05.100.
URL `http://www.sciencedirect.com/science/article/pii/S0168900209011425`

[Bha08] M. Bhattacharya, D. Melconian, A. Komives, S. Triambak, A. García, E. G. Adelberger, B. A. Brown, M. W. Cooper, T. Glasmacher, V. Guimaraes, P. F. Mantica, A. M. Oros-Peusquens, J. I. Prisciandaro, M. Steiner, H. E. Swanson, S. L. Tabor and M. Wiedeking. *ft* value of the $0^+ \rightarrow 0^+$ β^+ decay of ^{32}Ar: A measurement of isospin symmetry breaking in a superallowed decay. *Phys. Rev. C*, **77**: (2008) 065503. doi:10.1103/PhysRevC.77.065503.
URL `http://link.aps.org/doi/10.1103/PhysRevC.77.065503`

[Bla96] B. Blank, S. Andriamonje, F. Boué, S. Czajkowski, R. Del Moral, J. P. Dufour, A. Fleury, P. Pourre, M. S. Pravikoff, K.-H. Schmidt, E. Hanelt and N. A. Orr. First spectroscopic study of ^{22}Si. *Phys. Rev. C*, **54**: (1996) 572–575. doi:10.1103/PhysRevC.54.572.
URL `http://link.aps.org/doi/10.1103/PhysRevC.54.572`

[Bla97] B. Blank, F. Boué, S. Andriamonje, S. Czajkowski, R. Del Moral, J. P. Dufour, A. Fleury, P. Pourre, M. S. Pravikoff, E. Hanelt, N. A. Orr and K. H. Schmidt. Spectroscopic studies of the βp and β2p decay of ^{23}Si. *Zeitschrift für Physik A Hadrons and Nuclei*, **357 3**: (1997) 247–254. ISSN 1431-5831. doi:10.1007/s002180050241.
URL `http://dx.doi.org/10.1007/s002180050241`

[Bla05] B. Blank, A. Bey, G. Canchel, C. Dossat, A. Fleury, J. Giovinazzo, I. Matea, N. Adimi, F. De Oliveira, I. Stefan, G. Georgiev, S. Grévy, J. C. Thomas, C. Borcea, D. Cortina, M. Caamano, M. Stanoiu, F. Aksouh, B. A. Brown, F. C. Barker and W. A. Richter. First observation of ^{54}Zn and its decay by two-proton emission. *Phys. Rev. Lett.*, **94**: (2005) 232501. doi:10.1103/PhysRevLett.94.232501.
URL `http://link.aps.org/doi/10.1103/PhysRevLett.94.232501`

[Bla08] B. Blank and M. Borge. Nuclear structure at the proton drip line: Advances with nuclear decay studies. *Progress in Particle and Nuclear Physics*, **60 2**: (2008) 403 – 483. ISSN 0146-6410. doi:http://dx.doi.org/10.1016/j.ppnp.2007.12.001.
URL `http://www.sciencedirect.com/science/article/pii/S0146641007000956`

[Bro] B. A. Brown. Private communication.

[Bru97] R. Brun and F. Rademakers. Root - an object oriented data analysis framework. *Nuclear Instruments and Methods in Physics Research Section A: Accelerators, Spectrometers, Detectors and Associated Equipment*, **389**: (1997) 81 – 86. ISSN 0168-9002.
URL `http://root.cern.ch/`

[Buc05] L. Buchmann, M. Comyn, J. Thomson, M. Trinczek, C. Jewett, J. D'Auria, S. Bishop, L. Buchmann, A. Chen, S. Engel, D. Gigliotti, U. Greife, D. Hunter, A. Hussein, D. Hutcheon, J. Jos, A. Laird, M. Lamey, R. Lewis, A. Olin, D. Ottewel, P. Parker, M. Pavan, J. Pearson, J. Rogers, C. Ruiz and C. Wrede. Direct measurement of the ^{21}Na(p, γ)^{22}Mg reaction: resonance strengths and γ-γ analysis. *Nuclear Physics A*, **758**: (2005) 729 – 732. ISSN 0375-9474. doi: http://dx.doi.org/10.1016/j.nuclphysa.2005.05.131.
URL `http://www.sciencedirect.com/science/article/pii/S0375947405008250`

[Cli89] E. Clifford, E. Hagberg, J. Hardy, H. Schmeing, R. Azuma, H. Evans, V. Koslowsky, U. Schrewe, K. Sharma and I. Towner. The decay of ^{20}Na: Measurements of isospin mixing and the weak vector coupling constant as well as other new decay data. *Nuclear Physics A*, **493 2**: (1989) 293 – 322. ISSN 0375-9474. doi: http://dx.doi.org/10.1016/0375-9474(89)90399-0.
URL `http://www.sciencedirect.com/science/article/pii/0375947489903990`

[Col98] B. J. Cole. Proton and two-proton drip lines in the sd shell. *Phys. Rev. C*, **58**: (1998) 2831–2839. doi:10.1103/PhysRevC.58.2831.
URL `http://link.aps.org/doi/10.1103/PhysRevC.58.2831`

[Cza97] S. Czajkowski, S. Andriamonje, B. Blank, F. Bou, R. D. Moral, J. Dufour, A. Fleury, E. Hanelt, N. Orr, P. Pourre, M. Pravikoff and K.-H. Schmidt. βp, β2p and $\beta\alpha$ spectroscopy of ^{22,23,24}Si and ^{22}Al. *Nuclear Physics A*, **616 1**: (1997) 278 – 285. ISSN 0375-9474. doi:http://dx.doi.org/10.1016/S0375-9474(97)00098-5.
URL `http://www.sciencedirect.com/science/article/pii/S0375947497000985`

[Dét91] C. Détraz. The branching ratio ofβ-delayed two-proton emission. *Zeitschrift für Physik A Hadrons and Nuclei*, **340 3**: (1991) 227–230. ISSN 0939-7922. doi:

10.1007/BF01294668.
URL http://dx.doi.org/10.1007/BF01294668

[Dig08] C. A. Diget, P. Adrich, D. Bazin, M. D. Bowen, B. a. Brown, C. M. Campbell, J. M. Cook, a. Gade, T. Glasmacher, K. Hosier, S. McDaniel, D. McGlinchery, a. Obertelli, L. a. Riley, K. Siwek, J. R. Terry, J. a. Tostevin and D. Weisshaar. Structure of excited states in ^{21}Mg studied in one-neutron knockout. *Physical Review C - Nuclear Physics*, **77**: (2008) 1–7. ISSN 05562813. doi:10.1103/PhysRevC.77.064309.

[Dos05] C. Dossat, A. Bey, B. Blank, G. Canchel, A. Fleury, J. Giovinazzo, I. Matea, F. d. O. Santos, G. Georgiev, S. Grévy, I. Stefan, J. C. Thomas, N. Adimi, C. Borcea, D. C. Gil, M. Caamano, M. Stanoiu, F. Aksouh, B. A. Brown and L. V. Grigorenko. Two-proton radioactivity studies with ^{45}Fe and ^{48}Ni. *Phys. Rev. C*, **72**: (2005) 054315. doi:10.1103/PhysRevC.72.054315.
URL http://link.aps.org/doi/10.1103/PhysRevC.72.054315

[Dos07] C. Dossat, N. Adimi, F. Aksouh, F. Becker, A. Bey, B. Blank, C. Borcea, R. Borcea, A. Boston, M. Caamano, G. Canchel, M. Chartier, D. Cortina, S. Czajkowski, G. de France, F. de Oliveira Santos, A. Fleury, G. Georgiev, J. Giovinazzo, S. Grvy, R. Grzywacz, M. Hellstrm, M. Honma, Z. Janas, D. Karamanis, J. Kurcewicz, M. Lewitowicz, M. L. Jimnez, C. Mazzocchi, I. Matea, V. Maslov, P. Mayet, C. Moore, M. Pftzner, M. Pravikoff, M. Stanoiu, I. Stefan and J. Thomas. The decay of proton-rich nuclei in the mass $a = 36 - 56$ region. *Nuclear Physics A*, **792 1**: (2007) 18 – 86. ISSN 0375-9474. doi:http://dx.doi.org/10.1016/j.nuclphysa.2007.05.004.
URL http://www.sciencedirect.com/science/article/pii/S0375947407005507

[Fae84] T. Faestermann, A. Gillitzer, K. Hartel, P. Kienle and E. Nolte. Evidence for proton radioactivity of ^{113}Cs and ^{109}I. *Physics Letters B*, **137 1**: (1984) 23 – 26. ISSN 0370-2693. doi:http://dx.doi.org/10.1016/0370-2693(84)91098-0.
URL http://www.sciencedirect.com/science/article/pii/0370269384910980

[Fer34] E. Fermi. Versuch einer theorie der β-strahlen. i. *Zeitschrift für Physik*, **88 3**: (1934) 161–177. ISSN 0044-3328. doi:10.1007/BF01351864.
URL http://dx.doi.org/10.1007/BF01351864

[Fre77] S. Freedman, R. Cousins, C. Gagliardi, G. Garvey and J. Greenhalgh. $\beta\alpha$ correlation in the decay of ^{20}Na. *Physics Letters B*, **67 2**: (1977) 165 – 168. ISSN 0370-2693. doi:http://dx.doi.org/10.1016/0370-2693(77)90093-4.
URL http://www.sciencedirect.com/science/article/pii/0370269377900934

[Gio01] J. Giovinazzo, B. Blank, C. Borcea, M. Chartier, S. Czajkowski, G. de France, R. Grzywacz, Z. Janas, M. Lewitowicz, F. de Oliveira Santos, M. Pfützner,

M. Pravikoff and J. Thomas. Decay of proton-rich nuclei between 39ti and 49ni. *The European Physical Journal A - Hadrons and Nuclei*, **10 1**: (2001) 73–84. ISSN 1434-601X. doi:10.1007/s100500170146.
URL http://dx.doi.org/10.1007/s100500170146

[Gio07] J. Giovinazzo, B. Blank, C. Borcea, G. Canchel, J.-C. Dalouzy, C. E. Demonchy, F. de Oliveira Santos, C. Dossat, S. Grévy, L. Hay, J. Huikari, S. Leblanc, I. Matea, J.-L. Pedroza, L. Perrot, J. Pibernat, L. Serani, C. Stodel and J.-C. Thomas. First direct observation of two protons in the decay of ^{45}Fe with a time-projection chamber. *Phys. Rev. Lett.*, **99**: (2007) 102501. doi:10.1103/PhysRevLett.99.102501.
URL http://link.aps.org/doi/10.1103/PhysRevLett.99.102501

[Gla15] B. E. Glassman, D. Pérez-Loureiro, C. Wrede, J. Allen, D. W. Bardayan, M. B. Bennett, B. A. Brown, K. A. Chipps, M. Febbraro, C. Fry, M. R. Hall, O. Hall, S. N. Liddick, P. O'Malley, W. Ong, S. D. Pain, S. B. Schwartz, P. Shidling, H. Sims, P. Thompson and H. Zhang. Revalidation of the isobaric multiplet mass equation for the <math> <mrow> <mi>A</mi> <mo>=</mo> <mn>20</mn> </mrow> </math> quintet. *Physical Review C*, **92 4**: (2015) 042501. ISSN 0556-2813. doi:10.1103/PhysRevC.92.042501.
URL http://link.aps.org/doi/10.1103/PhysRevC.92.042501

[Goi16] T. Goigoux, P. Ascher, B. Blank, M. Gerbaux, J. Giovinazzo, S. Grévy, T. Kurtukian Nieto, C. Magron, P. Doornenbal, G. G. Kiss, S. Nishimura, P.-A. Söderström, V. H. Phong, J. Wu, D. S. Ahn, N. Fukuda, N. Inabe, T. Kubo, S. Kubono, H. Sakurai, Y. Shimizu, T. Sumikama, H. Suzuki, H. Takeda, J. Agramunt, A. Algora, V. Guadilla, A. Montaner-Piza, A. I. Morales, S. E. A. Orrigo, B. Rubio, Y. Fujita, M. Tanaka, W. Gelletly, P. Aguilera, F. Molina, F. Diel, D. Lubos, G. de Angelis, D. Napoli, C. Borcea, A. Boso, R. B. Cakirli, E. Ganioglu, J. Chiba, D. Nishimura, H. Oikawa, Y. Takei, S. Yagi, K. Wimmer, G. de France, S. Go and B. A. Brown. Two-proton radioactivity of ^{67}Kr. *Phys. Rev. Lett.*, **117**: (2016) 162501. doi:10.1103/PhysRevLett.117.162501.
URL http://link.aps.org/doi/10.1103/PhysRevLett.117.162501

[Gol60] V. Goldansky. On neutron-deficient isotopes of light nuclei and the phenomena of proton and two-proton radioactivity. *Nuclear Physics*, **19**: (1960) 482 – 495. ISSN 0029-5582. doi:http://dx.doi.org/10.1016/0029-5582(60)90258-3.
URL http://www.sciencedirect.com/science/article/pii/0029558260902583

[Gol61] V. Goldansky. Two-proton radioactivity. *Nuclear Physics*, **27 4**: (1961) 648 – 664. ISSN 0029-5582. doi:http://dx.doi.org/10.1016/0029-5582(61)90309-1.
URL http://www.sciencedirect.com/science/article/pii/0029558261903091

[Gol04] V. Z. Goldberg, G. V. Rogachev, W. H. Trzaska, J. J. Kolata, A. Andreyev, C. Angulo, M. J. G. Borge, S. Cherubini, G. Chubarian, G. Crowley, P. Van Duppen, M. Gorska, M. Gulino, M. Huyse, P. Jesinger, K.-M. Källman, M. Lattuada, T. Lönnroth, M. Mutterer, R. Raabe, S. Romano, M. V. Rozhkov, B. B. Skorodumov, C. Spitaleri, O. Tengblad and A. Tumino. Investigation of the α-cluster structure in ^{22}Ne and ^{22}Mg. *Physical Review C*, **69 2**: (2004) 024602. ISSN 0556-2813. doi: 10.1103/PhysRevC.69.024602.
URL `http://link.aps.org/doi/10.1103/PhysRevC.69.024602`

[Gor92] J. Gorres, M. Wiescher, K. Scheller, D. J. Morrissey, B. M. Sherrill, D. Bazin and J. A. Winger. β-delayed proton decay of ^{20}Mg and its astrophysical implications. *Phys. Rev. C*, **46**: (1992) R833–R837. doi:10.1103/PhysRevC.46.R833.
URL `http://link.aps.org/doi/10.1103/PhysRevC.46.R833`

[Gri00] L. V. Grigorenko, R. C. Johnson, I. G. Mukha, I. J. Thompson and M. V. Zhukov. Theory of two-proton radioactivity with application to ^{19}Mg and ^{48}Ni. *Phys. Rev. Lett.*, **85**: (2000) 22–25. doi:10.1103/PhysRevLett.85.22.
URL `http://link.aps.org/doi/10.1103/PhysRevLett.85.22`

[G83] J. Grres, H. Becker, L. Buchmann, C. Rolfs, P. Schmalbrock, H. Trautvetter, A. Vlieks, J. Hammer and T. Donoghue. Proton-induced direct capture on ^{21}Ne and ^{22}Ne. *Nuclear Physics A*, **408 2**: (1983) 372 – 396. ISSN 0375-9474. doi: http://dx.doi.org/10.1016/0375-9474(83)90588-2.
URL `http://www.sciencedirect.com/science/article/pii/0375947483905882`

[Har76] J. Hardy, J. MacDonald, H. Schmeing, T. Faestermann, H. Andrews, J. Geiger, R. Graham and K. Jackson. A new series of β-delayed proton precursors. *Physics Letters B*, **63 1**: (1976) 27 – 30. ISSN 0370-2693. doi:http://dx.doi.org/10.1016/0370-2693(76)90460-3.
URL `http://www.sciencedirect.com/science/article/pii/0370269376904603`

[Har15] J. C. Hardy and I. S. Towner. Superallowed $0^+ \to 0^+$ nuclear β decays: 2014 critical survey, with precise results for V_{ud} and ckm unitarity. *Phys. Rev. C*, **91**: (2015) 025501. doi:10.1103/PhysRevC.91.025501.
URL `http://link.aps.org/doi/10.1103/PhysRevC.91.025501`

[Hei32] W. Heisenberg. Uber den Bau der Atomkerne. II. *Zeitschrift für Physik*, pp. 156–164.

[Hey04] K. Heyde. *Basic Ideas and Concepts in Nuclear Physics: An Introductory Approach, Third Edition*. Series in fundamental and applied nuclear physics (2004). ISBN 9781420054941.

[Hol13] J. D. Holt, J. Menéndez and A. Schwenk. Three-body forces and proton-rich nuclei. *Phys. Rev. Lett.*, **110**: (2013) 022502. doi:10.1103/PhysRevLett.110.022502.
URL `http://link.aps.org/doi/10.1103/PhysRevLett.110.022502`

[Hub89] F. Hubert, J. P. Dufour, R. Del Moral, A. Fleury, D. Jean, M. S. Pravikoff, H. Delagrange, H. Geissel, K. H. Schmidt and E. Hanelt. β decay of ^{22}O. *Zeitschrift für Physik A Atomic Nuclei*, **333 3**: (1989) 237–246. ISSN 0939-7922. doi: 10.1007/BF01294511.
URL `http://dx.doi.org/10.1007/BF01294511`

[Iac06] V. E. Iacob, Y. Zhai, T. Al-Abdullah, C. Fu, J. C. Hardy, N. Nica, H. I. Park, G. Tabacaru, L. Trache and R. E. Tribble. β decay of proton-rich nucleus ^{23}Al and astrophysical consequences. *Phys. Rev. C*, **74**: (2006) 045810. doi: 10.1103/PhysRevC.74.045810.
URL `http://link.aps.org/doi/10.1103/PhysRevC.74.045810`

[Ich09] Y. Ichikawa, T. Kubo, N. Aoi, V. Banerjee, A. Chakrabarti, N. Fukuda, H. Iwasaki, S. Kubono, T. Motobayashi, T. Nakabayashi, T. Nakamura, T. Nakao, T. Okumura, H. J. Ong, T. K. Onishi, D. Suzuki, H. Suzuki, M. K. Suzuki, T. Teranishi, K. N. Yamada, H. Yamaguchi and H. Sakurai. β-decay study of $T_z = -2$ proton-rich nucleus ^{24}Si. *The European Physical Journal A*, **42 3**: (2009) 375–378. ISSN 1434-601X. doi:10.1140/epja/i2008-10761-8.
URL `http://dx.doi.org/10.1140/epja/i2008-10761-8`

[Kar63] V. A. Karnaukhov. Proceedings of the third conference on reactions between complex nuclei. pp. 434–438.

[Kis98] Z. Kis, B. Fazekas, J. str, Z. Rvay, T. Belgya, G. Molnr and L. Koltay. Comparison of efficiency functions for Ge γ-ray detectors in a wide energy range. *Nuclear Instruments and Methods in Physics Research Section A: Accelerators, Spectrometers, Detectors and Associated Equipment*, **418 23**: (1998) 374 – 386. ISSN 0168-9002. doi:http://dx.doi.org/10.1016/S0168-9002(98)00778-5.
URL `http://www.sciencedirect.com/science/article/pii/S0168900298007785`

[Kol14] G. Koldste, B. Blank, M. Borge, J. Briz, M. Carmona-Gallardo, L. Fraile, H. Fynbo, J. Giovinazzo, J. Johansen, A. Jokinen, B. Jonson, T. Kurturkian-Nieto, T. Nilsson, A. Perea, V. Pesudo, E. Picado, K. Riisager, A. Saastamoinen, O. Tengblad, J.-C. Thomas and J. V. de Walle. Sizeable β-strength in ^{31}Ar (β3p) decay. *Physics Letters B*, **737**: (2014) 383 – 387. ISSN 0370-2693. doi: http://dx.doi.org/10.1016/j.physletb.2014.09.015.
URL `http://www.sciencedirect.com/science/article/pii/S0370269314006650`

[Lal98] G. Lalazissis, A. Farhan and M. Sharma. Light nuclei near neutron and proton drip lines in relativistic mean-field theory. *Nuclear Physics A*, **628 2**: (1998) 221 – 254. ISSN 0375-9474. doi:http://dx.doi.org/10.1016/S0375-9474(97)00630-1.
URL `http://www.sciencedirect.com/science/article/pii/S0375947497006301`

[Lau13] K. L. Laursen, O. S. Kirsebom, H. O. U. Fynbo, a. Jokinen, M. Madurga, K. Riisager, a. Saastamoinen, O. Tengblad and J. Äystö. High-statistics measurement of the β-delayed α spectrum of ^{20}Na. *The European Physical Journal A*, **49 6**: (2013) 79. ISSN 1434-6001. doi:10.1140/epja/i2013-13079-6.

[Lor12] G. Lorusso, A. Becerril, A. Amthor, T. Baumann, D. Bazin, J. S. Berryman, B. A. Brown, R. H. Cyburt, H. L. Crawford, A. Estrade, A. Gade, T. Ginter, C. J. Guess, M. Hausmann, G. W. Hitt, P. F. Mantica, M. Matos, R. Meharchand, K. Minamisono, F. Montes, G. Perdikakis, J. Pereira, M. Portillo, H. Schatz, K. Smith, J. Stoker, A. Stolz and R. G. T. Zegers. β-delayed proton emission in the ^{100}Sn region. *Phys. Rev. C*, **86**: (2012) 014313. doi:10.1103/PhysRevC.86.014313.
URL `http://link.aps.org/doi/10.1103/PhysRevC.86.014313`

[Lun] M. V. Lund. A search for exotic decay modes on the proton drip-line - the case of ^{20,21}Mg.
URL `https://cds.cern.ch/record/2153139/files/CERN-THESIS-2016-036.pdf`

[Lun16] M. V. Lund, A. Andreyev, M. J. G. Borge, J. Cederkäll, H. De Witte, L. M. Fraile, H. O. U. Fynbo, P. T. Greenlees, L. J. Harkness-Brennan, A. M. Howard, M. Huyse, B. Jonson, D. S. Judson, O. S. Kirsebom, J. Konki, J. Kurcewicz, I. Lazarus, R. Lica, S. Lindberg, M. Madurga, N. Marginean, R. Marginean, I. Marroquin, C. Mihai, M. Munch, E. Nacher, A. Negret, T. Nilsson, R. D. Page, S. Pascu, A. Perea, V. Pucknell, P. Rahkila, E. Rapisarda, K. Riisager, F. Rotaru, C. Sotty, M. Stanoiu, O. Tengblad, A. Turturica, P. Van Duppen, V. Vedia, R. Wadsworth and N. Warr. Beta-delayed proton emission from 20mg. *The European Physical Journal A*, **52 10**: (2016) 304. ISSN 1434-601X. doi:10.1140/epja/i2016-16304-x.
URL `http://dx.doi.org/10.1140/epja/i2016-16304-x`

[Ma15] Y. Ma, D. Fang, X. Sun and P. Z. et al. Different mechanism of two-proton emission from proton-rich nuclei ^{23}Al and ^{22}Mg. *Physics Letters B*, **743**: (2015) 306 – 309. ISSN 0370-2693. doi:http://dx.doi.org/10.1016/j.physletb.2015.02.066.
URL `http://www.sciencedirect.com/science/article/pii/S0370269315001574`

[Mac] M. MacCormick. Private communication.

[Mac14] M. Maccormick and G. Audi. Evaluated experimental isobaric analogue states from T=1/2 to T=3 and associated IMME coefficients. *Nuclear Physics A*, **925**: (2014)

61–95. ISSN 0375-9474. doi:10.1016/j.nuclphysa.2014.01.007.
URL http://dx.doi.org/10.1016/j.nuclphysa.2014.01.007

[May48] M. G. Mayer. On closed shells in nuclei. *Phys. Rev.*, **74**: (1948) 235–239. doi:10.1103/PhysRev.74.235.
URL http://link.aps.org/doi/10.1103/PhysRev.74.235

[Mei16] Z. Meisel. To be published (2016).

[Mie07] K. Miernik, W. Dominik, Z. Janas, M. Pfützner, C. R. Bingham and Czyrkowski. First observation of β-delayed three-proton emission in ^{45}Fe. *Phys. Rev. C*, **76**: (2007) 041304. doi:10.1103/PhysRevC.76.041304.
URL http://link.aps.org/doi/10.1103/PhysRevC.76.041304

[Mor03a] D. Morrissey, B. Sherrill, M. Steiner, A. Stolz and I. Wiedenhoever. Commissioning the A1900 projectile fragment separator. *Nuclear Instruments and Methods in Physics Research Section B: Beam Interactions with Materials and Atoms*, **204 0**: (2003) 90 – 96. ISSN 0168-583X. doi:http://dx.doi.org/10.1016/S0168-583X(02)01895-5. 14th International Conference on Electromagnetic Isotope Separators and Techniques Related to their Applications.
URL http://www.sciencedirect.com/science/article/pii/S0168583X02018955

[Mor03b] A. C. Morton. β-decay studies at the NSCL using a double-sided silicon strip detector. *AIP Conference Proceedings*, **680 1**: (2003) 550–553. doi:http://dx.doi.org/10.1063/1.1619777.
URL http://scitation.aip.org/content/aip/proceeding/aipcp/10.1063/1.1619777

[Mue01] W. Mueller, J. Church, T. Glasmacher, D. Gutknecht, G. Hackman, P. Hansen, Z. Hu, K. Miller and P. Quirin. Thirty-two-fold segmented germanium detectors to identify γ-rays from intermediate-energy exotic beams. *Nuclear Instruments and Methods in Physics Research Section A: Accelerators, Spectrometers, Detectors and Associated Equipment*, **466 3**: (2001) 492 – 498. ISSN 0168-9002. doi:http://dx.doi.org/10.1016/S0168-9002(01)00257-1.
URL http://www.sciencedirect.com/science/article/pii/S0168900201002571

[Per00] K. Perjrvi, T. Siiskonen, A. Honkanen, P. Dendooven, A. Jokinen, P. Lipas, M. Oinonen, H. Penttil and J. yst. Measurement of the IAS resonance strength in ^{23}Mg. *Physics Letters B*, **492 12**: (2000) 1 – 7. ISSN 0370-2693. doi:http://dx.doi.org/10.1016/S0370-2693(00)01074-1.
URL http://www.sciencedirect.com/science/article/pii/S0370269300010741

[Pfü12] M. Pfützner, M. Karny, L. V. Grigorenko and K. Riisager. Radioactive decays at limits of nuclear stability. *Reviews of Modern Physics*, **84 2**: (2012) 567–619. ISSN 00346861. doi:10.1103/RevModPhys.84.567.

[Pf03] M. Pftzner, B. Blank, J. Giovinazzo, E. Badura, C. Bingham, C. Borcea, B. Brown, M. Chartier, S. Czajkowski, F. De Oliveira Santos, A. Fleury, H. Geissel, L. Grigorenko, R. Grzywacz, M. Hellstrm, Z. Janas, J. Kurcewicz, A. Lalleman, M. Lewitowicz, M. Lopez Jimenez, V. Maslov, C. Mazzocchi, I. Mukha, G. Mnzenberg, C. Plettner, M. Pravikoff, E. Roeckl, K. Rykaczewski, K. Schmidt, R. Simon, M. Stanoiu and J. Thomas. *Discovery of the two-proton decay of* ^{45}Fe, vol. 34, pp. 2363–2371 (2003), 4 ed.

[Pie95] A. Piechaczek, M. Mohar, R. Anne, V. Borrel, B. Brown, J. Corre, D. Guillemaud-Mueller, R. Hue, H. Keller, S. Kubono, V. Kunze, M. Lewitowicz, P. Magnus, A. Mueller, T. Nakamura, M. Pftzner, E. Roeckl, K. Rykaczewski, M. Saint-Laurent, W.-D. Schmidt-Ott and O. Sorlin. β decay of ^{20}Mg. *Nuclear Physics A*, **584 3**: (1995) 509 – 531. ISSN 0375-9474. doi:http://dx.doi.org/10.1016/0375-9474(94)00791-K. URL `http://www.sciencedirect.com/science/article/pii/037594749400791K`

[Pom11a] M. Pomorski, K. Miernik, W. Dominik, Z. Janas, M. Pfützner, C. R. Bingham and H. Czyrkowski. β-delayed proton emission branches in ^{43}Cr. *Phys. Rev. C*, **83**: (2011) 014306. doi:10.1103/PhysRevC.83.014306.
URL `http://link.aps.org/doi/10.1103/PhysRevC.83.014306`

[Pom11b] M. Pomorski, M. Pfützner, W. Dominik, R. Grzywacz, T. Baumann, J. S. Berryman, H. Czyrkowski, R. Dabrowski, T. Ginter, J. Johnson, G. Kamiński, A. Kuźniak, N. Larson, S. N. Liddick, M. Madurga, C. Mazzocchi, S. Mianowski, K. Miernik, D. Miller, S. Paulauskas, J. Pereira, K. P. Rykaczewski, A. Stolz and S. Suchyta. First observation of two-proton radioactivity in ^{48}Ni. *Phys. Rev. C*, **83**: (2011) 061303. doi:10.1103/PhysRevC.83.061303.
URL `http://link.aps.org/doi/10.1103/PhysRevC.83.061303`

[Pri03] J. Prisciandaro, A. Morton and P. Mantica. Beta Counting System for fast fragmentation beams. *Nuclear Instruments and Methods in Physics Research Section A: Accelerators, Spectrometers, Detectors and Associated Equipment*, **505 12**: (2003) 140 – 143. ISSN 0168-9002. doi:http://dx.doi.org/10.1016/S0168-9002(03)01037-4. Proceedings of the 10^{th} Symposium on Radiation Measurements and Applications. URL `http://www.sciencedirect.com/science/article/pii/S0168900203010374`

[Rad] D. Radford. Notes on the use of the program gf3.
URL `http://radware.phy.ornl.gov/gf3/gf3`

[Rat75] A. Ratkowski. Energy response of silicon surface-barrier particle detectors to slow heavy ions. *Nuclear Instruments and Methods*, **130 2**: (1975) 533 – 538. ISSN 0029-554X. doi:http://dx.doi.org/10.1016/0029-554X(75)90053-1.
URL `http://www.sciencedirect.com/science/article/pii/0029554X75900531`

[Ren96] Z. Ren, W. Mittig, B. Chen, Z. Ma and G. Auger. Relativistic mean-field study of light proton-rich nuclei ^{18}Ne,^{20}Mg and^{22}Si. *Zeitschrift für Physik A Hadrons and Nuclei*, **353 4**: (1996) 363–365. ISSN 0939-7922. doi:10.1007/BF01285147.
URL `http://dx.doi.org/10.1007/BF01285147`

[Rog09] T. Roger, H. Savajols, I. Tanihata, W. Mittig, M. Alcorta, D. Bandyopadhyay, R. Bieri, L. Buchmann, M. Caamaño, B. Davids, N. Galinski, A. Gallant, D. Howell, R. Kanungo, W. Mills, S. Mythili, M. Notani, R. Openshaw, E. Padilla-Rodal, P. Roussel-Chomaz, G. Ruprecht, G. Savard, G. Sheffer, A. C. Shotter, M. Trinczek and P. Walden. Mass of ^{11}Li from the ^{1}H(^{11}Li,^{9} Li)^{3}H reaction. *Phys. Rev. C*, **79**: (2009) 031603. doi:10.1103/PhysRevC.79.031603.
URL `http://link.aps.org/doi/10.1103/PhysRevC.79.031603`

[Saa11] A. Saastamoinen, L. Trache, A. Banu, M. A. Bentley, T. Davinson, J. C. Hardy, V. E. Iacob, M. McCleskey, B. T. Roeder, E. Simmons, G. Tabacaru, R. E. Tribble, P. J. Woods and J. Aysto. Experimental study of β-delayed proton decay of ^{23}Al for nucleosynthesis in novae. *Phys. Rev. C.*, **045808**: (2011) 1–10. doi:10.1103/PhysRevC.83.045808.
URL `http://dx.doi.org/10.1103/PhysRevC.83.045808`

[Sch82] D. Schardt. Direct proton decay of ^{147}Tm. pp. 256–266. doi:10.1007/BFb0018101.
URL `http://dx.doi.org/10.1007/BFb0018101`

[Sik12] F. Siklér. A parametrization of the energy loss distributions of charged particles and its applications for silicon detectors. *Nuclear Instruments and Methods in Physics Research, Section A: Accelerators, Spectrometers, Detectors and Associated Equipment*, **691**: (2012) 16–29. ISSN 01689002. doi:10.1016/j.nima.2012.06.064.

[Sin98] B. Singh, J. Rodriguez, S. Wong and J. Tuli. Review of log ft values in β decay. *Nuclear Data Sheets*, **84 3**: (1998) 487 – 563. ISSN 0090-3752. doi:http://dx.doi.org/10.1006/ndsh.1998.0015.
URL `http://www.sciencedirect.com/science/article/pii/S0090375298900151`

[SL87] M. G. Saint-Laurent, J. P. Dufour, R. Anne, D. Bazin, V. Borrel, H. Delagrange, C. Détraz, D. Guillemaud-Mueller, F. Hubert, J. C. Jacmart, A. C. Mueller,

F. Pougheon, M. S. Pravikoff and E. Roeckl. Observation of a bound T_z=-3 nucleus: ^{22}Si. *Phys. Rev. Lett.*, **59**: (1987) 33–35. doi:10.1103/PhysRevLett.59.33.
URL http://link.aps.org/doi/10.1103/PhysRevLett.59.33

[Sto69] R. H. Stokes and P. G. Young. ^{18}N and ^{22}F Ground States, ^{22}F Excited States, and $T = 2$ Analogs in ^{22}Ne. *Phys. Rev.*, **178**: (1969) 1789–1794. doi: 10.1103/PhysRev.178.1789.
URL http://link.aps.org/doi/10.1103/PhysRev.178.1789

[Sza83] E. Szanto, A. D. Toledo, H. Klapdor, G. Rosner and M. Schrader. Yrast and high-spin states in ^{22}Ne. *Nuclear Physics A*, **404 1**: (1983) 142 – 166. ISSN 0375-9474. doi:http://dx.doi.org/10.1016/0375-9474(83)90419-0.
URL http://www.sciencedirect.com/science/article/pii/0375947483904190

[Tow15] I. S. Towner and J. C. Hardy. Parametrization of the statistical rate function for select superallowed transitions. *Phys. Rev. C*, **91**: (2015) 015501. doi: 10.1103/PhysRevC.91.015501.
URL http://link.aps.org/doi/10.1103/PhysRevC.91.015501

[Tri99] W. Trinder, J. Anglique, R. Anne, J. yst, C. Borcea, J. Daugas, D. Guillemaud-Mueller, S. Grvy, R. Grzywacz, A. Jokinen, M. Lewitowicz, M. Lopez, F. de Oliveira, A. Ostrowski, T. Siiskonen and M. Saint-Laurent. β-decay of ^{35}ca. *Physics Letters B*, **459 13**: (1999) 67 – 72. ISSN 0370-2693. doi:http://dx.doi.org/10.1016/S0370-2693(99)00655-3.
URL http://www.sciencedirect.com/science/article/pii/S0370269399006553

[TUN] Tunl nuclear data evaluation project.
URL http://www.tunl.duke.edu/nucldata/chain/20.shtml

[Val09] L. Valentin. *Physique subatomique: noyaux et particules*. Collection Enseignement des sciences (2009). ISBN 2705660963.

[Wal12] J. P. Wallace, P. J. Woods, G. Lotay, a. Alharbi, a. Banu, H. M. David, T. Davinson, M. McCleskey, B. T. Roeder, E. Simmons, a. Spiridon, L. Trache and R. E. Tribble. β-Delayed proton-decay study of ^{20}Mg and its implications for the ^{19}Ne(p,γ)^{20}Na breakout reaction in X-ray bursts. *Physics Letters, Section B: Nuclear, Elementary Particle and High-Energy Physics*, **712 1-2**: (2012) 59–62. ISSN 03702693. doi: 10.1016/j.physletb.2012.04.046.
URL http://dx.doi.org/10.1016/j.physletb.2012.04.046

[Wan12] M. Wang, G. Audi, A. Wapstra, F. Kondev, M. MacCormick, X. Xu and B. Pfeiffer. The AME2012 atomic mass evaluation. *Chinese Physics C*, **36 12**: (2012) 1603. URL `http://stacks.iop.org/1674-1137/36/i=12/a=003`

[Wei35] C. F. v. Weizsäcker. Zur theorie der kernmassen. *Zeitschrift für Physik*, **96 7**: (1935) 431–458. ISSN 0044-3328. doi:10.1007/BF01337700. URL `http://dx.doi.org/10.1007/BF01337700`

[Wei05] L. Weissman, A. F. Lisetskiy, O. Arndt, U. Bergmann, B. A. Brown, J. Cederkall, I. Dillmann, O. Hallmann, L. Fraile, S. Franchoo, L. Gaudefroy, U. Kster, K.-L. Kratz, B. Pfeiffer and O. Sorlin. β decay of ^{22}o. *Journal of Physics G: Nuclear and Particle Physics*, **31 7**: (2005) 553. URL `http://stacks.iop.org/0954-3899/31/i=7/a=002`

[Wig57] E. Wigner. Nuclear analogue states. *Proceedings of the Robert. A. Welch Foundation Conference on Chemical Research*, **1**: (1957) 67–91.

[Wil87] A. Willis, M. Morlet, N. Marty, C. Djalali, G. M. Crawley, A. Galonsky, V. Rotberg and B. A. Brown. Excitation of 1^+ and 2^- states in the Neon isotopes. *Nuclear Physics, Section A*, **464 2**: (1987) 315–325. ISSN 03759474. doi:10.1016/0375-9474(87)90340-X.

[Zel60] Y. B. Zeldóvich. The existence of new isotopes of light nuclei and the equation of state of neutrons. *Soviet Physics JETP*, **11 4**: (1960) 812.

Résumé

Les ions d'intérêts riches en protons de ^{20}Mg, de ^{23}Si et de ^{22}Si ont été produits par fragmentation au laboratoire NSCL, MSU (USA), puis implantés dans un dispositif composé de 3 détecteurs Si pistes (DSSD) entouré de 16 détecteurs HPGe. Cet ensemble a permis la détection des particules chargées émises depuis les états non liés, en coincidence avec les rayons γ émis par la désexcitation des noyaux fils. La décroissance βp du ^{20}Mg, particulièrement bien connue, a été étudiée afin de tester et d'optimiser l'analyse. En particulier, les voies de décroissance βp peuplant les 3 premiers états excités du ^{19}Ne ont pu être identifiées. Le temps de demi-vie, les rapports d'embranchement des transitions et les énergies d'excitation des états, y compris l'état isobarique analogue (IAS), ont été mesurés. L'étude de la décroissance β du ^{23}Si a permis l'identification de 14 états dans l'^{23}Al. L'émission de deux protons depuis l'IAS dans l'^{23}Al a pu être mise en évidence avec certitude. La mesure de l'énergie de l'IAS a permis une détermination plus précise de la masse de l'état fondamental du ^{23}Si, 23.27 (7) MeV. Une possible transition $\beta 3p$ a également été observée. La plupart des prédictions théoriques de la masse du ^{22}Si sont en accord avec une radioactivité 2-protons (2p). Les décroissances $\beta 2p$ vers le premier état excité et l'état foncamentale du ^{20}Na ont été identifiées. Le rapport d'embranchement vers l'IAS est de 2.05 (44) %, et son energie d'excitation a été mesurée 9040 (54) keV. La mesure supplémentaire du temps de demi-vie, $T_{1/2} = 30.38$ (45) ms, a permis de calculer le temps de vie partiel de cette transition. Dans cette étude, nous proposons une paramétrisation de la fonction statistique de Fermi f pour les décroissances de Fermi super-permises, permettant la première mesure indirecte de l'excès de masse de l'état fondamental du ^{22}Si, 31.49 (14) MeV. L'énergie seuil correspondante est alors $S_{2p} = 645$ (100) keV, et ne permet pas une radioactivité 2p depuis l'état fondamental.

Abstract

The neutron-deficient nuclei ^{20}Mg, ^{23}Si and ^{22}Si were produced by fragmentation at NSCL, at MSU (USA), and implanted into an array of 3 double sided stripped Si detectors, surrounded by 16 high-purity Ge detectors. This novel arrangement allowed the detection of the charged particles emitted by the unbound excited states in coincidence with the γ rays emitted by the de-excitation of the daughter. The βp decay of ^{20}Mg is very well-known and therefore was used to test and optimize the analysis programm. The β-delayed proton transitions to the first 3 excited states in ^{19}Ne were identified and compared to previous measurements. The half-life, the branching ratio of the transitions and the excitation energies, including the IAS, were measured and are in good agreement with the adopted values. The study of the β^+ decay of ^{23}Si allowed the identification of 14 excited states in ^{23}Al. The emission of 2 protons from the IAS was unambiguously identified. The measurement of the IAS energy allowed a better determination of the mass excess of ^{23}Si, giving 23.27 (7) MeV. A possible $\beta 3p$ decay channel was also tentitavely identified. Most of the theoritical predictions are in favor of a 2-proton radioactivity in ^{22}Si. The $\beta 2p$ decays to the first excited state and the ground state of ^{20}Na were identified. The branching ratio of the decay to the IAS is 2.05 (44) %, and the IAS excitation energy was measured to be 9040 (54) keV. The additional measurement of the half-life gives $T_{1/2} = 30.38$ (45) ms, and allowed the determination of the partial half-life. In this study, we propose a parametrization of the statistical rate function f for the superallowed Fermi β decays. This allow the first indirect mass measurement of ^{22}Si ground state, 31.49 (14) MeV. The two-proton threshold is then $S_{2p} = 645$ (100) keV and does not allow 2p radioactivity.